1-2022

Surface-functionalized chemiresistive films that exploit h-bonding, cation-pi, and metal-halide interactions.

Prasadanie Karunarathna Adhihetty
University of Louisville

SURFACE-FUNCTIONALIZED CHEMIRESISTIVE FILMS THAT EXPLOIT H-BONDING, CATION-π, AND METAL-HALIDE INTERACTIONS

By

Prasadanie Karunarathna Adhihetty
B. Sc., University of Kelaniya, Sri Lanka, 2014
M.S., University of Louisville, USA, 2019

A Dissertation

Submitted to the Faculty of the
College of Arts & Sciences of the University of Louisville
in Partial Fulfillment of the Requirements
for the Degree of

Doctor of Philosophy in Chemistry

Department of Chemistry
University of Louisville
Louisville, Kentucky

May 2022

SURFACE-FUNCTIONALIZED CHEMIRESISTIVE FILMS THAT EXPLOIT H-BONDING, CATION-π, AND METAL-HALIDE INTERACTIONS

By

Prasadanie Karunarathna Adhihetty

B. Sc., University of Kelaniya, Sri Lanka, 2014

M.S., University of Louisville, USA, 2019

A Dissertation Approved on

April 14, 2022

by the Following Dissertation Committee:

……..
Dissertation Director: Dr. Michael H. Nantz

……
Dr. Xiao-An Fu

…….
Dr. Frederick A. Luzzio

…….
Dr. Francis P. Zamborini

DEDICATION

This dissertation is dedicated

to my loving parents
and
to my husband

ACKNOWLEDGEMENTS

Foremost, I would like to express my deepest appreciation and gratitude to my research advisor Dr. Michael H. Nantz. As an international student who is far away from the relatives, I am so blessed to have Dr. Nantz as my boss. He played two characters in my graduate school life as a supervisor and a father. During my hard times he guided me with his dynamic vision, sincerity, and inspired me to be who I am today. His balanced mentoring and management style causes us to work with him throughout the program without any stress. Dr. Nantz is full of knowledge but always he supports our ideas and encourages us to work independently. I really enjoyed his company and am fortunate to be a part of "The Baus" family.

I am profoundly grateful to my co-advisor Dr. Xiao-An Fu for his guidance, support and encouragement. All the work presented in this thesis resulted from collaborations with Dr. Fu and his research group.

A debt of gratitude is owed to my thesis committee members, Dr. Xiao-An Fu, Dr. Frederick A. Luzzio, and Dr. Francis P. Zamborini. I greatly appreciate the help of Dr. Zamborini. He constantly supported and helped me to understand the basics of Au MPCs synthesis and characterization. Specially, I want to express my gratitude to Dr. Luzzio, who kindly accepted my request to serve on my research and dissertation committees after Dr. Rich's retirement. Dr. Christine Rich served on my literature and original research proposal (ORP) committees. I would like to especially thank her for the moral support she gave to

me. I would like to thank given to me. I am very grateful to all of them for their time, suggestions, encouragement and help throughout these years.

I am particularly grateful to the University of Louisville (U*of*L), the U*of*L Superfund Research Center, and the National Institute of Environmental Health Sciences (NIEHS) for financial support of my projects.

Also, thank you for the great minds of Dr. Zhenzhen Xie, and Sujoy Halder from Dr. Fu's research group. They provided continuous support to complete the sensor projects described in this thesis. More importantly, I am grateful to all my lab-mates: Drs. Tirtha Sibakoti, Fisal Ibrahim, and Stephanie Mattingly, and my great friend Saurin Sutaria. I really enjoyed working with them. Saurin and I joined to the Nantz group at the same time. We shared all the ups and downs from the beginning to the present. Thank you, Saurin, for being my best buddy. Specially, I would like to thank Dr. Stephanie the smart and kindhearted lady in the lab. She was with me in my hard times, and I really enjoyed her company. Also, I have been very fortunate to work and train my undergrads Emma Ison and Drew M. Smith. Drew worked with me three semesters and I really enjoyed working with her in the lab.

Moreover, I am grateful and proud to have been part of the U*of*L Department of Chemistry. I am pleased for its warm welcome and the supportive faculty members and the staff.

I am deeply indebted to Prof. Priyani A. Paranagama, Prof. Dinesh Pandithavidana, and Dr. Russel De Silva at University of Kelaniya, Sri Lanka for their encouragement, motivation, and support in pursuing graduate studies. Without their guidance and support I was not able to enter to the graduate school.

I am blessed to have the company of Dilmi, Dinushika, and Hirumani. They are the humble souls I have found in my USA life. We all are thousand miles away from our families. We smiled, danced, and fought together. But we are always there for each other. Thank you for giving me all the precious memories. Thank you so much for being there for me when I really needed you. Thank you for everything you all have done for me. I am really going to miss you all. As always, I am so thankful to have you all in my life.

Finally, I want to thank my parents for their unconditional love and constant support to make me who I am today. As the youngest in a family with two elder sisters and brothers, I would like to thank you for everything you all have done so far. And last, but not least, I want to thank my loving and supportive husband for his sacrifice. He is the hero behind the scenes. It has been almost five years that we have been living in two different countries. Thank you for believing in me, understanding me, supporting me, and standing with me when I really need you.

ABSTRACT

SURFACE-FUNCTIONALIZED CHEMIRESISTIVE FILMS THAT EXPLOIT H-BONDING, CATION-π, AND METAL-HALIDE INTERACTIONS

Prasadanie Karunarathna Adhihetty

April 14, 2022

The development of gas sensors for detection of volatile organic compounds (VOCs) has been of interest in the sensing field for decades. To date, the use of metal nanoparticle-based chemiresistors for trace VOC detection, particularly gold nanoparticle-based sensors, is of great interest due to their high chemical stability, ease of synthesis, unique optical properties, large surface to volume ratio, and high level of conductivity. Much effort has been devoted towards gold monolayer protected clusters (Au MPCs) as chemiresistors to detect harmful VOCs. The present thesis documents the results of our efforts to exploit the advantages of functionalized Au MPCs chemiresistors for selective VOCs sensing by changing Au MPCs surface functionality.

Our concept is to incorporate binding motifs onto Au MPCs to selectively bind target VOCs and thereby improve the sensing capabilities of chemiresistors derived from casting the functionalized Au MPCs on interdigitated electrodes (IDEs). Chapter 1 in this thesis provides a review of nanoparticle-based chemiresistors for VOCs detection, the

use of MEMS technology to prepare Au MPCs-based chemiresistors, and surface functionalized Au MPCs for VOCs detection. As inceptive studies, we were able to prepare urea-functionalized Au MPCs that demonstrated remarkable sensitivity and selectivity toward acetone serving as a representative carbonyl VOC. Chapter 2 describes the urea-functionalized Au MPCs approach for acetone sensing. We examined several structural elements of thiol urea ligands to change the degree of H-bonding between adjacent urea motifs on the Au MPCs surface as well as varied the steric properties of terminal groups on the urea-functionalized chains. The responses of the developed sensors were notably affected by the urea functional motifs. A *tert*-butyl end group on the thiol urea sensors resulted in high sensitivity and selectivity toward acetone and delivered a sensor capable of detecting acetone in air at concentrations from 10 ppb to 10 ppm.

Next, we expanded our functionalized Au MPCs-based chemiresistive studies toward detection of aromatic VOCs. We explored metal carboxylate-functionalized Au MPCs chemiresistors as a means to selectively detect aromatic hydrocarbons, such as benzene, toluene, ethylbenzene, and xylene (BTEX), at trace levels in outdoor and indoor air. Here, we exploited the strong cation-π noncovalent interactions between metal cations bound to the Au MPCs-based chemiresistor surface and the π-systems of BTEX as a principal sensing mechanism. In this study, we synthesized alkali-metal carboxylate-functionalized Au MPCs by modifying the surface chemistry of Au MPCs via an oxime ether approach. Chapter 3 includes our alkali-metal carboxylate-functionalized Au MPCs chemiresistor synthesis and their selective binding strategy for aromatic VOCs capturing over non-aromatic VOCs. For our study, Li^+, Na^+, and K^+ ion functionalized Au MPC sensors were developed. The K^+- and Na^+- functionalized Au MPCs sensors show a higher

response to electron rich BTEX VOCs over electron deficient nitrobenzene, cyclohexene, acetone, and methanol vapors. Response of Li^+ sensor for all the analytes were very low than the Na^+ and K^+ ion sensors. The developed sensors response to selected aromatic and non-aromatic VOCs suggests cation-π interactions arising between the positively charged cations and the electron-rich aromatic π-systems. The results open a promising research direction for harnessing cation-π interaction to create aromatic VOC-selective sensors.

Chapter 4 details our primary investigation into the use of the unusual binding ability of a cesium cation to vicinal alkyl and vinyl chlorides to detect trichloroethylene (TCE). This chapter describes the sensor response patterns of cesium carboxylate-functionalized Au MPCs chemiresistors on exposure to different alkyl and vinyl chlorides to explore the influence of structural features on TCE detection. The developed Cs^+-Au MPCs sensor exhibits a higher response to analytes with vinyl 1,2-dichlorounit than the other chloro analytes. Moreover, TCE exhibits a high sensor response at 1 ppm – 5 ppm vapor concentration than the other declared harmaful chloro analytes. Hence, this study revealed the different binding affinities of cesium cation toward the geminal, vicinal and vinyl halides and how it affects for sensor response.

In summary, these results show that the outer ligand structure of thiolate-protected Au MPCs plays a major role in enhancing selectivity and sensitivity toward VOCs and suggests this approach as an effective means for targeting analytes.

TABLE OF CONTENTS

LIST OF TABLES

LIST OF FIGURES

LIST OF SCHEMES

CHAPTER 1

SENSORS FOR VOCs DETECTION: GENERAL INTRODUCTION

1.1. SENSORS

As a result of modern technology, sensors are widely used in everyday life, often with other electronics. A sensor is a device that detects changes in its environment and gives a response in a measurable way. This device converts a physical stimulus, like light, heat, sound, pressure, particular motion, or magnetism (one energy domain), into a measurable analog (electrical domain). LDR or Light Dependent Resistor is a simple example of a sensor. According to the intensity of the light to which it is subjected, the resistance of the device varies. The resistance of an LDR increases with decreasing light falling on the LDR and vice versa. Another example is a microphone that converts sound to an electrical signal which can be amplified, transmitted, recorded, and reproduced.[1,2,3]

Classification of Sensors

Sensors can be classified in several ways, such as:[4]

1. Active and passive sensors

   Active sensors require an external excitation signal, while passive sensors do not require an external signal as they directly generate an output signal.[5]

2. Based on sensor detection type

   Chemical, biological, electrical, neuromorphic, and radioactive

3. Based on conversion phenomenon

   Electrochemical, thermoelectric, photoelectric, electromagnetic, and thermotic

4. Analog and digital sensors

   Analog sensors produce a continuous analog output signal, such as voltage and resistance, with respect to the quantity being measured whereas digital sensors work with digital data.

Types of Sensors

Different types of sensors have been developed for several applications and they are used to measure physical properties like resistance, capacitance, temperature, conduction, etc. The commonly used sensor types include the following:[2,4,5]

1. Smoke, gas, and alcohol sensors
2. Temperature sensor – thermocouples and thermistors
3. Strain and gage sensor (strain, weight, shock)
4. Vibration sensors – accelerometers
5. Sound sensors – microphones
6. Voltage transformers – potential transformers
7. Optical sensors – sensing light, UV radiation, or IR
8. Digital sensors – proximity sensors

Generally, a good sensor is sensitive to the measured property and insensitive to any other properties encountered in the application and does not influence the measured property. Also, most sensors have a linear regression, and the sensitivity of the sensor is measured by the slope of the linear regression. The sensitivity indicates the amount of a sensor output change in relation to the input quantity being measured.[6]

1.2. CHEMICAL SENSORS

Chemical sensors are analytical devices that can provide information about the chemical composition of a surrounding environment, whether in a liquid or gas phase. In this type of sensor, the concentration of one or more chemical species in a sample is considered. The target species is commonly referred as the analyte.[2] A glass electrode was

the first chemical sensor; it was developed for pH determination by indicating the hydrogen ion composition in a solution. Chemical sensing is a kind of information-acquisition process where we can obtain the real-time chemical composition of the system. In the chemical sensing process, an interaction occurs between the chemical species and the sensor to produce an amplified electrical signal.

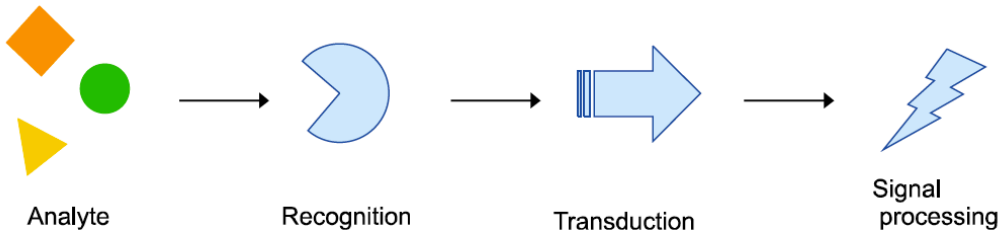

Figure 1.1. Representation of a chemical sensor process. (Copied from Ref. 9)

Generally, a sensor consists of a receptor and a transduction (signaling) unit as shown in Figure 1.1. The receptor unit shows an affinity to a specific analyte in a less or more selective way. First, in the recognition phase, the analyte molecules selectively interact with the receptor molecules or sites included in the sensor's recognition element structure. In a chemical sensor, the recognition and transduction functions are embedded in the same device.[2,3,7] As a function of analyte concentration, some physical or chemical property of the sensing element is varied by its interaction with the analyte. The sensor transforms this change into a measurable physical signal. This sensor process is known as signaling or signal transduction. The transducer is a device which translates the information from one form (e.g., chemical) to another form (e.g., physical).[8]

1.3. CHEMIRESISTORS (RESISTIVE GAS SENSORS)

A chemiresistor is a device that changes its electrical resistance upon changes in the surrounding chemical environment. Usually this occurs in response to a direct chemical interaction between analyte molecules (gases, vapors) and the sensing material of the chemiresistor.[2,10] Generally, chemiresistors are a type of chemical sensor wherein the sensing material and the analyte reversibly interact with each other through noncovalent interactions, such as hydrogen bonding, ionic bonding, halogen bonding, pi-pi interactions, or Van der Waals interactions. To effectively associate and interact, the sensing material and the analyte species should be compatible with respect to chemical reactivity. For instance, if one species presents an electropositive H-atom, then the other species should contain an electronegative atom capable of hydrogen bonding.

A basic chemiresistor is made up of a sensing material that is deposited between two metal electrodes or a set of interdigitated electrodes. The resistance between the electrodes can be easily measured using a multimeter in the absence or presence of an analyte. Examples of commonly used sensing materials are conductive polymers, metals and metal-oxides, nanomaterials (carbon nanotubes, nanoparticles, and graphene), and carbon black polymer composites.[11] Among them, metals, metal oxide semiconductors, conducting polymers, polymer/carbon composites are used as large chemiresistive films while nanowires, nanotubes and nanoparticles are used as small chemiresistive films or the sensing materials. As shown in Figure 1.2, when the chemiresistive sensor is exposed to analytes, analyte-sensor interactions change the initial resistance. Moreover, this resistance change is directly proportional to the amount of analyte present in the environment.

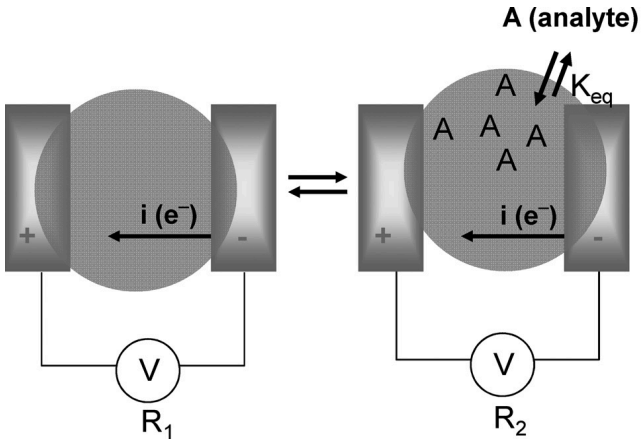

Figure 1.2. Representation of a sensing material placed between metal electrodes of a basic chemiresistor that is subjected to a constant voltage (V). The initial resistance R_1 changes to resistance R_2 when analyte **A** interacts with the sensing material. (Copied from Ref. 11)

1.3.1. Development of Chemiresistors

In 1985, Wohltjen and Snow developed a vapor sensitive chemiresistor using planar microelectrodes and a Langmuir-Blodgett organic semiconductor film.[12] They coined the name "chemiresistor" to describe the device. Figure 1.3 is a schematic representation of the first chemiresistor developed by Wohltjen and Snow. Their vapor sensing method was compatible with monolithic silicon microelectronics technology. Characteristically, vapor interactions with very thin films of organic semiconductors were caused to change the electronic conductance of this chemiresistor and those changes were reproducible and rapid in terms of to make a sensitive and stable chemical detector. They used functionalized copper phthalocyanine as the sensing material and deposited onto the planar microelectrode arrays using Langmuir-Blodgett technique to detect ammonia. Wohltjen *et al.,* were able to detect drops in resistance in the presence of ammonia vapors at sub-ppm concentration levels.[12]

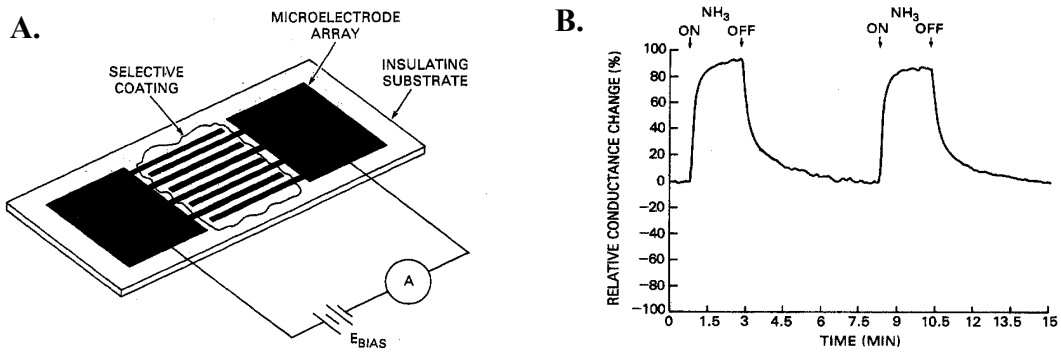

Figure 1.3.A. Representation of the chemiresistor developed by Wohltjen and Snow. Under a constant voltage the current changes as a result of changes in the sensor resistance when vapors interact with the semiconductive film and **B.** 45-layer CuPccp (copper tetracumylphenoxy phthalocyanine) chemiresistor response to successive pulses of 2 ppm ammonia at 30 °C with 1 V bias voltage. (Copied from Ref 12)

1.3.2. Gas and Vapor Sorption

Detection of gases and vapors is crucial for applications like monitoring air quality, controlling hazardous gases in industrial environments, and various physiological studies. Generally, gases and vapors are detected by their adsorption at the surface or absorption into a solid material. Different sensing materials have been studied for gas and vapor detection depending on the target analyte. In the past few years, chemiresistor technology has been widely studied to develop gas sensors for gaseous ammonia detection,[13] for aromatic VOCs like benzene, toluene, ethylbenzene, and xylene (BTEX) detection,[14,15] and even for cigarette smoke detection.[16,17] Chemiresistors are of great interest due to the ability to produce accurate, real-time information about the nearby environment with only a minimal power (e.g., electricity) requirement, as they generally are small devices.[11]

1.3.3. Design of Chemiresistors

Chemiresistors are mainly developed by coating interdigitated electrodes (IDEs) with thin films of sensing materials to fill the gaps between the electrodes (Figure 1.4). IDEs are not conductive before coating a sensing material, but after applying sensing material between the electrodes, IDEs become conductive. Conductive metals like Au, Cr, and Pt are commonly utilized to make these electrodes and the conductance between the electrodes is controlled by the chemiresistive sensing material.[11,12] The use of IDEs in chemiresistors offers both advantages and disadvantages. IDEs increase the surface area of the sensing material film that contacts the electrodes. The overall conductivity of the system is increased by making more electrical connections between the electrodes. IDEs can be arranged in sensor arrays to detect multiple analytes efficiently.[18] MEMS technology

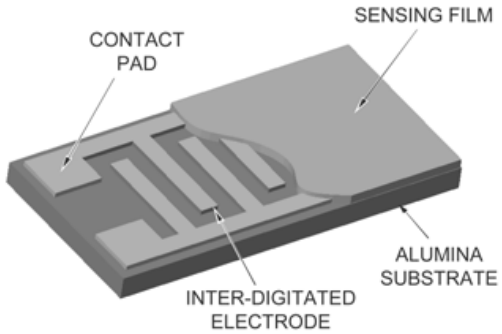

Figure 1.4. Common IDEs used in chemiresistors. (Copied from Ref. 19)

(photolithography) is used to design micron-sized comb finger-shaped IDEs. It is necessary to use a clean room facility to fabricate comb finger IDEs. Compared to such small-sized IDEs, larger electrodes are much easier to design and fabricate. For example, techniques like thermal evaporation can be used for fabrication.[16]

1.3.3.1. Micro-Electro-Mechanical-System (MEMS) Technology

MEMS is a process technology utilized to design small-scale integrated systems or devices that combine electrical and mechanical components having physical dimensions from one micron to several millimeters (Figure 1.5).[20] These devices are fabricated using integrated circuit (IC) batch processing techniques and can recognize, control, and actuate on the micro scale followed by generation of effects on the macro scale.

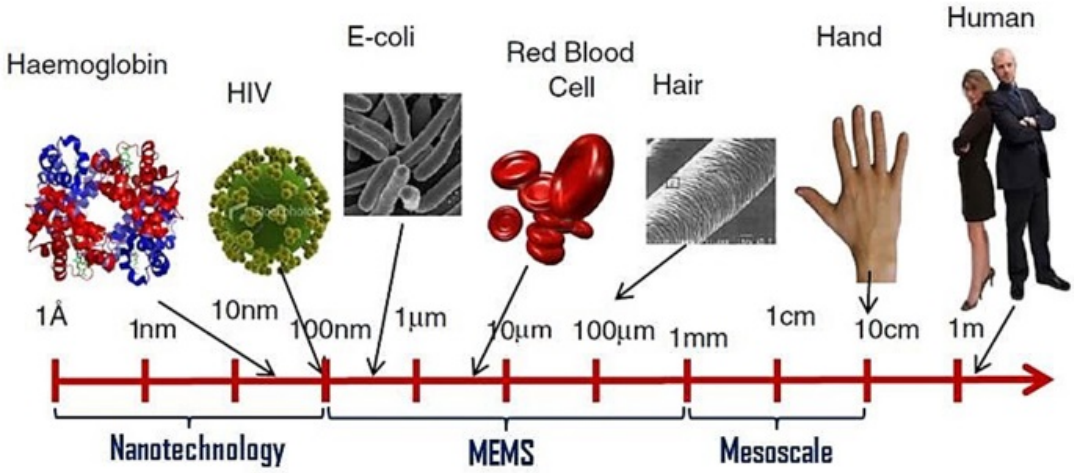

Figure 1.5. Illustration of the MEMS microscopic scale. (Copied from Ref. 20)

MEMS technology requires design, engineering and manufacturing expertise from a wide range of technical areas including mechanical, electrical, and chemical engineering as well as integrated circuit fabrication technology, chemistry, optics, packaging and instrumentation.[20] Many MEMS fabricated devices, such as infrared detectors, ink jet printer heads, pressure sensors, and micro-mirror arrays for high-definition projectors, air bag sensors, computer disk read/write heads, biosensors, and microvalves, are commercially available. Figure 1.6 shows an example for a surface micromachined electrostatically actuated micromotor fabricated using MEMS.

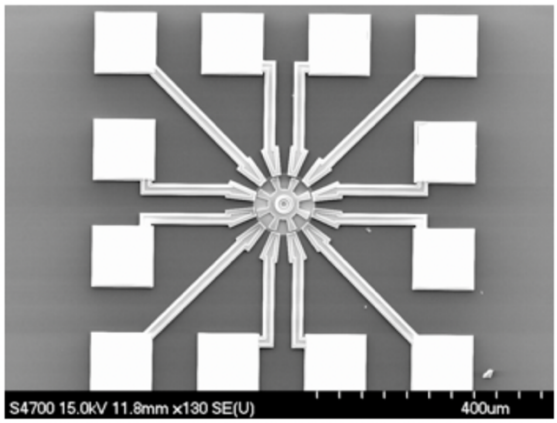

Figure 1.6. Illustration of a MEMS-based micro actuator. (Copied from Ref. 20 b)

MEMS devices have several advantages as a manufacturing technology.

Some of them are:[10,20]

- high sensitivity
- low power consumption
- high frequencies
- cost effective when mass produced (can change the size or scale in manufacturing)
- easy to integrate with microelectronics to produce embedded mechatronic systems
- designs can be achieved by leveraging scaling effects at microscopic levels

Also, MEMS technology has several disadvantages, such as:

- not cost effective at the research and development level (high initial cost for fabrication and assembly using cleanrooms and foundry facilities)
- expensive characterization techniques

1.3.3.2. Design and Fabrication of MEMS Devices

Generally, silicon is used to micromachine MEMS devices. There are different types of silicon wafers available, and silicon is doped to vary the conductivity levels. Electrode layers or piezoelectric layers can be added to introduce various capabilities. There are several steps and cycles involved in MEMS design and fabrication, as summarized in Figure 1.7.[20]

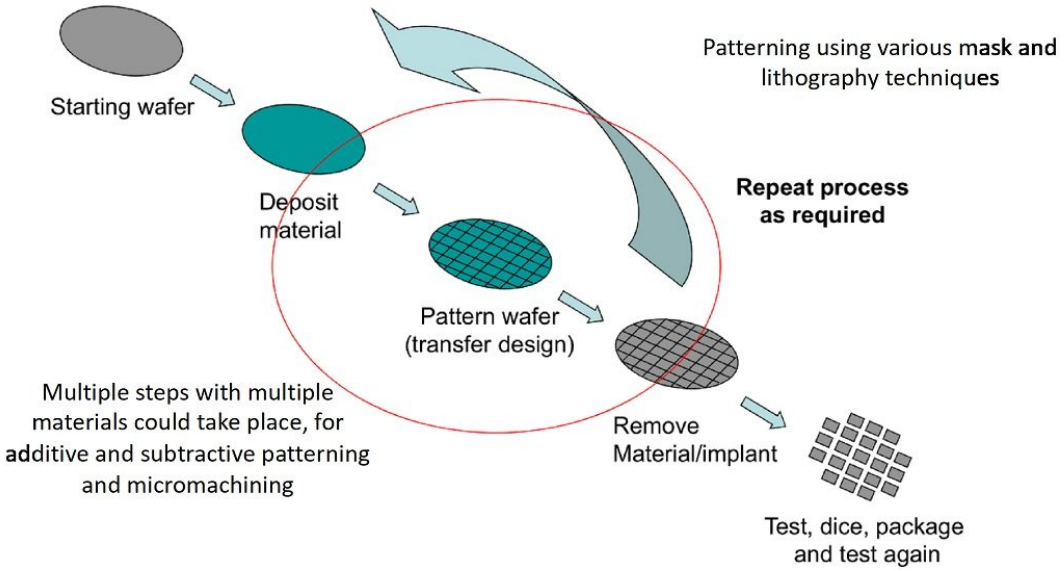

Figure 1.7. Steps involved in MEMS design and fabrication. (Copied from Ref. 20)

The manufacturing steps involved in MEMS are as follows:[20,21]

- design, modelling, and simulation (analytical, numerical, computer-aided design (CAD) and finite element analysis (FEA) methods are used)
- layout and wafer tape-out (layout editor is used)
- starting wafer substrate (silicon, glass, quartz, stainless steel, plastics)
- microfabrication process

- additives (chemical vapor, sputtering, evaporation, oxidization steps are used for material deposition)
- patterning (masks, photolithography, contact lithography, projection lithography)
- material etching (wet chemical, dry ion or plasma, deep reactive ion etching (DRIE))
- die dicing (laser, diamond saw, plasma etch)
- wire bonding (connecting interface circuitry)
- packaging and encapsulation (hermetic seal, plastic / metal / ceramic seal, wafer-level packaging)

Miniaturized structures, actuators, sensors, and microelectronics are the functional devices and structures (elements) of MEMS. However, the most useful and notable elements are the microactuators and microsensors that are categorized under "transducers". Transducers mainly convert energy from one form to another form, such as converting a measured mechanical signal into an electrical signal.[21] To maximize the capacitive surface area of the transducer, comb finger designs (interdigitated electrodes) are widely used in MEMS electrostatic transducers, as shown in Figure 1.4. Over the past several years, most sensors have been manufactured as microsensors on a microscopic scale using MEMS technology and these sensors are mainly used to measure pressure, temperature, chemical species, radiation, etc. Microsensors show higher sensitivity and have a faster measurement time and become excellent candidates for gas sensors.[20]

1.3.4. Sensing Materials

1.3.4.1. Nanoparticles or Nanomaterials

Au-, Ag- and Pt-based nanoparticles with different sizes, structures, and composition have been widely studied as the sensing materials in the chemiresistive sensors.[11,22] Among these nanoparticles, Au MPCs (Au monolayer-protected clusters) or Au NPs (Au nanoparticles) coated with self-assembled monolayers (SAMs) are commonly used.[23-26] The physical and chemical properties of organic SAMs greatly influence the stability of the derived Au NPs and can prevent them from aggregating.[27] Additionally, the structures of SAMs can determine the separation distance between nanoparticle cores, and this property can act as a barrier to electron tunneling through the SAMs when a voltage is applied.[11,28] Consequently, SAMs influence the electrical resistivity of the nanoparticle assembly.[29-31] Furthermore, chemical species (e.g., analytes, other gases) can diffuse into the matrix formed by SAMs around the Au NPs causing swelling, which also will influence the electrical resistivity. Also, SAMs surface structure can control or even enhance interactions between analytes and the NP matrix. When analytes diffuse into the matrix or when they interact directly with SAMs functionality, the distance between nanoparticle

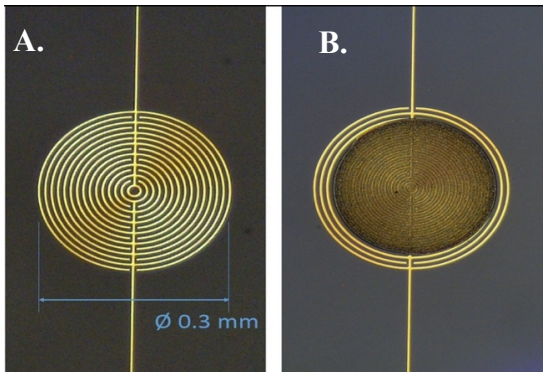

Figure 1.8. Circular shaped IDEs. **A.** without Au NPs film and **B.** with Au NPs film as a chemiresistor. (Copied from Ref. 32)

cores can increase and thereby effect the electrical resistance of the device.[11] Figure 1.8 shows how the IDEs looks like after Au NPs coating. As mentioned earlier non-conductive IDEs become conductive in the presence of Au NPs film as a sensing material.

1.3.4.2. Metal Oxide Semiconductors

Different metal oxide semiconductors have been studied as sensing materials in chemiresistors.[11,33-35] These sensors are mostly used as gas sensors, and they are sensitive for both reduced and oxidized species of each gas. Thus, this type of chemiresistive sensor is ideal to use in industrial situations to ensure a safer environment for employees.

Table 1.1. Metal oxides studied in chemiresistors for vapor sensing.[36]

Metal oxide used as the sensing material	Detected vapors
Tungsten oxide	NO_2
Chromium titanium oxide	H_2S
Indium oxide	O_3
Tin oxide	Reducing gases
Gallium oxide	O_2, CO
Molybdenum oxide	NH_3
Zinc Oxide	Hydrocarbons, O_2

The main disadvantage of metal oxide sensors is that they do not operate at room temperature - high temperatures, above 100 °C, are required to overcome the activation barriers for metal oxide sensors.[37] Table 1.1 summarizes several metal oxide chemiresistive sensors developed for vapor detection.[36]

1.3.4.3. Carbon Nanotubes (CNT)

The use of carbon nanotubes as a sensing material is a recent development. Single-walled carbon nanotube-based (SWCNT) chemiresistors were made in 2000 for the first-time by Kong *et al.*,[38] Since then, several studies involving chemiresistor fabrication using individual single-walled carbon nanotubes (Figure 1.9A),[39] bundles of single-walled carbon nanotubes,[40,41] multi-walled carbon nanotubes (MWCNT, Figure 1.9B),[42,43] and polymer mixtures of carbon nanotubes[44-47] have been reported. These studies have shown that the resistances of carbon nanotube-fabricated devices are readily altered by chemical species or analytes through several mechanisms.

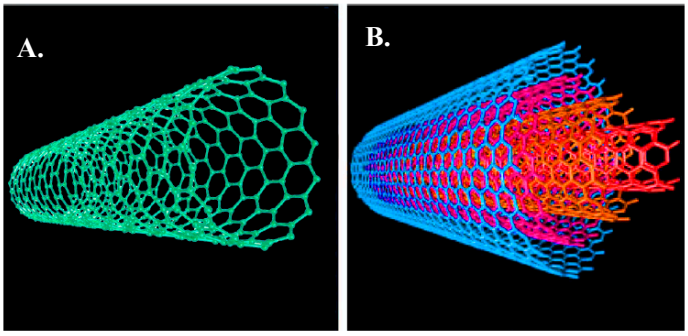

Figure 1.9. Schematics of **A.** SWCNT and **B.** MWCNT. (Copied from Ref. 48 a)

Carbon nanotube-based sensing materials have become more popular for sensors as they have fast response times and low detection limits. However, normal carbon nanotube sensors are not very selective. They can respond to a wide range of analytes. several research groups have aimed to improve the selectivity of carbon nanotube sensors by adding functional groups to the CNT surface,[48a.] by doping with heteroatoms,[48b.] or using polymer barriers.[48c.]

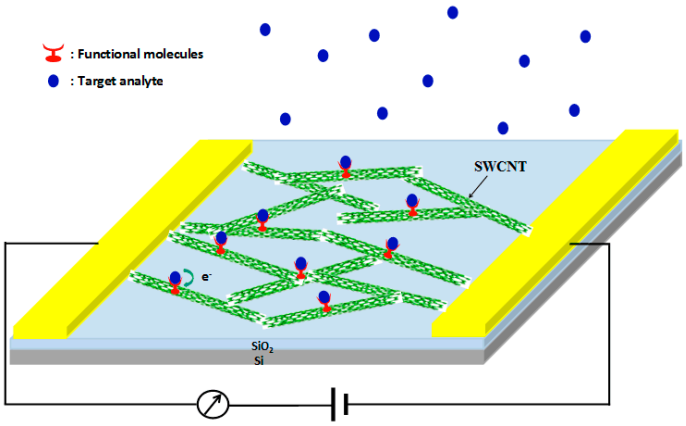

Figure 1.10. Representation of CNT chemiresistive sensor. (Copied from Ref. 49)

1.3.4.4. Conductive Polymers

Polyaniline and polypyrrole conductive polymers are mostly studied as sensing materials. Conductivity of this type of sensor devices are changed by direct interact of target analytes with the polymer chain (Figure 1.10.).[16,50] Like bare carbon nanotubes, conductive polymers also show low selectivity as the most analytes can interact with the polymer material and to increase the selectivity, molecularly imprinted polymers are used.[51] Here, the molecular imprinting technique is utilized to create cavities in the polymer matrix by removing the target molecules from the matrix. This technique also increases the sensitivity of the cemiresistive sensor.[50,51]

1.3.4.5. Graphene

Graphene is another candidate that widely studied as a sensing material which shows excellent sensitivity over most sensing materials.[52,53] This is an allotrope of carbon which consists of a graphite single layer. Graphene chemiresistors are mostly used to detect VOCs,[54-56] proteins,[57] and several simulated chemical species.[58]

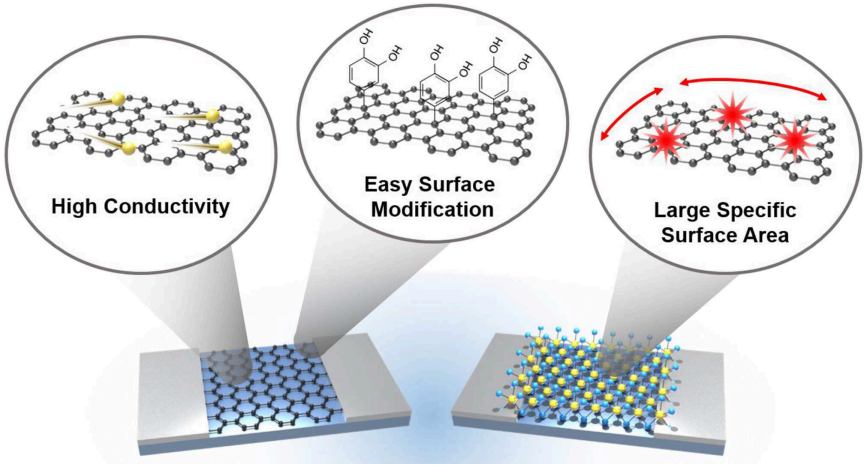

Figure 1.11. Illustration of graphene use as a sensing material and its advantages. (Copied from Ref. 58 b)

1.4. CHEMIRESISTORS CONSTRUCTED FROM NANOPARTICLES

As previously mentioned, metallic nanoparticles have been widely utilized as sensing material in chemiresistive sensing application studies. These nanoscale materials provide various advantages over traditional bulk materials for sensing, such as:[11]

- Small size
  - low cost
  - low power consumption
  - perform fast measurements in the field
  - analyte measurement in highly confined spaces
- High surface to volume ratio
- Electronic properties of the nanomaterial are dominated by the surface atoms
  - analytes interact with the surface atoms more effectively and produce a large resistance change compared to bulk materials

- lower detection limit

- Small analyte diffusion length
  - fast analyte equilibration with the sensing material
  - fast response time

Various conductive metals such as Ag, Au, Pd, Pt and alloys of these metals have been used as sensing materials in most chemiresistive sensors. These chemically modified metal nanoparticles have a metallic core (pure metal or alloyed form) and a chemical coating. Depending on the sensing application, several modifications have been studied in these NPs. In most of the research studies, the nanoparticles are functionalized with organic self-assembled monolayers (SAMs), surfactants, polymers, biomolecules, and ions.[11] Different chemically modified metal nanoparticle and their chemiresistive sensing applications are summarized in Table 1.2.

1.4.1. Chemically Modified Metal Nanoparticles Synthesis and Functionalization

1.4.1.1. Electrostatically Stabilized Metal Nanoparticles

The Turkevich method[59] is used to synthesize negatively charged citrate ion-coated metal nanoparticles, which are the most common electrostatically stabilized nanoparticles. In this method, the metal ion precursor is reduced at high temperature using trisodium citrate in aqueous medium to generate nanoparticles with a 12 to 20 nm core diameter. Trisodium citrate serves as both a weak stabilizer and a reducing agent. To synthesize small nanoparticles with diameters in the 4-5 nm range, borohydride is used as a reductantat at room temperature in the presence of trisodium citrate. And these small nanoparticles are used as seed particles to synthesize various shaped larger nanoparticles, such as nanorods, nanocubes, nanowires, and triangles.[60-62] Sometimes, it is very difficult to make the drop-

Table 1.2. Different types of chemically modified metal and alloy nanoparticles.[11]

Metal composition	NP size + STD [nm]	Modifier	Linker	Film deposition method	Sensing environment	Analytes detected	LOD	Current increase (↑) decrease (↓)
Au	NR	octanethiol (C8S)	—	airbrush	air	water, IPA, tetrachloroethylene, Tol	2.7 ppm (Tol)	↑ and ↓
Au	2.9–6.0	hexanethiol C6S-X with X = OH, NH_2, CH_3, COOH	—	spin-coating	air	MeOH, IPA, Hx, pentane, Tol, acetic acid	20-10 ppm (EtOH)	↑
Au	2.0 ± 0.8	$CH_3(OCH_2CH_2)_nSH$ n = 2,3,4	—	airbrush	air	water, IPA, Tol	NR	—
Au	3.0–5.0	n-(3-thienyl)alkane-thiols n = 2,6,12	—	spin-coating	air	EtOH, chloroform, Hx, Tol	NR	—
Au	4.3 ± 0.9	C8S; $PtCl_2$(olefin)-pyridine) +C8S	—	airbrush	air	EtOH, acetone, 2-butanone, isooctane, trichloroethylene, 1-4 dioxane, Tol, perchloro-ethylene, n-butyl acetate, chlorobenzene, m-xylene, styrene, ethylene, 1-octane, 1.3-butadiene	≈5.5 ppb (styrene)	↓
Au	3.0–4.0	C8S; octanetrithiol ($C8S_3$)	—	inkjet-printing	NR	Tol, EtOH, dichloroethane, MeOH, and acetone	300 ppm (Tol)	↓
Au	4.3 ± 0.9	C8S	—	spray-coating	N_2	28 different vapor analytes	0.0079 ppm (n-decane)	↓
Au	3.9–4.5	1-octanethiol (C8); 1-mercapto-6-phe-noxyhexane (OPH); 7-hydroxy-7,7-bis(trifluoromethyl)-heptane-1-thiol (HFA), or mercapto-dipheny-lacetylene (DPA)	—	micro-dispensing	NR	n-propanol 2-butanone	NR	↓
Pt	17 ± 0.5	oleylamine (ODA),11-mercaptounde-canol, MUA, and benzylmercaptan	—	drop-casting	dry and humid air	Hx, octane, decane, ethyl Bz, EtOH, and water	40 ppm (octane)	↓
Au	NR	chlorobenzen-emethanethiol (CBMT), C8S	—	immersion	air	IPA, acetone, cyclohexane	185 ppm (Tol)	↓
Au	6.0–7.0	$C12NH_2$	—	drop-casting	air	water, acetone, Tol, methane-thiol, propanethiol, octane-thiol, and thiols diluted in N_2	1.5 ppm (methane-thiol)	↑
Au; AuAg	4.1 ± 0.8	tetraoctylammonium bromide (TOABr)	—	drop-casting	air	MeOH, EtOH, IPA, Tol, acetone	2.0 ppm (EtOH)	↑
Au	5.2 ± 0.3 1.9 ± 0.7	C12S	(1,9 nonanedithiol, NDT), (MUA)	place-exchange cross-linking precipitation	air	EtOH, Hx, Tol	NR	—
Au	2.0 ± 0.7	C12S	$X–(CH_2)_n–X$; X = COOH,HS; n = 6,9,12,16	place-exchange cross-linking precipitation	air	Bz, Hx, Tol	NR	—
AuAg	2.0–3.0 (±0.5)							
Au	≈1.6	C6S	hexanedithiol	microcontact printing	N_2	IPA, Tol	NR	—

Metal composition	NP size + STD [nm]	Modifier	Linker	Film deposition method	Sensing environment	Analytes detected	LOD	Current increase (↑) decrease (↓)
Au	NR	$C12NH_2$	[1,12-dodecanedithiol]; [(4)-staffane-3,3‴-dithiol]; [4,4′-terphenyldithiol]	layer-by-layer	air	Tol, 1-propanol, 4-methyl-2-pentanone, water	NR	—
Au	≈1.1	[poly(ethylene glycol) thiol (HSPEG)]; [phenyl ethane thiol (-SC_2Ph)]	octanedithiol and decanedithiol	liquid-phase cross-linking	air	Hx, EtOH, CO_2	NR	—
Au	4.0 ± 1.2	$C12NH_2$	dodecanedithiol	layer-by-layer	air	Tol, 4-methyl-2-pentanone, water, 1-propanol	NR	—
Au	NR	C_nS, n = 4,6,8,10,12, MUA, MHA, MHDA	$HS(CH_2)_nCO_2H$, n = 5,10,15	drop-casting	N_2	EtOH	NR	—
Au; Ag; Pd	1.0–3.0	C6S; MUA	Carboxylate-M^{n+}-carboxylate, n = Cu^{2+}, Zn^{2+}, Ag^{+}, or methyl viologen	layer-by-layer	air	EtOH	NR	—
Au	≈4.0	$C12NH_2$	[disulfide polyphenylene]; [poly-(amidoamine)]; [poly(propylene imine)]	layer-by-layer	air	water, 1-propanol, Tol	NR	—
Pt, Au	3.0 ± 0.8	$C12NH_2$	1,9 nonanedithiol	layer-by-layer	air	water, NH_3, CO, Tol, tetrachloroethylene	100 ppb (NH_3)	↓
Au	3.0	1H, 1H, 2H, 2H Perfluorodecanthiol (PFDT)	—	drop-casting	N_2	hexafluorobenzene, MeOH, Hx, chloroform, Tol, water	NR	↑
Au	NR	C_nS, n = 4-11	—	drop-casting	NR	*n*-hexane, *n*-heptane, *n*-octane, iso-octane, cyclohexane,Tol, ethyl acetate, MeOH, EtOH, IPA 1-butanol	NR	↑ and ↓
Au	NR	C8S	1,6 Hexanedithiol and 1,4 benzenedimethanethiol	place-exchange cross-linking precipitation	N_2	water vapor, Tol, EtOH, ethylacetate, IPA, and acetonitrile	4 ppm (Tol)	↓
Pd	1.7–113.8	λ-DNA	—	drop-casting	air	H_2	1000 ppm	↑
Au	NR	C6S; C10S; 4-methylbenzethiol	—	Langmuir–Schaeffer	air	Tol, NO_2	0.5 ppm (NO_2)	↑ and ↓
Au	3.2–11.8	C6S	—	immobilized on SAM-modified surface	air	Hx, Tol, ethyl ether, THF, $CHCl_3$, CH_2Cl_2, acetone	NR	—
Pd; PdAg PdAu	≈3.0	C6S; $C8NH_2$; $C12NH_2$; $C16NH_2$; TOABr, mix-monolayer (C6S+$C8NH_2$)	—	drop-casting	N_2 and air	H_2	800 ppm	↑
Au	≈6.0	C6S; [4-mercaptophenol]; [6, Hydroxyexanethiol]	—	inkjet-printing	liquid	EtOH, Cl_2CH_4, Tol, octane	0.1 ppm (Tol)	↓
Au	≈3.0	C8S	—	drop-casting	liquid	C8S and Galvinol	pH sensitive	—
Au	≈6.0	polymethtylene	—	immobilized on a redox-gate	liquid	bypiridinium	oxidation/ reduction	—
Au	≈13	oligonucleotides	—	Immobilized on a oligonucleotide-strands	liquid	DNA	500 femtomolar	—
Au	13.0 ± 20	3-mercaptopropionic acid	Zn^{4+}	immobilized on a peptide nucleic acid	liquid	DNA	50 femtomolar	—

cast films using these nanoparticles as they have high tendency for particle aggregation. To avoid particle aggregation, post synthesis steps, such as place exchange reactions, cross linking reactions, biomolecular functionalization and layer by layer deposition, are used.[63]

1.4.1.2. Metal Nanoparticles Stabilized with Surfactants or Polymers

Surfactant-stabilized metal nanoparticles have been synthesized recently and mainly used for chemiresistive gas and vapor sensing applications.[24,64] Zamborini *et al.*, synthesized Au and Pd nanoparticles as well as AuAg and PdAg alloyed metal nanoparticles coated with tetraoctylammonium bromide (TOAB) using $AuCl_4^-$, $PdCl_4^{2-}$, and Ag^+ precursors in the presence of $NaBH_4$ as the metal ion reducing agent in toluene.[24] These nanoparticles can be easily drop-cast between IDEs for gas and vapor sensing applications. [24,64]

1.4.1.3. Monolayer Protected Nano Clusters (MPCs)

MPCs are the most common and widely studied type of metal nanoparticles used for chemiresistive sensing applications. MPCs are generally synthesized by reducing a metal ion precursor using stabilizing ligands such as organoamines or organomercaptans in a two-phase or even single-phase solvent system.[65] In the synthesis process, the metal ion is reduced to its zero-valent metallic form followed by nucleation and growth steps to form nanoparticles while a single self-assembled monolayer (SAM) coating is formed by adsorption of organic ligands onto the nanoparticle surfaces. SAM coating offers several advantages like passivation of nanoparticle surface, prevention of nanoparticle aggregation, and control over nanoparticle solubility.[11] Furthermore, the SAM molecule to metal ion ratio can determine the overall nanoparticle size. The nanoparticle core size

decreases as this ratio increases. Generally, alkanethiolate-coated Au MPCs can be synthesized in the 2 – 5 nm core diameter range.[66] Moreover, thermal treatment of MPCs can be used to decrease the size dispersity and increase particle size.[11] Also, alkanethiolate-coated Au MPCs are widely synthesized over other ligand Au MPCs as the formation of the strong Au–S bond provides extra chemical stability to the metal NPs.[11] Some examples of thiol-coated Au MPCs include octanethiol-coated Au MPCs,[67] hexanethiol-coated Au MPCs,[65] and a mixture of alkane thiols and ω-carboxylate alkanethiol-coated Au MPCs.[68] Amines also are often used as ligands for synthesis of MPCs, as is seen in the organoamine-coated MPCs derived from octylamine[64] and dodecylamine[69,70] coated Pd and PdAg alloy as well as in dodecylamine-coated Au and Pt MPCs,[71] and PdAu alloy MPCs.[72]

In an alternate method, MPCs can be synthesized by reduction of the metal ion precursor in the presence of a weak ligand (citrates, surfactants) followed by exchange reactions with strong alkanethiolate ligands.[11] Also, Murray *et al*., developed a method for ligand functionalization of Au MPCs known as a place-exchange reaction. Here, the primary monolayer is exchanged partially or completely with an incoming new ligand having an extra functionality.[73,74] This method introduces several reactive groups to the MPCs and increases the selectivity of resultant chemiresistive sensors.

1.4.2. Electrode Fabrication and Nanoparticles Deposition in Chemiresistors

As mentioned in Section **1.3.3.1**, electrodes in a chemiresistor device can be microfabricated using MEMS technology in a clean room. To complete the chemiresistive device fabrication, chemically modified metal nanoparticles must be deposited between two metal electrodes to produce electrical conductivity. Polyelectrolytes[75] or bifunctional cross-linkers (dithiols)[76] have been used to assemble electrostatically stabilized metal

nanoparticles in one approach. For this, the electrodes are sequentially dipped in metal nanoparticles and a cross linker or polyelectrolyte solution. Layer-by-layer assembly or drop-cast deposition can also be used for surfactant or polymer coated nanoparticles.[24] Moreover, DNA- or protein-coated nanoparticles are deposited using special biological interactions.[11]

Depending on the polarity of the SAMs, MPCs are soluble in different organic solvents and thus drop casting,[77] spin coating[25,78-80] and airbrushing[67,78] deposition methods can be used to fabricate electrodes. For SAMs with dendrimers,[81] metal ion-carboxylate linkages[68,82] and dithiols[83] layer -by-layer deposition method is also possible. Also, a cross-

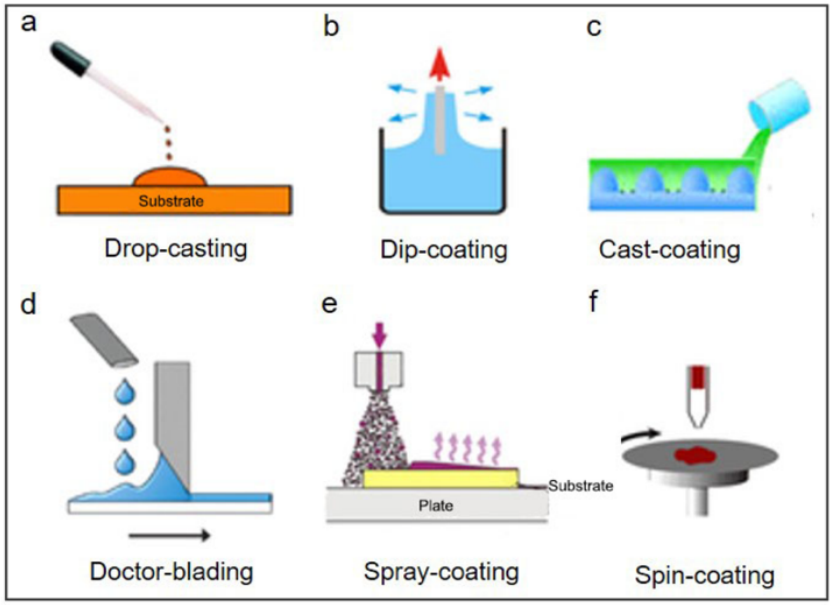

Figure 1.12. Diagrammatic representation of common film coating techniques. (Copied from Ref. 89)

linking precipitation method was developed by Zhong *et al.*,[84] and here the organic soluble nanoparticles become insoluble after adding ligands as formation of new dithiol or hydrogen bonding interactions (cross linking of MPCs).[11] Interestingly, several new

deposition methods like lithography techniques,[85] micro dispensing,[86] inject printing,[87] and microcontact printing[88] have been studied recently. Figure 1.12. summarizes common film coating techniques.

1.4.3. Electronic Properties of Metal Nanoparticles

1.4.3.1. Electronic Conductivity of MPCs

Several research groups have studied the electronic properties of chemically modified metal nanoparticles. The conductivity of 3-D films fabricated from Au MPCs has been reported to arise as a result of core-to-core electron hoping (along the atoms of the ligands), as explained by the following equation:[11]

$$\sigma_{EL} = \sigma_0 \exp[-\beta_d \delta_{edge}] \exp[-E_A/RT] \quad (1)$$

Where,

σ_{EL} = Electronic conductivity of the film (W^{-1} cm^{-1})

σ_0 = pre-exponential constant

δ_{edge} = Core edge-to-edge distance

β_d = Electron tunneling coefficient ($Å^{-1}$)

E_A = Activation energy (kJ mol^{-1})

T = Temperature (K)

Figure 1.13 shows the electron hopping process that occurs through the MPCs. As shown in the figure, the metal cores are separated by SAMs around each metallic nanoparticle core. When a voltage (V) is applied, electron hopping occurs from one metal core to the next metal core. According to the equation (1), nanoparticle core edge-to-edge distance (δ_{edge}) and the electron tunneling coefficient (β_d) exponentially determines the

conductivity of the fils (σ_{EL}). The distance between the cores (d_{edge}) is determined by the thickness of the organic shell or the number of carbons in the SAM alkyl chain (molecular composition and the structure of the SAM). As the distance between the cores increases, electron transfer or tunneling coefficient (β_d) decrease exponentially. Furthermore, the dielectric constant of the monolayer (ε_s) also effects the tunneling coefficient. For instance, aromatic groups have a higher ε_s than alkanechains hence they might have different β_d. Au MPCs with Functionalization also influences tunneling. For example, mercaptohexanol-coated Au MPCs have a different β_d value than hexanethiol-coated Au MPCs due to the different end groups.[11] As shown in equation (1), film conductivity also depends on the activation energy and the temperature. Temperature effect for conductivity is different for continuous and discontinuous metal films. When increasing the temperature, the conductivity increases in discontinuous films like ultrathin films or MPCs with 2-8 nm

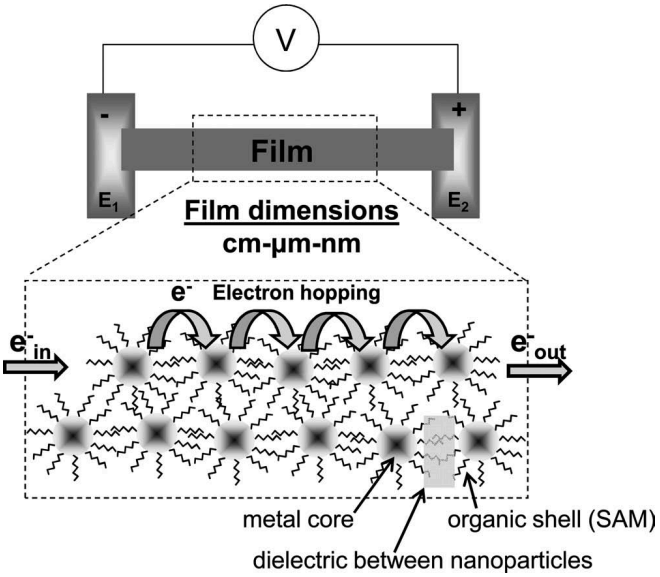

Figure 1.13. Simplified representation of a metal monolayer protected clusters (MPCs) chemiresistive film deposited in-between IDEs. (Copied from Ref. 11)

metal cores while conductivity decreases in continuous metal films.[11] Terrill *et al*., studied both Arrhenius and granular models for temperature effect on conductivity of Au MPCs films and found that film conductivity is dependent on T^{-1} and $T^{-1/2}$.[29] Also, Terrill *et al*.,[29] and Sheng *et al*.,[90] mentioned that the dielectric constant of the surrounding medium and the particle core radius also influence the activation energy. The film conductivity increases by decreasing the activation energy as increasing the dielectric constant of the medium.

Generally, when an analyte interacts with the nanoparticle film, it increases the particle core-to-core distance through film swelling, thus changing the electronic conductivity of the film. Also, dielectric properties of the SAM significantly change the electron tunneling and the activation energy, which leads to a change in the conductivity of the film. At constant temperature for sensing experiments, all these variables will influence the overall film conductivity and it can be difficult to explain the dominant factor for a change.[11]

1.4.3.2. Analyte Partitioning and Chemiresistive Sensor Response

As mentioned earlier, chemical sensors include a target analyte delivery method, a chemically sensitive film coating, and a transducer. As the analyte interacts with the sensing material, the transducer converts this physical or chemical interaction into a measurable electronic signal. Generally, an inert carrier gas (N_2 or Ar) is used to transport the vapor phase analytes to the sensing device. In a chemiresistor, when the vapor phase analytes interact and partition along the sensing material or the film, the resistance changes and this resistance change is directly proportional to the analyte concentration. The following equation explains the relationship between the concentration of the analyte in the sensing film (C_f) and the analyte concentration in the vapor phase (C_v). Both species in

an equilibrium by the partition coefficient K_d and the relationship of analyte concentration in each phase to K_d is shown by the following equation (2),[11]

$$K_d = C_f/C_v \quad (2)$$

Assuming that the sensor response (R_s) is directly proportional to the C_f, where,

$$C_f = K_d\, C_v$$

$$R_s \propto (K_d C_v)$$

$$R_s = f\,(K_d C_v) \quad (3)$$

Where, f is the proportionality constant, and it can be defined as $R_s = f$ when $K_d C_v = 1$

The partition coefficient depends on the relative affinity of vapor phase analyte molecules for the vapor phase versus the sensing film. Generally, polar vapor phase molecules will have a higher affinity for a polar film and vice versa. Sometimes, a very large partition coefficient value may result when there is a specific chemical interaction, such as H bonding, that occurs between the film and the analyte.[83]

1.5 VOLATILE ORGANIC COMPOUNDS (VOCs) AND CHEMIRESISTIVE SENSORS FOR VOCs DETECTION

1.5.1. What are VOCs?

VOCs are a group of organic chemicals containing carbon and hydrogen that can readily vaporize at ambient conditions. VOCs have common properties like low molecular weight, low vapor pressure, and low boiling point, and they comprise a variety of functional groups, such as aromatic rings, aldehydes, ketones, ethers, esters, nitriles, halogenated hydrocarbons, and sulfides.[90] Most VOCs are man-made and are common air pollutants in both indoor and outdoor air. They are formed from burning fuels like gasoline, coal, natural

gas, or wood. VOCs are also found in several consumer products and in solvents used by industries that make cigarettes, dry-cleaning fluids, air fresheners, adhesives, paints and paint thinners, disinfectants and cleaners, glues, and wood preservation chemicals.[91,92] People can be exposed to VOCs at any time. Children, elderly individuals, and asthma patients are at a high risk. Breathing is the most common route of entry of VOCs into the body. Skin contact is another. Many VOCs are toxic, so short- and long-term exposure to them can cause several adverse health problems. Health effects from short-term exposure to harmful VOCs include irritated eyes, dizziness, headaches, respiratory irritations, allergies, memory problems, asthma, and other breathing difficulties. Birth defects, cancers, fatigue, eye irritations, damage to kidneys, liver, and central nervous system are the health effects from long-term exposure to harmful VOCs.[90,91,92]

1.5.2. Regulation of Harmful VOCs

Table 1.3. Several harmful VOCs and their PEL (Permissible Exposure Limits) as annotated by OSHA.[94]

Substance	OSHA PEL as of 1/5/22
Acrolein	0.1 ppm
Benzene	1.0 ppm
Formaldehyde	0.75 ppm
Vinyl chloride	1.0 ppm
Toluene	10 ppm
Xylene (o-, m-, p-isomers)	100 ppm
Tetrachloroethylene	25 ppm
1,3-Butadiene	1.0 ppm

Mainly, the Environmental Protection Agency (EPA) and the Occupational Safety and Health Administration (OSHA) regulate the carcinogenic VOCs such as formaldehyde, acetone, benzene, xylene, toluene, ethylbenzene, and trichloroethylene. To prevent deaths and harmful effects from inhalation of VOCs in the work environment, the Occupational Safety and Health Act of 1970 (OSHAct) was declared by OSHA.[93,94] As shown in Table 1.3, OSHA has released a Permissible Exposure Limit (PEL) for each of these VOCs. A PEL value gives the maximum exposure concentration of each chemical that an employee can be exposed to under OSHA regulations in their working environment.

1.5.3. Detection of VOCs

VOCs are present in very low concentrations, ranging from ppb to the ppm range. So, it is important to detect and track the concentration of these harmful VOCs in both indoor and outdoor air to maintain the air quality. To do so, gas chromatography coupled with a mass spectrometer (GC-MS), or GC with a photoionization detector (GC-PID), or GC with a flame ionization detector (GC-FID) are widely used for VOCs detection.[92,95] Sample preconcentration is generally employed for VOC analyses due to the low sensitivity of these common GC-detector tandems. Highly skillful people are needed to operate these complex analytical instruments. Currently, various transduction methods, such as piezoelectric, colorimetric, fluorescence, and chemiresistors, have been studied as alternative methods for VOCs analysis. Several research groups have contributed significant effort to develop chemiresistors for VOCs sensing with improved selectivity.[11] The fabrication of portable, inexpensive, and selective chemical sensors are of great interest. Along these lines, organic ligand-capped or cross-linked metal nanoparticle-based

chemiresistors exhibit great potential and have attracted significant interest for VOCs detection.[11,96,97] Highly sensitive, metal oxide-based chemiresistors[30-35] are commercially available and operated at high temperature where the analyte is combusted on the sensor surface. In contrast to metal oxide-coated chemiresistors, metal nanoparticle-based chemiresistors are used at room temperature and therefore the chemical and physical properties of target analytes are preserved. As mentioned in section **1.4.3.**, metal nanoparticle based chemiresistors mainly interact with analytes through sorption processes where the swelling of the organic matrix (sensing material) changes the chemiresistor resistance.

The present thesis is mainly focused on chemiresistive sensing applications using chemically modified, pure Au metallic nanoparticles.

1.6. Au MPCs BASED CHEMIRESISTORS FOR VOCs DETECTION

Among metal nanoparticle chemiresistors, Au MPCs-based chemiresistors are widely studied due to the strong chemical and physical properties of the Au metal. It is straightforward to incorporate a wide variety of cross linkers and organic ligands (thiols and amines) possessing different functional groups onto the Au surface to thereby change the Au MPCs surface chemistry which in turn, influences VOCs sensing. Incorporating surface functional groups onto Au MPCs can increase the affinity and selectivity towards different target analytes. Further it may enable differentiation of an analyte from others in a mixture.[11, 97, 98]

1.6.1. Organomercaptans Coated Au MPCs for VOCs Sensing

1.6.1.1. Effect of Functional Groups on VOCs Sensing

Wohltjen and Snow were the first to report Au NPs chemiresistors for sensing VOCs.[67] They synthesized octanethiol-coated 2 nm-sized Au MPCs, which then were drop cast onto IDEs to make the sensor. Chemiresistive sorption behavior was observed using

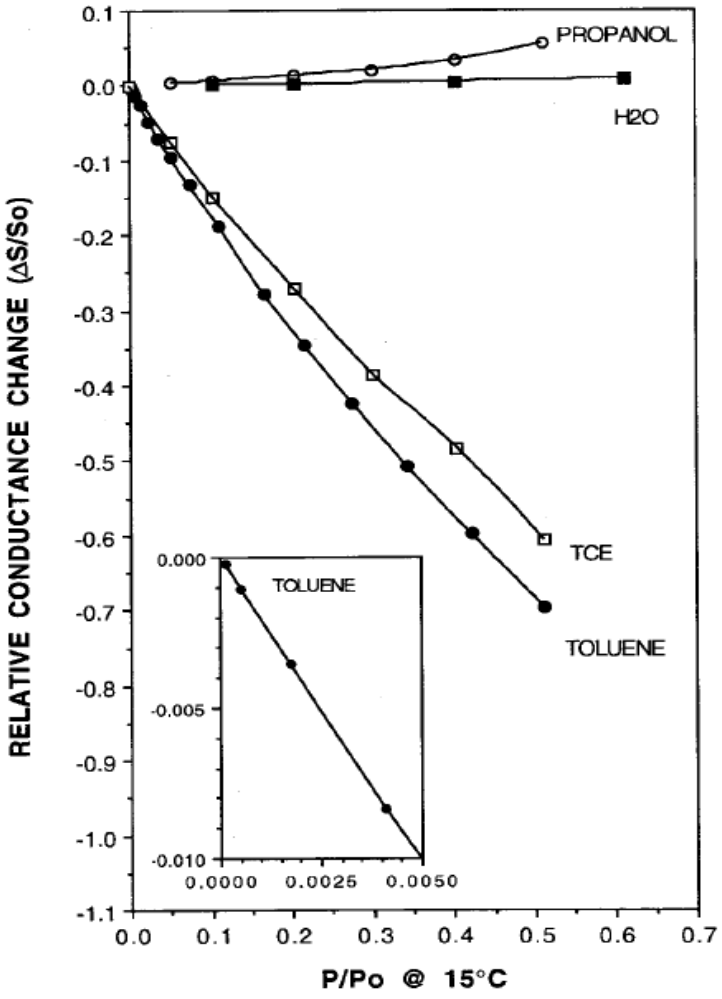

Figure 1.14. Vapor response isotherms of the Au:C8 (1:1) MEMS sensor to toluene, tetrachloroethylene (TCE), 1-propanol, and water based at 15 °C vapor pressures. (Copied from Ref. 67)

several non-polar and polar vapor analytes including toluene, tetrachloroethylene, 2-propanol, and water, representing a hydrocarbon, a chlorocarbon, a hydrogen bonding polar molecule, and a very polar inorganic molecule.[67] Figure 1.14 summarizes the relative conductance change to the different vapor pressures of these four analytes and shows that in the presence of toluene vapor the film conductivity decreases drastically. The sensor is unresponsive at all the water vapor concentrations examined. In contrast to toluene, in

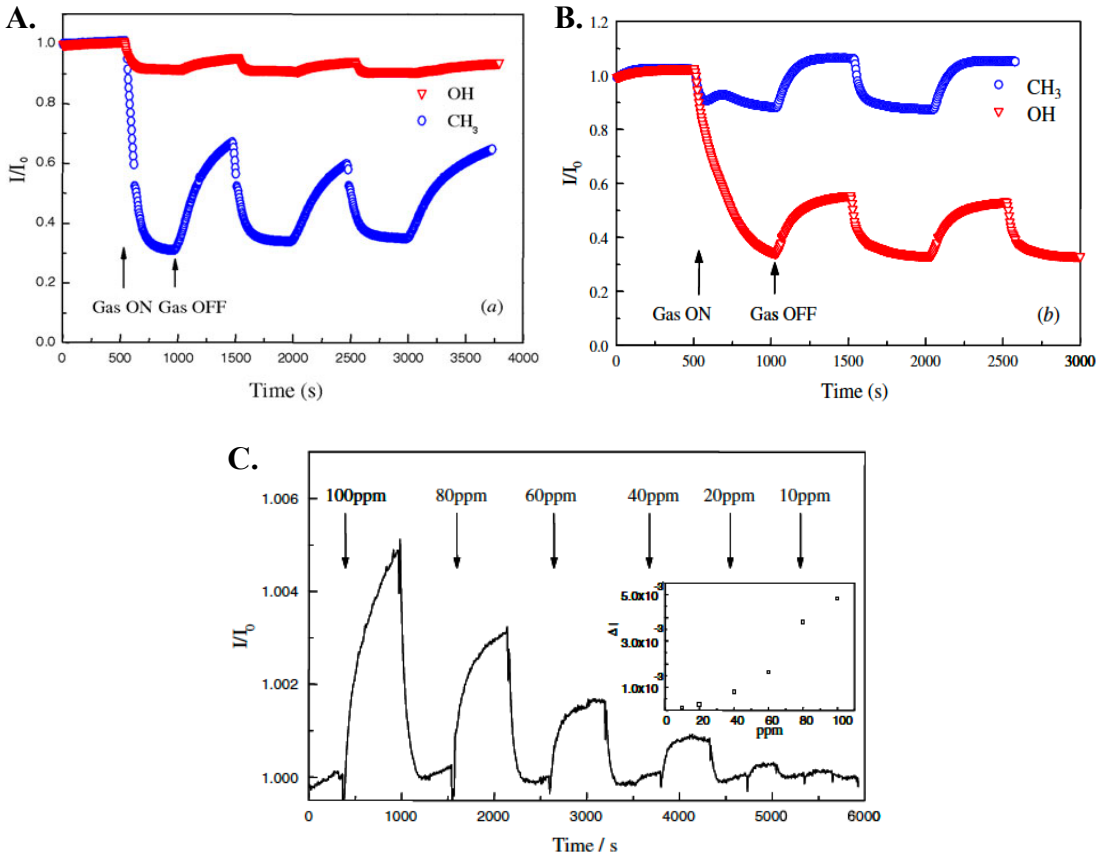

Figure 1.15. Chemiresistive response of HO- and CH_3-functionalized Au MPCs films to **A.** DCM vapor, **B.** methanol vapor, and **C.** sensor response of HO-functionalized Au MPCs film to different concentrations of ethanol vapor. (Copied from Ref. 100)

presence of hydrogen-bonding polar 2-propanol vapors, the film conductivity increases slightly. The investigators believed that electron transport in the film could occurs via the following two mechanisms:[11, 67] (1) electrons tunneling between the metal cores and (2) electron hopping along the atoms of the thiol ligand. Wohltjen and Snow concluded that the toluene vapors dominate the swelling mechanism, where hydrocarbon nonpolar toluene vapors absorb into the nonpolar thiol layer (like dissolves like). The toluene vapor absorption causes to increase the interparticle distance hence perturbs the electron transport and produce a large film response. Furthermore, Wholtjen and Snow suggested to add different chemical functionalities to the organic ligand shell to improve the selectivity and sensitivity for variety of chemical analytes.[67]

In later studies, Murray *et al.,* introduced two synthetic pathways to synthesize poly-hetero-ω-functionalized alkanethiolate-stabilized gold cluster compounds.[98] Evans *et al.,* also synthesized aromatic organothiol-coated Au MPCs as the sensing material for chemiresistive vapor sensing of pentane, hexane, toluene, methanol, ethanol, 2-propanol, acetic acid, and chloroform vapors using the drop cast method. In their study, HS-C_6H_4-X derivatives were prepared where, X = OH, -COOH, -NH_2 and -CH_3.[99] They observed that the X = -CH_3 Au MPCs sensors showed a higher response to non-polar analytes like hexane and pentane than to the other, more polar analytes, which can be expected based on chemical similarities. In contrast, the polar -OH Au MPCs showed a higher response to the polar analytes than to the non-polar analytes. From this data, they concluded that the nature of the X functional group controls the strength of particle-solvent and particle-particle interactions as well as the interaction with different vapor analytes,[99] which set the stage for the design of future functionalized Au MPCs-based sensors. To further study the vapor

sensing ability of functionalized MPCs, the -OH and -CH_3 Au MPCs were selected, as the -COOH and NH_2 functionalized Au MPCs were not stable in solution. The -CH_3 functionalized Au MPCs dissolved well in non-polar solvents and the -OH Au MPCs were soluble in polar solvents. DCM, ethanol, and methanol vapors were selected as analytes for the studies.[100] Figure 1.15 represents the chemiresistive responses to the vapor analytes examined. The polar HO-containing films were more responsive to polar methanol vapor than to DCM, while the CH_3-containing films were more responsive towards the non-polar DCM than to methanol. The authors explained their observations based on equation (1). At low methanol vapor concentrations, film permittivity increases (ε_s) as methanol vapor molecules partition into the Au MPCs film, hence current increases. At higher methanol vapor concentrations, the current decreases as an increase in the edge-to-edge distance (δ_{edge}) occurs, when the swelling process dominates over the permittivity of the film. Figure 1.15. C depicts the response of the HO-containing Au MPCs sensor to concentrations of ethanol vapors from 100 ppm to 10 ppm. When increasing the concentration of ethanol vapor, a conductivity increase was observed similar to the observations in studies conducted by Wohltjen and Snow[67] and Han *et al.*[101] Several research groups have observed increases in current when polar sensors are exposed to high concentrations of ethanol vapors, ascribed to increases the permittivity (dielectric constant) in the medium around Au MPCs.[11,99,101]

Foos *et al.,* synthesized di-, tri-, and tetraethylene oxide-functionalized Au MPCs using the thiol exchange reaction of C_6S-Au MPCs by $CH_3(OCH_2CH_2)_nSH$.[102] and measured the vapor sensing properties of toluene, water and 2-propanaol vapora. They observed a decrease in current in the presence of toluene. This observation was most

prominent for the Au MPCs containing the shorter ethylene oxide chains (n=2). Furthermore, these films displayed a weaker response toluene. Moreover, their observations were like the studies of Wohltjen and Snow about C_8S Au MPCs[67] and Evans *et al*., about aromatic thiol coated Au MPCs.[99] With a low content of oligomer units present, the best response for toluene was observed and the response to non-polar vapors such as toluene decreases as the oligomer units in the Au MPCs increases.[102] However, this observation suggest a discrepancy in polarity between the vapor analyte and the chemiresistive film.

Kim *et al.,* synthesized Au MPCs with mixed monolayers of 1-octanethiol and chlorobenzenemethanethiol as chemiresistive films for vapor sensing of cyclohexane, acetone, and 1-propanol.[25] They observed that the Au MPCs films with a content of 1-octanethiol at 50% were more responsive towards acetone and Au MPCs films with a higher content of 1-octanethiol at 80% were more responsive to the non-polar cyclohexane and 1-propanol. Ahn *et al.,* synthesized thiophene-functionalized Au MPCs from 12-(3-thienyl)-dodecanethiol and then spin coated the particles onto IDEs to prepare a chemiresistor.[79] Ethanol, chloroform, hexane, and toluene vapors were examined as analytes in vapor sensing studies. They observed the response trend as toluene > chloroform > hexane >> ethanol order due to the chemical selectivity of the MPCs film. In summary, the aforementioned studies support the trend that non-polar films are more selective towards to non-polar analytes and the non-polar analytes partition into the nonpolar film more readily than do polar analytes. This behavior leads to an increase in film swelling and increases the chemiresistor response by increasing the film resistance.[11]

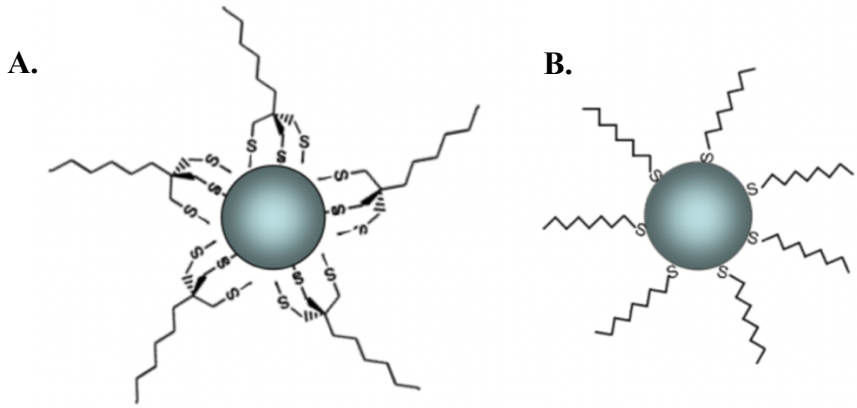

Figure 1.16. Representation of **A.** trithiol and **B.** monothiol-coated Au MPCs synthesized by Garg *et. al*. (Copied from Ref. 103)

Grag and coworkers studied the use of trithiols as a stabilizer for Au MPCs synthesis for chemiresistive sensors to improve the stability and selectivity for several polar and nonpolar VOCs.[103] Figure 1.16. shows the trithiol and monothiol-coated Au MPCs synthesized by Garg *et. al.* They observed that trithiol-coated Au MPCs films have more stability than conventional Au MPCs films since multiple thiol-Au bonds are resistant to oxidation. More importantly, these trithiol-coated Au MPCs chemiresistor show excellent response to the vapors of toluene, ethanol, methanol, acetone, and DCM and these response patterns are alike to those of mono thiol-coated Au MPCs sensors in same chain length.[11,103]

Several research groups have tried to combine the GC retention times of VOCs with their chemiresistive response patterns. Cai *et al.* were the first to report on this topic.[104] They developed a dual-chemiresistor vapor sensing array using 1-octanethiol-coated Au MPCs and phenylethanethiol-coated Au MPCs as interfacial layers on the chemiresistor (Figure 1.17). This array was placed on the top of a GC pre-concentrator to desorb the adsorbents thermally. Their study proves that the VOCs response patterns and the GC retention times together improves the vapor analysis with compared to single systems

alone.[104] Later on several studies have been done using this sensing arrays and GC/MS to improve the VOCs analysis.[105,106]

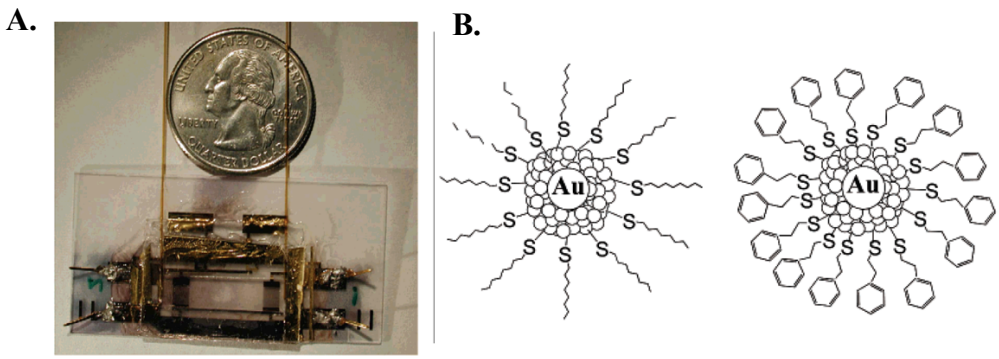

Figure 1. 17. A. Representation of dual chemiresistor array kept in a detector cell and **B.** Nanostructures of 1-octanethiol-coated Au MPCs (left) and phenylethanethiol-coated Au MPCs (right) used as interface layers. Copied from Ref. (104)

1.6.1.2. Effect of Thiol Chain Length on VOCs Analysis

Electronic properties of the Au MPCs film can be modified by changing the monolayer length. Ahn and coworkers synthesized Au MPCs coated with thiophene functionalized alkanethiols having different alkane chain lengths where Th-$(CH_2)_n$-SH (Th=3-thiophene) with n = 2, 6, 12.[79] Hexane, toluene, chloroform, and ethanol were used as the vapor analytes and all the sensors show the response pattern of toluene > chloroform > hexane >> ethanol for all the concentration they used. They described that the solubility properties of the synthesized thiophene-terminated alkanethiols control the sensor response to each analyte. The sensor with a large number of methylene units produced a high resistance (low conductivity) as they facilitate the more vapor absorption having more sites, hence the vapor sensitivity of the thiophene alkanethiols coated Au MPCs films increases

with the number of methylene units in the alkane chain.[79] García-Berríos *et al.*[107] synthesized a series of normal alkanethiols (C4-C11) coated Au MPCs films and studied their chemiresistive sensing ability for several organic vapors including, methanol, ethanol, isopropanol, 1-butanol, n-hexane, n-heptane, n-octane, isooctane, cyclohexane, toluene, and ethyl acetate. They observed that when increasing the alkane chain length of the monolayer, the sensor sensitivity for non-polar and aprotic polar vapors increased proportionally. Furthermore, when they increased the sensor alkane chain length, the sensor sensitivity to polar alcohol vapors decreased as the film resistance decreased due to the increase in film permittivity as mentioned earlier. Moreover, the authors thought that the concentration of the vapors in the film (C_f) would be affected to dielectric (ε_s) of the film and due to the absorbed vapor molecules, the dielectric constant of the film changes. Quartz crystal microbalance (QCM) measurements were performed, and they concluded that vapor analyte sorption or the partitioning only in the organic ligand matrix and this suggested that the sensor resistance response is dominated by the morphological changes in the alkane chain or the inter particle distance changes.[107]

1.6.2. Alkyl Amine-Coated Au MPCs

Briglin and coworkers used dodecylamine-coated Au MPCs as chemiresistive films to detect organic mercaptan vapors.[70] When they used non-thiol vapors, like water, toluene, and acetone, they observed a reversible increase in resistance according to the previously described swelling mechanism. Surprisingly, irreversible current change was displayed when thiol vapors used due to the formation of strong Au-S covalent bonds formed on place exchange reactions between the incoming thiols and the dodecylamine ligands. They observed a rapid increment in the irreversible current for the shorter thiol vapors, such as

H_2S, CH_3SH, and propanethiol. The authors concluded that decrease in core-to-core distance after ligand exchange may cause the current increment. However, in the presence of octanethiol vapor, the irreversible current decreased but the authors were not able to explain the reason for this observation.[11,70]

1.6.3. Formation of Chemically Linked Au NPs Films

Several research groups have utilized the cross-linking precipitation mechanism to form Au MPCs films across the IDEs.[11] Leibowitz *et al.,* introduced the one-step exchange-cross linking-precipitation route to develop NP thin films similar as layer-by-layer construction method.[84] For this study, several thiolate-coated Au NPs and α,ω-alkanedithiol cross-linkers were used. In solution, they simply mixed these two units and precipitated the dithiol-cross-linked Au MPCs as a thin film on the substrate by place exchange-cross linking mechanism. Later, Han *et al*.,[101] followed this method to develop Au NP chemiresistive films for VOCs sensing studies. First, they synthesized 1-decanethiolate-coated Au MPCs. Then 11-mercaptoundecanoic acid (MUA) and 1,9-nonanedithiol (NDT) were utilized as molecular linkers to prepare NDT linked Au NPs and MUA-linked Au NPs with 2 or 5nm core size using place exchanging-cross linking-precipitation route. Here, the cross linking and the precipitation occurs through Au-S bond formation in NDT and hydrogen bonding in MUA – COOH terminal. Following Table 1.4. summarizes the response sensitivity data for the synthesized two different shell linkage sensing films. According to this data, both 5 nm Au MPCs films with NDT and MUA linkers show a higher response sensitivity to toluene than to polar vapors. The response pattern is nearly identical to the previously presented results. The authors demonstrated that the response patterns are dependent on the Au NPs core size and the organic shell

structure.[101]

Table 1.4. Chemiresistor response data for different VOCs vapor sorption at NDT and MUA shell linkage films. Note: Toluene = Tol, Hexane = Hx, Water = Wa. (Copied from Ref. 101)

Shell linkage	Vapor	Responses for different core sizes			
		$Au_{5\ nm}$		$Au_{2\ nm}$	
		$(\Delta R/R_i)/\Delta C$	$\Delta f/\Delta C$	$(\Delta R/R_i)/\Delta C$	Df/DC
MUA	Tol	2.24×10^{-3}	−0.24	8.28×10^{-4}	−0.23
	Hx	4.17×10^{-4}	−0.042	1.87×10^{-4}	−0.030
	MeOH	7.04×10^{-5}	−0.010	b)	–
	Wa	2.96×10^{-5}	−0.014	b)	–
NDT	Tol	2.71×10^{-4}	−0.18	3.14×10^{-4}	−0.24
	Hx	5.23×10^{-5} a)	−0.028	5.49×10^{-5} a)	−0.036
	MeOH	1.89×10^{-5}	–	b)	–
	Wa	1.11×10^{-5}	–	b)	–

b) No entry due to unusual response profiles.

It is important to tune the interparticle properties of nanoparticle arrangements to improve the sensitivity and selectivity towards VOCs sensing. Wang *et al.*,[108] developed a chemiresistive sensing array consist of a non-linked and linked Au MPCs. (non-linker ligands do not have any specific end group while linker ligands consist of an ω functionality) Here, they changed the alkyl chain length to vary the interparticle distance and difunctional linkers ($X\text{-}(CH_2)_n\text{-}X$) like dithiols and dicarboxylate acids (MUA) were used to make the crosslinked films through place exchanging-crosslinking-precipitation route. Using their data, authors concluded that the chemiresistor responses to VOCs

correlate with both linker ligand and non-linker ligand alkyl chain length. Joseph *et al*.,[69] synthesized Au MPCs films by dipping the IDEs into solutions of Au MPCs coated with $C12NH_2$ and alkanedithiols with different chain lengths such as C6, C8, C12, C16. They observed that all amine capping molecules were replaced by dithiols. Furthermore, when increasing the alkane chain length of alkanedithiols, the chemiresistive response increases exponentially for a given concentration of toluene vapor. This study summarized that the nanoparticle film conductivity decreases as the alkane chain length of the linker ligands increases, hence sensor sensitivity increases by increasing the core-to-core distance or the interparticle distance. This finding is in agreement with the observations described by Wang *et al*.[108] Guo *et al*., also used the exchange-crosslinking-precipitation method to crosslink C8S Au MPCs with benzenedimethanethiol and hexanedithiols ligands.[109] Toluene, acetonitrile, ethyl acetate, isopropanol, ethanol, and water vapors were used to study the chemiresistive sensing ability of the synthesized crosslinked films. Here they highlighted that tetraoctylammonium bromide (TOAB) residue coming from the Brust-Schiffrin two-phase synthesis method can influence the sensor resistance change.

Vapor induced swelling mechanism is the widely considered sensing mechanism for VOCs detection using Au MPCs chemiresistive films. Film flexibility plays an important role for vapor sorption and particle swelling in the film. Murray and co-workers have studied Au MPCs broadly and they observed the importance of the NP film flexibility for VOCs sensing when they used metal-ion-carboxylate linked Au MPCs films.[68] Zamborini and co-workers studied the influence of film flexibility for VOCs sensing using dithiol cross-linked C6S Au MPCs. Here they changed the degree of crosslinking, and chemiresistive response for 2-propanol and toluene vapors were measured.[88] Prior to VOCs

sensing, the C6S Au MPCs films were crosslinked by introducing hexanedithiol vapors in different time scales to prepare Au MPC-[S-$(CH_2)_6$-S]-Au MPC linkages in the film. The authors found that the crosslinked chemiresistive sensor response to toluene vapor decreases as the increasing exposure time to dithiol vapors. The longer exposure time to hexanedithiol increases the degree of cross-linking and thereby decreases the film flexibility. These studies demonstrated the importance of Au MPCs film flexibility in VOCs sensing.

Joseph *et al*.,[110] studied the effect of film thickness and the structure for VOCs sensing using dithiol linked Au MPCs. They used layer-by-layer deposition of Au NPs with 1,12-dodecanedithiol to change the film thickness. The authors observed that the sensor response trend to water, toluene, 1-propanol and 4-methyl-2-pentanone changed from lower value to higher value as the film become thicker by increasing the number of deposition cycles. They suggested that the initial decrease in resistance is due to the film swelling and increasing the core-to-core distance. When the number of deposition cycles increases, the distance between the nanoparticle cores decreases and hence enhances the electron conductivity of the film. Thus, they concluded that film thickness and the structure play a vital role in VOCs sensing mechanism. Han *et al.,* also studied the role of film thickness.[26] Both of the studies showed that when the NPs film becomes thicker, the analyte vapors may not be able to penetrate further into the film to increase the film resistance.

Murray and coworkers[68,82] developed a place exchange reaction method to synthesize a mixed monolayer of Au MPCs using two different thiols as a non-linker and linker ligand where linker ligand carries a chemical functionality. Using this place exchange reaction, thiols with different functional groups can be introduced to the Au surface to enhance the

chemiresistive sensor selectivity to interested VOCs analytes. In their study, mixed monolayer coated Au MPCs were synthesized using alkanethiolates and carboxylic acid functionalized alkanethiolates. These MPCs were linked together by a network of carboxylate-M^{n+}-carboxylate bridges in the film. Solutions of Cu^{2+}, Zn^{2+}, Ag^{+} and methyl viologen were used to introduce M^{n+}.[68,82] These Au MPCs films linked by carboxylate-M^{n+}-carboxylate bridges were used for chemiresistive vapor sensing studies. The vapor sensing ability of these films will be discussed further in Chapter 3.

1.7. THESIS PROJECT MOTIVATION

Development of real time, portable gas sensors with high sensitivity and selectivity for detection of harmful VOCs at trace levels is a burgeoning research area. Many harmful VOCs are present in very low concentrations at the ppm to ppb range. So, detection of trace level VOCs using traditional analytical methods is challenging, especially since they are often mixed with other interfering gases. As mentioned earlier, the use of GC/MS based techniques has several disadvantages including the difficulty in using this method for on-site environmental air quality monitoring. Metal oxide-based gas sensors are widely studied and developed for VOCs sensing as they offer several advantages, like simple instrumentation, low cost, rapid response, and low recovery time. However, these metal oxide sensors suffer from several disadvantages, such as high-power consumption, poor selectivity, and low sensitivity. So, it is important and challenging to develop VOCs sensors that address the above-mentioned requirements including high sensitivity and selectivity.

Au NPs-based chemiresistors developed using MEMS technology are of great interest for VOCs sensing. IDEs sensor arrays can be designed and made with MEMS

technology and mass production of these sensor chips is very economical. Moreover, the surface chemistry of the Au NPs can be easily tuned by adding different functional groups to the thiolate ligands. We hypothesize this approach will help to achieve selectivity for analysis of VOCs of interest. Also, the shell formed by the organothiolate ligands around the Au NPs helps to precipitate, redissolve, and preserve these NPs without complications arising from aggregation.

Herein, we propose, prepare, and test three different classes of novel surface-functionalized Au MPCs chemiresistors for the selective detection of trace levels of (1) carbonyl compounds, (2) aromatic hydrocarbons, such as BTEX, and (3) TCE in air.

CHAPTER 2

INCORPORATION OF A UREA BINDING MOTIF ON GOLD NANOPARTICLE-BASED CHEMIRESISTORS TO SENSE CARBONYL VOCs[a]

---

a The research presented in this chapter has been published in *Sensors* **2020**, *20*, 7024 and *RSC Adv*. **2018**, *8*, 35618.

2.1. INTRODUCTION

Acetone is considered a hazardous vapor by the EPA and OSHA. Its airborne PEL is 1000 ppm.[1] Acetone is widely utilized in industry as a solvent to prepare rubber cements, waxes, resins, lacquers, leather, artificial silk, and some plastics. Also, it is used to synthesize some other chemicals such as ketene, methyl methacrylate, methyl isobutyl ketone, diacetone alcohol, acetic anhydride, chloroform, isophorone, vitamin C, and iodoform. Acetone can be also found in nail-polish remover, paint, varnish removers, fishing rod, drawing inks, and shoe cements.[1,2] Acetone can threaten human health as it can enter the respiratory system by inhalation or absorption through the skin. Prolonged exposure to acetone can cause irritation to the skin, eyes, nose, and throat as well as headaches, dizziness, kidney, and liver failures, vomiting and in some cases death.[2] Moreover, acetone in breath also has been recognized as a specific biomarker for diabetes.[3] For these reasons, methods for acetone detection and accurate quantification at trace levels are continually being developed.

Currently, gas chromatography-based techniques, ion mobility spectrometry, and selected ion flow tube mass spectrometry are widely used for acetone detection.[1,4,5] But these techniques still have several drawbacks, such as low sensitivity, the need for sample preconcentration, low selectivity, and high associated instrumentation costs. Therefore, there is a need to develop highly sensitive, selective, low power, portable, and real-time gas sensor devices to detect acetone at low concentrations, such as in the ppm to ppb range.

2.1.1. Chemiresistors for Acetone Detection

Several research groups have explored developing inexpensive and selective chemiresistive gas sensors for acetone detection. Metal oxide semiconductor based

chemiresistors, such as WO_3, Fe_2O_3, ZnO, Co_2O_3, In_2O_3, NiO, SnO_2, are of great interest as efficient acetone sensors.[6,7,8,9,10,11,12] Among them, Wang and coworkers demonstrated in 2006 that the ferroelectric WO_3 NPs chemiresistor selectively detects acetone in breath-simulated media.[7] By using this nanosensor, they obtained a < 0.8 ppm acetone sensitivity for a healthy human breath sample and > 1.8 ppm sensitivity for a diabetic patient. Importantly, they observed the same sensitivity after repetition of acetone flow cycles, which indicates good stability of the chemiresistor. In selectivity studies, they used a panel of common VOCs present in human breath including NH_3, methanol, NO, CO_2, ethanol, NO_2, and CO. Wang *et al*. observed good selectivity for acetone detection at 400 °C. Later, Jia *et al*. developed WO_3 nanorods with (100) and (002) facets and they found that hexagonal WO_3 samples with (002) facets show better selectivity and sensitivity with a low response time than those with (100) facets.[8] The WO_3 microspheres with (002) facets showed a 0.25 ppm detection limit for acetone vapors. Additionally, this sensor was operated at 230 °C and showed a 3.53 response to 1 ppm acetone within a 9 s response time. Jia and co-workers were able to obtain a fast recovery time of 14 s using a chemiresistor fabricated from WO_3 microspheres with (002) facets. The authors believe that the hexagonal WO_3 has a large dipole moment on (002) facets, hence acetone is easily absorbed and strongly interacts with the (002) facets. Due to the excellent acetone sensing properties of WO_3 semiconductors, other WO_3 based chemiresistors were widely studied to further enhance the detection sensitivity and to decrease the operating temperature.[9] Spinal type zinc ferrite ($ZnFe_2O_4$) nanostructures are conductive and also have been studied as sensing materials for chemiresistors. Pure $ZnFe_2O_4$ nanostructures have a poor sensing capabilities and metal nanoparticles have been used to improve its sensing capabilities

towards VOCs detection. Nemufulwi *et al.,* developed a Au-modified $ZnFe_2O_4$ nanostructure chemiresistor and studied the effects of $ZnFe_2O_4$ surface modifications for acetone detection.[13] Their comparative gas sensing studies between the Au modified and pure $ZnFe_2O_4$ displayed that Au modified $ZnFe_2O_4$ nanosensor showed a high selectivity with a low detection limit of 2.5 ppm and high response towards acetone vapors at 120 °C operating temperature than the pure $ZnFe_2O_4$ nanosensor. However, the Au modified $ZnFe_2O_4$ sensor exhibits a higher response time (13 s) and recovery time (69 s) than the pure $ZnFe_2O_4$ based sensor which shows a recovery time of 3 s and response time of 15 s. For both type of sensors, they obtained a longer recovery time than the response times. The Au modified $ZnFe_2O_4$ sensor selectivity towards acetone was compared using ethanol, methanol, propanol, CO_2, and methane at 40 ppm vapor concentration. Acetone exhibited the highest response of 25 than the other vapors. Nemufulwi and co-workers were able to improve the acetone sensing behavior of $ZnFe_2O_4$ based sensors by modifying its surface with Au NPs. The authors concluded that highly distributed pores in Au modified $ZnFe_2O_4$ can enhance the gas diffusion and high concentration of defects in Au modified $ZnFe_2O_4$ structure will promote oxygen chemisorption, and all together will improve the acetone detection ability.

Graphene based additives has been added to metal oxide chemiresistors to enhance the acetone sensing ability to the metal oxide used by itself. Several researchers found that the use of graphene as an additive to metal oxide chemiresistors is an effective way to amplify the chemiresistor ability to detect aceone.[9,10,11,14] For instance, Choi and coworkers developed WO_3 hemitube nanostructures functionalized by either graphene oxide (GO) or graphite (GR) layers for acetone sensing in exhaled human breath.[9] Among those sensors,

0.1 wt% GR functionalized WO_3 hemitube nanosensor demonstrated a higher response (6.45 fold for 5 ppm acetone) with compared to pure WO_3 hemitube sensor at 300 °C operating temperature. Furthermore, 0.1 % GR-WO_3 exhibited fast response (< 15 s) and recovery time (< 30 s) towards acetone. By this study, authors showed that the morphological changes in the WO_3 hemitubes functionalized by thin GR and GO can provide a larger number of surface reaction sites for incoming acetone vapors hence electron density across the chemiresistive film can be modulate.[9] Wang *et al.,* showed that modification of CuO-ZnO material with reduced graphene oxide (rGO) sheets could enhance the acetone sensing ability.[10] The synthesized CuO-ZnO/rGO-based sensor exhibits the highest sensitivity at 10 ppm acetone, which is 1.5 times higher than the CuO-ZnO composite and 2.0 times higher than the ZnO/rGO composite at a 340 °C operating temperature.[10] Large sized reduced graphene sheets were used in all these studies and as they wrapped around the metal oxide composite, most of the active sites on metal oxides could be decreased. Later, Pt NPs with small sized reduced graphene oxide nanosheets coupled with hexagonal WO_3 were studied by Chen *et al*., to develop a portable chemiresistive acetone gas sensors. In these studies, effective catalytic properties of transition metal NPs and large surface area of graphene nanosheets were utilized.[15] However, the operating temperatures, sensitivity, response, and recovery time of these synthesized sensors have yet to be improved to achieve the requirements of a proper acetone gas sensor.

Carbon nanotubes (CNT) have been also studied for acetone sensing at room temperature.[12,16,17,18,19] Young *et al.,* modified the surface of the CNTs networked films using Au nanoparticles to enhance the acetone sensitivity.[16] Au modified CNT sensor

displayed a higher sensitivity for acetone with 2-fold increment than the CNTs itself. The CNT/Au – based sensor shows the lowest detection limit of 50 ppm for acetone at room temperature. Authors believed that the Au nanoclusters do not contribute for acetone selectivity, but it does enhance the sensor selectivity. However, this acetone sensor exhibits a lower sensitivity than the previously described acetone sensors. Also, Hwang *et al.*, fabricated a chemiresistor with oxidized single-walled carbon nanotubes functionalized with titanium dioxide (SWCNT@TiO_2) for detection of acetone in dry breath samples.[17] They designed a dehumidifier to dehydrate breath samples before analysis. Furthermore, Luo *et al*., developed an Au nanoparticle-structured thin films of chemiresistor sensor array for acetone sensing in breath samples. Several thiol functionalized nanoparticles (decanethiol, 11-mercaptoundecanoic acid, 1,4-butanedithiol, 1,5-pentanedithiol, 1,3-propanedithiol) were used in their study to introduce different chemical and physical properties including hydrogen bonding ability, hydrophobicity, chain length or structural differences.[20] In addition to the discussed studies, polymer based chemiresistors,[21] nanofiber chemiresistors,[22] nanowires,[23] optical, mixed potential and mass sensitive devices have been developed and studied for acetone sensing.[6,12,24]

2.1.2. Harnessing the H-bonding Ability of Urea Moieties to Develop an Au MPCs-Based Chemiresistor for Sensing Acetone

To overcome the common challenges of selectivity and sensitivity in gas sensors, molecular level control of functional motifs is necessary.[25] For instance, highly selective and unusual stability of gas absorption was achieved by using microporous H-bonded entities in supramolecular structures.[26,27] So, it is proved that H-bonds play a vital role in controlling the existence and stability of molecular assemblies.[28] Furthermore, thiourea or

urea moieties or their derivatives are considered as a well-known, prominent binding site for several analytes, and widely utilized in molecular recognition field due to their strong H-bonding formation ability.[29,30,31] Figure 2.1 demonstrates the intramolecular (**A**) and intermolecular (**B**) H-bonding formation of urea moieties.[31]

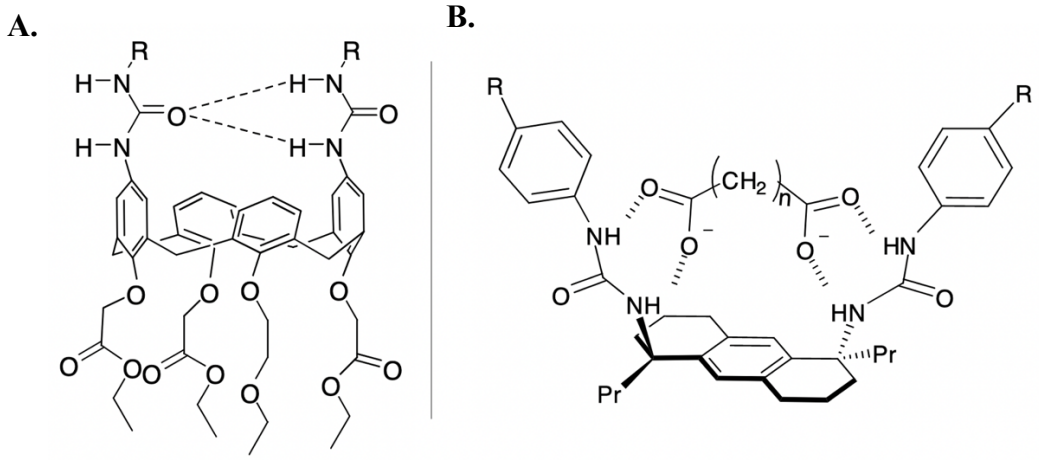

Figure 2.1. Illustration of **A.** intramolecular and **B.** intermolecular H-bonding of urea moieties. (Copied from Ref. 31 b).

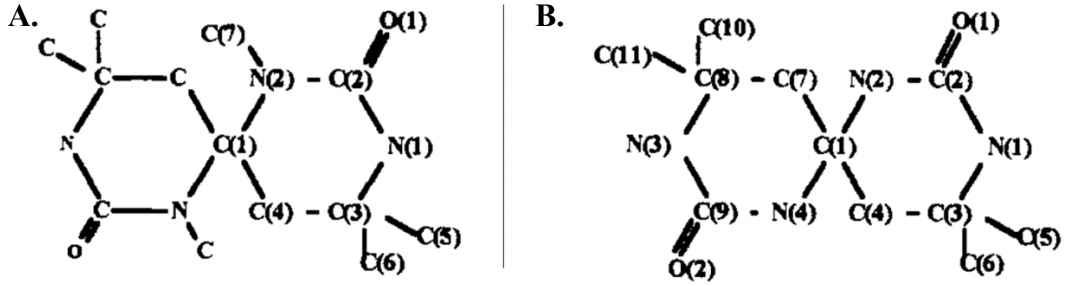

Figure 2.2. Structures of **A.** ACMU adduct (acetone and 1-methylurea) and **B.** ACURD adduct (acetone and urea). (Copied from Ref. 28)

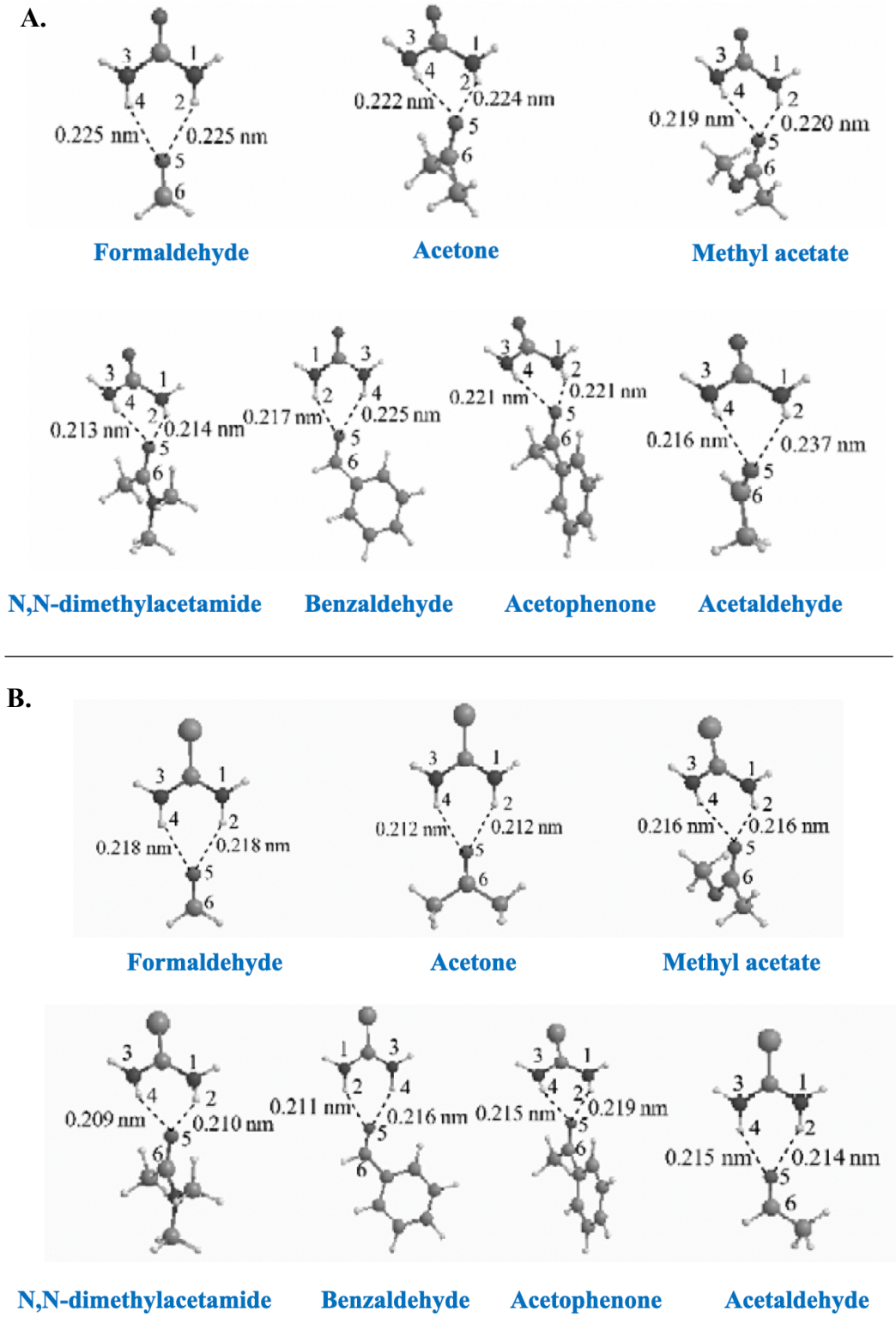

Figure 2.3. Computationally optimized hydrogen bonding molecular complexes of **A.** urea and **B.** thiourea with different carbonyl compounds. (Copied from Ref. 32)

In 1994, Kaftory *et al.,* studied the importance of H-bonding between acetone and urea derivatives to determine their crystal structures.[28] The following adducts (Figure 2.2) were synthesized by reacting three acetone molecules and two urea or 1-methylurea molecules in the presence of DMSO or water as the solvent. The different hydrogen bonding patterns of these adducts were analyzed using crystallographic techniques. The authors concluded that all the NH groups and the carbonyl oxygen atoms are engaged in H-bonding.

In addition to this work, Zheng *et al*., demonstrated the degree of H-bonding formation between urea or thiourea and different carbonyl compounds computationally.[32] The substituent effect for H-bonding ability was also investigated by adding several electron donating and withdrawing groups on urea (thiourea) and carbonyl compounds (Figure 2.3). As shown in the figure 2.3, thiourea exhibits stronger H-bonding interaction than for urea. Among all the complexes, H-bonding interaction between the thiourea and *N,N*-dimethylacetamide is strongest due to the shortest bond length values. The authors concluded that H-bonding formation can be facilitated by adding electron donating groups on carbonyl compounds and electron withdrawing groups on urea (thiourea) compounds.[32]

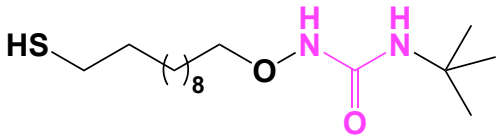

Figure 2.4. Synthesized thiol ligand with urea motif and *tert*-butyl end group (urea motif is highlighted in pink).

The Xio-An Fu research group (Department of Chemical Engineering, University of Louisville) in collaboration with our group started to harness the H-bonding formation ability of urea moieties to develop a Au MPCs based chemiresistive gas sensor to detect trace levels of acetone with high sensitivity and selectivity.[33] Initially, they developed a urea motif that contained a *tert*-butyl end group on one end and a long-chain thiol group at the other (Figure 2.4). Using this thiol urea, they prepared a Au MPCs chemiresistor[33] and they demonstrated a significant increase in acetone sensing relative to several commercially available, non urea-containing thiol functionalized Au MPCs chemiresistive sensors. Figure 2.5 shows their proposed acetone sensing mechanism between the urea functionality and the acetone vapors on the surface of the Au MPCs. The urea motifs in the capping thiol ligands can form hydrogen bonds between the adjacent ligands on the surfaces of the Au NPs as well as with the incoming acetone gas molecules. However, it is reasonable to believe that the *tert*-butyl group of the urea functionality weakens the hydrogen bonding formation capability between adjacent urea functionalities. As a result, binding with an incoming acetone molecule can readily interrupt the intermolecular H-bonding between adjacent chains and accommodating more acetone gas molecules occurs as the acetone concentration increases. This urea-functionalized chemiresistive sensor showed a good selectivity and high sensitivity (10 ppb to 10 ppm) for acetone in reproducible and reversible way at ambient temperature. For example, the sensor was insensitive to water and ethanol due to the weak interactions with the urea motif and having strong intermolecular interactions with other water or ethanol molecules. They also observed a higher response of this sensor to benzene and ethyl benzene than to water and ethanol, presumably because of the hydrophobic molecules embed within the hydrophobic

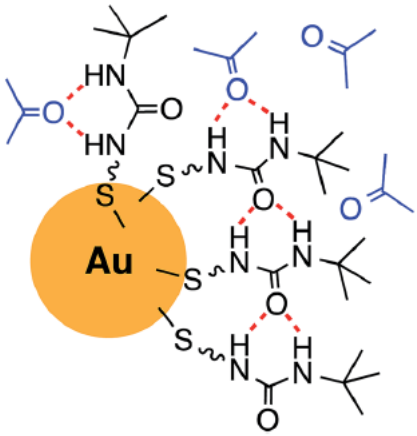

Figure 2.5. Graphical representation of hydrogen bonding between the urea motif on Au MPCs surface and incoming acetone molecules. (Copied from Ref. 33)

chain matrix of the sensor due to the lack of any significant intermolecular interactions at the surface. More importantly, the new urea-based sensor worked under high humidity conditions at ambient temperature and showed a linear relationship between the chemiresistor response and the logarithm of analyte concentration. Also, this sensor showed a low detection limit (LoD 1 ppb) to acetone, among the lowest LoDs for acetone chemiresistors reported so far. The authors concluded that the H-bonding formation between urea and carbonyl functionality may serve as a powerful means for enhancing the sensitivity for acetone detection as well as for other carbonyl VOCs.[33]

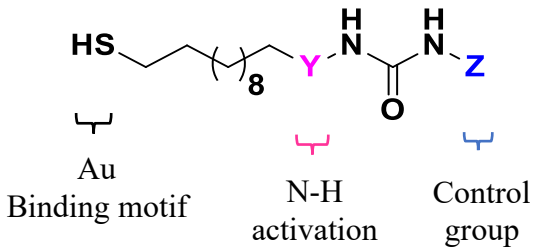

Figure 2.6. Thiol urea ligand structure (Y = O or -CH_2- Z= R or OR).

Given that the influence of the thiol molecular structure at the Au MPCs surface on carbonyl VOC sensing had not been thoroughly studied and understood, we aimed to study the influence of electronic and steric effects by preparing a series of similarly substituted thiol-urea compounds and testing Au MPCs-based chemiresistors derived from these ligands. In this study, we changed the initial thiol urea ligand structure (Figure 2.6) by incorporating different structural elements to the indicated Y and Z positions to change the degree of H-bonding between the adjacent urea motifs to possibly influence interactions with carbonyl VOCs. Here, we assumed that NH acidity of the urea binding motif could be varied by changing the Y position as well as by varying the steric bulk of the terminal group Z, and those changes may lead to high functional group selectivity and sensitivity for carbonyl groups.

Table 2.1 Panel of thiol-urea ligands synthesized for comparison.

Series I Alkoxy	Series II Dialkyl or Alkylaryl	Series III Dialkoxy
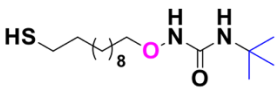	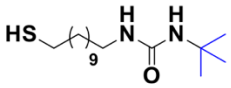	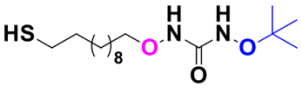
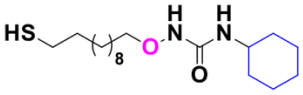	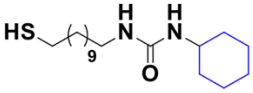	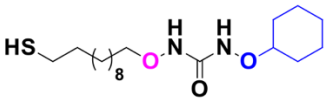
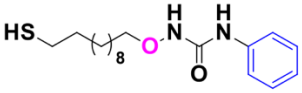	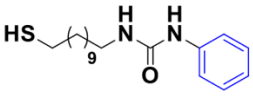	N/A
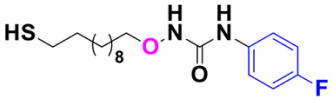	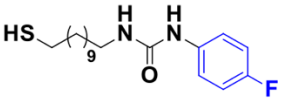	N/A

For our study, we synthesized a panel of substituted thiol-urea compounds with different peripheral end groups to develop different Au MPCs chemiresistors (Table 2.1). Our approach used highly flexible synthetic routes to introduce variability to the urea groups.[34] Selection of synthetic routes to these thiol ureas was influenced by previously reported molecular recognition studies.[35] This Chapter details the syntheses of the thiol urea compounds, the fabrication of the derived Au MPCs chemiresistors, and the resultant sensor response data for acetone sensing. The response data is also included as a section in Dr. Zhenzhen Xie's Ph.D. dissertation.[34, 36]

2.2. RESULTS AND DISCUSSION

The thiol-urea compounds were initially prepared by Dr. M. V. R. Raju (former post-doc, Nantz Research Group, Department of Chemistry, University of Louisville) and later resynthesized by me for additional studies. The thiol-urea functionalized Au MPCs synthesis and VOCs sensing studies were done by Dr. Zhenzhen Xie (Fu Research Group, J. B. Speed School of Engineering, University of Louisville).

2.2.1. Thiol Ligand Synthesis

Three series of thiol-urea ligands (Table 2.1) were synthesized according to the schemes 2.1-2.3, which are similar to the reported synthesis of 1-(*tert*-butyl)-3-((11-mercaptoundecyl)oxy)urea of our previous study.[33] All the synthetic procedures were discussed in chapter 5.3 with the scales and their shelf-stability and the synthesized compounds were characterized by ^{1}H and ^{13}C NMR spectroscopy (see Appendices A). Hybrid linear ion trap (LIT) FT-ICR mass spectrometer was used to obtain the exact masses of synthesized compounds.

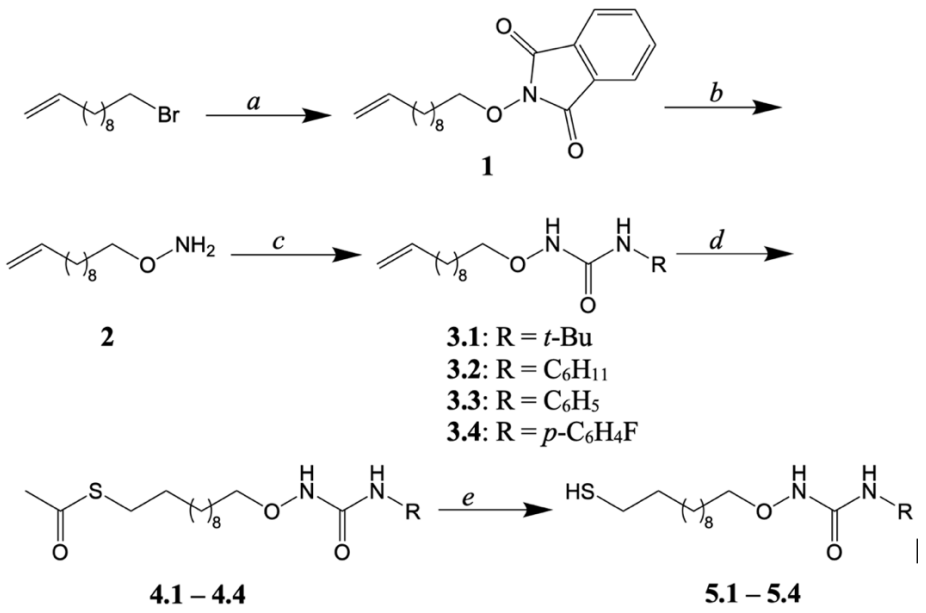

Scheme 2.1. Synthetic route for synthesis of monoalkoxyurea thiols (Series I) Reagents and conditions: *a.* NHP, $NaHCO_3$, DMF, 80 °C; b. H_2NNH_2, CH_2Cl_2, 0 °C to rt; c. R-NCO, Et_3N, CH_2Cl_2, 0 °C to rt; d. $CH_3C(O)SH$, cat. AIBN, THF, reflux; e. HCl, EtOH, reflux. NHP = *N*-hydroxyphthalimide, AIBN = azoisobutyronitrile.

As shown in schemes 2.1 and 2.2, *N*-hydroxyphthalimide or potassium hydrogen phthalate was used respectively to introduce the amine functionality to the hydrocarbon alkane chain. In the next step, hydrazinolysis of phthalimide group was carried out using hydrazine to reveal the aminooxy (Scheme 2.1) or amine (Scheme 2.2) group. The required urea moiety was introduced by reacting the aminooxy or amine intermediate with the interested isocyanate reagent. AIBN initialized catalytic reaction was used to add the thioester group to the terminal alkene followed by acidic thioester cleavage to synthesize the Series I and Series II thiol-urea ligands.

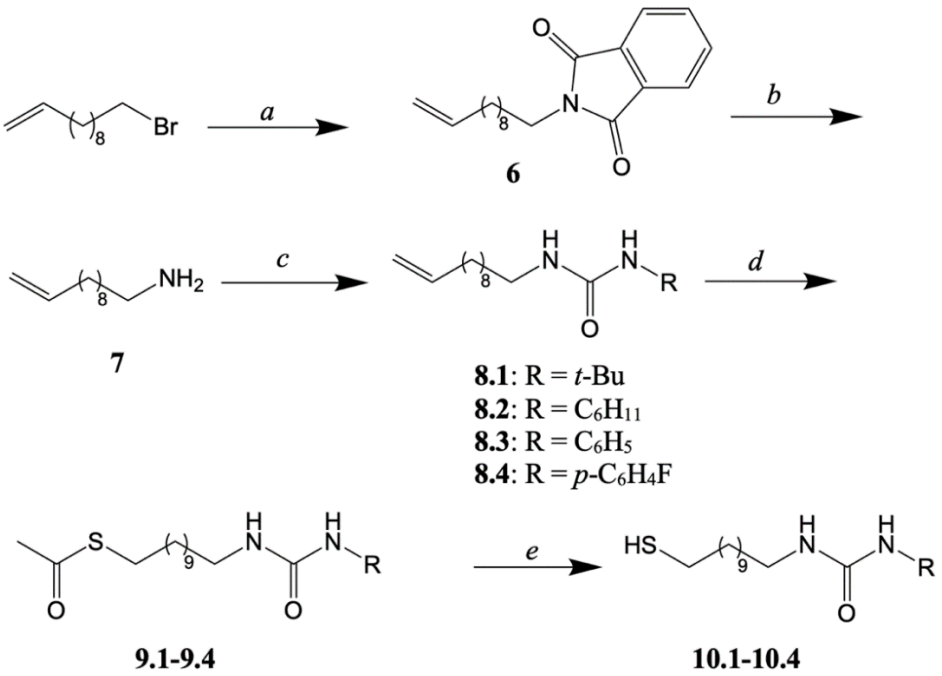

Scheme 2.2. Synthetic route for synthesis of dialkylurea or *N*-alkyl-*N′*-arylurea thiols (Series II). Reagents and conditions: *a.* KHP, DMF, 80 °C; b. H_2NNH_2, CH_2Cl_2, 0 °C to rt; c. R-NCO, Et_3N, CH_2Cl_2, 0 °C to rt; d. $CH_3C(O)SH$, cat. AIBN, THF, reflux; e. HCl, EtOH, reflux. KHP = Potassium hydrogen phthalate, AIBN = azoisobutyronitrile.

In the Series III, oxycarbamate was initially synthesized by using 4-nitrophenyl chloroformate. The formed oxycarbamate was reacted with the aminooxy intermediate synthesized in Series I, to introduce the dialkoxy property to the ligand. Figure 2.7 shows the NMR spectra of *tert*-butyl substituted urea thiols in all the series and the NMR spectra of other urea thiols were attached in the Appendix A. Disappearance of the methyl protons in thioacetate (singlet peak at ~ 2.3 ppm) and appearance of upfielded methylene protons next to S atom (~ 2.85 ppm to ~ 2.52 ppm) in each ^{1}H NMR spectra support a thioester cleavage and thiol-urea ligand formation for all the thiol-urea ligands in Table 2.1.

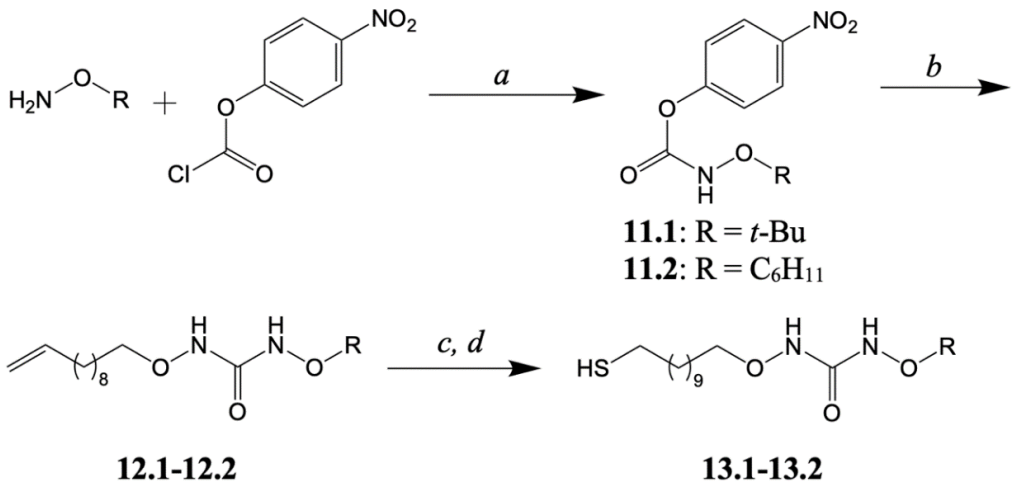

Scheme 2.3. Synthetic route for synthesis of bisalkoxyurea thiols (Series III). Reagents and conditions: *a.* Pyridine, CH_2Cl_2 reflux; *b*. $H_2C{=}CH(CH_2)_9ONH_2$, Et_3N, CH_2Cl_2, 0 °C to rt; c. $CH_3C(O)SH$, cat. AIBN, THF, reflux; e. HCl, EtOH, reflux. AIBN = azoisobutyronitrile.

2.2.2. Thiol-Urea Functionalized Au MPCs Synthesis

The synthesized thiol-urea compounds shown in Table 1 (Series I to Series III) were used to prepare urea-functionalized Au MPCs chemiresistors for sensing studies. The resistance changes of each sensor decreased in the presence of each analyte with compared to resistance change in the presence of synthetic air. Thus, the following equation was used to define the sensor response to acetone in synthetic air,[37]

$$\text{Response} = (R_o - R_{gas}) / R_{gas} \qquad (1)$$

where, R_o and R_{gas} are the resistance of the sensor in the presence of synthetic air and the analyte gas, respectively. First, we studied the effect of different peripheral group functionality on the urea motif of each thiol for acetone sensing in all three series.

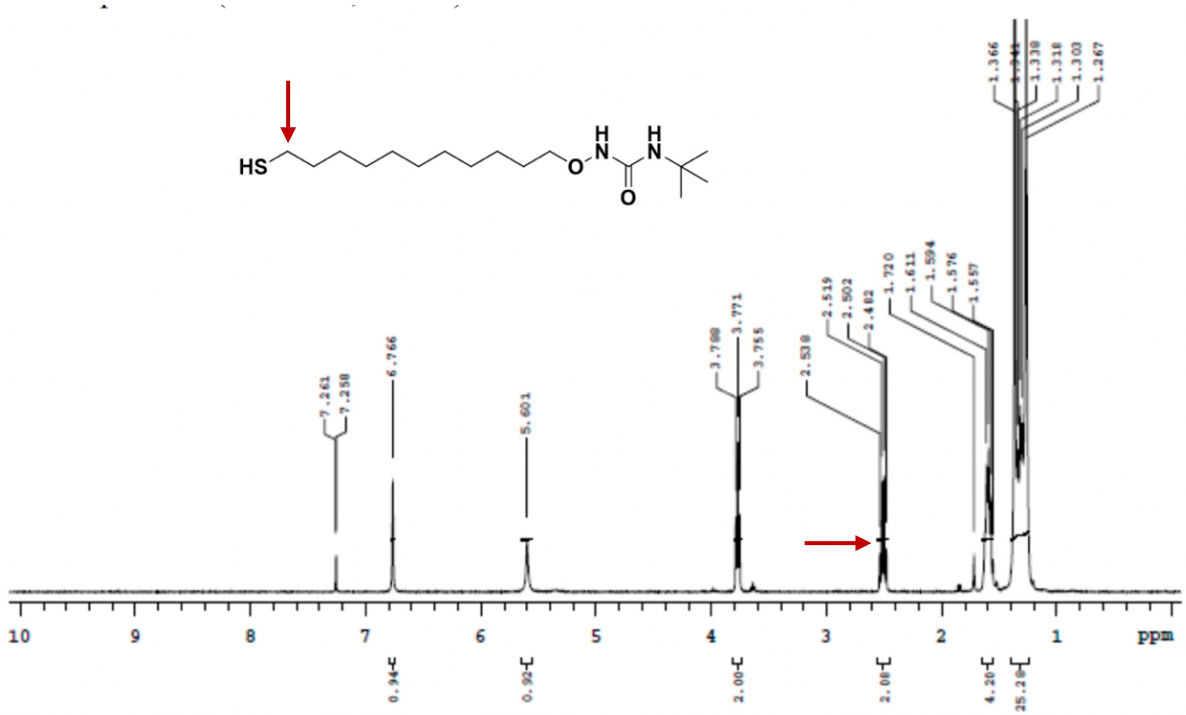
HS
O
H
N
H
N
O
7.261
7.250
6.766
5.601
3.788
3.771
3.755
2.538
2.519
2.502
2.482
1.720
1.611
1.594
1.576
1.557
1.366
1.338
1.318
1.303
1.267
10
9
8
7
6
5
4
3
2
1
ppm
0.94
0.92
2.00
2.08
4.20
25.28

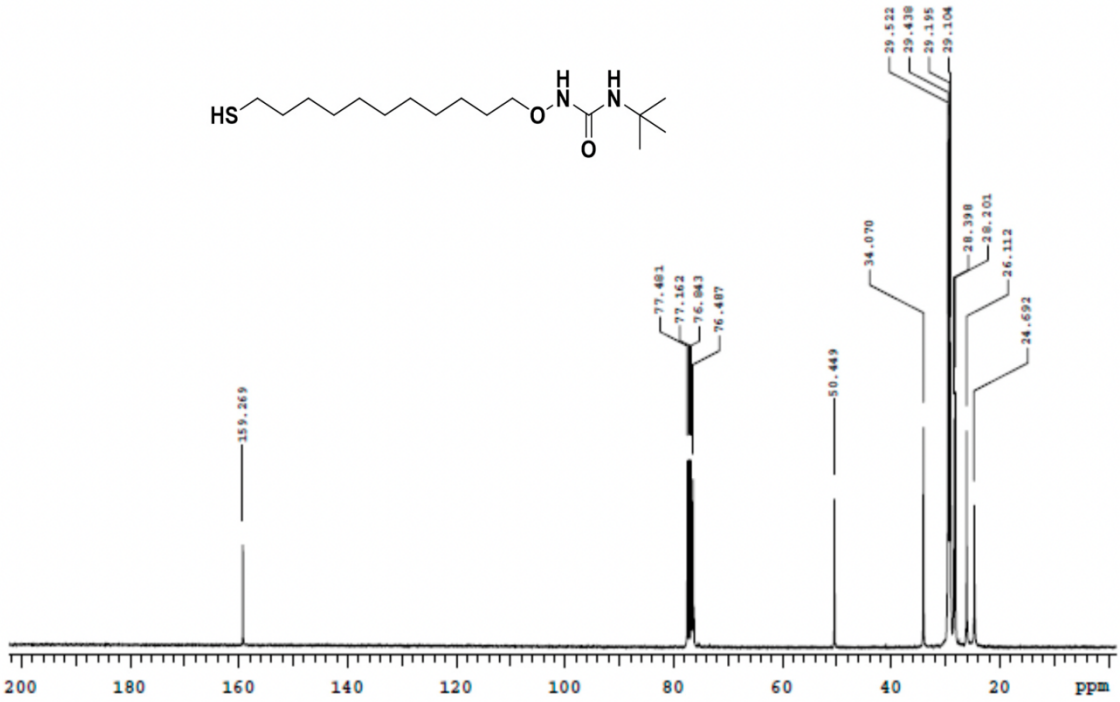
HS
O
H
N
H
N
O
159.269
77.481
77.162
76.843
76.487
50.449
34.070
29.522
29.438
29.195
29.104
28.398
28.201
26.112
24.692
200
180
160
140
120
100
80
60
40
20
ppm

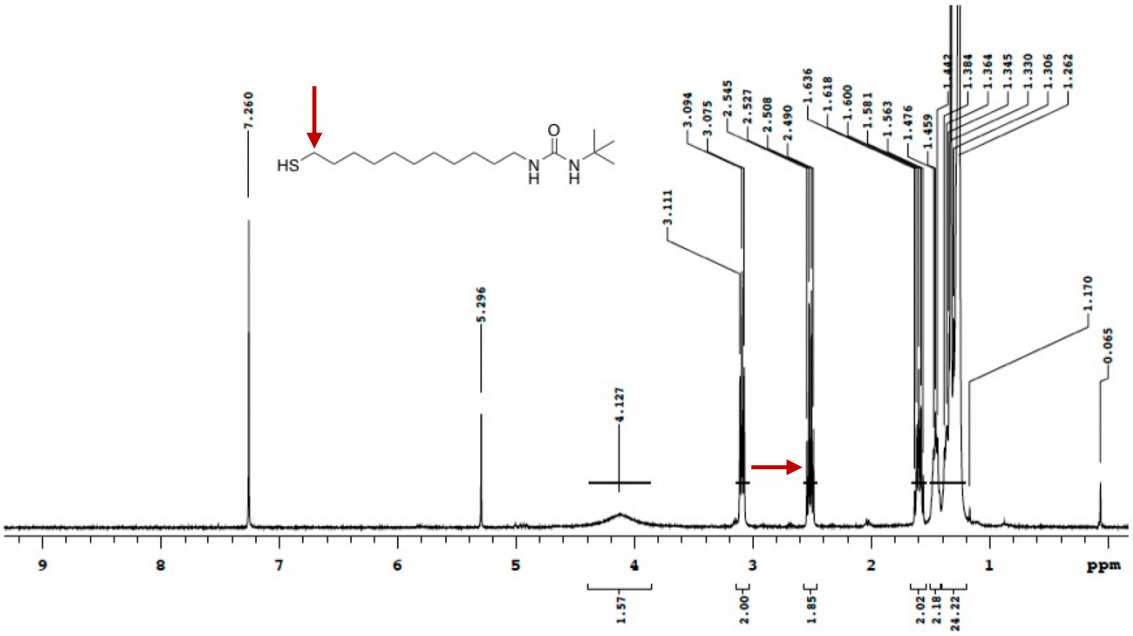
HS
O
N
H
N
H
7.260
5.296
4.127
3.111
3.094
3.075
2.545
2.527
2.508
2.490
1.636
1.618
1.600
1.581
1.563
1.476
1.459
1.442
1.384
1.364
1.345
1.330
1.306
1.262
1.170
0.065
9
8
7
6
5
4
3
2
1
ppm
1.57
2.00
1.85
2.02
2.18
24.22

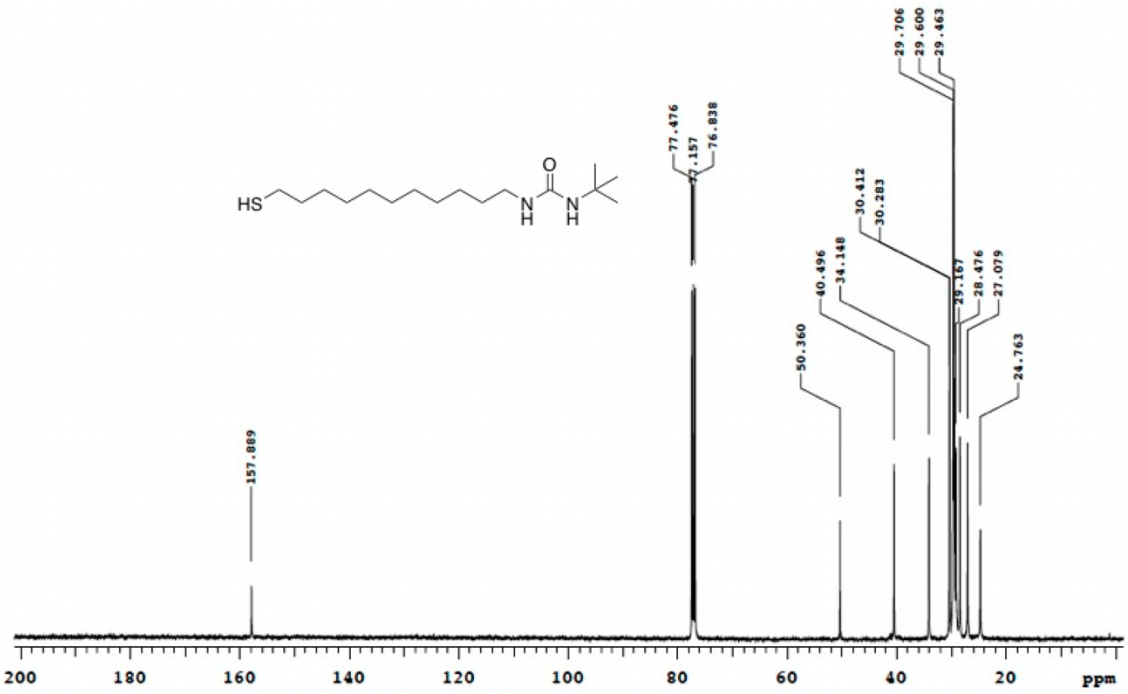
HS
O
N
H
N
H
157.889
77.476
77.157
76.838
50.360
40.496
34.148
30.412
30.283
29.706
29.600
29.463
29.167
28.476
27.079
24.763
200
180
160
140
120
100
80
60
40
20
ppm

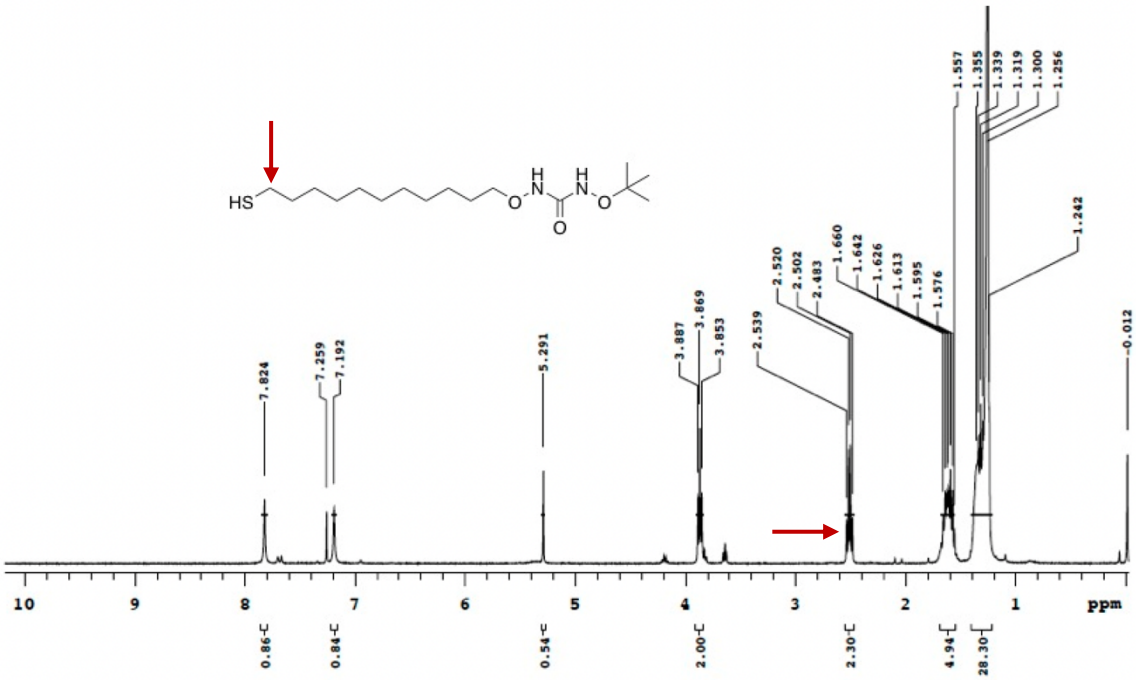

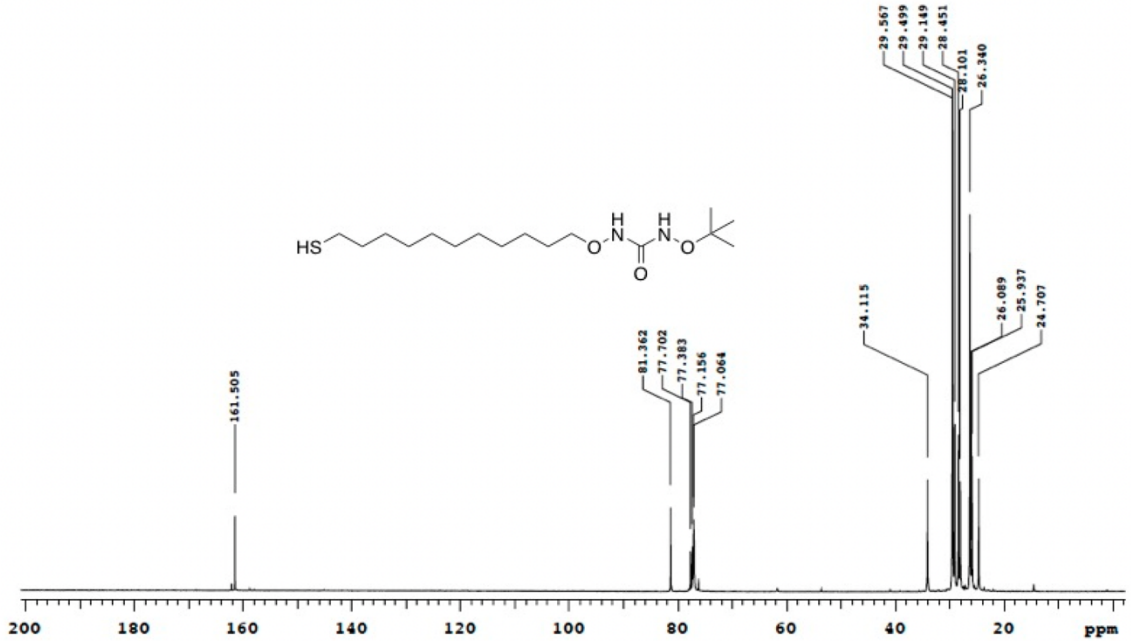

Figure 2.7. ^{1}H NMR spectra ($CDCl_3$, 400 MHz) and ^{13}C NMR spectra ($CDCl_3$, 100 MHz) confirming syntheses of *tert*-butyl substituted thiol urea ligands.

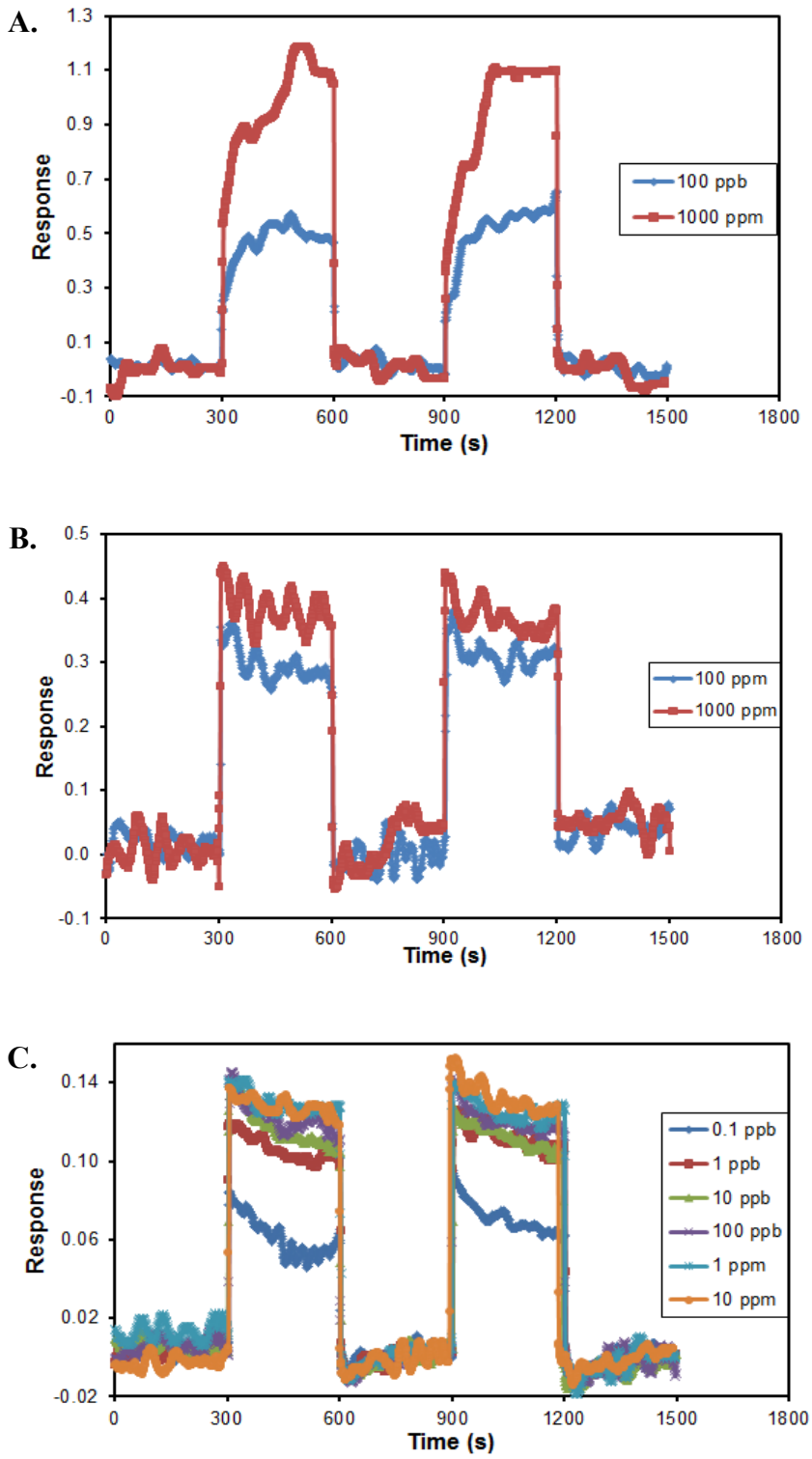

Figure 2.8. Monoalkoxyurea thiol sensor response profiles for exposure to acetone vapor. **A.** cyclohexyl, **B.** phenyl, and **C.** *p*-fluorophenyl. (Copied from Ref. 36)

Figure 2.8 shows the response values of cyclohexyl, phenyl and *p*-fluorophenyl functionalized monoalkoxyurea thiol capped Au MPCs sensors for acetone vapor in synthetic air. According to these response profiles, we observed the lower response values of cyclohexyl, phenyl and *p*-fluorophenyl functionalized monoalkoxyurea thiol capped Au MPCs sensors for acetone vapor than the previously studied *tert*-butyl monoalkoxyurea thiol sensor which had 0.1 ppb LoD (Figure 2.9). Interestingly, we did not observe any resistance change in cyclohexyl, and phenyl functionalized monoalkoxyurea thiol sensors for acetone concentrations lower than 100 ppb. These data highlighted that it is important to control the hydrogen bonding network formation between the urea moieties to enhance the acetone sensing. As mentioned in the introduction, the large response of *tert*-butyl monoalkoxyurea thiol sensor for acetone may be due to the steric bulkiness of *tert*-butyl group and it is enough to disrupt the hydrogen bonding network between the urea moieties. This substituent bulkiness can be explained using the "A-values" for substituted cyclohexanes.

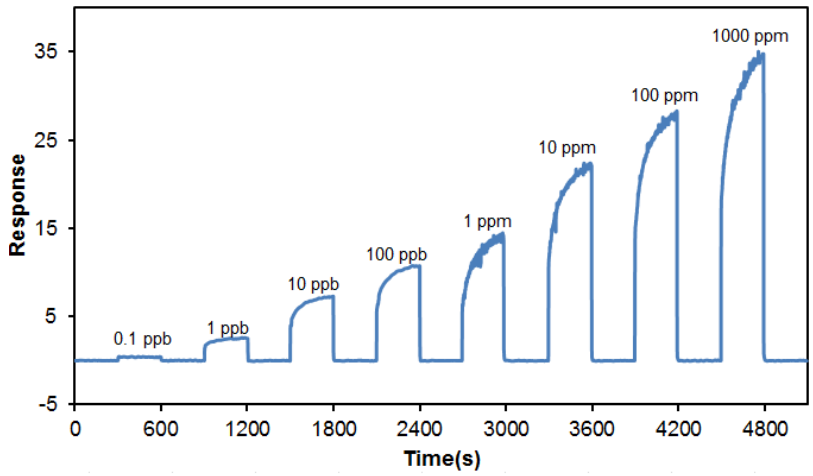

Figure 2.9. Response profile of the *tert*-butyl substituted monoalkoxyurea thiol sensor to acetone exposure at 0.1 ppb to 1000 ppm.

Bulkiness of any substituent on a cyclohexane ring is represented in a numerical way by "A-value" where the greater the A-value the "bulkier" the group is considered.[38] Among the substituents we examined, *tert*-butyl has the highest A value (~ 4.9), so it is bulkier than the other peripheral groups and hence disrupts hydrogen bonding network formation among adjacent urea motifs. The disruption enhances the ease with which hydrogen bonding formation can occur between the urea motif and any incoming acetone vapors.[38,39]

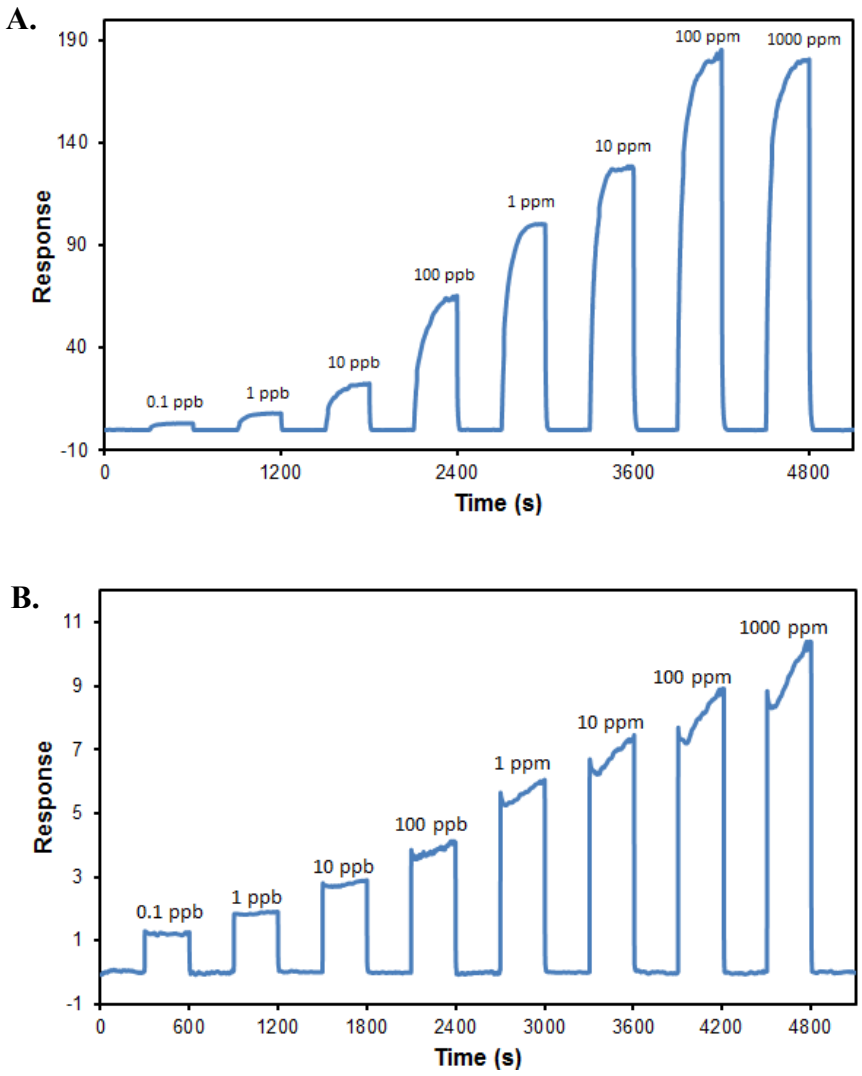

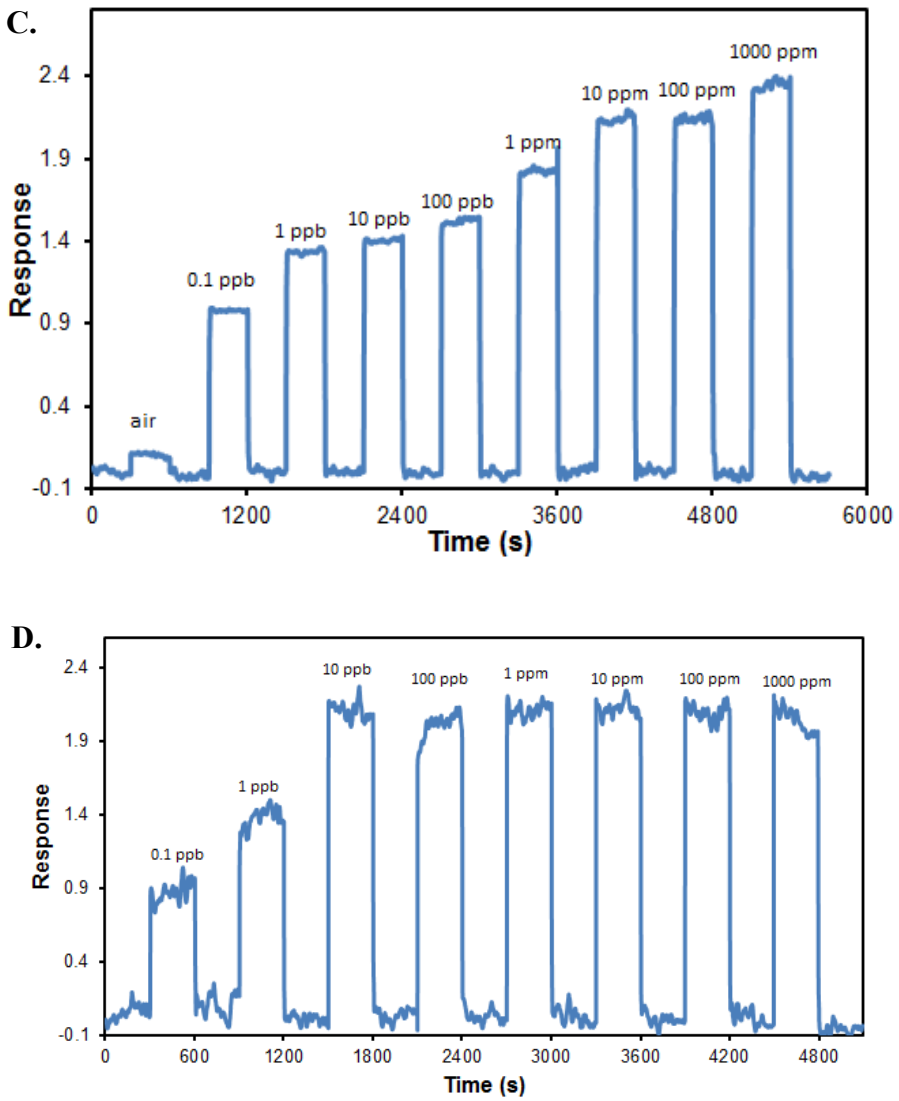

Figure 2.10. *N*-Alkyl-*N'*-arylurea thiol sensor response profiles to acetone vapor. **A.** *tert*-butyl, **B.** cyclohexyl; **C.** phenyl; and **D.** *p*-fluorophenyl. (Copied from Ref. 36)

Figure 2.10 summarizes the sensor response values of thiols in series II (dialkyl = *N*-alkyl-*N'*-arylurea thiol) to acetone vapor in synthetic air. Similar to what we observed with Series I, the *tert*-butyl alkylurea functionalized thiol sensor showed the highest sensitivity to acetone vapors relative to the other sensors in Series II. In contrast to the

cyclohexyl and phenyl sensors in Series I, all the sensors in series II shows response to lower acetone concentrations than 100 ppb. However, sensor saturation can be observed in the *p*-fluorophenyl substituted urea thiol sensor above 10 ppb acetone concentration levels. When compared, the *tert*-butyl substituted thiol sensors of Series I and Series II, it is clear that the dialkylurea thiol shows a larger response for different acetone concentrations than the monoalkoxyurea thiol sensor. The presence of an electronegative atom adjacent to urea motif possibly exerts an influence in this case that can explain the difference between the two *tert*-butyl sensors.[40,41] The overall nucleophilicity as well as acidity of a heteroatom-H moiety is influenced by the presence of an electron withdrawing atom in an α-position to the nucleophilic atom. A good example is the acidity difference between H_2O ($pK_a = 15$) and H_2O_2 ($pK_a = 12$). The α-electron withdrawing atom, an oxygen in both this example and in our alkoxyurea cases, increases the acidity of -NH in both the mono- and bisalkoxyurea series. The increase in NH acidity in turn enhances the H- donating ability of the urea functionality. Due to this effect, urea motifs with α-O make a strong hydrogen-bonded network between the adjacent urea motifs. The dialkyl and N-alkyl-N'arylurea thiol sensors form a weaker hydrogen-bonded network between the urea motifs than the monoalkoxyurea thiol sensors, and this facilitates the acetone vapor interaction which leads to a higher sensor response.

As shown in the figure 2.11, *tert*-butyl bisalkoxyurea thiol sensor has a large response for acetone than the cyclohexyl bisalkoxyurea thiol sensor and this trend was consistent with the Series I and II sensors which supports our α-O effect explanation. However, *tert*-butyl substituted bisalkoxyurea thiol sensor has a low sensitivity than the *tert*-butyl substituted thiol sensors in Series I and II.

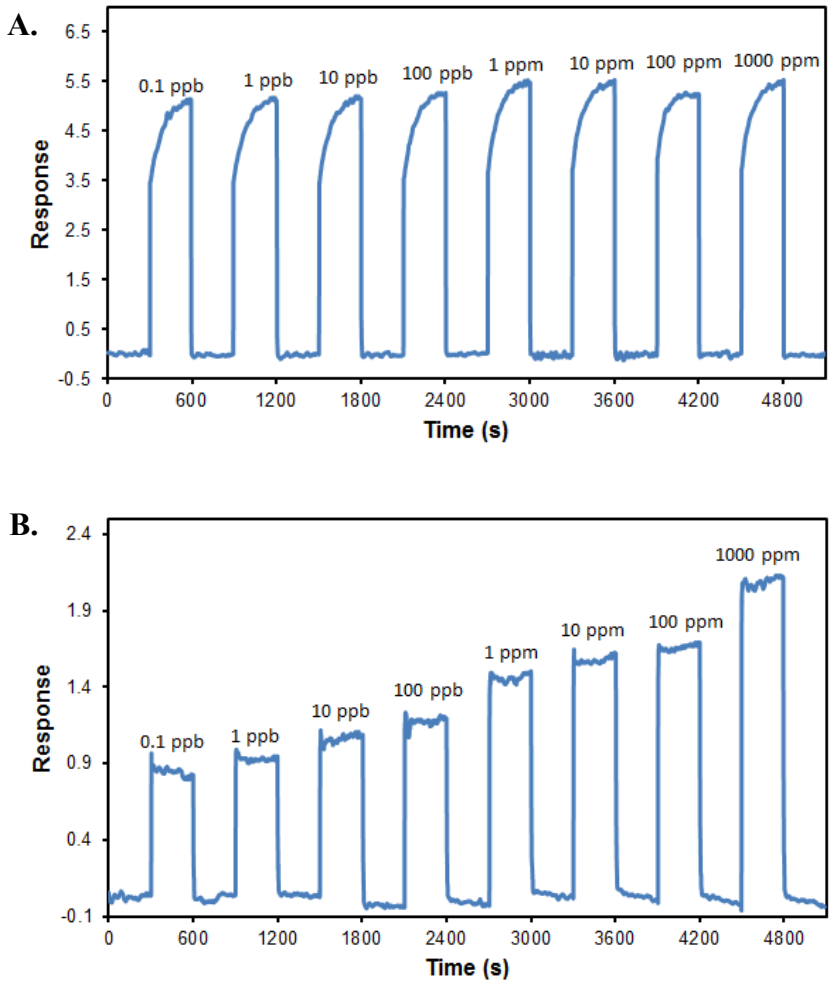

Figure 2.11. Bisalkoxyurea thiol sensors response profiles to different concentrations of acetone vapor. **A.** *tert*-butyl and **B.** cyclohexyl. (Copied from Ref. 36)

Using the bar chart in figure 2.12, we summarize the Series I-III sensors response data for 1 ppm acetone sensing. Here, it clearly demonstrated that *tert*-butyl bulky group substituted thiols sensors have a higher sensing ability towards acetone than the other *N*-substituted functional groups. Furthermore, *tert*-butyl sensor in series II exhibits the highest response for 1 ppm acetone vapor due to the steric and electronic effects in the

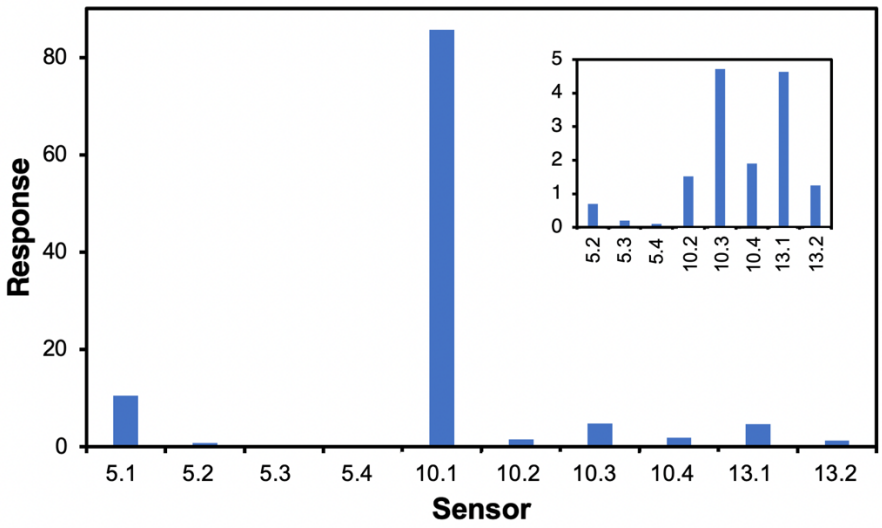

Figure 2.12. Response patterns of sensors functionalized with urea-thiol for sensing 1 ppm acetone in synthetic air.[34]

urea-thiol molecule. Bisalkoxyurea thiol ligands consist of two α-O atoms and make the NH protons more acidic than the NH protons in monoalkoxyurea thiol ligands[42,43] hence, make a strong hydrogen bonding network between the adjacent urea motifs and decreases the acetone vapor access into the matrix which leads to show overall low response among the three series. Figure 2.13 summarizes the electronic effect changes in *tert*-butyl urea thiols in Series I-III in presence of α-O atoms next to urea motifs. As mentioned earlier, *tert*-butyl group is bulkier than the other *N*-substituted functionalities and due to the special arrangement of *tert*-butyl group substituted sensors, it weakens the previously described hydrogen bonding network formation and enhances the acetone migration into the matrix. This phenomenon strengthens the hydrogen bonding formation between the urea motif in the sensor and incoming acetone vapors.

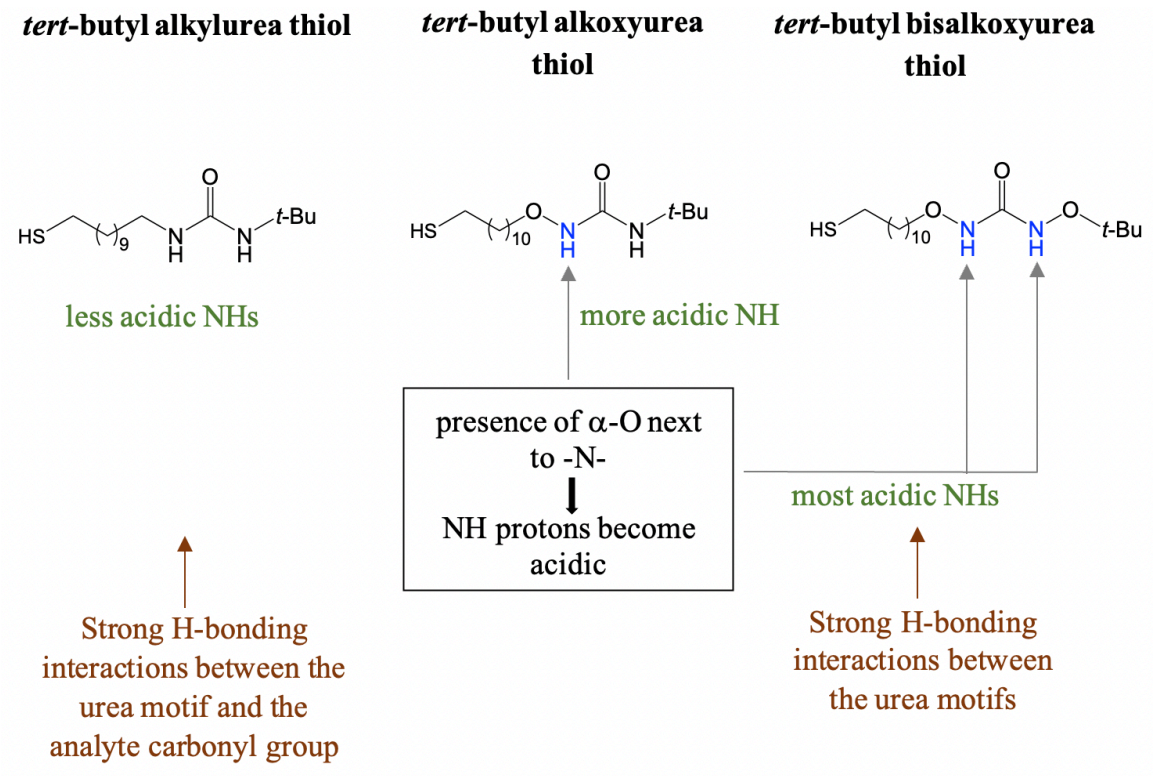

Figure 2.13. Illustration of the α-O effect for H-bonding network formation in *tert*-butyl urea thiols.

Tert-butyl dialkylurea thiol coated Au MPCs sensor selectivity towards acetone was studied in the presence of several analytes, which can form intermolecular H-bonding with urea motif. For this study, ethanol, water, and benzene were used as the analytes, and the collected sensor response values for the above VOCs were compared with the acetone vapor response. Figure 2.14 displays the response profile and the sensitivity for each analyte is directly measured by the slope of the linear regression curve. Proportionately, ethanol, benzene, and water analytes show a flat slope which imply that the urea motif in the *tert*-butyl dialkylurea thiol coated Au MPCs sensor has a weak hydrogen bonding interaction towards the above analytes than the acetone. Furthermore, the sensor response

to acetone is strong and significant thus exhibits a high sensitivity (slope 33.2). These data indicates that the hydrogen bonding interaction is highly influenced or affected by electronic factors of a molecule.

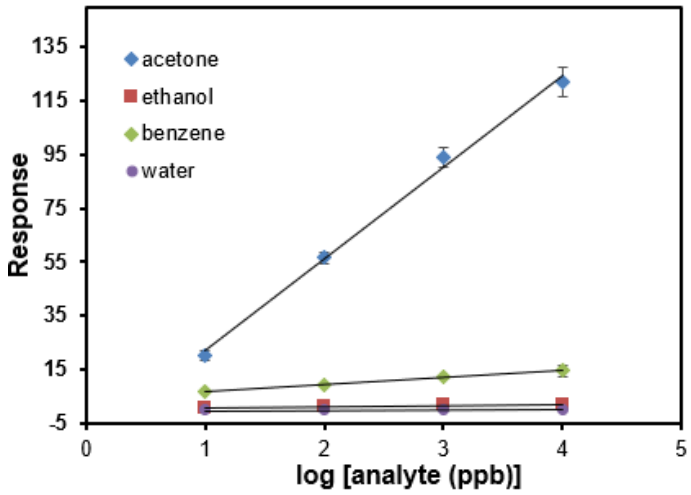

Figure 2.14. Response profile of *tert*-butyl dialkylurea thiolated Au MPCs sensor (series II) for in detection of acetone, ethanol, benzene, and water.

2.3. CONCLUSION

Chemiresistors derived from functionalized thiol ligands coated onto Au MPCs are promising materials for sensing VOCs at trace levels. As the above research has demonstrated, chemiresistive films formed from urea motif-functionalized thiol Au MPCs can be used to detect trace levels of carbonyl VOCs as low as 1 ppb. In this study, monoalkoxy–alkyl-, dialkyl-, and dialkoxyurea thiol ligands bearing different peripheral substituents were synthesized to prepare Au MPCs sensors. Among them, the chemiresistors with *tert*-butyl end group-substituted thiol ligands exhibited the highest sensitivity and selectivity towards acetone vapors. The obtained data suggest that the

sensitivity and selectivity of this type of sensor for carbonyl VOCs detection is influenced greatly by modulating the intermolecular H-bonding network between the urea moieties of thiol ligands by adjusting urea NH acidity and end group structure to destabilize chain-chain interactions.

CHAPTER 3

HARNESSING THE CATION-π INTERACTIONS OF METALATED GOLD MONOLAYER-PROTECTED CLUSTERS TO DETECT AROMATIC VOLATILE ORGANIC COMPOUNDS[b]

---

b The research presented in this chapter has been submitted in *Talanta* for review **2022**.

3.1. INTRODUCTION

Aromatic hydrocarbons are of great interest as a subgroup of VOCs that are present in urban and semi-urban environments. BTEX, an acronym that refers to benzene, toluene, ethyl benzene and xylenes, is a group of anthropogenic aromatic compounds that is considered to be harmful and is often measured in polluted environments.[1] The source of BTEX is primarily the petrochemical industry, but BTEX is also emitted by motor vehicles, aircraft exhausts, cigarette smoke, gasoline spills, and during petrol manufacturing. Volcanoes and wildfires also emit BTEX vapors to the air.[1] BTEX is widely used in refined petroleum products as well as in the production of adhesives, cosmetics, inks, thinners, pharmaceutical products, paints, and lacquers.[2] According to the World Health Organization (WHO), exposure to BTEX contaminated air or even breathing air that is contaminated with BTEX vapors at very low concentrations can cause short- and long-term adverse health effects to the central nervous system, lungs, and liver as well as cause disease including leukemia and cancer.[1,3] In particular, benzene, which is considered the primary source of fugitive BTEX emissions, can cause cancers at low concentrations, as low as 1 ppb.[2] Though benzene is known as a carcinogen, the other BTEX members are not identified as carcinogens to date.[1] According to environmental and health administrations, the OSHA PEL value for benzene is 1 ppm for an 8 h work shift and it is recommended not to exceed 5 ppm for short term exposure over a period of 15 min. The PEL values for the other BTEX VOCs are near 100 ppm or higher.[4] So, it is required to monitor these anthropogenic VOCs frequently to minimize their direct health effects, environmental damage, and contribution to photochemical smog.

3.1.1. BTEX Detection Methods

BTEX is measured extensively in industrial and urban environmental air. To date, several gas sensors and technologies are available for real-time monitoring of BTEX in ambient air. Gas chromatography coupled to a photo ionization detector (GC-PID),[2,5,6] proton-transfer-reaction mass spectrometry (PTR-MS),[3] Aeroqual AQM BTEX monitor,[7] and radiello passive air sample collector with gas chromatography-flame ionization detector (GC-FID)[8,9] are commercially available instruments that are currently used in the field for BTEX monitoring. However, these commercialized techniques suffer from several disadvantages, like high initial cost, low selectivity, and susceptibility to humidity effects. To overcome these problems, various research studies have sought to improve the existing technologies by introducing new techniques over the past several years.[10,11] Among them, tandem mass spectrometry-based techniques,[12] solid phase microextraction-based GC/MS approaches,[13,14] GC preconcentration methods,[15,16] microfluidic devices,[17,18] acoustic wave sensors based on plasticized polymer films,[19] film-based fluorescent sensors,[20] adsorption on activated carbon,[21] the use of zeolite adsorbents,[22] phenyl-modified PDMS sol-gel adsorption methods,[23] colorimetric methods,[24] electrochemical gas sensors,[25] and chemiresistors with sensing films consisting of metal oxides,[26,27] graphene,[28] carbon nanotubes,[29,30] and Au NPs-doped MWCNTs (multi wall carbon nanotubes)[31,32] have been widely studied.

3.1.2. Au MPC-Based Chemiresistors for Aromatic VOCs Detection

The use of Au NPs-based chemiresistors for trace VOC detection has become a widely studied technique for preparing sensory probes due to the inherent properties of Au NPs, such as high chemical stability, ease of synthesis, unique optical properties, large

surface to volume ratio, and high level of conductivity.[33,34] By changing the size, shape and surface chemistry, the electronic and optical properties of Au NPs can be tuned depending on the application. Over the past several years, gold monolayer protected clusters (Au MPCs), where the metal nanoparticle core is surrounded by a self-assembled monolayer of organic ligand, generally thiolate-based, have been studied for VOC sensing.[35,36] Few thiolate-coated Au MPCs chemiresistors have been reported for BTEX detection in air, but several research groups have studied changes in thiol ligand structure in regard to sensitivity and selectivity toward selected aromatic VOCs. Wohltjen and Snow synthesized an octanethiolate-coated Au MPCs chemiresistor and studied the sensing responses to toluene vapors.[37] They observed a large and rapid drop in conductance of the sensor when exposed to toluene vapor, which was different than the responses to the other vapors studied. Due to the hydrocarbon nature of toluene, toluene vapors rapidly diffused into the hydrophobic organic matrix (like dissolves like) and the swelled matrix caused a decrease in the electron tunneling and electron hoping current. Han *et al.,*[38] also studied thiolate-coated Au MPCs sensing arrays for the aromatic VOCs sensing of benzene, toluene, xylenes (*o, p, m*), 4-nitrobenzene, 2-nitrotoluene, 3-nitrotoluene.[38] They used Au nanostructured arrays consisting of thin films of alkane-thiolate Au MPCs synthesized from dodecanethiol as the capping ligand and 1,9-nonanedithiol, 1,5-pentadithiol, 16-mercaptohexadecanoic acid (MHA), 11-mercaptoundecanoic acid (MUA), 3-mercaptopropanoic acid (MPA) as linker ligands. The synthesized sensing materials differed from each other in terms of hydrogen bonding, hydrophobicity, and chain length (structure). As a result, different conductivity properties were obtained for each analyte and each sensor. The sensor response sensitivity was strongly dependent on the linker ligand

structure.[38] Huang *et al*.,[39] also explored the shell structure effect on vapor selectivity of Au MPCs sensors using VOCs with different functionality, including toluene, *n*-octane, butyl acetate, anisole, 2-heptanone, and *n*-butanol.[39] Four types of sensors were synthesized using four thiols with different functionalities. Toluene vapor elicited the highest response for the Au MPCs sensor fitted with a 4-pyridinethiolate shell structure compared to the other sensors that featured ester, carboxylic acid, or *n*-hydrocarbon functionalities, presumably due to possible π-π interactions with the pyridine ring. Kim *et al.*[40] studied the response profiles of benzene- and methyl ester-functionalized thiolate-coated Au MPCs chemiresistors against benzene and toluene vapors. These studies all revealed that functionalized thiolate shell structures of Au MPCs chemiresistors are promising candidates for development of chemiresistive gas sensors for air quality monitoring.

3.1.3. Harnessing Cation-π Interactions to Develop Au MPCs-Based Chemiresistors for BTEX Detection

Having noted this, our interest in thiolate ligands fitted with pendant functionality to impart derived Au MPCs with selective VOC-sensing properties[41] has led us to develop an Au MPCs-based chemiresistor approach for aromatic VOCs (BTEX) sensing that exploits the use of cation-π interactions. As mentioned earlier, several research groups have studied the effect of polar-π interactions and π-π interactions (Figure 3.1) for aromatic VOCs sensing[32,38,42] but the use of cation-π interactions for aromatic VOCs sensing has not been reported. We describe herein a method to promote cation-π interactions wherein the non-covalent interactions between Au MPCs-bound metal ions and aromatic π-systems elicits a selective chemiresistor response.

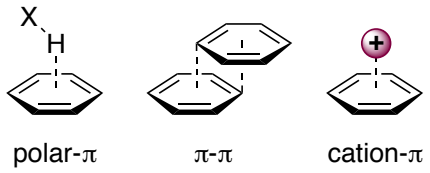

Figure 3.1. Common types of π interactions.

Recently the cation-π interaction has been discussed as a strong attraction that can be expected to make a remarkable contribution to molecular recognition phenomena.[43,44,45] Mainly this interaction is considered as an electrostatic attraction between a quadrupole moment of the electron-rich aromatic region and electron-deficient cation. Several factors influence the strength of the cation-π bonding, such as the nature of the cation and π system[43,44] solvation[45] and geometry of interaction.[46] π-Systems strongly bind with cations that have larger charge density, as confirmed by several research groups that have examined these interactions in the gas phase.[45,47,48] While cation- π attractions are very prominent in the gas phase, these forces are attenuated in the presence of solvents. Gallivan *et al.*[45] studied the change in K^+-benzene binding energy in different solvents computationally and observed a decrease in binding energies in polar solvents relative to gas phase interactions. Kumpf *et al.,*[47] demonstrated the highest cation- π interaction strengths for K^+ and Rb^+, more so than for Li^+ and Na^+, in aqueous media.

Cation-π interactions have been studied widely in relation to supramolecular chemistry, where these interactions assume significant roles in synthetic receptors[43,44] as well as in host-guest assemblies.[49,50] Furthermore, the interactions between cations and aromatic π-systems also have been studied for synthesis applications, such as in catalysis,[51] and in biomolecule recognition events to determine protein structure and function.[52] These studies strongly support developing the cation-π interaction as a sensing mechanism for

detection of aromatic VOCs.

Our approach to harnessing the cation-π interaction for aromatic VOCs sensing was motivated in part by the studies of Leopold *et al.,*[53] and Zamborini *et al.,*[54] in which metal ion-carboxylate linked nanoparticle films were prepared and studied for electron hopping conductivity and vapor sensing properties. Further motivation for using carboxylate functionality was provided by Han *et al.,*[38] who observed sensitivity for aromatic compounds over non-polar hydrophobic vapor analytes when using a sensing array derived from 16-mercaptohexadecanoic acid-coated Au MPCs. In this case, the response to aromatic compounds increased with an increase in polar functional groups on the aromatic analytes due to polar-π interactions.[38] We thus aimed to develop a chemiresistor-based sensor for aromatic VOCs sensing by applying alkali metal ion-carboxylate functionalized Au MPCs to interdigitated electrodes (IDEs) prepared using micro-electromechanical system (MEMS) technology, as depicted in Figure 3.2.

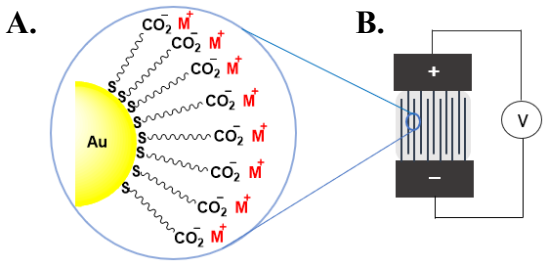

Figure 3.2. **A**. Metal ion-carboxylate linked Au MPCs (M^+ = alkali metal) and **B**. Structure of a chemiresistor with interdigitated electrodes. The Au MPCs are drop-cast onto the chemiresistor electrodes to create a closed circuit.

This Chapter describes our initial studies using Au MPCs derived from a short-chain thiolate ligand fitted with aminooxy functionality for ready introduction of

carboxylate salts. Lithium, sodium, and potassium carboxylate-linked Au MPCs were examined for their ability to sense vapors of benzene, toluene, ethyl benzene and xylene (BTEX) as well as in comparison studies to probe the role of the cation-π interaction.

3.2. RESULTS AND DISCUSSION

We prepared aminooxy-functionalized Au MPCs by reaction of thiol **4** (Scheme 3.1) under two-phase Brust-Shiffrin conditions.[55] The synthesized aminooxy Au MPCs **9/C6** (Scheme 3.1) were characterized using ^{1}H NMR and ^{13}C NMR (Appendix), FT-IR (Appendix, Figure 3.15), TEM (Appendix, Figure 3.24), and UV-visible spectroscopy

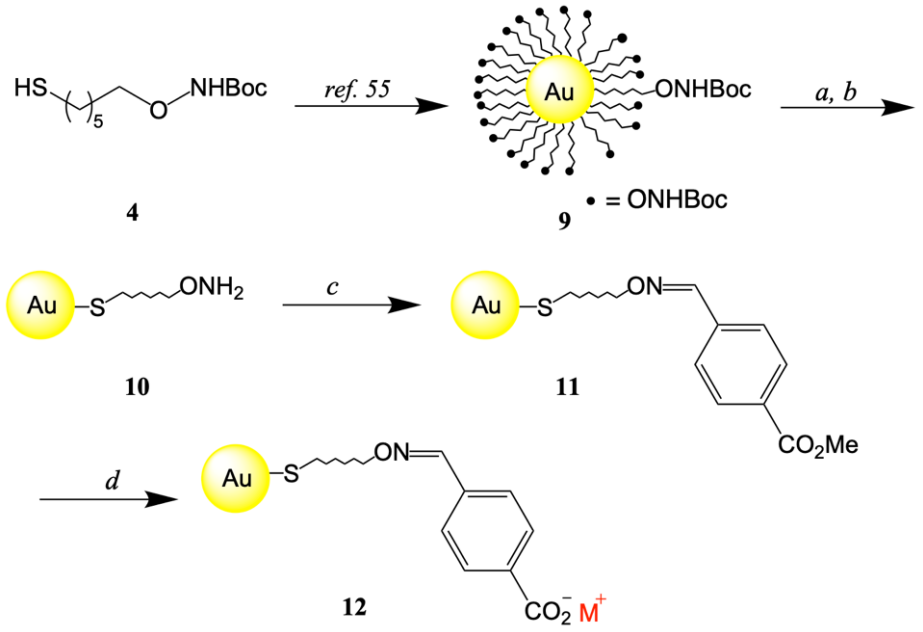

Scheme 3.1. Synthesis of *n*-alkane C6 length metal-ion functionalized Au MPCs. Only one ligand is emphasized in MPCs 9-12. Reagents and conditions: a. 50% CF_3CO_2H, CH_2Cl_2, 0 °C, 15 min.; b. Et_3N, MeOH:CH_2Cl_2 (2:1), rt, 3 h; c. methyl 4-formylbenzoate, CH_2Cl_2, rt, 17 h; d. M^+OH^- (LiOH, NaOH or KOH), MeOH:CH_2Cl_2 (1:9), 0 °C to rt, 17 h.

(Appendix, Figure 3.26). The characterization data confirm formation of thiolate-bound Au MPCs with <3 nm diameter. TEM data on Au MPCs **9**, obtained by taking 200 measurements from 100 particles horizontally and perpendicular to the plane of each particle, reveal an average particle size of 2.3 nm. TGA data on Au MPCs **9/C6** (Appendix, Figure 3.22) indicate an organic composition of 35%. The *N*-Boc deprotection (**9** → **10**, Scheme 3.1) was readily monitored using FT-IR spectroscopy, which showed disappearance of the carbamate C=O stretch at 1714 cm^{-1} as the carbamate groups are removed (Appendix, Figure 3.16). Aminooxy Au MPCs **10** can serve as a platform for incorporation of a wide variety of surface functionality by reaction with aldehydes, a convenient synthetic approach that we have found to be highly useful when seeking to tailor Au MPCs.[60]

To introduce surface carboxylic ester functionality, Au MPCs **10** were reacted with methyl 4-formylbenzoate. Oxime ether formation was readily verified by ^{1}H NMR spectroscopy on the resultant Au MPCs **11/C6**, which showed the oximyl-H resonances at δ 8.15-7.80 ppm (*E* isomer) in addition to the aryl-H resonances at δ 8.15-7.80 ppm and 7.65-7.50 ppm (Figure 3.3 A). Furthermore, downfield shift of the methylene adjacent to the aminooxy moiety ($-CH_2ONH_2$) from δ 3.64 ppm in **10/C6** to δ 4.15 ppm in the oxime ether **11** is highly characteristic of the ligation reaction.[60] Figure 3.3 B shows the ^{1}H NMR spectroscopy of the oxime ether adduct formation between the aminooxy thiol (Compound **3,** Scheme 3.2) and the methyl 4-formylbenzoate. This spectrum can be used as a reference to study the oxime ether adduct formation on the Au MPCs surface. As noted, oximyl-H resonances at δ 8.09 ppm (*E* isomer) in addition to the aryl-H resonances at δ 8.04-8.01 ppm and 7.65-7.63 ppm. Furthermore, the methylene adjacent to the aminooxy moiety (-

CH_2ONH_2) down fielded to δ 4.19 ppm in the oxime ether adduct. The chemical shift values of Figure 3.3 B spectra correlate with the Figure 3.3 A spectral data and validate the

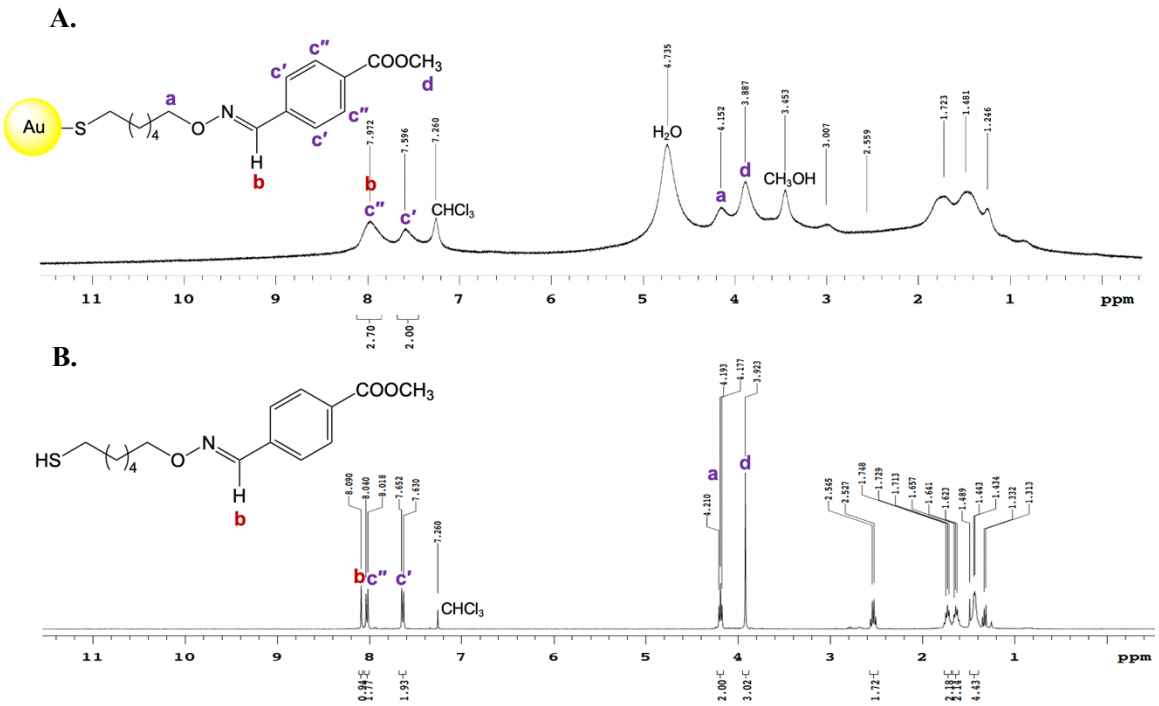

Figure 3.3. ^{1}H NMR spectrum ($CDCl_3$, 400 MHz) of **A.** Au MPCs **11/C6** synthesized by reaction of MPCs 10 with methyl 4-formylbenzoate and **B.** oxime ether addcut synthesized by reaction of aminooxy thiol (**3**, Scheme 3.2 in Chapter 5) with methyl 4-formylbenzoate. Residual solvent peaks for $CHCl_3$, water, and methanol are indicated.

characteristic oxime ether formation on the Au surface. Theoretically in the oximation reaction, both *E* and *Z* geometric isomers are possible to form in the solution. However, it is experimentally proved that aldimines exist only the *E* configuration (> 99%) where aldimine formation with benzaldehydes or monosubstituted benzaldehydes.[61] In aldimines, the C=N bond conjugates with the aromatic π electrons and the nitrogen lone pair preferentially in *E* isomer and they are more stable than the corresponding Z isomer.

Conversely, the steric effects of Z isomer will create less effective bond orbital overlap hence destabilize the molecule.[62] FT-IR spectroscopy on Au MPCs **11/C6** (Appendix, Figure 3.16) indicates a strong broad absorption at 1609 to 1714 cm^{-1}, which is the result of overlap between the ester carbonyl stretch and newly formed C=N bond.

Ester hydrolyses using alkali metal hydroxide salts afforded the target metal ion-carboxylate linked Au MPCs **12**-M^+ (Scheme 3.1), where the M^+ studied included Li^+, Na^+, and K^+. Alkali metal incorporation for the Au MPCs **12**-Na^+ and **12**-K^+ preparations were confirmed using EDS. As can be expected, we obtained EDS spectra (Appendix, Figure 3.27, and Figure 3.29) that showed emission bands characteristic of Na^+ incorporation (K_α 1.05 keV) and K^+ incorporation (K_α 3.37 keV) when the ester Au MPCs **11/C6** were treated with either NaOH or KOH, respectively. Confirming the presence of Li^+ ions required XPS. The emission at 57.4 eV in the XPS scan of Au MPCs **12**-Li^+/C6 (Appendix, Figure 3.30) confirms the presence of lithium in the sample.[63]

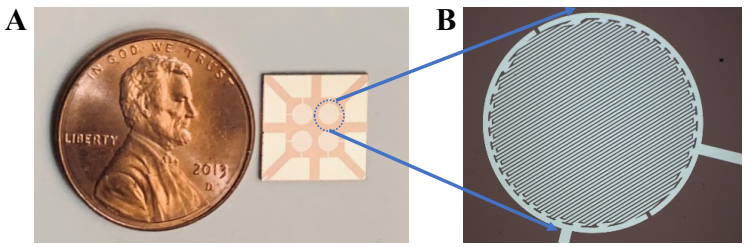

Figure 3.4. A. Microfabricated chip with four circular IDEs and **B.** Optical micrograph of the IDE.

With the metal ion-carboxylate linked Au MPCs **12**-M^+ in hand, we next evaluated the responses of chemiresistors formed on cladding this panel of Au MPCs onto individual

IDEs as previously described.[41,64] Figure 3.4 A shows a photo of the fabricated chip with four circular IDEs. Figure 3.4 B shows an optical micrograph of the structure of the IDEs. Microfabricated chip was designed by Sujoy Halder (Graduate student, Dr. Xian-An Fu's research group) and all the sensor measurements were performed by him. Figure 3.5 shows the resistance changes of the chemiresistor formed from **12**-K^+/C6 for sensing benzene at the concentration range 100 ppb to 5 ppm. With an increasing concentration of benzene, the response increased as the deviation of resistance from the baseline increased. The resistance changes were rapid and reversible. From the resistance profile, we note that the resistance of this sensor decreases in the presence of benzene, which can be the result of an increase of analyte permittivity into the organic matrix surrounding the metal cores or due to analyte surface binding, as with postulated targeted cation–π interactions.[65]

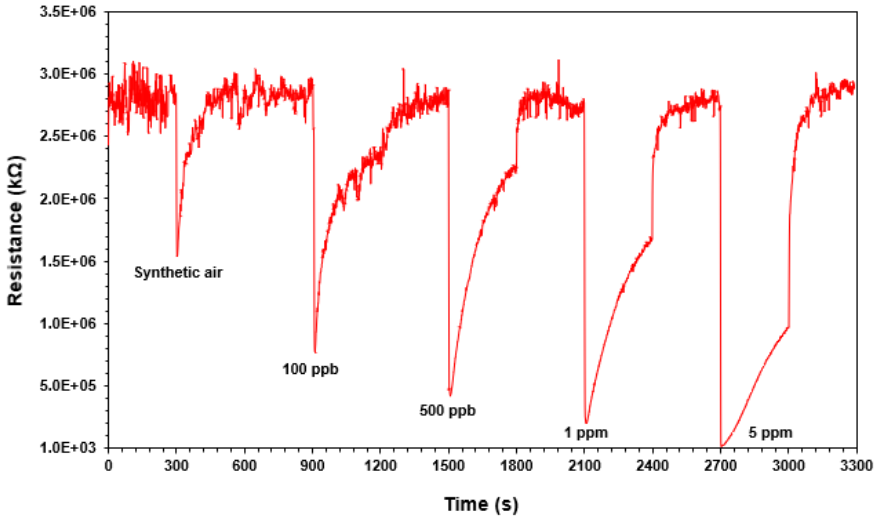

Figure 3.5. Resistance of chemiresistor **12**-K^+ upon exposure to 100 ppb, 500 ppb, 1 ppm and 5 ppm of benzene at 22 °C.

To further examine the dominant factor between these two influences for resistance change, we measured sensor responses to vapors of other aromatic and non-aromatic

compounds. For this study, *n*-alkane C11 length (Scheme 3.3) Na^+-functionalized Au MPCs were synthesized using the same synthetic route in scheme 3.1. The two chemiresistors **12**-Na^+/C6 and **12**-Na^+/C11 with two different hydrocarbon chains were used to measure the sensor responses to vapors of aromatic benzene, toluene, xylene, ethylbenzene, and nitrobenzene and as well as non-aromatic cyclohexane at 1 ppm vapor concentration. Figure 3.6 summarizes the responses of **12**-Na^+/C6 and **12**-Na^+/C11 functionalized sensors on exposure to a panel of VOCs used. From the response profile, we note that the hydrophobic *n*-alkane chain length greatly influences the sensitivity and selectivity of the analyte. **12**-Na^+/C6 chemiresistor shows the higher responses for all the analytes used and the selectivity for each analyte is significant. Herein, it supports the idea that the analyte permittivity into the organic matrix increases with decreasing the hydrophobicity of the matric by reducing the n-alkane chain length of the organic thiol surrounding the metal core.

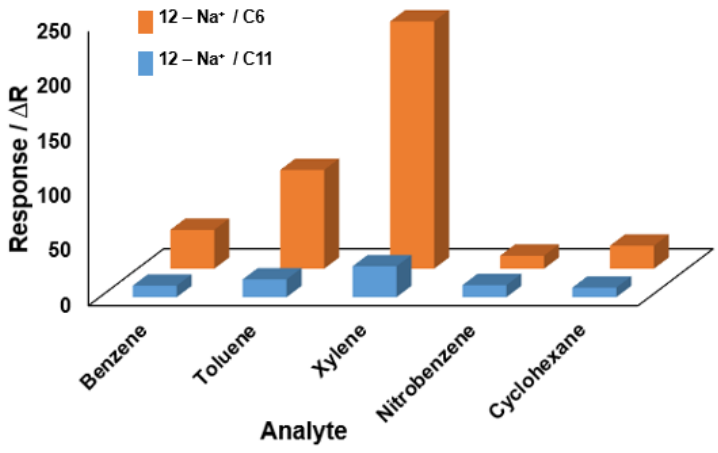

Figure 3.6. Response pattern of chemiresistor **12**-Na^+/C6 and **12**-Na^+/C11 upon exposure to 1 ppm analyte vapors at 22 °C.

To validate the analyte surface binding through cation-π interaction was examined using the three different **12**-M^+/C6 chemiresistors. We measured sensor responses to vapors of selected aromatic and non-aromatic compounds. Figure 3.7 shows the responses of Li^+-, Na^+- and K^+-functionalized sensors on exposure to a panel of aromatic VOCs as well as cyclohexane, ethanol, and acetone. The Au MPCs **12**-M^+/C6 show a linear relationship between response and analyte concentration in the range of 100 ppb to 5 ppm. In that the slope of the linear regression curve is a direct measurement of sensitivity, the sensors show higher sensitivity for analytes containing a π system (benzene, toluene, ethylbenzene, and xylene), a result that is consistent with a sensing mechanism elicited by cation-π interactions. Further support for involvement of cation-π interactions is noted by the higher sensitivity toward the aromatic VOCs containing alkyl substitution. Alkyl substituents increase π-electron density in the ring via induction, which in turn can be expected to promote greater association of the π system with an electron-deficient metal ion, a relationship that has been previously reported.[66] Indeed, the alkyl substituted analytes of the lithium sensor is not surprising since lithium is more tightly bound by carboxylate anion than either sodium or potassium, thus decreasing its electrostatic potential for engaging in cation-π interactions.[67] The heightened sensitivity of the Na^+- and K^+-bound sensors relative to the Li^+-bound sensor also agrees with studies on cation-π interactions in the solid state by Fukin *et al.*,[68] who studied the cation-π interactions for alkali metals with π- and σ-modalities using polyfunctional arene ligands with ether groups and concluded that larger cations undergo M^+---π interactions more readily. Limit of detection (LOD) was calculated from the response curve for these tested analytes using linear regression according to the formula: LOD = 3.3 (S_y/S) [S_y = the standard deviation of the response

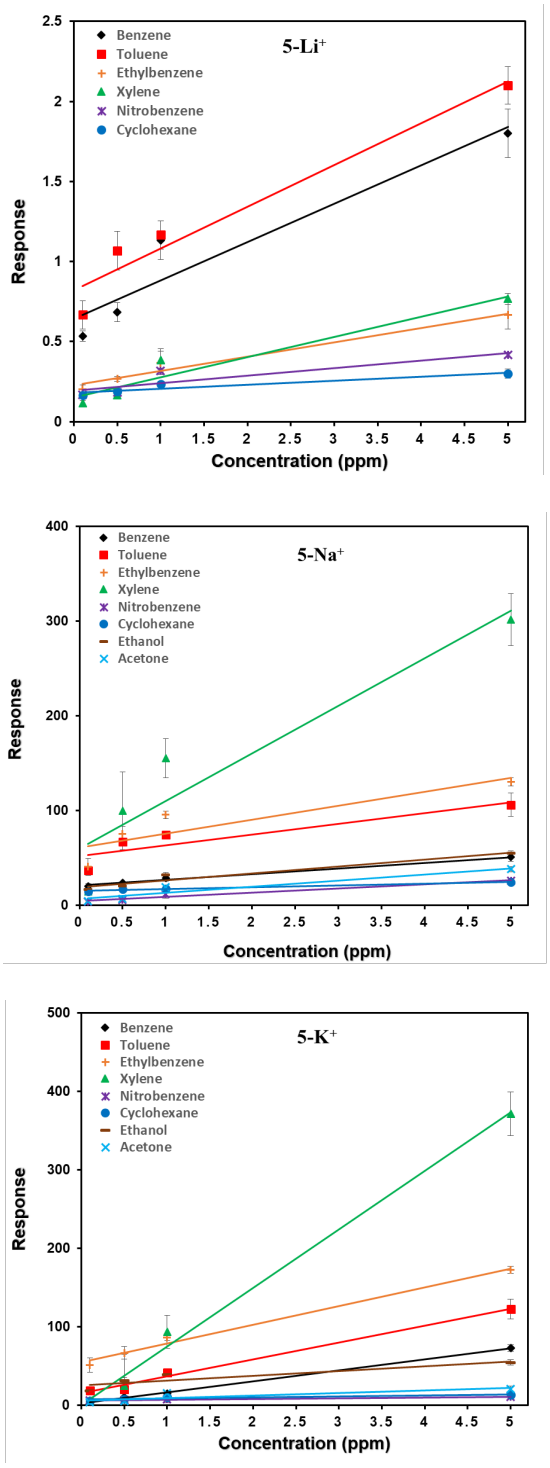

Figure 3.7. Sensor response of Au MPCs **12**-M^+/C6, where $M^+ = Li^+$, Na^+ or K^+. Each point indicates the average of n = 3 measurements. The variability of these measurements is shown by the error bars.

and S = the slope of the response curve]. The calculated LOD ranges from 0.1 – 3 ppb for these compounds.

Of particular interest for the analytes examined are the relatively flat slopes obtained for cyclohexane, ethanol, and acetone. Cyclohexane and ethanol cannot engage in cation-π interactions, and cation-π interactions of nonaromatic π-systems, such as in acetone, are little known and limited to the complex of ethylene-ammonium cation,[69] acetylene-calcium cation,[70] and intramolecular complexations of carbonyl π-systems.[71] Cation-π interactions often must compete with polar M^+-hydrophilic interactions, but with the present sensors, the polar substrates did not elicit significant responses, suggesting the dominant response for the synthesized chemiresistors corresponds to cation-π interactions and not to hydrophilic interactions or analyte permittivity into the hydrophobic monolayer core.

Although nitrobenzene contains an aromatic π-system, the response curves of the three chemiresistors examined to nitrobenzene also are flat (Figure 3.7). The lack of response of the Na^+- and K^+-functionalized chemiresistors to nitrobenzene at a concentration of 5 ppm is shown in Figure 3.8, which compares sensor responses to the BTEX VOCs and cyclohexane, ethanol, and acetone at the same concentration to represent the sensitivity of the sensors toward electron-rich aromatic VOCs. A reasonable interpretation of this result is that the nitro group diminishes the π-electron density of the aromatic ring via a resonance withdrawing effect to substantially reduce the ability for metal ion coordination via cation π-interactions. Also, both the Na^+- and K^+-functionalized chemiresistors show a low response to cyclohexene, in which the alkene-π bond is not as coordinating as the π-system of an aromatic substrate.

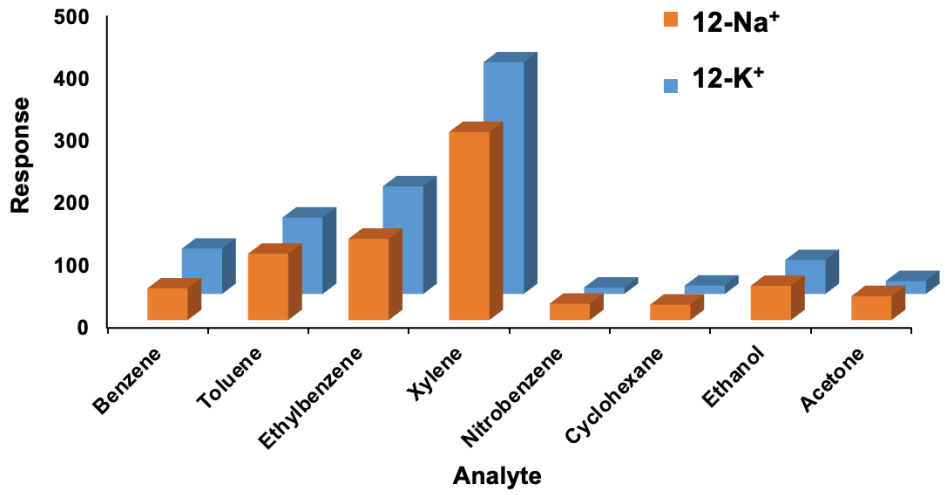

Figure 3.8. Chemiresistor response to VOCs at a concentration of 5 ppm. Sensors were prepared from Au MPCs **12**-M^+/C6, where $M^+ = Na^+$ or K^+.

Apart from cation-π interactions, these sensor materials also show strong interaction with water. To examine the effects of hydration, the responses of the sensors to water spiked into synthetic air were studied. In this study, predetermined amounts of water were injected into 1 L tedlar bags containing synthetic air to achieve the desired relative humidity (RH). Theoretically, 1% RH is equivalent to 312 ppm water at 25 °C. For instance, 29 µL of water was injected into a 1 L tedlar bag to make 25% RH and heated a little until all the water was evaporated. The same procedure was carried out to prepare 50%, 75%, and 100% RH. Figure 3.9 shows the responses of Li^+-, Na^+- and K^+-functionalized Au MPCs sensors to relative humidity (25 – 100%) at 22 °C. Similar to the VOCs response profile, the interaction of Au MPCs **12**-M^+/C6 to water moisture shows the order $K^+ > Na^+ > Li^+$. The large responses of Na^+- and K^+-functionalized Au MPCs to humidity cause significant interference in measuring BETX in environmental air. One way

to eliminate the effect of humidity is to use a sorbent tube to absorb water from environmental air samples. Another approach is to use a preconcentrator with selective sorbents to capture and concentrate BTEX target analytes and then to use synthetic air for elution of the preconcentrator. The preconcentration process will not only eliminate humidity, but also concentrate target compounds for more accurate analysis. Further study using these sensors for detection of BTEX in environmental air after a preconcentration process is needed.

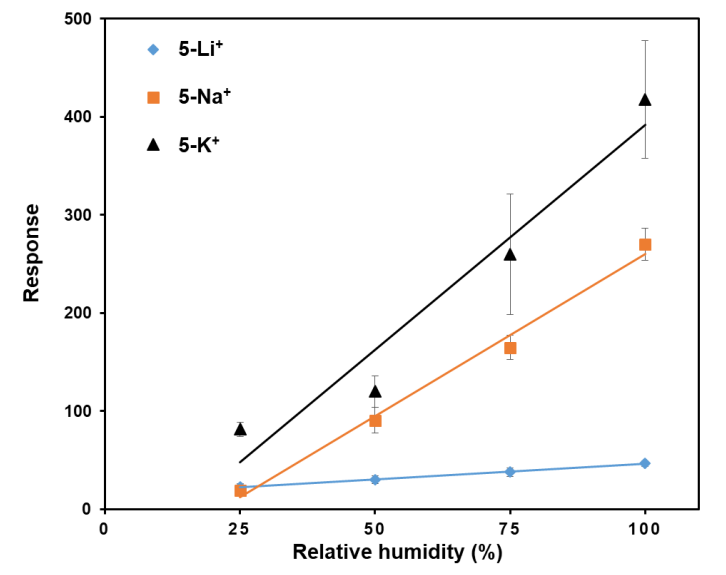

Figure 3.9. Au MPCs **12-M$^+$/C6** sensor responses to relative humidity (25 – 100 %).

To further validate that sensor resistance changes are due specifically to cation-π interactions of carboxylate-linked metal cations, we examined the sensor responses to both the structurally analogous methyl ester-functionalized Au MPCs (**11/C6**, Scheme 3.1) and to potassium hydroxide-treated Au MPCs. No significant changes in resistance were observed by introducing BTEX at different concentrations to Au MPCs **11/C6**, which do

not contain bound alkali metal ions (data not shown). To eliminate the possibility that the ester hydrolysis procedure in which **11** is treated with metal hydroxide can deposit metal ions onto Au MPCs other than as a metal ion-carboxylate, we reacted dodecane thiolate-coated Au MPCs with 0.1 M KOH in the same manner as in the synthesis of Au MPCs **12**-K^+ (we thank Prof. Sachin Handa for his suggestion to test this possibility). The response of the resultant KOH-treated Au MPCs to benzene then was examined. We did not observe any notable response to benzene at all concentrations examined. These results underscore that the attachment of metal ions to the Au MPCs monolayer in the form of metal carboxylates is crucial for sensor recognition of aromatic VOCs.

To examine further the high sensor response of the **12**-K^+/C6 sensor to aromatic VOCs, we prepared additional Au MPCs-based chemiresistive films using different commercially available thiols (Table 3.1). The initial resistance of the each chemiresistive film is mentioned in the table 3.1. The initial resistance of the chemiresistive film in sensor **f** (**12**-K^+/C6) shows the highest initial resistance than the other films. Place exchanged chemiresistive film in sensor **c** exhibits the lowest initial resistance and it might be due to less steric hindrance between the coated thiolates and short core edge-to-edge distance (δ_{edge}) due to the densely packed continuous chemiresistive film. Figure 3.10 shows sensor responses to benzene at a concentration range from 100 ppb to 5 ppm. The sensor made from 4-mercaptobenzoic acid (4-MBA), which has -COOH functionality at its surface, did not respond to benzene vapor even at high concentrations. However, the analogous sensor fitted with K^+ (4-MBA/K^+) did respond to benzene vapor, albeit not at the level of the **12**-K^+/C6 sensor. Due to the lack of aromatic analyte binding sites (cation-π) at the surface of the Au MPCs of sensors made using a place-exchange method (Experimental Section,

Table 3.1. Commercially available thiols coated onto Au MPCs chemiresistive films for benzene sensing studies.

Sensor	Coated thiol	Au MPCs chemiresistive film	Initial film resistance
a	4-mercaptobenzoic acid or 4-MBA	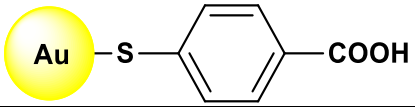	17 x 10^6 Ω
b	4-mercaptobenzoic acid / K^+ or 4-MBA (K^+)	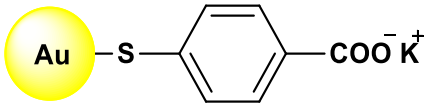	15 x 10^6 Ω
c	1-hexanethiol and 4-MBA / K^+ or MCH/4-MBA (K^+): synthesized by place-exchange method	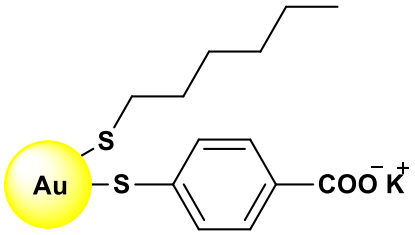	28 x 10^3 Ω
d	1-dodecanethiol and 4-MBA / K^+ or DDT/4-MBA (K^+): synthesized by place-exchange method	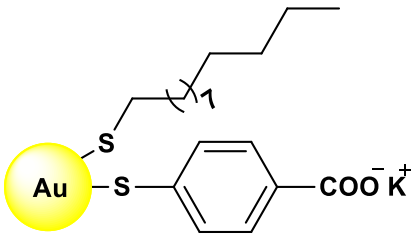	0.6 x 10^6 Ω
e	16-mercaptohexadecanoic acid / K^+ or MHDA (K^+)	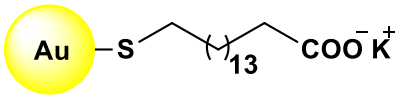	0.8 x 10^6 Ω
f	12-K^+/C6	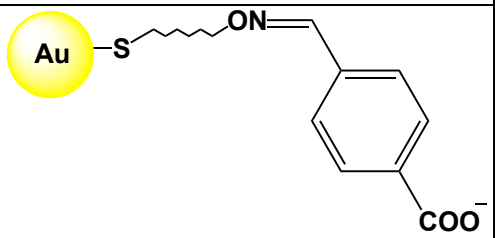	5.0 x 10^9 Ω

5.4.2.4.) show a little response to the benzene, but it is lower than the response of **4-**MBA/K^+ sensor. The utilized place exchange method will remove approximately 50% of the non-linker 1- hexanethiol ligand and introduce approximately 50% of the linker 4-mercaptobenzoic acid.[57] Also, the response of dodecanethiol coated mixed monolayer of Au MPCs sensor (**C12/4**-MBA (K^+)) is lower than the hexanethiol coated mixed monolayer of Au MPCs sensor (**C6/4**-MBA (K+)). Furthermore, **16**-MHDA/K+ sensor also responded to all the benzene vapor concentrations used but it shows a lower response value than 4-MBA/K+ sensor. The data suggests that if the hydrophobic nature of the organic matrix of the sensor increases, then the sensor response to aromatic VOCs will decrease. The self- assembled monolayer (SAM) of the 4-MBA/K+ sensor consist of an aromatic ring thus it increases the dielectric constant of the matrix than the organic matrixes with hydrocarbon alkane chains. The dielectric constant can affect electron tunneling

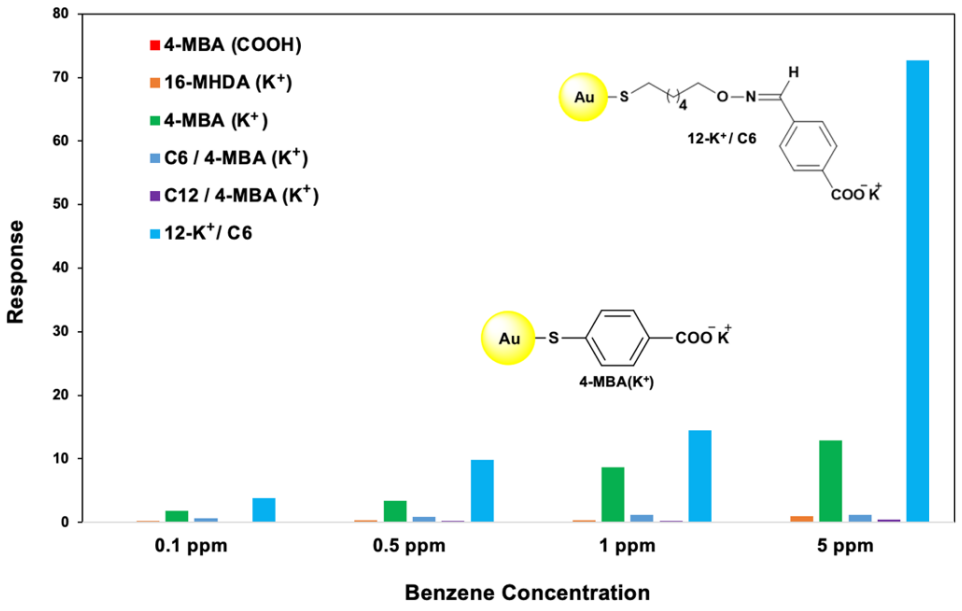

Figure 3.10. 12-K+/C6 Sensor response pattern comparison with commercially available thiols coated Au MPCs sensors for sensing benzene in synthetic air.

coefficient (β_d). Due to the electron delocalization in aromatic rings, they also have a smaller electron tunneling coefficient compared to hydrocarbon alkane chains. These factors can be used to rationalize the high sensor response of **4**-MBA/K^+ to benzene. Interestingly, the **12-**K^+/C6 sensor showed the highest response to benzene among all the sensor types examined. This **12-**K^+/C6 sensor consist of an oxime ether bond (-C=N-O-) and form a highly conjugated π system with the aromatic ring. This arrangement may increase the electron delocalization where inductive effect pulls electrons towards the most polarized atom. This electron distribution will make the cation more electrophilic which could enhance a cation-π interaction with an aromatic compound. Indeed, these K+ functionalized Au MPCs sensors exhibit a higher response to benzene (BTEX) than the responses of previously studied thiolate-coated Au MPCs sensors mentioned in section 3.1.

3.3. CONCLUSION

Harnessing the strong, non-covalent interactions between aromatic π-systems and cations has been the focus of numerous efforts to explain biomolecular organization, establish new architectures, and to catalyze reactions, but these forces have yet to be explored as a sensing mechanism for detecting trace levels of aromatic VOCs. The research presented in this Chapter showed that linking alkali metal ions to the surface of Au MPCs-based chemiresistors delivers sensors with appreciable selectivity toward electron-rich aromatic VOCs. The trends in the observed response curves for the metal ion chemiresistors toward aromatic and non-aromatic VOCs, both in terms of metal ion composition and aromatic ring π-electron density, support cation-π interactions as a dominant mechanism for the responses. The many possible interactions between analytes

and Au MPCs functionalized with metal ions preclude a single mode of molecular association as being responsible for the overall sensor response. However, the present results point toward cation-π interactions as a promising research avenue to explore for selectively sensing aromatic VOCs due to the inherent polarizable and electrostatic nature of these molecular interactions.

CHAPTER 4

INTRODUCING A NEW APPROACH FOR SENSING TRICHLOROETHYLENE (TCE) IN AIR[c]

---

c A manuscript is being prepared including the research presented in this chapter for submission 2022.

4.1. INTRODUCTION

In this modernized world, synthetic chemicals are extensively utilized to achieve different industrial purposes. Among them, most organic solvents have been identified as harmful airborne volatile organic compounds (VOCs). Trichloroethylene (TCE) is one of the most harmful carcinogenic VOCs, as declared so by United States Environmental Protection Agency (EPA).[1,2] TCE is a halogenated alkene that is widely utilized as a chlorinated solvent in several industries. For instance, metal industries, such as automobile manufacturers, use TCE to degrease manufactured metal parts. TCE is used to spot-clean stains on clothing. It is also used as an extraction solvent in the textile industry.[3] Moreover, TCE is utilized as a chemical reagent to produce flame retardants, pharmaceutical compounds, pesticides, and poly(vinyl chloride) (PVC) plastics. In the aerospace industry, TCE is used to flush $O_{2\ (liquid)}$ and in refrigerants by serving to transfer low-temperature heat. Finally, TCE is present in several household items, such as adhesives, paints, varnishes, lubricants, paint removers, and in correction fluids.[1,3] TCE evaporates quickly to contaminate environmental air and any spilled TCE (e.g., industrial accidents) penetrates through soil to dissolve in ground water.[4] In cases involving spills, TCE in ground water can deposit in sediment and remain there for a long time. TCE enters our bloodstream by inhalation of TCE-contaminated air, through skin contact with TCE vapors or solvent, and ingestion of TCE contaminated water.[4] Once it is absorbed into the bloodstream, TCE travels into tissues having a good blood supply, such as kidneys, brain, liver, and body fat. Inside these tissues, TCE metabolizes into toxic trichloroacetic acid (TCA), and trichloroethanol (TCOH) (Scheme 4.1.) and these toxic metabolites alter the regular cellular functions, which leads to an increase in health risks.[5,6] Short term exposure to TCE

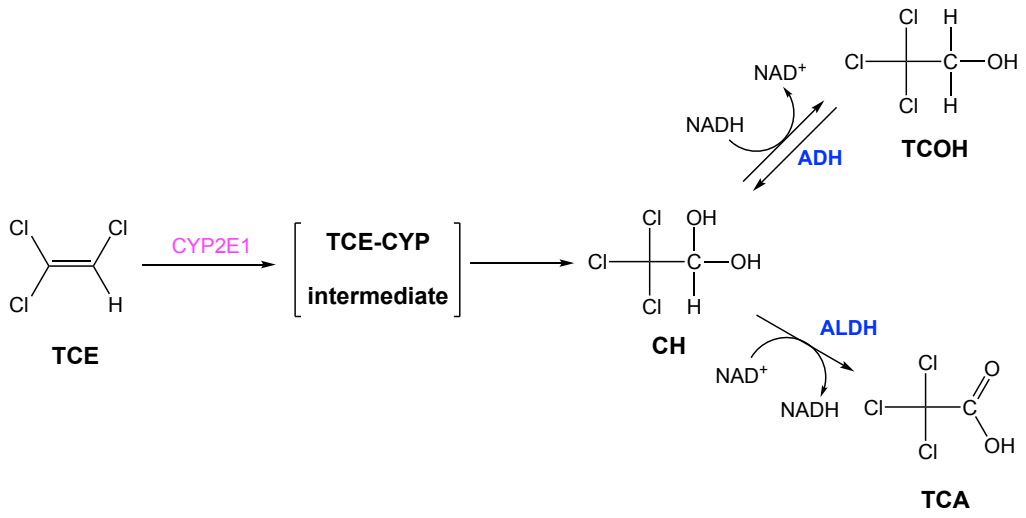

Scheme 4.1. Metabolism pathway of TCE to its carcinogenic trichloroacetic acid (TCA) and noncarcinogenic trichloroethanol (TCOH) by cytochrome P450 enzyme CYP2E1; Note: ADH = Alcohol dehydrogenase, ALDH Aldehyde dehydrogenase.[6]

will cause sleepiness, headache, blurred vision, dizziness, fatigue, eye irritations, and respiratory tract irritations, while long term exposure to high levels of TCE will increase the risks of liver and kidney cancers and non-Hodgkin's lymphoma.[7] Pregnant women and infants are also at high risk.[8] Thus, it is highly recommended to reduce TCE exposure by practicing good occupational health behavior by cleaning any contaminated environmental areas. TCE is of great interest and has been widely studied in terms of its chemical and physical properties, industrial and medical uses, metabolism, toxicity, prevention, and its detection in air, soil, and water.[7,9,10] Naturally, to protect human health, TCE environmental remediation is an important area of research.

4.1.1. TCE Detection Methods in Air, Water, and Soil

Table 4.1. Analytical methods used to detect TCE quantitatively.

Analytical method	Utilized technique	Reference
Gas Chromatography (GC)	for sample collection: - headspace analysis - membrane interface probe (MIP) - halogen specific probe - adsorbent (charcoal) based sample capturing and desorbing (CS_2) for analysis: - mass spectrometer (MS) - photoionization detector (PID) - electron capture detector (ECD) - flame ionization detector (FID) - helium detector	12, 13, 14, 15, 16
High Performance Liquid Chromatography (HPLC)		16
Ion Chromatography (IC)		16
Capillary Electrophoresis (CE)		16
High-Field Asymmetric waveform Ion Mobility Spectrometry (FAIMS)		16
Liquid Chromatography coupled with mass spectrometry (LC/MS)		16
Fourier Transform Infra-Red Spectroscopy (FT-IR)	- TCE Photooxidation on TiO_2	

	- piecewiselinear discriminant analysis (PLDA) - photoactivation of TCE by diphenylamine	17, 18
Spectrofluorimeter	- fluorescence measurements	19
Spectrophotometric colorimetry	- Fujiwara reaction	20
Raman Spectroscopy	- Fujiwara reaction - polyethylene polymer to concentrate TCE vapors and fiber optic probe for detection	20, 21, 22, 23
Tandem Mass Spectrometer (TAGA)		24
Potentiometer		25
Near – Infrared optical absorption spectroscopy	- multiplexed photonic crystal waveguides (PCWs)	26
Electrodeposition sensors		27
Fiber optic sensors	- Fujiwara reaction	28
Microbial bio sensors		29
Surface Acoustic Wave microchemical sensors	- carbon adsorbent polymer film with a quartz piezoelectric output transducer	30
Chemiresistors	- carbon polymer based	31
Microfabricated gas chromatography (μGC)	- thiol coated Au MPCs for chemiresistor arrays	32, 33

According to section 5(a) (2) of the Occupational Safety and Health Administration (OSHA) Act, the regulatory permissible exposure limit (PEL) for TCE is 100 ppm (an 8 hour time weighted average).[11] The EPA and National Institute for Occupational Safety

and Health (NIOSH) have established several analytical methods for TCE detection in air, soil, and water. As mentioned, gas chromatography (GC)[12] and GC coupled with mass spectrometry (GC/MS) are widely employed in the field.[13] Table 4.1 summarizes several analytical methods that have been utilized to analyze TCE quantitatively in air, water, and soil. Most of these methods are not well suited for detecting low concentrations (ppb to ppt) of TCE in air due to lack of sensitivity and selectivity, the need for sample preconcentration, high power consumption, sampling limitations, instrument cost and instrument complexity.

In addition to the above methods, several commercially available portable analyzers including GC/MS based CMS 200, CMS 100[34] and INFICON HAPSITE portable GC-MS[35] are used for TCE monitoring at ppm – ppt range within less than 10 minutes. (Figure 4.1.) These portable instruments are very effective for real time measurements of TCE in water and air than the previously mentioned laboratory instrumentation.

Figure 4.1. INFICON HAPSITE portable GC-MS. (Copied from Ref. 35)

Since TCE detection and environmental clean-up is a foremost responsibility, different analytical and engineering approaches have been extensively studied over several years to develop a simple, low-cost sensor for effective onsite measurement of harmful TCE vapors and its principal metabolites at ppb to ppt levels. Recent approaches include techniques such as infra-red spectroscopy,[17,18,26] spectrofluorimeter (fluorescence) measurements,[19] spectrophotometric colorimetry,[20] and Raman spectroscopy.[20-23] (Table 4.1) In most of these techniques, Fujiwara pyridine-alkali reaction has been improved and widely studied to determine TCE in air[20] and water.[22] In this specific reaction, a red color is developed in the reaction mixture when an organic halide is mixed with pyridine in the presence of an alkali (e.g., NaOH). The intensity of the color primarily depends on the halide reactivity. As not all the techniques are effective for real time analysis of TCE vapors in air, some groups have succeeded in developing real time monitoring of TCE, such as Karellas and Chen,[24] who developed a real time monitor to detect TCE and perchloroethylene (PCE) in ambient air by using a low-pressure chemical ionization source (LPCI) connected to a tandem mass spectrometer (TAGA).

Many researchers now are pursuing convenient means to directly measure TCE by developing sensors with properties like low cost, low power consumption, portability, and high sensitivity and selectivity. For example, fiber-optic-based sensors,[28] electrodeposition sensors,[27] and microbial biosensors[29] have been studied to monitor TCE. Some research groups have utilized the MEMS technology to detect TCE in air, soil, and water. Among them, Ho and coworkers[30,31,36] developed a microchemical sensor array and a surface-acoustic-wave (SAW) sensor using a GORE-TEX membrane to monitor several chlorinated VOCs including TCE in air, soil, and ground water *in-situ*. Also, they studied

the ability of carbon loaded polymeric chemiresistor arrays to characterize TCE quantitatively where sensing mechanism depend on TCE adsorption on to the matrix.[37]

4.1.2. Au MPCs-based Chemiresistors for TCE Detection in Air

Not many researchers have addressed the use of Au MPCs chemiresistors for TCE vapor monitoring in air. Of those that have, the studies were untargeted and relied solely on hydrophobic interactions for signal induction. Wohltjen and Snow[38] developed an alkanethiolate (octanethiol) coated Au MPCs chemiresistor and demonstrated its vapor sensing properties for toluene, TCE, water, and 1-propanol. They observed non-linear responses for all vapors and high selectivity and sensitivity for the hydrophobic analyte toluene and TCE vapors with negligible responses for the polar analytes water and 1-propanol. Organically interlinked Au MPCs based chemiresistors were synthesized by Joseph *et al*.,[39] using dodecylamine coated Au MPCs and either poly(propyleneimine) dendrimers of generation (G) G1-G5 or 1,6-hexanedithiol as linkers. The conductivity properties of each linked sensor film were demonstrated using the same panel of analytes studied by Wohltjen and Snow.[38] Joseph and co-workers observed strong responses to toluene and TCE vapors for the hexanedithiol linked Au MPCs chemiresistor. In both studies, (Joseph study and the Wohltjen study) van-der-Waals interactions causes the fast diffusion of TCE into the organic matrix to change the resistance. Furthermore, the modified GC/MS technique of microfabricated gas chromatographic instrumentation (μGC) has been widely utilized to improve the sensitivity and selectivity of GC for airborne VOCs sensing including TCE. Zellers and coworkers[32,33,40,41] have extensively studied the use of microsensor arrays in μGC as detectors to achieve desired limits of detection (LOD)

in very low concentration levels of ppb to ppt TCE onsite monitoring in indoor air. Their μGC consist of a micro-preconcentrator, dual-column temperature and pressure programmed separation module, and an integrated array of thiolate-monolayer protected Au MPCs chemiresistors.

4.1.3. Utilizing Cesium Ion-Chlorine Unusual Binding Ability to Detect TCE in Air

The use of functionalized Au MPCs based chemiresistors for selective TCE sensing in indoor and outdoor air has yet to be realized. This is our aim. We seek to use the thiol tuning ability inherent to Au MPCs to add cesium carboxylate functionality to the surface of the Au clusters to selectively interact with TCE. Our chemiresistor design and motivation for this project was influenced by several X-ray crystallography studies on Cs metal ion coordination to vinyl-chlorides as well as to other saturated chloro-substituted compounds. As reported by Bryan *et al.,*[42,43] a bidentate host-guest type coordination of two 1,2-dichloroethane (1,2-DCE) solvent molecules to the Cs^+ ion in the cesium complex of tetrabenzo-24-crown-8 via the four chlorine atoms[43] (Figure 4.2) and dichloromethane (DCM) via two chlorine atoms (Figure 4.3).[42]

Furthermore, Cametti *et al*.,[44] observed coordination of a Cs^+ ion of a CsF-Uranyl-Salen complex to a chlorine atom of a chloroform solvent molecule in η^1 fashion (Figure 4.4). Figure 4.4. A. shows the molecular structure of Uranyl-salen complex which was used to prepare a complex with CsF and this study was the first example of chloroform ligation to an alkali metal cation. Importantly, Smith *et al*.,[45] reported the coordination of a vinyl 1,2-dichloro unit to a Cs^+ ion of the herbicide picloram, and this interaction formed a stable metallocycle complex through a vinyl 1,2-dichloro unit (Figure 4.5).

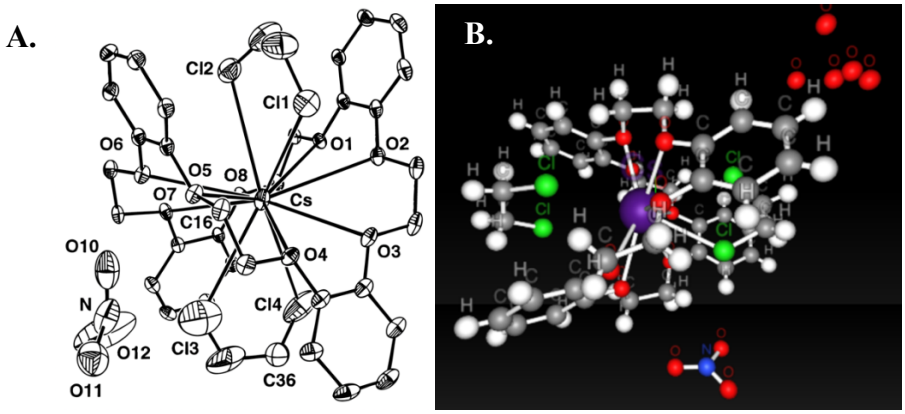

Figure 4.2. A. ORTEP plot and **B.** Computationally optimized molecular structure of [Cs-(tetrabenzo-24-crown-8)(1,2-dichloroethane)$_2$](NO$_3$)•H$_2$O and illustration of 1,2-dichloroethane coordination to Cs$^+$ ion. (Copied from Ref. 43)

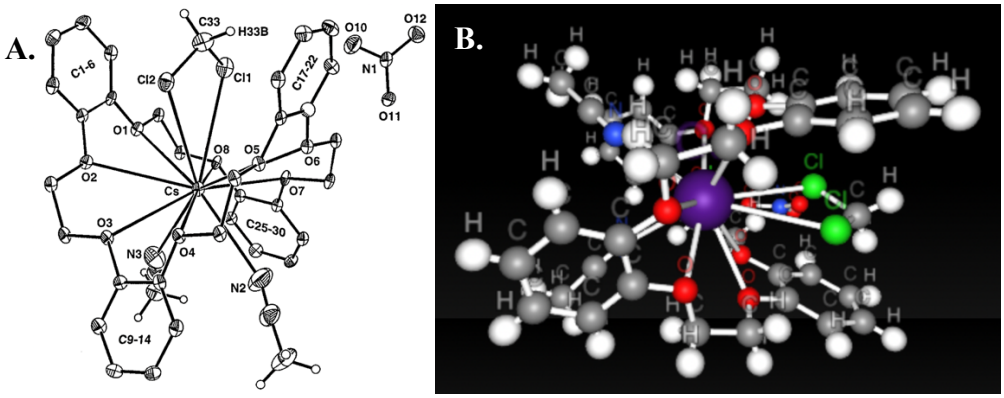

Figure 4.3. A. ORTEP drawing and **B.** Computationally optimized molecular structure of [Cs(tetrabenzo-24-crown-8)(η^1-NCMe)$_2$(η^2-CH$_2$Cl$_2$)][NO$_3$) and illustration of DCM coordination to Cs$^+$ cation. (Copied from Ref. 42)

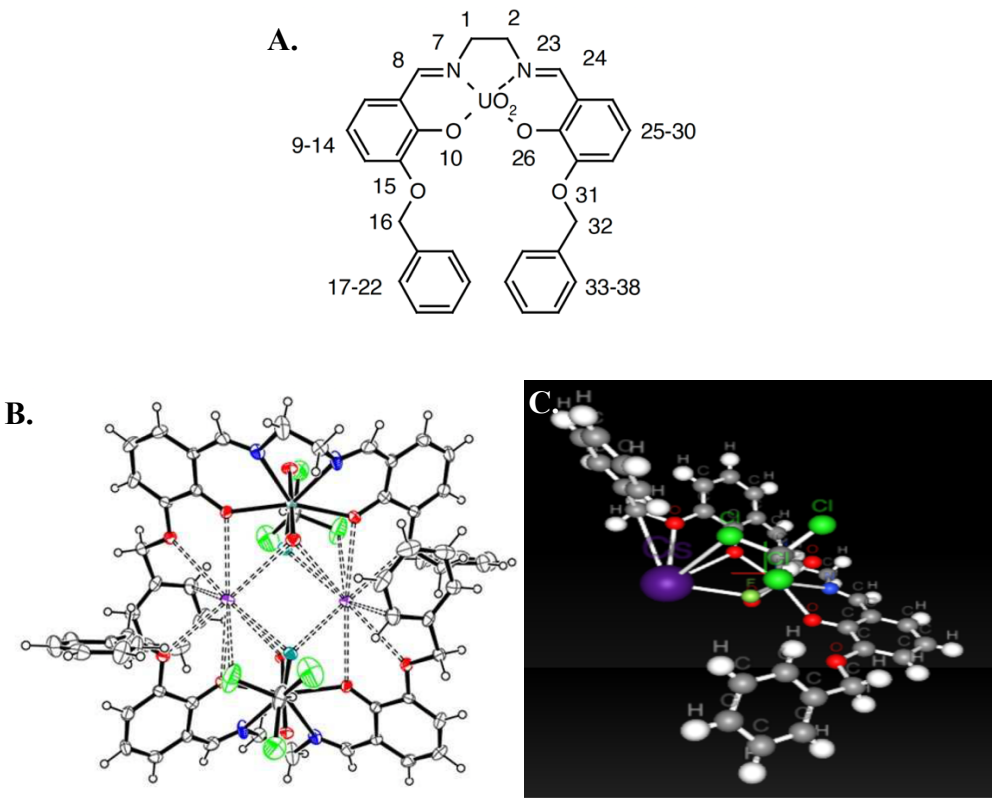

Figure 4.4. A. Molecular structure of Uranyl-salen complex, **B.** ORTEP illustration, and **C.** Computationally optimized molecular structure of Uranyl-salen.CsF.$CHCl_3$ complex and ligation of $CHCl_3$ to Cs^+ ion. (Copied from Ref. 44)

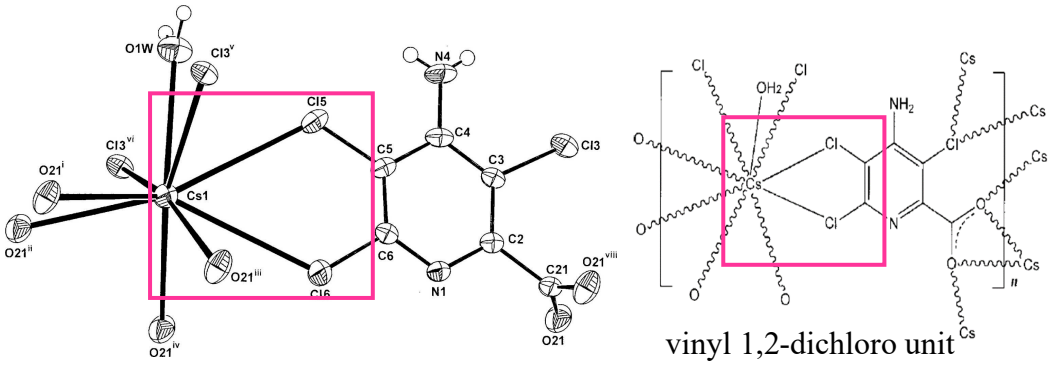

Figure 4.5. A. ORTEP plot and **B.** Illustration of divinyl chloride coordination to Cs^+ ion in $[Cs(C_6H_2Cl_3N_2O_2)(H_2O)]_n$ complex. (Copied from Ref. 45)

Also, Smith and coworkers[46,47] studied the crystal structures of Na^{+}, Mg^{2+}, Cu^{2+} and Mn^{2+} salts of herbicide picloram and did not report any metal ion coordination to organochlorine for any of these cations-chlorine coordination appears to highly favor the cesium ion. In addition to these X-ray crystallography studies, close association of the cesium cation with chlorine substituents is further noted in work by Aggarwal *et al.,*[48] who studied the TCE sorption ability of smectite clay exchanged separately with Cs^{+}, K^{+}, or Ca^{2+} ions as interlayer cations (Figure 4.6.). According to their report, the Cs^{+}-saturated

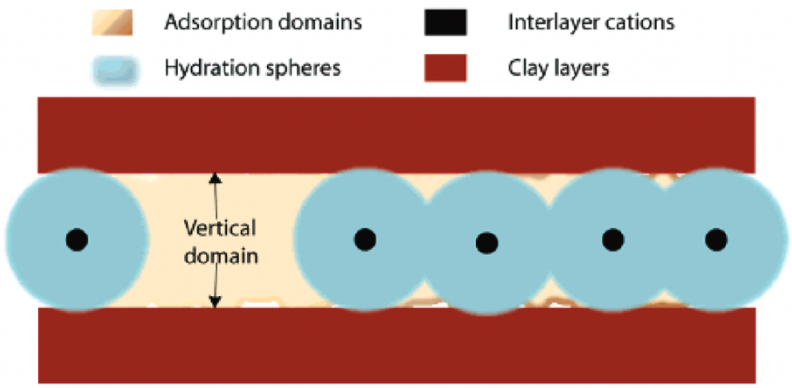

Figure 4.6. Schematic illustration of smectite clay mineral interlayers for TCE adsorption. (Copied from Ref. 48)

smectite clay absorbed more TCE than the clays exchanged using the other metal cations. Together, these studies strongly support that there is a significant interaction between the Cs^{+} ion and Cl atoms of organochlorine compounds, which is an interaction that remains to be thoroughly studied (or exploited). We surmise this interaction can be influenced by the electronic and steric environment of both the Cs cation and chlorine ligand. Therefore, it may be possible to observe differences in binding energy and the bond strength of the

coordination based on how the Cs^+ is presented. Based on this background, we seek to harness the Cs^+ ion coordination to TCE of a Cs^+-functionalized Au MPCs chemiresistor to selectively detect TCE. Figure 4.7. illustrates the overall idea of our approach graphically. This study is the first attempt at using a Cs^+ ion-functionalized Au MPCs chemiresistive sensor for detection of TCE and other chlorinated VOCs in polluted air.

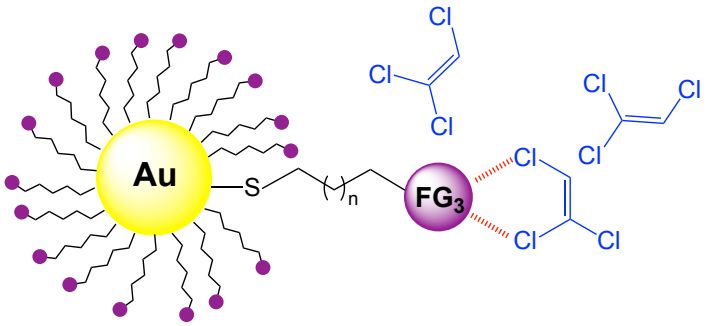

Figure 4.7. Graphical Illustration of the functionalized Au MPCs chemiresistor to selectively detect TCE. Note: Only one ligand is emphasized in Au MPCs and FG_3 represents the Au MPCs surface bound functionality.

4.2. RESULTS AND DISCUSSION

All the Au MPCs in this study were synthesized by me. The microsensor chip developed by Sujoy Halder in Chapter 3 was used to prepare the Au MPCs chemiresistors. Sensor measurement studies were carried out by Sujoy and me.

In this work, morphology, hydrophilic-hydrophobic character, and ionic strength of the Au MPCs chemiresistive film for chlorinated TCE vapor sensing was studied. For our study, the oxime ether functionalized Au MPCs **11**/C6 in Chapter 3 was utilized to synthesize cesium-carboxylate functionalized Au MPCs **12**-Cs^+/C6 by ester saponification

using cesium hydroxide. The synthesized Au MPCs **12-**Cs^+/C6 (particle diameter ~ 2 nm) were characterized using UV-Vis and EDS methods. As explained in the experimental section, another three different Cs^+ ion functionalized Au MPCs chemiresistive films were prepared for further investigations. All these films were drop casted onto the IDEs to prepare reasonably consistent four different chemiresistors.

As described in previous chapters, the sensing materials are the dominant component of a chemiresistive array. The sensor response is highly dependent on the morphology of the materials and vapor selectivity is decidedly affected by materials' specific non-covalent interactions with the vapor analytes, like through cation-π interactions, halogen bonding, metal ion coordination, Van der Waals, and hydrogen bonding. So, in this study the morphology of the thiol ligand was decorated with an oxime ether functionality to increase the sensor sensitivity and cesium-carboxylate functionality to enhance the selectivity towards chlorinated vapors.

Au MPCs **12-**Cs^+/C6 sensor exhibits the same resistance changing patterns for all the analyte vapors used as the previously described **12**-K^+, Na^+ and Li^+ sensors in Chapter 3. The rapid increase in the conductance (decrease in the resistance) might be due to the high dielectric constant of the organic matrix and the specific non-covalent interaction between the analyte vapors and the cesium cation at the surface of the functionalized Au MPCs. Furthermore, electron delocalization in the aromatic ring offers a small β_d (tunneling coefficient) and it enhances the electronic conductivity through the film. These factors are prominent at changing the sensor resistance via the well-known film swelling phenomenon.

Initially, the sensor **12**-Cs^+/C6 response pattern for different vapor analytes including chlorinated, aromatic, polar, and non-polar were studied. In this section, the chemiresistive film morphology for analyte selectivity was observed. Figure 4.8 shows the **12**-Cs^+/C6 sensor response data for all the analytes used at 0.1 ppm, 0.5 ppm, 1.0 ppm, 2.5 ppm and 5.0 ppm vapor concentrations. To our surprise, we observed non-linear responses for both chlorinated vapors with high selectivity and sensitivity and linear, low responses for all other analytes. It is not a surprise that response of Au MPCs **12**-Cs^+/C6 sensor towards benzene is mainly due to the cation-π interaction between the cesium cation and the π-electron density of the benzene (delocalized π electron density) and that this response is higher than the cyclohexene, which has a lower π-electron density than benzene. Among

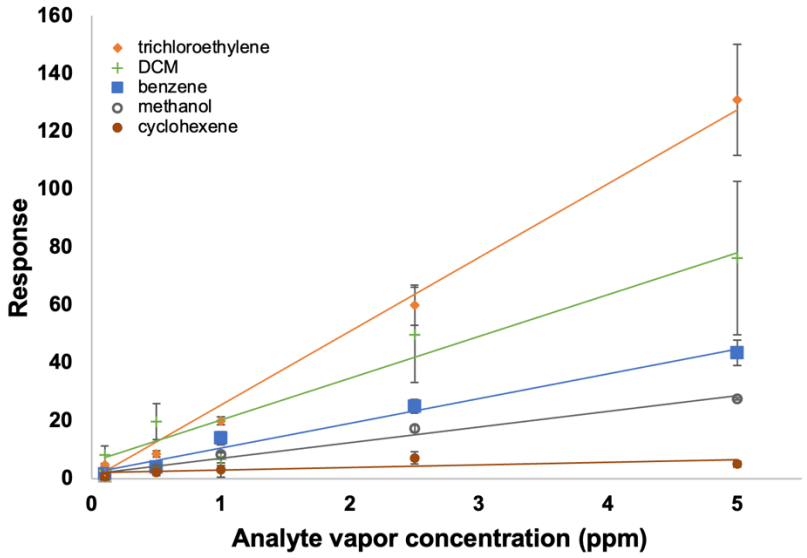

Figure 4.8. Response of Au MPCs **12**-Cs^+/C6 sensor to different VOCs. (Chlorinated vs aromatic vs polar vs non-polar). Each point indicates the average of n = 3 measurements. The variability of these measurements is shown by the error bars.

the chlorinated analytes, TCE exhibits the highest response at high vapor concentrations than DCM. TCE consists of three high electronegative chlorine atoms and those atoms pull σ and π electron density toward themselves and create a high electron density around the Cl atoms. This high electron density arrangement around the Cl atoms can enhance the stable 5-membered metalocylcle formation between the vinyl 1,2-dichlorounit and the Cs^+ and it might be the reason to exhibit higher sensor response than the other analytes. Due to the presence of high electronegative chlorine atoms, TCE has a low π electron density relative to benzene and cyclohexene. The choro substituents are electron withdrawing, and these substituents decrease the π electron density of TCE and make them less favorable for cation-π interaction. So, it is reasonable to expect that TCE will not interact with the cesium cation at the surface of the Au MPCs through the π electron density of alkene functionality, but they do interact with the chemiresistive film, presumably through the aforementioned, unusual cesium-chlorine coordination. However, the strength of cation-π interaction in benzene is lower than the chlorine-cesium cation coordination in TCE and DCM. Furthermore, Au MPCs **12-**Cs^+/C6 sensor responded to polar methanol vapors in a considerable strength. This might be due to the methanol oxygen coordination to the cesium cation which is known.[49] Importantly, this sensor shows a reversible and fast response for all the vapor analytes used.

In the interest of this large Au MPCs **12-**Cs^+/C6 sensor responses towards chlorinated analytes, we continued our study using chlorinated alkanes. Figure 4.9 compares the sensor response values of chlorinated alkane vapors with TCE vapors. Interestingly, TCE still exhibits a higher response for this sensor. Structurally, TCE, and

1,2-dichloroethane features vicinal 1,2 dichlorides where chloroform, DCM and 1,1-dichloroethane bear geminal chlorides. So, it can be suggested that analytes with vicinal vinyl 1,2-dichloro units and vicinal 1,2-dichlorounits might have the affinity to develop a metallocycle via coordination of 1,2-dichloro unit to cesium cation as proposed by Smith *et al*.,[45] and this formation is stronger in analytes with vicinal vinyl 1,2-dichloro units (TCE) due to the high electron density distribution around the chlorine atoms. Also, the cesium cation interacts more favorably with chlorine due their soft Lewis acid–base nature. DCM has a relatively high dipole moment (Table 4.2) compared to chloroform and exhibits a higher response than chloroform. DCM has two geminal chorines and their electron density is higher than the electron density around Cl atoms in chloroform and this high

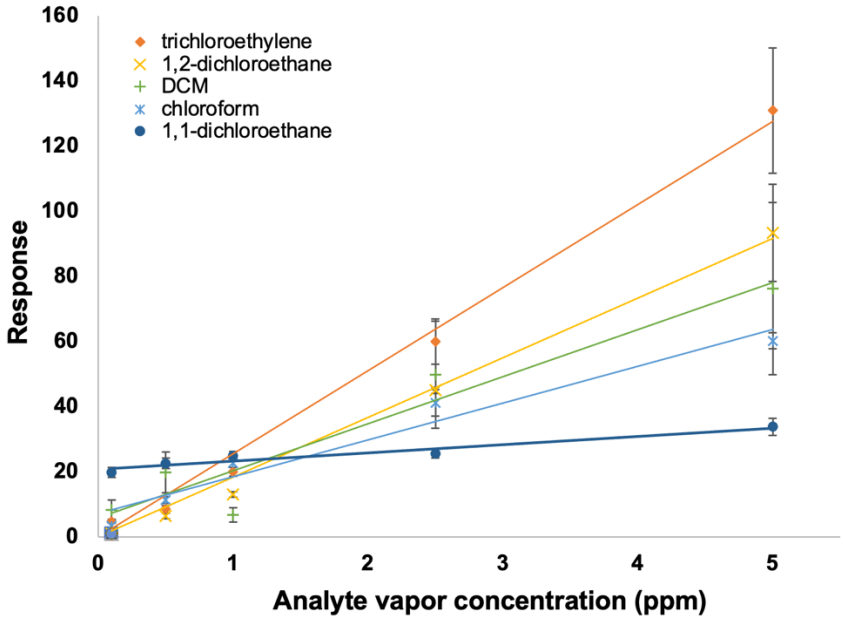

Figure 4.9. Response of Au MPCs **12**-Cs^+/C6 sensor to chloroalkanes. Each point indicates the average of n = 3 measurements. The variability of these measurements is shown by the error bars.

electron density on Cl atoms might be enhanced the Cs-Cl coordination in DCM than chloroform. It suggests suggests that net molecular dipole moment also plays a role to enhances the cesium-chlorine coordination. But conversely, geminal chlorinated 1,1-dichloroethane, which has a higher dipole moment than DCM and chloroform, shows a lower response to Au MPCs **12-**Cs^+/C6 sensor at high vapor concentrations (above 1 ppm) and higher responses at low vapor concentrations (below 1 ppm) than other analytes. However, when increasing the 1,1-dichloroethane concentration, the sensor response did not increase significantly. So, it can be assumed that the **12-**Cs^+/C6 sensor is already saturated for 1,1-dichloroethane and the sensing material is not sensitive to 1,1-dichloroethane vapor. Below 1 ppm chloro analyte vapor concentrations, this sensor is not discriminative, and it might be due the other molecular interactions that we are not able to understand at this point.

Table 4.2. Dipole moments μ (D) of analytes used.[50]

Analyte	**Net dipole moment μ / D**
1,2-Dichlorobenzene	2.54
1,1-Dichloroethane	2.35
cis-1,2-dichloroethylene	1.9
1,2-Dichloroethane	1.86
Methanol	1.70
Dichloromethane (DCM)	1.55
1,1-dichloethylene	1.3
Chloroform	1.02
Trichloroethylene (TCE)	0.88
Cyclohexene	0.33
Benzene	0
trans-1,2-dichloroethylene	0
Tetrachloroethylene (PCE)	0

To further understand this specific coordination interaction for TCE and other chlorinated compounds as well as Au MPCs **12**-Cs^+/C6 sensor selectivity for those analytes, a new panel of chlorinated hydro alkenes were utilized as analyte vapors. Figure 4.10 summarizes the Au MPCs **12**-Cs^+/C6 sensor responses data for several chloroalkenes. Excitingly, Au MPCs **12**-Cs^+/C6 sensor shows higher responses for all the concentrations of vicinal vinyl 1,2-dichloro unit-containing alkenes than the geminally chlorinated 1,1-dichloroethene. This observation strongly suggested that the previously explained metallocycle formation via vinyl 1,2-dichlorounit coordination to cesium cation is prominent and can be harnessed as a recognition element for TCE sensing. Among all the analytes used, 1,2-dichlorobenzene features the highest net dipole moment (Table 4.2) and

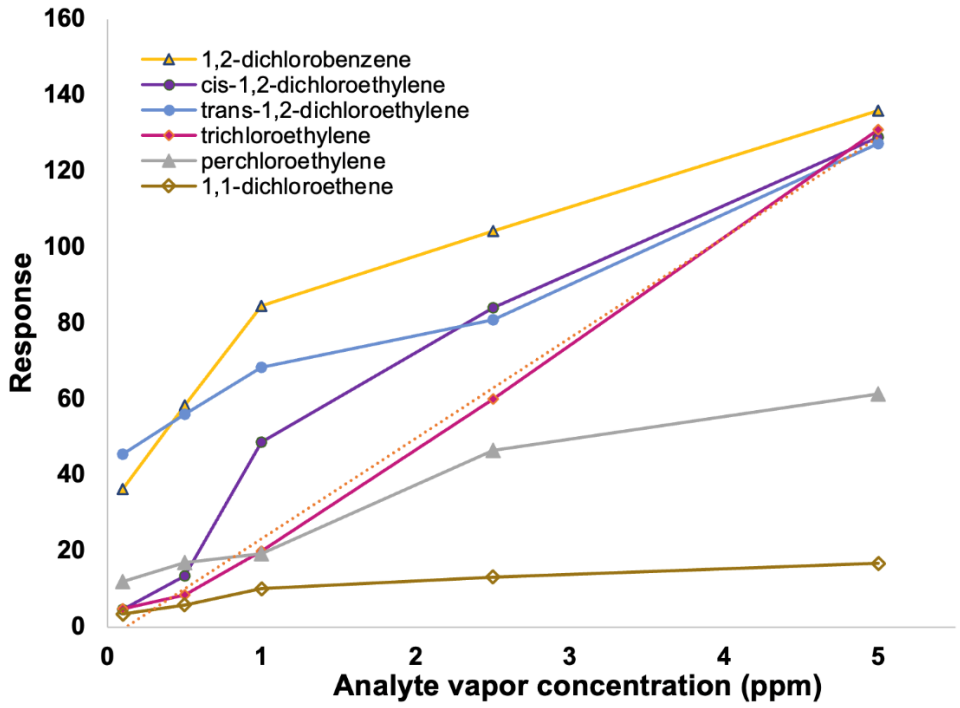

Figure 4.10. Response of Au MPCs **12**-Cs^+/C6 sensor to chloroalkenes.

the vinyl 1,2-dichlorounit which strongly contributes to chlorine coordination to cesium cation. Cation-π interaction is also possible between the cesium cation and the aromatic π electron density, but it appears not to be the dominant factor for this high response value. Due to the combination of all the factors, 1,2-dichlorobenzene exhibits the highest sensor response for Au MPCs 12-Cs^+/C6 sensor at high vapor concentrations (above 1 ppm) than other analytes. Also, 1,2-dichlorobenzene shows a linear response at high concentration vapors (above 1 ppm). According to the same reasons as 1,2-dichlorobenzne, *cis* 1,2-dichloroethylene shows overall higher sensor response than TCE due the high electron density around the chlorine atoms which enhances the Cs-Cl binding interaction. *cis*-1,2-Dichloroethylene, *trans*-1,2-dichloroethylene and 1,1-dichloethylene are geometric isomers, but they are differing significantly in dipole moments. *trans*-1,2-Dichloroethylene exhibits higher sensor response than TCE and it might be due to the high electron density around the chlorines in *trans*-1,2-dichloroethylene. Since the two chlorine atoms in *trans*-1,2-dichloroethylene are positioning in two sides, there is not any possibility to form a stable 5-membered metallocycle through interaction between the cesium cation and the vinyl 1,2-dichloro unit. But those two chlorine atoms can easily interact with two cesium cations, and it might be the reason to exhibit high response to this sensor. Perchloroethylene shows lower response than TCE and this might be due to the low electron density around the chlorine atoms than TCE. This observation suggested that if the electron density around the chlorine atom is low, the Cs-Cl interaction will be less, and it will produce a low sensor response. Interestingly, 1,1-dichloroethene which has two geminal chlorines shows lower response to this sensor for all the concentrations of 1,1-dichloroethene vapor used. This observation supported the previously explained sensor response trend (Figure 4.9) for

anlytes with vicinal vinyl 1,2-dichloro unit, vicinal 1,2-dichlorounit and geminal chlorines. However, 1,2-dichlorobenzene, *trans* 1,2-dichloroethylene, and *cis* 1,2-dichloroethylene are neither widely employed in industry nor declared as a harmful VOC. The Au MPCs 12-Cs^+/C6 sensor response profile in Figure 4.11 indicates the sensor responses for all the analytes we used and TCE vapor responses are relatively significant.

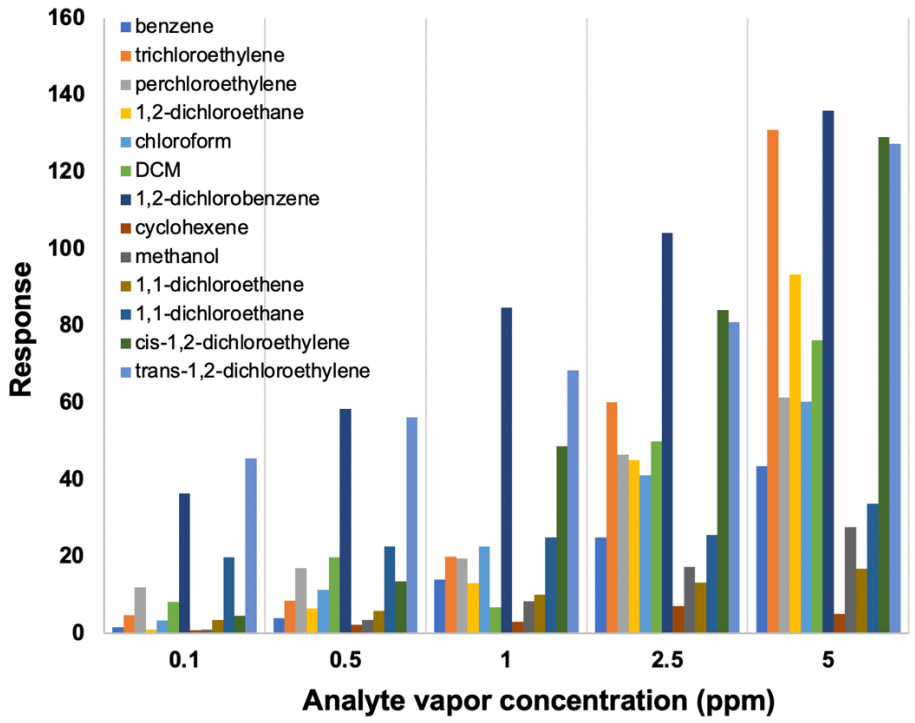

Figure 4.11. Response of Au MPCs **12-Cs^+/C6** sensor to different VOCs including aromatic, polar, non-polar, chloroalkanes and chloroalkenes.

To study the effect of morphology and the hydrophobic-hydrophilic character of Au MPCs chemiresistive film for TCE sensing, another three different Au MPCs/Cs^+ sensors were prepared (Table 4.3) and their response pattern for TCE vapors were observed (Figure 4.12). The initial film resistance value for each sensor was mentioned in the table

Table 4.3. Different Au MPCs chemiresistive films for TCE selectivity studies.

Sensor	Au MPCs chemiresistive film	Initial film resistance
C12/Cs$^+$-MUA	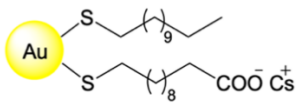	0.75 x 10^6 Ω
Cs$^+$-MUA	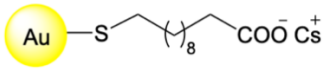	0.4 x 10^9 Ω
19-Cs$^+$	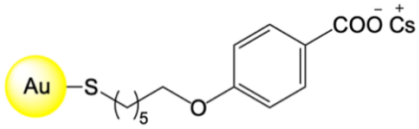	60 x 10^9 Ω
12-Cs$^+$/C6	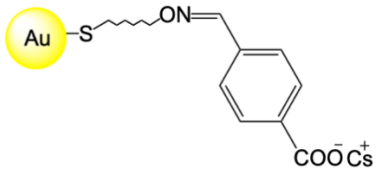	2 x 10^9 Ω

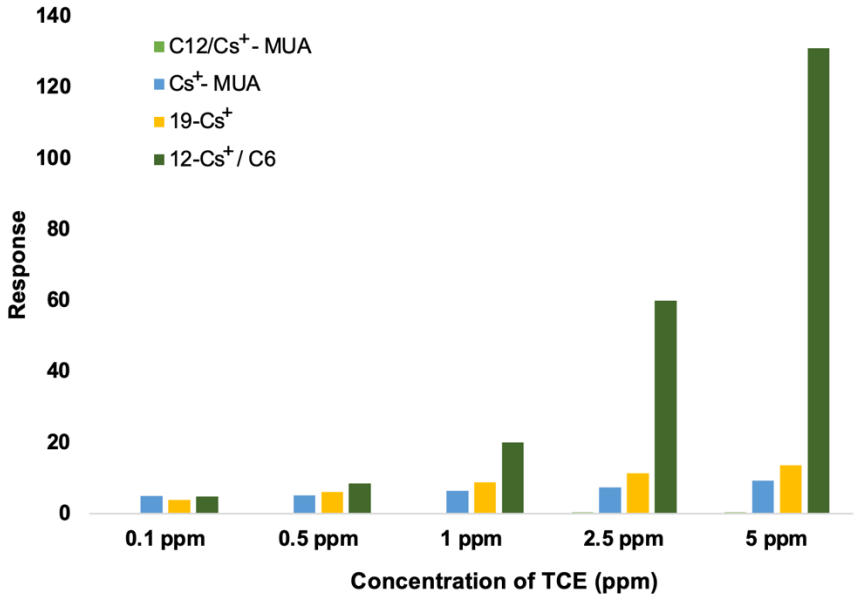

Figure 4.12. Sensors' response to TCE in synthetic air

4.3. As mentioned in the chapter 3, place-exchanged film exhibts the lowest initial resistance and the highest resistance is given by the chemiresistive film with ether linkage in sensor 19-Cs^+. Interestingly, all the sensors have different TCE selectivity and sensitivity. The sensor developed with mixed monolayer Au MPCs (C12/Cs^+-MUA) show a negligible response for all the TCE vapor concentrations than other sensors. When compared to the Cs^+-MUA sensor, the C12/Cs^+-MUA sensor provides a low cesium cation density for dominant chlorine-cesium cation coordination interactions, hence it shows lower sensor response to TCE vapors. Also, the C12/Cs^+-MUA sensor consists of more hydrophobic organic matrix environment than the other sensors. As we know, the polarity of a molecule is given by its molecular net dipole moment, and it shows the overall electron distribution among the atoms of the molecule. Chlorine has a much larger atomic mass and is more electronegative than hydrogen and carbon. TCE consists of unevenly distributed chlorine atoms (vicinal (1,2) and geminal (1,1)), so its electron density distribution produces a net molecular dipole moment to make TCE a polar molecule. The polar TCE vapor molecules have a negligible interaction with the hydrophobic organic matrix of both Cs^+-MUA and C12/Cs^+-MUA sensors. The response profile (Figure 4.12) indicates that sensors with high hydrophobicity showed lower sensor response to TCE with low sensitivity and this suggested that hydrophobicity also contributed to the sensor response. Thus, it can be concluded that dipole moment does not have a major influence on response. But it may contribute to the analyte adsorption.

The electronic properties of matrix organic ligands in each sensor are of great interest. Sensor 19-Cs^+ and 12-Cs^+/C6 have a less hydrophobic organic matrix with compared to the previously described other two sensors. Also, these aromatic

functionalized Au MPCs display different sensory responses depending on the nature of the thiol chain attached to the aromatic group. Our major sensor 12-Cs^+/C6 offers high response for all the TCE vapors and the only difference between the sensor 19-Cs^+ and sensor 12-Cs^+/C6 is the presence of an oxime ether linkage in 12-Cs^+/C6 sensor. So, this arrangement provides a highly conjugated electronic system which enhances the electron tunneling through the organic matrix than is possible in the other ligands studied. Furthermore, the nitrogen in the oxime ether linkage might also provide a coordination sphere for cesium cations, which could influence the cesium-chlorine coordination. The coordination chemistry of alkali metal ions with the organic ligands is not well studied compared to the transition metal ion coordination. This may be due to the weak complexing abilities of alkali metal ions than the transition metal ions. Alkali metal ions consist of filled *d* and *f* shells and lack of partially filled *d* or *f* shells cause the weak complexing abilities with other ligands. However, it can be believed that the oxygen of the ether functionality (sensor 19-Cs^+) or the nitrogen of the oxime ether functionality (sensor 12-Cs^+/C6) may coordinate with Cs^+ ion through electron donor acceptor interaction, hence accommodating more binding motifs for chlorinated hydrocarbons. In general, due to the high electronegativities of oxygen and nitrogen, they have sufficient ionization potentials and can interact with metal ions attractively. For instance, X-Ray crystallography studies on alkali metal ion coordination proves that crown ethers and macropolycylic amines have high cation binding affinities and that driving force is based on this electronegativity nature.[51] The formation of macrocyclic motif of oximic nitrogen interaction with the transition metal ions are known.[52] However no study has been reported about the chemistry of oxime/alkali metal complexes. As mentioned earlier, sensor 12-Cs^+/C6 carries an oxime

ether functionality and if the cesium cation bound with oximic nitrogen as well as with the carboxylate functionality, this sensor should carry high cesium content than the sensor 19-Cs^+. The EDX studies (Figure 4.15 and 4.16.) showed that the sensor 12-Cs^+/C6 has 64.02 % and the sensor 19-Cs^+ has 62.11 % of cesium content by total atomic weight of Au and Cs. These results suggested that both sensors have similar binding interactions with Cs^+ ions and that the 12-Cs^+/C6 sensor provides slightly a little more binding sites for incoming TCE vapors than sensor 19-Cs^+.

It appears that the high response and selectivity of the 12-Cs^+/C6 sensor towards TCE is primarily dependent on some form of cesium-chlorine coordination between the analyte TCE vapors and the cesium cation in the organic matrix of the Au MPCs chemiresistive film. This interaction has not been studied for chlorinated VOCs sensing previously, hence it is crucial to understand the factors that affect this interaction to further improve sensitivity and selectivity of an Au MPCs chemiresistor for TCE sensing. The research studies about halocarbon interaction with the cations are known. As mentioned earlier, halocarbons have an attached high electronegative halogen, C-X (X = F, Cl, Br, I), and it has been shown that this functionality can interact with electron deficient cations through cation-dipole interactions.[53] Electron donor acceptor property on C-Cl----M^+ (M^+ = metal cations) studies are not known however, C-F----M^+, C-Br---- M^+ are known.[54] Takemura *et al*., investigated the C-F----M^+ interaction between several alkali metal cations (Li^+, Na^+, K^+, Cs^+ and NH_4^+) and the oxygen and nitrogen bearing cage compounds having fluorobenzene units as donor atoms.[54,55] Crystallographic studies were used to analyze the bond strengths and they demonstrated that shorter bond length for C-F----M^+ than those of O----M^+, and N----M^+ for all the metal cations used. According to this study,

it is a fact that C-F----M^+ cation-dipole interaction involves a relatively significant attractive force and C-F (C-X) interacts more strongly with metal cations than amine nitrogen and ether oxygen. Takemura *et al*., stated that the cation-dipole interaction can be the dominant factor in C-F----M^+ interaction rather than a coordination bond. Also, it is proved that there is an electron transfer from the fluorine atom to the metal cation.[55] Due to the large ionization potential of F and lack of available d orbitals of alkali metal cations for dative bond, fluorine forms a smaller dative bond with the cation. In our study, we focus on the C-Cl----Cs^+ interaction, where chlorine atom has relatively the same electronegativity strength (3.15) as nitrogen (3.04) and lower strength than oxygen (3.44).[56] By considering the electron distribution and atomic radius of N, O, and Cl, it is reasonable to believe that electron-donating ability is higher in C-Cl since the electrons are loosely attached to Cl nucleus than N.

4.3. CONCLUSION

Cesium ion functionalized Au MPCs chemiresistor (Au MPC/Cs^+) responses to chlorohydrocarbons are greatly affected by the morphology, hydrophilic-hydrophobic nature, and the dielectric constant of the chemiresistive film (organic matrix). The net molecular dipole moment, strength of C-Cl----Cs^+ dipole-cation interaction, and presence of a vicinal or vinyl 1,2-dichloro unit that can form a stable metallocycle also influence the selectivity and the sensitivity of the Au MPC/Cs^+ chemiresistor for chlorohydrocarbons detection. Moreover, the strength of the C-Cl----Cs^+ dipole-cation interactions is correlated with the dipole moment magnitude of the chlorohydrocarbons and the alignment of the cesium cation with the dipole moment vector in the C-Cl----Cs^+ complex.

We have observed that Cs^+-carboxylate functionalized Au MPCs chemiresistive films function as highly selective chemiresistors for TCE sensing in air. We surmise the key interaction that contributes to sensor response harnesses a bidentate (i.e., metallocycle-like) coordination of TCE to cesium cation in the organic matrix. Further studies are required to examine the robustness of the stable metallocycle complex formation with cesium cation. This work suggests that additional research be conducted to expand the potential of CX---M^+ interactions as a means to develop chemiresistors for halogenated VOCs analysis.

4.4. FUTURE STUDIES

Further experimental studies are required to optimize Cs^+-carboxylate functionalized Au MPCs chemiresistors for detection of harmful TCE vapors in air. It is possible to alter the electronic properties of the Cs^+-carboxylate functionalized thiol ligand to enhance the sensitivity and selectivity for TCE by changing the molecular structure of thiol ligand. For instance, additional Cs^+ molecules can be added through di or monosubstituted aryl ester saponification strategy. Furthermore, carboxylate ion fuctionality can be replaced by other aninons like sulfonates or phenoxides to alter the electronic properties of the thiol ligand as well as strength of binding interactions of Cs^+ to Cl atoms. Different metal ion-carboxylate functionalized Au MPCs of 12-Cs^+/C6 sensor can be used to further confirm the metallocycle formation between the cesium cation and the vinyl 1,2-dichloro unit.

CHAPTER 5

EXPERIMENTAL PROCEDURES

5.1. GENERAL EXPERIMENTAL

5.1.1. Materials

All solvents and reagents used in this thesis were reagent grade and were purchased either from Sigma Aldrich, VWR or TCI. All the reagents were used as received unless otherwise indicated. Dry solvents were prepared in the lab according to the established methods. Dry dichloromethane (DCM), dimethylformamide (DMF), and acetonitrile were obtained by distillation from CaH_2. Dry toluene and tetrahydrofuran (THF) were prepared by distillation over sodium metal and benzophenone. Dry chloroform ($CHCl_3$), methanol (MeOH), and ethanol (EtOH) were obtained by storing over oven dried (300 °C, 48h) 4°A molecular sieves. Nanopure water, obtained using a Barnstead water ultra-purification system (ThermoFisher, R_s = 18.2 MΩ•cm) was used to prepare the Au MPCs. Synthetic air (< 4 ppm of moisture) and nitrogen gas were purchased from Welders Supply Company, Louisville, KY, USA. Tedlar bags, acquired from Supelco (Bellefonte, PA, USA) were used to prepare the analyte samples.

5.1.2. Characterization

Thin-layer chromatography (TLC) technique was used to monitor the reaction progress and pre-coated silica plates (EMD Silica Gel 60 F254) were used. UV active compounds were visualized using the UV light (254 nm). General visualization was carried out by staining the TLC plates with PAA stain (2.5% p-anisaldehyde acid/ethanol solution) or ninhydrin stain (10 g ninhydrin in 100 mL of *n*-butanol and 3 mL of AcOH). Some of the synthesized compounds were purified using silica gel 60 (230-400 mesh) flash column chromatography. A Varian 400 MHz or 500 MHz spectrometer was used to obtain ^{1}H and

^{13}C nuclear magnetic resonance (NMR) spectra. The chemical shift values were reported in ppm relative to the solvent residual peak CD_3OD (3.31 ppm for ^{1}H NMR and 49.00 ppm for ^{13}C NMR), DMSO-*d6* (2.50 ppm for ^{1}H NMR and 39.52 ppm for ^{13}C NMR) or $CDCl_3$ (7.26 ppm for ^{1}H NMR and 77.23 ppm for ^{13}C NMR). A Perkin-Elmer Fourier-transform infrared (FTIR) spectrophotometer was used to record infrared spectra and a Varian CARY 50 Bio UV–visible spectrophotometer was used to collect UV-visible spectra. CH_2Cl_2 and MeOH were used as blank solutions in a 1 cm quartz cuvette to obtain fast scans between 400-900 nm wavelength range. Melting points were acquired using Fisher-Johns melting point apparatus. X-Ray photoemission spectroscopy (XPS) measurements were performed using a dry solid sample on K-alpha (ThermoFisher), which uses soft Al Kα X-ray as monochromatic source (E_{photon} = 1486.7 eV). Three points on the sample powders surface were used for analysis (X-ray probe size of 200 μm). Scanning Electron Microscopy (SEM) performed using a Tescan Vega 3 system equipped with an EDAX energy-dispersive X-ray spectroscopy (EDS) detector (acceleration voltage 200 kV under vacuum) was used to confirm the presence of potassium and sodium metals in the synthesized metal-ion functionalized Au MPCs. Thermogravimetric analysis (TGA) data were recorded using a TA Instruments Q600 SDT thermal analyzer with a heating rate of 10 °C min^{-1} from 25 to 800 °C under a nitrogen atmosphere.

The average Au MPCs particle size was measured using transmission electron microscopy (TEM) images that were acquired using a FEI Talos F200X (Thermo Scientific) high-resoultion transmission electron microscope (HRTEM) operated at 200 kV. Au MPCs sample powders were dispersed in CH_2Cl_2 by bath sonication and then transferred onto a lacey carbon grid for TEM imaging.

5.2. INDEX OF PROCEDURES

5.3. EXPERIMENTAL PROCEDURES OF CHAPTER 2

5.4. EXPERIMENTAL PROCEDURE OF CHAPTER 3

5.5. EXPERIMENTAL PROCEDURE OF CHAPTER 4

5.3. EXPERIMENTAL PROCEDURES OF CHAPTER 2

5.3.1. Thiol Ligands Synthesis

The organic compounds in this chapter were initially synthesized by Dr. M. V. R. Raju. The following described compounds were resynthesized by me.

5.3.1.1. Synthesis of Alkoxyurea Thiol – Series I

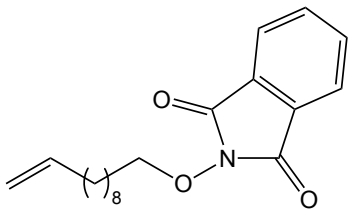

2-(Undec-10-en-1-yloxy)isoindoline-1,3-dione (1). *N*-hydroxyphthalimide (NHP) (11.15 g, 68.38 mmol) and sodium bicarbonate (5.744 g, 68.38 mmol) were dissolved in dry DMF (100.0 mL) and degassed the mixture under argon for 5 min. The solution mixture was slowly heated up to 80 °C and 11-bromo-1-undecene (5.00 mL, 22.8 mmol) was added drop wise followed by refluxing the reaction mixture for 18 h under argon. The reaction was stopped after 12 h and allowed to cool down to room temperature. The mixture was diluted with water (80.0 mL) and extracted with ethyl acetate (4 × 60.0 mL). The organic layers were combined and washed with 5% LiCl solution (3 × 50.0 mL) to remove remained DMF, and then it was concentrated by rotary evaporation. SiO_2 column chromatography was used to purify the crude product using 4:1 mixture of Hexane: EtOAc, to afford 5.887 g (82%) of **1** as a white solid; TLC, R_f = 0.55 (4:1 Hexane: EtOAc); IR 2923, 2851, 1787, 1730, 1464, 1399, 1186 cm^{-1}; 1H NMR ($CDCl_3$, 500 MHz) δ 7.82-7.81(m, 2H), 7.73-7.71 (m, 2H), 5.80-5.78 (m, 1H), 4.99-4.90 (m, 2H), 4.19 (t, J= 5.6 Hz,

2H), 2.02-2.00 (m, 2H), 1.78-1.75 (m, 2H), 1.46-1.44 (m, 2H), 1.32-1.27 (m,10H) ppm; ^{13}C NMR ($CDCl_3$, 100 MHz) δ 163.7, 139.2, 134.5, 129.1, 123.5, 114.2, 78.7, 33.9, 29.5, 29.4, 29.3, 29.2, 29.0, 28.2, 25.6 ppm.

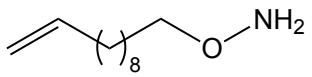

***O*-(undec-10-en-1-yl)hydroxylamine (2).** The compound **1** (2.850 g, 9.048 mmol) was dissolved in dry CH_2Cl_2 (25 mL) and purged with argon for 5 min. Next, the solution was cooled to 0 °C and hydrazine (1.41 mL, 29.1 mmol) was added dropwise at 0 °C followed by stirring the reaction mixture for 30 min at 0 °C and 12 h at room temperature under argon. The formed precipitate (phthalhydrazide) was filtered out and filtrate was concentrated by rotary evaporation. The obtained crude aminooxy product **2** 1.484 g (88%) was used to the next step directly without any further purification.

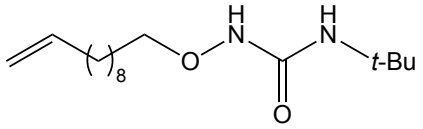

1-(*tert*-Butyl)-3-(undec-10-en-1-yloxy)urea (3.1). The crude aminooxy compound **2** (1.450 g, 7.838 mmol) was dissolved in dry CH_2Cl_2 (30.0 mL) and the solution was first purged with argon for 5 min. After 5 min, Et_3N (1.30 mL, 9.41 mmol) was added, and the reaction mixture was cooled to 0 °C followed by addition of *t*-butyl isocyanate (1.08 mL, 9.48 mmol) dropwise. After stirring at 0 °C, the reaction mixture was allowed to reach to the room temperature and stirred another 12 h. Afterward, the mixture was concentrated using rotary evaporation and the obtained crude product was purified by SiO_2 column

chromatography using 4:1 mixture of hexane:EtOAc solvent mixture to yield 1.640 g (74 %) of urea **3.1** as a colorless liquid; TLC, R_f = 0.35 (4:1, hexane:EtOAc); IR 3422, 3194, 2923, 2855, 1674, 1525 cm^{-1}; 1H NMR ($CDCl_3$, 500 MHz) δ 6.63 (br, NH), 5.82-5.80 (m, 1H), 5.61 (br, NH), 5.00-4.92 (m, 2H), 3.78 (t, *J* = 6.4 Hz, 2H), 2.05-2.02 (m, 2H), 1.62-1.60 (m, 2H), 1.37-1.25 (m, 21 H) ppm; ^{13}C NMR ($CDCl_3$, 100 MHz) δ 159.3, 139.1, 114.2, 76 .4, 50.4, 33.8, 29.5, 29.4, 29.18, 29.12, 28.9, 28.1, 26.1 ppm.

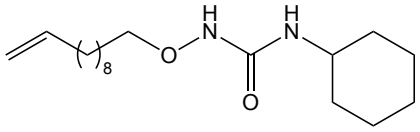

1-Cyclohexyl-3-(undec-10-en-1-yloxy)urea (3.2). The crude aminooxy compound **2** (0.410 g, 2.216 mmol) was dissolved in dry CH_2Cl_2 (30.0 mL) and the solution was first purged with argon for 5 min. After 5 min, Et_3N (0.46 mL, 3.32 mmol) was added, and the reaction mixture was cooled to 0 °C followed by addition of cyclohexyl isocyanate (0.35 mL, 2.77 mmol) dropwise. After stirring at 0 °C, the reaction mixture was allowed to reach to the room temperature and stirred another 12 h. Afterward, the mixture was concentrated using rotary evaporation and the obtained crude product was purified by SiO_2 column chromatography using 3:2 mixture of hexane:EtOAc solvent mixture to yield 0.562 g (81%) of urea **3.2** as a white solid; TLC, R_f = 0.35 (4:1, hexane:EtOAc); IR 3226, 3201, 2921, 2852, 1639 cm^{-1}; ^1H NMR ($CDCl_3$, 400 MHz) *δ* 6.83 (br, NH), 6.10 (br,NH), 5.81-5.79 (m, 1H), 5.60 (d J = 8.0 Hz, 1H), 5.00-4.92 (m, 2H), 3.80 (t, *J* = 6.8 Hz, 2H), 3.68-3.66 (t, *J* = 4.0 Hz, 1H), 2.05-2.01 (m, 2H), 1.97-1.93 (m, 2H), 1.74-1.69 (m, 2H), 1.68-1.61 (m, 3H), 1.44-1.29 (14H), 1.23-1.14 (m, 3H) ppm; ^{13}C NMR ($CDCl_3$, 100 MHz) δ

159.5, 139.2, 114.2, 76.7, 48.4, 33.9, 33.6, 29.6, 29.5, 29.2, 29.0, 28.2, 26.2, 25.6, 24.9 ppm.

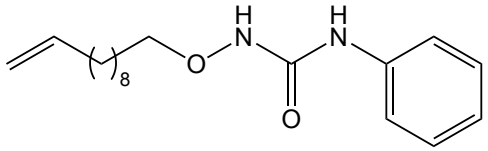

1-Phenyl-3-(undec-10-en-1-yloxy)urea (3.3). The crude aminooxy compound **2** (1.083 g, 5.854 mmol) was dissolved in dry CH_2Cl_2 (30.0 mL) and the solution was first purged with argon for 5 min. After 5 min, Et_3N (1.22 mL, 8.78 mmol) was added, and the reaction mixture was cooled to 0 °C followed by addition of phenyl isocyanate (0.80 mL, 7.32 mmol) dropwise. After stirring at 0 °C, the reaction mixture was allowed to reach to the room temperature and stirred another 12 h. Afterward, the mixture was concentrated using rotary evaporation and the obtained crude product was purified by SiO_2 column chromatography using 4:1 mixture of hexane:EtOAc solvent mixture to yield 1.482 g (84 %) of urea **3.3** as a white solid; TLC, R_f= 0.35 (4:1, hexane:EtOAc); IR 3332, 3172, 2915, 2849, 1655 cm^{-1}; ^1H NMR ($CDCl_3$, 400 MHz) δ 7.56 (br, NH), 7.47 (d, J = 8.0 Hz, 2H), 7.32 (t, J = 8.0 Hz, 2H), 7.09 (t, J = 7.8 Hz, 1H), 5.81-5.79 (m, 1H), 5.00-4.91 (m, 2H), 3.93 (t, J = 6.4 Hz, 2H), 2.06-2.00 (m, 2H), 1.71-1.68 (m, 2H), 1.39-1.29 (m, 12H) ppm; ^{13}C NMR ($CDCl_3$, 100 MHz) δ 157.3, 139.2, 137.4, 129.2, 124.0, 119.6, 114.3, 77.4, 33.9, 29.6, 29.5, 29.2, 29.0, 28.2, 26.1 ppm.

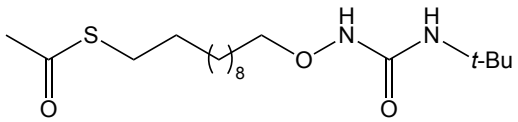

***S*-(11-((3-tert-Butyl)ureido)oxy)undecyl)ethanethioate (4.1).** The compound **3** (2.941 g, 10.36 mmol) and azobisisobutyronitrile (AIBN) (0.255 g, 1.553 mmol) were dissolved in dry THF (30.0 mL) and heated to reflux thereupon thioacetic acid (1.48 mL, 20.7 mmol) was added drop wise followed by stirring the reaction mixture at reflux for 8 h. Afterward, the reaction mixture was concentrated by rotary evaporation and the crude product was purified using SiO_2 column chromatography using 1:1 elution solvent mixture of hexane:EtOAc to yield 2.860 g (76 %) of compound **4.1** as a pale yellow liquid; TLC, R_f = 0.43 (1:1 hexane : EtOAc); ^{1}H NMR ($CDCl_3$, 500 MHz) δ 6.90 (br, NH), 5.59 (br, NH), 3.78 (t, J = 6.8 Hz, 2H), 2.85 (t, J = 6.8 Hz, 2H), 2.30 (s, 3H), 1.61-1.51 (m, 4H), 1.39-1.24 (m, 23H) ppm; ^{13}C NMR ($CDCl_3$, 100 MHz) δ 196.1, 159.2, 76.4, 50.5, 30.7, 30.6, 29.5, 29.2, 28.8, 28.2, 26.1 ppm.

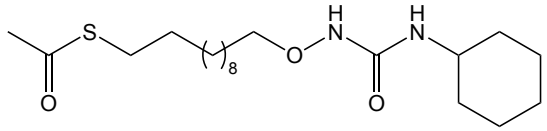

***S*-(11-((3-Cyclohexylureido)oxy)undecyl)ethanethioate (4.2).** The procedure mentioned under 4.1 synthesis was followed to transfer **3.2** (0.554 g, 1.787 mmol) into the title thioester **4.2** (0.542 g, 79%) as a pale white solid; IR 3322, 3200, 2919, 2851, 1690, 1639, 1535 cm^{-1}; ^{1}H NMR ($CDCl_3$, 400 MHz) δ 6.84 (d, J = 5.6 Hz, NH), 5.59 (d, J = 7.6 Hz, NH) 3.81 (t, J = 6.4 Hz, 2H), 3.68 (t, J = 4.4 Hz, 1H), 2.87 (t, J = 7.6 Hz, 2H), 2.32 (s, 3H), 1.96-1.94 (m, 2H), 1.73-1.69 (m, 2H), 1.64-1.42 (m, 5H), 1.39-1.22(m, 16H), 1.19-1.14 (m, 3H) ppm; ^{13}C NMR ($CDCl_3$, 100 MHz) δ 196.1, 159.4, 76.6, 48.4, 48.3, 33.6, 30.8, 30.7, 29.6, 29.4, 29.2, 29.1, 28.9, 28.2, 26.1, 25.6, 24.9 ppm.

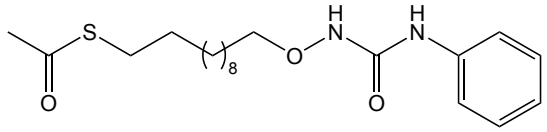

***S*-(11-((3-Phenylureido)oxy)undecyl)ethanethioate (4.3).** The procedure mentioned under 4.1 synthesis was followed to transfer **3.3** (0.865 g, 2.841 mmol) into the title thioester **4.3** (0.832 g, 77%) as a white solid; IR 3363, 3195, 2922, 2848, 1681, 1655, 1596 cm^{-1}; ^{1}H NMR ($CDCl_3$, 400 MHz) δ 7.56 (br, NH), 7.48-7.45 (m, 2H), 7.34-7.30 (m, 2H), 7.09(t, J = 7.2Hz, 1H), 3.93 (t, J = 6.8 Hz, 2H), 2.89 (t, J = 7.2 Hz, 2H), 2.32 (s, 3H), 1.70-1.67 (m, 2H), 1.57-1.52 m, 2H), 1.41-1.27(m, 14H) ppm; ^{13}C NMR ($CDCl_3$, 100 MHz) δ 196.2, 157.3, 137.4, 129.1, 124.0, 119.6, 77.4, 30.8, 30.7, 29.5 x 2, 29.4, 29.2, 29.1, 28.9, 28.2, 26.1 ppm.

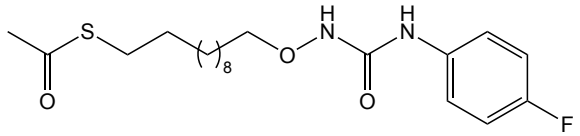

***S*-(11-((3-(4-Fluorophenyl)ureido)oxy)undecyl)ethanethioate (4.4).** The procedure mentioned under 4.1 synthesis was followed to transform **3.4** (0.060 g, 0.186 mmol) into the title thioester **4.4** (0.055 g, 74%) as a white solid; IR 3384, 3184, 2922, 2854, 1678, 1660, 1525 cm^{-1}; ^{1}H NMR ($CDCl_3$, 400 MHz) δ 7.52 (br, 1H), 7.74 (m, 2H), 7.06-7.00 (m, 2H), 3.93 (t, J = 6.8 Hz, 2H), 2.88 (t, J = 7.2 Hz, 2H), 2.32 (s, 3H), 1.72-1.68 (m, 2H), 1.58-1.54 (m, 2H), 1.34-1.23 (m, 14H) ppm; ^{13}C NMR ($CDCl_3$, 100 MHz) δ 196.2, 160.6, 158.2, 157.4, 133.4, 121.5, 115.9, 115.7, 77.4, 30.8, 30.7, 29.5 (2), 29.4, 29.2, 29.1, 28.9, 28.2, 26.0 ppm.

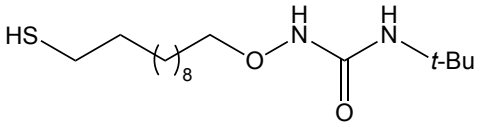

1-(tert-Butyl)-3-((11-mercaptoundecyl)oxy)urea (5.1). The intermediate **4.1** (1.974 g, 5.483 mmol) was dissolved in dry EtOH (30.0 mL) followed by addition of conc. HCl (3.66 mL, 43.86 mmol) and the reaction mixture was refluxed at 70 °C for 4 h. Afterward, it was cooled to room temperature and concentrated under reduced pressure to yield the crude product. This residue was diluted by adding H_2O (10.0 mL). The resultant solution mixture was cooled to 0 °C and saturated $NaHCO_3$ solution was added carefully to make the mixture slightly alkaline. The aqueous layer was extracted with CH_2Cl_2 (5 × 20.0 mL) and saturated NaCl (2 × 20.0 mL) was used to wash the combined organic layers. $MgSO_4$ was used to dry the organic layer, which was then filtered and concentrated by rotary evaporation to afford 1.540 g (86%) of **5.1** as a pale-yellow liquid. Compound **5.1** was directly used to synthesize Au MPCs; TLC, R_f = 0.48 (7:3, hexane:EtOAc); ITMS for $C_{16}H_{34}N_2O_2S$ calcd 319.2419, found 319. 2419 $[M+H]^+$; IR 3422, 3194, 2923, 2855, 1674, 1525, 1457, 1364, 1235 cm^{-1}; ^1H NMR ($CDCl_3$, 500 MHz) δ 5.60 (br s, 1H, NH), 3.78 (t, J = 6.8 Hz, 2H), 2.53 (t, J = 7.4 Hz, 2H), 1.62-1.60 (m, 4H), 1.39-1.28 (m, 23H, t-butyl + aliphatic chain) ppm; ^{13}C NMR ($CDCl_3$, 100 MHz) δ 159.2, 76.4, 50.4, 34.0, 29.5, 29.4, 29.2, 29.1, 28.3, 28.2, 26.1, 24.6 ppm.

5.3.1.2. Synthesis of dialkyl urea thiols – Series II

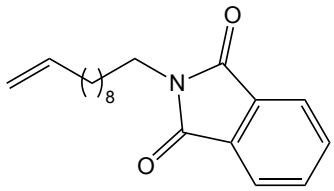

2-(undec-10-en-1-yl)isoindoline-1,3-dione (6). Potassium hydrogen phthalate (KHP) (15.20 g, 82.05 mmol) was dissolved in dry DMF (100.0 mL) and degassed the mixture under argon for 5 min. The solution mixture was slowly heated up to 80 °C and 11-bromo-1-undecene (6.00 mL, 27.4 mmol) was added dropwise followed by refluxing the reaction mixture for 12 h under argon. The reaction was stopped after 12 h and allowed to cool down to room temperature. The mixture was diluted with water (80.0 mL) and extracted with ethyl acetate (4 × 60.0 mL). The organic layers were combined and washed with 5% LiCl solution (3 × 50.0 mL) to remove remained DMF, and then it was concentrated by rotary evaporation. SiO_2 column chromatography was used to purify the crude product using 4:1 mixture of Hexane: EtOAc, to afford 8.694 g (81%) of **6** as a pale yellow solid; TLC, R_f = 0.55 (4:1 Hexane: EtOAc); ^{1}H NMR ($CDCl_3$, 500 MHz) δ 7.85-7.83 (m, 2H), 7.71-7.69 (m, 2H), 5.80-5.79 (m, 1H), 5.00-4.90 (m, 2H), 3.69 (t, J = 7.2 Hz, 2H), 2.04 (q, J = 7.2 Hz, 2H), 1.68-1.65 (m, 2H), 1.35-1.26 (m, 12H) ppm.

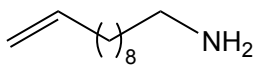

Undec-10-en-1-amine (7). Compound **6** (7.593 g, 25.40 mmol) was dissolved in dry CH_2Cl_2 (100.0 mL). The solution was purged with argon for 5 min. Next, the solution was cooled to 0 °C and hydrazine (4.31 mL, 88.9 mmol) was added dropwise at 0 °C followed by stirring the reaction mixture for 30 min at 0 °C and then 12 h at room temperature under argon. The formed precipitate was filtered, and the filtrate was concentrated by rotary evaporation. The crude aminooxy product (3.433 g) was obtained as a white solid and was used in the next step without any further purification.

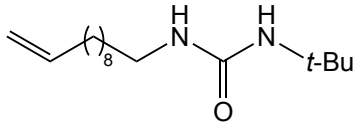

1-(tert-Butyl)-3-(undec-10-en-1-yl)urea (8.1). To a stirred solution of amine **7** (3.440 g, 20.36 mmol) in dry CH_2Cl_2 (70.0 mL) at rt under argon, Et_3N (4.34 mL, 31.2 mmol) was added dropwise via syringe and the reaction mixture was cooled to 0 °C followed by addition of *t*-butyl isocyanate (3.60 mL, 31.2 mmol) dropwise. After stirring at 0 °C, the reaction mixture was allowed to reach room temperature and stirred another 12 h. Afterward, the mixture was concentrated using rotary evaporation and the obtained crude product was purified by SiO_2 column chromatography using 3:2 mixture of hexane:EtOAc solvent mixture to yield urea **8** (4.675 g, 86 %) as a colorless liquid; TLC, R_f = 0.49 (3:2, hexane:EtOAc); IR 3321, 2971, 2922, 2852, 1738, 1630, 1562 cm^{-1}; ^1H NMR ($CDCl_3$, 500 MHz) δ 5.81-5.79 (m, 1H), 5.00-4.90 (m, 2H), 4.30-4.21 (br, 2H), 3.10 (t, J = 6.8 Hz, 2H), 2.03-2.02 (m, 2H), 1.46-1.43 (m, 2H), 1.36-1.20 (m, 21H) ppm. ^{13}C NMR ($CDCl_3$, 100 MHz) δ 157.8, 139.3 x 2, 114.4, 11.2, 50.4, 40.5, 33.9, 30.4, 29.7, 29.6, 29.5 x 2, 29.2, 29.0, 27.1 ppm.

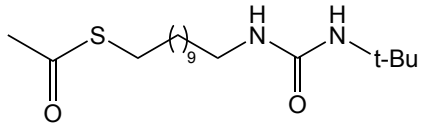

***S*-(11-(3-(*tert*-Butyl)ureido)undecyl)ethanethioate (9.1).** Compound **8** (4.093 g, 15.27 mmol) and azobisisobutyronitrile (AIBN) (0.376 g, 2.290 mmol) were dissolved in dry THF (30.0 mL) and heated to reflux; thereupon thioacetic acid (2.18 mL, 30.6 mmol) was added dropwise followed by stirring the reaction mixture at reflux for 8 h. Afterward, the reaction mixture was concentrated by rotary evaporation and the crude product was

purified using SiO_2 column chromatography using 7.5:2.5 elution solvent mixture of hexane:EtOAc to yield compound **9** (2.654 g, 50 %) as a pale yellow liquid; TLC, R_f = 0.3 (2.5:1.5 hexane : EtOAc); IR 3368, 3315, 2964, 2922, 2849, 1683, 1633, 1281 cm^{-1};^1H NMR ($CDCl_3$, 400 MHz) δ 4.12 (br, NH), 3.10 (t, J = 6.8 Hz, 2H), 2.87 (t, J = 7.6 Hz, 2H), 2.31 (s, 3H), 1.55-1.53 (m 2H), 1.46-1.45 (m, 2H), 1.32-1.23 (m, 23H), ppm; ^{13}C NMR ($CDCl_3$, 100 MHz) δ 196.3, 157.8, 50.3, 40.7, 30.8, 30.7, 30.4, 29.7, 29.5 x 2, 29.4, 29.2, 29.1, 28.9, 27.0 ppm.

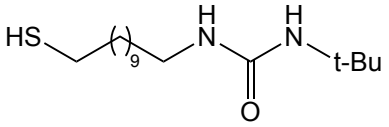

1-(*tert*-butyl)-3-(11-mercaptoundecyl)urea (10.1). Intermediate **9** (1.694 g, 4.924 mmol) was dissolved in dry EtOH (24.0 mL) followed by addition of conc. HCl (3.26 mL, 39.4 mmol). The reaction mixture was refluxed at 70 °C for 4 h. Afterward, it was cooled to room temperature and concentrated under reduced pressure to yield the crude product. This residue was diluted by adding H_2O (15.0 mL). The resultant solution mixture was cooled to 0 °C and saturated $NaHCO_3$ solution was added very carefully to make the mixture slightly alkaline. The aqueous layer was extracted with CH_2Cl_2 (5 × 20.0 mL) and saturated NaCl (2 × 20.0 mL) was used to wash the combined organic layers thereupon $MgSO_4$ was used to dry the organic layer, filtered, and concentrated by rotary evaporation to afford compound **10** (1.100 g, 74%) as a pale-yellow liquid. Compound **10** was used directly, without further purification, to synthesize Au MPCs; TLC, R_f = 0.45 (7:3, hexane:EtOAc); IR 3315, 2919, 2850, 1631, 1562, 1467, 1453 cm^{-1}; ^1H NMR ($CDCl_3$, 500 MHz) δ 4.15 (br s, 2H), 3.10 (t, J = 6.8 Hz, 2H), 2.53 (q, J = 7.2 Hz, 2H), 1.61-1.59 (m, 2H), 1.50-1.45 (m,

2H), 1.34-1.26 (m, 23H) ppm; ^{13}C NMR ($CDCl_3$,100 MHz) δ ppm 157.8, 50.3, 40.4, 34.1, 30.4, 30.2, 29.7, 29.6, 29.4, 29.1, 28.4, 27.0, 24.7 ppm.

5.3.1.3. Synthesis of *N-N'*-dialkoxyurea thiols - Series III

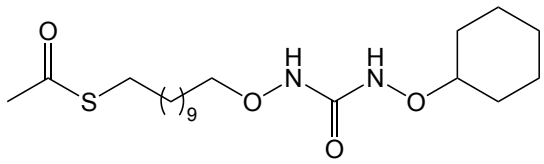

S-(11-((3-(Cyclohexyloxy)ureido)oxy)undecyl) ethanethioate (13). The compound **12.2** (0.163 g, 0.500 mmol) and AIBN (0.012 g, 0.075 mmol) were dissolved in dry THF (20.0 mL) and heated at reflux thereupon thioacetic acid (0.07 mL, 1.00 mmol) was added dropwise via a syringe. The reaction mixture was stirred at reflux for 12 h and cooled to rt followed by concentrated under reduced pressure. The obtained residue was purified by SiO_2 column chromatography with the eluting solvent mixture of 4:1 hexane:EtOAc to afford the corresponding thioester (0.142 g, 71%) as a colorless liquid; IR 3215, 2924, 2853, 1685 cm^{-1}; ^{1}H NMR ($CDCl_3$, 400 MHz) δ 7.83 (br, NH), 7.65 (br, NH), 3.87 (t, J = 6.8 Hz, 2H), 3.73-3.72 (m, 1H), 2.86 (t, J = 7.6 Hz, 2H), 2.31 (s, 3H), 1.98-1.96 (m, 2H), 1.76-1.74 (m, 2H), 1.64-1.53 (m, 5H), 1.36-1.20 (m, 20H) ppm; ^{13}C NMR ($CDCl_3$, 100 MHz) δ 196.2, 160.6, 83.7, 83.6, 77.2, 30.7, 29.5, 29.2, 29.1, 28.9, 28.0, 25.9, 25.6, 23.9 ppm.

5.3.2. Thiol-Urea Functionalized Au MPCs Synthesis

The Au MPCs synthesis was carried out by Dr. Zhenzhen Xie from Dr. Xiao-An Fu's research group.

Thiol urea ligands in series I-III (Table 1, Chapter 2) were directly used as capping agents to synthesize different urea thiol capped Au MPCs utilizing the well-known two-phase Brust-Shiffrin method.[44] $HAuCl_4.3H_2O$ (0.050 g, 0.127 mmol) was used as the Au metal ion precursor and dissolved in nano-pure water (4.0 mL) to yield a yellow color solution. Separately, tetraoctylammonium bromide (TOAB) (0.080 g, 0.146 mmol) was dissolved in toluene (20.0 mL) and $HAuCl_4$ aqueous solution was added to the TOAB solution. The reaction mixture was stirred at rt around 30 min until the aqueous layer became colorless. Afterwards, each urea thiol in Table 1 was added to the mixture at a 1:1 thiol:Au molar ratio and stirred further at rt for 2.5 h followed by dropwise addition of freshly prepared $NaBH_4$ (0.056 g, 1.480 mmol) dissolved in nano-pure water (4.0 mL) while vigorous stirring. Finally, the mixture was allowed to further stir at rt overnight. After the reaction, the toluene layer was separated, and Au MPCs were precipitated by dropwise addition of the toluene layer into ethanol (400.0 mL) with rapid stirring. After standing the ethanol solution at freezer, the suspension was centrifuged to isolate Au MPCs, and the collected particles were washed with ethanol several times to remove the unreacted thiols and the excess TOAB. The collected Au MPCs were dried at 40 °C in an oven to yield Au MPCs with ~ 2 nm diameter which was confirmed by TEM images for sensor formation.[33]

5.3.3. Interdigitated Electrodes (IDEs) Fabrication and Deposition of Thiol-Coated Au MPCs to Develop Chemiresistors

IDEs were designed and fabricated using the microelectromechanical systems (MEMS) software (Computer Aided Design (CAD) program) L-Edit by Dr. Zhenzhen Xie. The design of photomasks for use with photolithography are allowed by L-Edit program. All the IDEs used in this project were designed to fit into a 400 μm × 400 μm area using

20 μm wide and 3000 μm long metal lines connected to a 3 mm × 3 mm metal contact pads by placing similar IDEs in an arrangement to fit into a standard 4-inch silicon wafer. Lift-off microfabrication technique was used to fabricate the IDEs. This lift-off process starts with a sacrificial layer of photoresist coated on substrate. A metal layer is deposited after

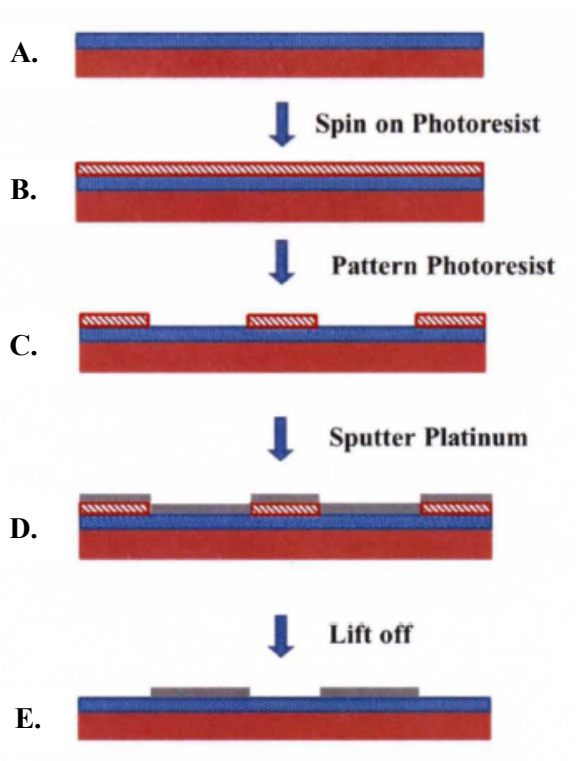

Figure 2.15 Illustration of IDEs fabrication process.
(Copied from Ref. 36)

the photoresist which is patterned by photolithography. At last, this sacrificial layer isremoved by dissolving in a solvent and IDEs and contact pads will remain on the silicon wafer. The figure 2.15 summarizes the lift-off process flow diagram that used to fabricate the IDEs. First, a standard 4-inch diameter silicon wafer (step A) with a thin insulating layer of silicon dioxide (SiO_2) having ~ 1 μm thickness was coated with LOR-3A, a lift-

off promoting resist, and then coated with a Shipley 1813 positive photoresist using spin casting technique (step B). An approximately 1.3 μm thick layer of photoresist was deposited on the wafer using recommended spinner settings for LOR-3A and Shipley 1813. In the next step, the wafer was placed on a Suss MA6/BA6 Mask Aligner and exposed to UV light (Ultraviolet) for 9 seconds using a dark field mask (step C) to sinter the positive photoresist in the exposed areas. Then the wafer was placed into a bath of MF319, a photoresist development solution for about 30 seconds. To confirm the complete development of the exposed photoresist, the wafer was inspected and ensure that IDE features would turn out functional. Next, the wafer was sputtered with platinum (Pt) using a Kurt J. Lesker PVD 75 DC Sputter (step D). A thin layer of chromium (Cr) was deposited prior to sputtering Pt, to promote Pt adhesion to the SiO_2 layer. Here, Cr was sputtered around 1 min. and the Pt for 4 min. to make a Pt/Cr layer with 163 nm thickness. In the last step, to complete the lift-off process, the wafer was placed into an N-methylpyrrolidin (NMP) bath with agitation for 24 h (step E). This wafer was diced into 1 cm × 1 cm IDEs chips, to complete the IDEs fabrication process. Again, the individual IDEs were inspected using a ZEISS Axioskop Optical Microscope, to ensure the completeness of the lift-off process.[36]

Figure 2.16 depicts the microscopic image of fabricated IDEs and an individual IDEs chip. To complete the sensor, the synthesized urea thiol-coated Au MPCs were dispersed in toluene (0.2 w/w %) and casted onto the IDEs area by dropwise addition. The prepared sensor was air dried to evaporate the toluene and to leave a flat, roughly circular film of Au MPCs. All the Au MPCs coated sensors were kept in an oven at 40 °C for sensor stabilization.[33,34,36] The gas sensors of Au MPCs coated with the three series of thiol-urea

ligands were utilized for sensing target analytes in air to compare the selectivity and sensitivity.

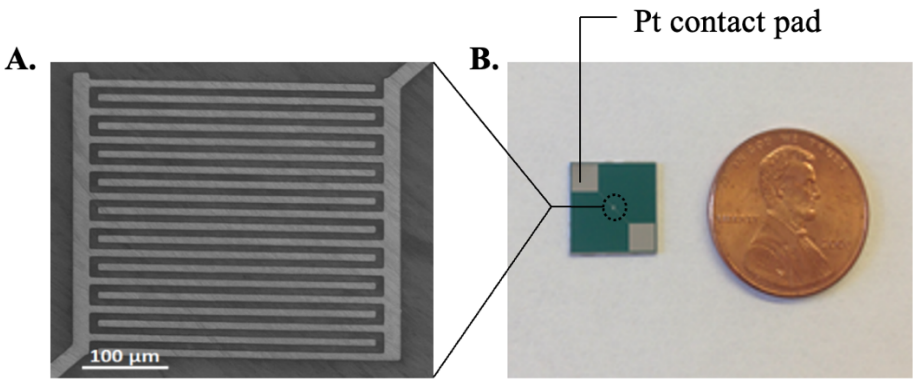

Figure 2.16. A. Scanning Electron Microscopy image of the microfabricated IDEs and **B.** Size difference between the sensor and a US one cent coin. (Copied from Ref. 33)

5.3.4. Sensor measurements

The sensor measurements were performed by Dr. Zhenzhen Xie (Dr. Xiao-An Fu's research group). The developed urea thiol-coated Au MPCs based gas sensors or the chemiresistors were placed inside a homemade stainless steel test chamber (total volume of about 300 mL) one at a time to perform the gas sensing studies (Figure 2.17). Initially, the test chamber was evacuated using vacuum and an interested VOC analyte, with a known concentration was introduced using a sample bag (Tedler bag) which was connected to the chamber. After the analyte entered to the test chamber, the pressure inside the chamber increased to the atmospheric pressure within a few seconds. Also, there were not any air flow occurs through the test chamber during the sensing measurement process. The analyte of each concentration was tested for a fixed time (5 min.) and the chamber was evacuated for the next cycle of measurement to study the reproducibility. Tedler bags were

used to prepare the VOC analyte samples. These bags were washed with synthetic air three times prior to analyte sample preparation, to remove the impurities. To prepare an interested VOC analyte with a known concentration, first an appropriate amount of each analyte was injected into a Tedler bag containing 1 L dry air to prepare 1000 ppm air sample. For instance, 3 μL of acetone was injected into a Tedler bag containing 1 L dry air and this acetone vaporizes within the bag and 1000 ppm gaseous concentration was

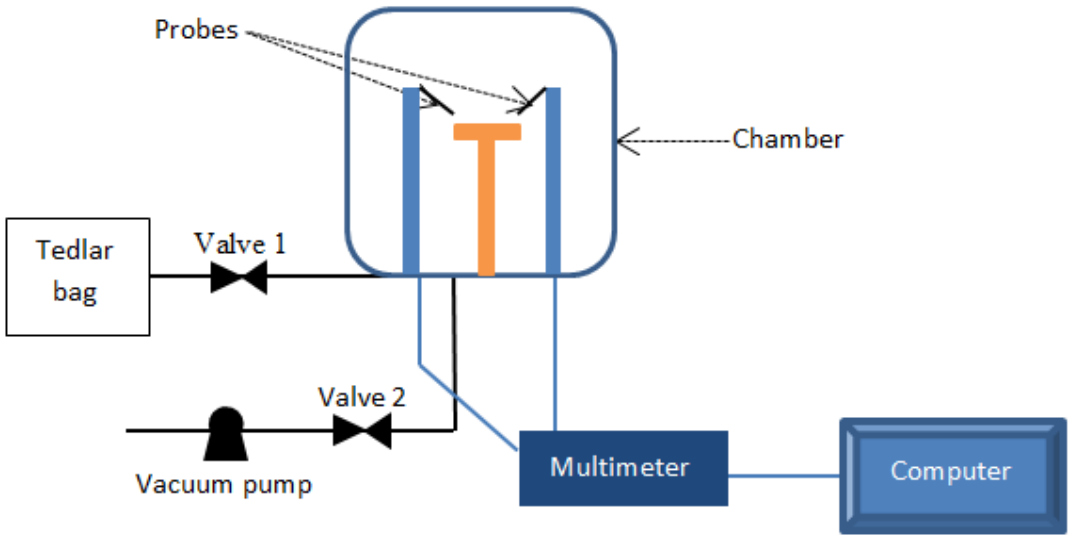

Figure 2.17. Illustration of the sensor measurement set-up used. (Copied from Ref. 36)

achieved. Using an air-tight glass syringe, 10 mL from the 1000 ppm acetone gas sample was collected and injected into a new 1 L cleaned Tedler bag followed by an addition of 990 mL dry air to prepare acetone concentration of 10 ppm. The similar process was carried out to prepare lower acetone concentration samples. This procedure was followed to prepare all the interested VOC analyte samples with each concentration. All the developed

sensors responded to analyte VOCs with different concentrations in synthetic air by changing the resistance of the IDEs coated with urea thiol functionalized Au MPCs.[34,36]

In the sensing process, a fixed applied voltage of 5 V was introduced by a Keithley 2400 I-V meter, and the resistance of an individual sensor was monitored and recorded as a function of time using the Labview program. All the chemiresistor resistances were first measured under a vacuum of 28-inch Hg below atmospheric pressure over 5 min whereupon VOC analyte sample was introduced at atmospheric pressure for 5 min., and again test chamber evacuation. The cycle of sensor resistance measurement in vacuum and the analyte exposure was repeated three times for all the analytes to test for sensor reproducibility. All experiments were performed at room temperature.

5.4. EXPERIMENTAL PROCEDURES OF CHAPTER 3

5.4.1. Functionalized Thiol Ligand Synthesis

n-Alkane thiol aminooxy ligands having C_6 (compound **3**, Scheme 3.2) and C_{11} (compound **7**, Scheme 3.3) chains were synthesized by modifying the reported synthetic route of Park S. *et al*.[59]

Synthesis of an *N*-Boc Protected Aminooxy Hexane Thiol Ligand

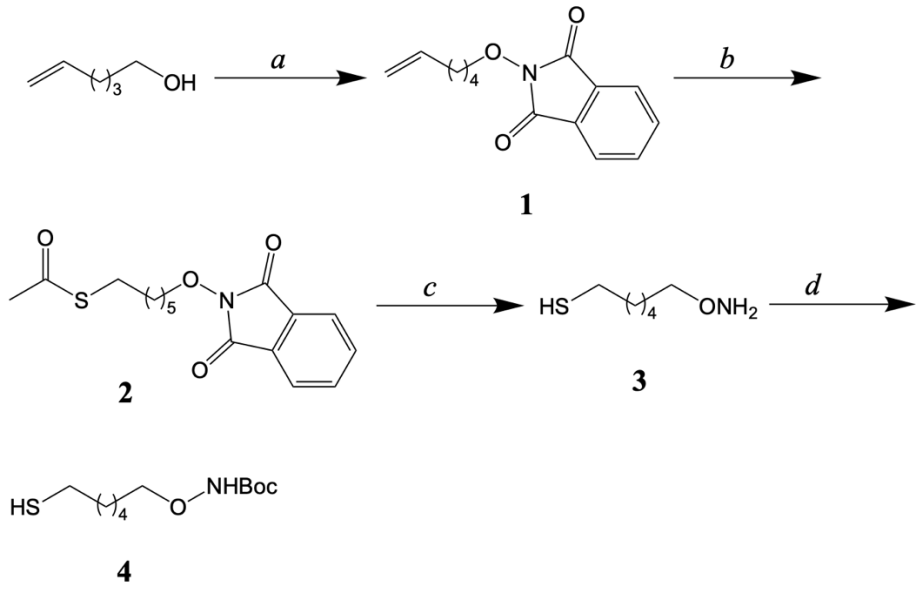

Scheme 3.2. Synthesis of an *N*-Boc protected aminooxy hexane thiol ligand; Reagents and conditions: a. NHP, PPh_3, DIAD, THF, 0 °C to rt, 16 h; b. $CH_3C(O)SH$, cat. AIBN, THF, reflux, 16 h; c. $H_2NNH_2.H_2O$, CH_2Cl_2, 0 °C to rt, 17 h; d. $(Boc)_2O$, MeOH : Et_3N (9:1), reflux, 1.5 h.; NHP = *N*-hydroxyphthalimide, PPh_3 = triphenylphosphine, DIAD = diisopropyl azodicarboxylate, AIBN = 2,2′-azobis(2-methylpropionitrile), $(Boc)_2O$ = di-*tert*-butyl dicarbonate.

2-(hex-5-en-1-yloxy) isoindoline-1,3-dione (1). Triphenylphosphine (13.09 g, 49.90 mmol) and *N*-hydroxy phthalimide (8.143 g, 49.90 mmol) were dissolved in dry THF (150.0 mL). 5-Hexene-1-ol (4.90 mL, 41.6 mmol) was added to the mixture drop wise and degassed the mixture using nitrogen stream for 15 min followed by stirring at 0 °C for 1 h under nitrogen. After 1 h, DIAD (9.83 mL, 49.9 mmol) was added dropwise to the mixture in an ice bath and further stirred at 0°C for 1 h followed by at rt for 16 hr under nitrogen. The reaction was quenched by adding diethyl ether (25.0 mL) before concentrated by rotary evaporation and residue was dissolved in ethyl acetate (20.0 mL). Then the crude product was washed with sat. aq. $NaHCO_3$ (5 x 25.0 mL) and sat. aq. NaCl (4 x 25.0 mL). The organic extract was separated, concentrated, and dissolved in diethyl ether (20.0 mL) followed by filtered through a short silica column in diethyl ether (100 %) to remove triphenylphosphine oxide (TPPO) byproduct. Again, the filtrate was concentrated and purified by column chromatography with 4:1 mixture of hexane : EtOAc, to afford 9.678 g (95 %) of **1** as a white solid; TLC, R_f = 0.46 (4:1 Hexane: EtOAc); ^{1}H NMR ($CDCl_3$, 400 MHz) δ 7.85-7.74 (m, 4H), δ 5.82 – 5.09 (m, 1H), δ 5.05 – 4.95 (m, 2H), δ 4.22 4.19 (m, 2H), δ 2.16-2.11 (m, 2H), δ 1.83-1.79 (m,2H), δ 1.63-1.41 (m,2H); ^{13}C ($CDCl_3$, 100 MHz) δ 163.44, 138.19, 134.39, 128.85, 123.33, 114.83, 78.17, 33.20, 27.48, 24.74.

***S*-(6-((1,3-dioxoisoindolin-2-yl) oxy) hexyl) ethanethioate (2).** Compound **1** (7.730 g, 31.55 mmol) was dissolved in THF (100.0 mL) and degassed after adding thioacetic acid (4.74 mL, 66.3 mmol) drop wise. the reaction mixture was heated to 40 °C for 10 min under nitrogen and catalytic amount of AIBN (0.777 g, 4.733 mmol) dissolved in THF (5.0 mL) was added drop wise. Finally, the mixture was refluxed for 17 h while stirring. The reaction mixture was quenched by diethyl ether (20.0 mL) after cooling to room temperature and

concentrated by rotary evaporation. The crude product was purified by using column chromatography 2:1mixture of hexane:EtOAc to obtain 9.014 g (89%) of the compound **2** as a pale yellow colored solid. TLC, R_f= 0.35 (2:1 Hexane:EtOAc); ^{1}H NMR ($CDCl_3$, 400 MHz) δ 7.84-7.73 (m, 4H), δ 4.21-4.17 (m, 2H), δ 2.89-2.85 (m, 2H), δ 2.31 (s, 3H), δ 1.79-1.76 (m, 2H), δ 1.64-1.43 (m, 6H); ^{13}C ($CDCl_3$, 100 MHz) δ 196.03, 163.74, 134.53, 129.11, 123.57, 78.47, 30.72, 29.46, 25.21.

6-(aminooxy) hexane-1-thiol (3). The intermediate **2** (8.512 g, 26.52 mmol) was dissolved in DCM (130.0 mL) and degassed using nitrogen stream for 15 min. The solution was cooled to 0 °C and hydrazine monohydrate (11.60 mL, 238.7 mmol) was added drop wise and the mixture was stirred 1h at 0 °C followed by stirring 12 h at rt under nitrogen. The reaction mixture was filtered inside a glove bag filled with nitrogen to remove the white precipitate (phthalhydrazide) and the filtrate was concentrated by rotary evaporation to afford 3.240 g (82%) of aminooxy thiol **3** as a pale-yellow viscous liquid. ^{1}H NMR ($CDCl_3$, 400 MHz) δ 3.66-3.63 (m, 2H), δ 2.54-2.49 (m, 2H), δ 1.63-1.54 (m, 4H), δ 1.42-1.32 (m,4H); ^{13}C ($CDCl_3$, 100 MHz) δ 34.32, 28.68, 25.85, 24.98.

***tert*-butyl (6-mercaptohexyl) oxycarbamate (4).** To a solution of aminooxy thiol **3** (3.200 g, 21.48 mmol) in a 9:1 mixture of methanol: Et_3N (100.0 mL) di-*tert*-butyl dicarbonate (5.43 mL, 23.6 mmol) was added drop wise and the mixture was refluxed 1.5 h under nitrogen atmosphere. After 1 h, the mixture was cooled to rt and concentrated under reduced pressure. The residue was dissolved in DCM (20.0 mL) and washed with D.I. water (5 x 25.0 mL) to remove the byproduct. The separated DCM layer was dried using

anhydrous Na_2SO_4 and evaporated the organic layer by rotary evaporation to get 2.720 g (85%) of the pure *N*-Boc protected thiol compound **4** as a pale-yellow viscous liquid. FT-IR 2574, 1716, 1105 cm^{-1}; UHPLC/MS $[M+H]^+$ calcd 249.1345 found 249.1335; ^1H NMR ($CDCl_3$, 400 MHz) δ 7.15 (s, 1H), δ 3.84-3.81 (m, 2H), δ 2.51-2.49 (m, 2H), δ 1.61-1.58 (m, 4H), δ 1.46 (s, 9H), δ 1.39-1.31 (m,4H). ^{13}C ($CDCl_3$, 100 MHz) δ 157.04, 81.72, 33.97, 28.28, 25.52, 24.65.

Synthesis of an *N*-Boc Protected Aminooxy Undecane Thiol Ligand

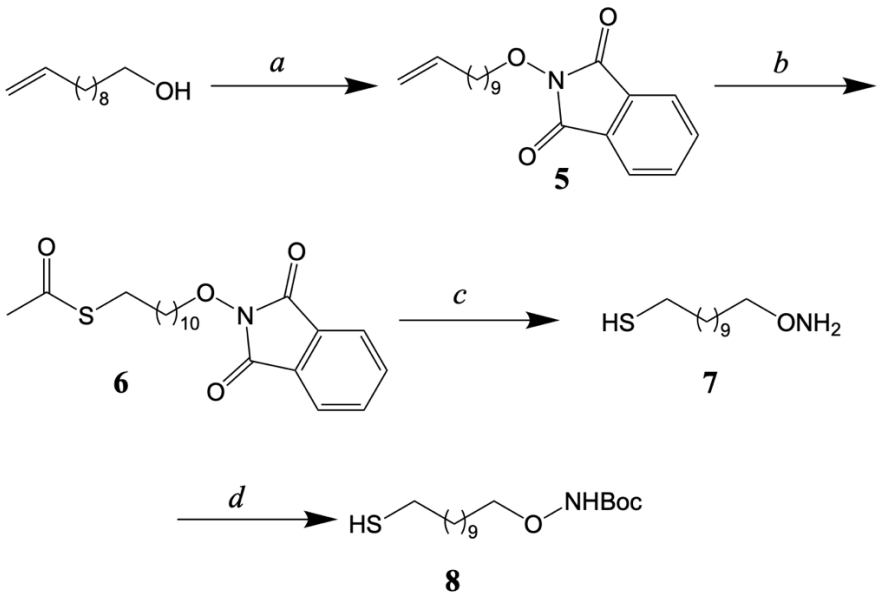

Scheme 3.3. Synthesis of an *N*-Boc protected aminooxy undecane thiol ligand; Reagents and conditions: a. NHP, PPh_3, DIAD, THF, 0 °C to rt, 16 h; b. $CH_3C(O)SH$, cat. AIBN, THF, reflux, 16 h; c. $H_2NNH_2.H_2O$, CH_2Cl_2, 0 °C to rt, 17 h; d. $(Boc)_2O$, MeOH : Et_3N (9:1), reflux, 1.5 h.; NHP = *N*-hydroxyphthalimide, PPh_3 = triphenylphosphine, DIAD = diisopropyl azodicarboxylate, AIBN = 2,2′-azobis(2-methylpropionitrile), $(Boc)_2O$ = di-*tert*-butyl dicarbonate.

2-(undec-10-en-1-yloxy) isoindoline-1,3-dione (5). The procedure mentioned under compound **1** synthesis was followed using 10-undecen-1-ol as the starting material to afford 7.586 g, (95%) of compound **5** as a white solid; TLC, R_f= 0.40 (4:1 Hexane:EtOAc); ^{1}H NMR ($CDCl_3$, 400 MHz) δ 7.81-7.71 (m, 4H), δ 5.78 – 5.76 (m, 1H), δ 4.98 – 4.87 (m, 2H), δ 4.18 4.15 (m, 2H), δ 2.01-1.99 (m, 2H), δ 1.77-1.73 (m, 2H), δ 1.45-1.43 (m, 2H) ; δ 1.34-1.26 (m, 10H) ^{13}C ($CDCl_3$, 100 MHz) δ 163.63, 139.18, 134.43, 129.00, 123.45, 114.14, 78.59, 33.80, 29.42, 29.10, 25.55.

***S*-(11-((1,3-dioxoisoindolin-2-yl) oxy) undecyl) ethanethioate (6).** The procedure mentioned under compound **2** synthesis was followed to afford 7.721 g, (82%) of compound **6** as a white solid; TLC, R_f= 0.33 (2:1 Hexane:EtOAc); ^{1}H NMR ($CDCl_3$, 400 MHz) δ 7.84-7.73 (m, 4H), δ 4.21-4.17 (m, 2H), δ 2.87-2.83 (m, 2H), δ 2.31 (s, 3H), δ 1.79-1.76 (m, 2H), δ 1.55-1.53 (m, 2H), δ 1.47-1.46 (m, 2H), δ 1.35-1.33 (m, 10H); ^{13}C ($CDCl_3$, 100 MHz) δ 196.18, 163.81, 134.54, 129.13, 123.60, 78.75, 30.77, 29.54-28.27, 25.65.

11-(aminooxy) undecane-1-thiol (7). The procedure mentioned under compound **3** synthesis was followed to afford 4.820 g, (75%) of compound **7** as a pale-yellow liquid; ^{1}H NMR ($CDCl_3$, 400 MHz) δ 3.54-3.51 (m, 2H), δ 2.43-2.37 (m, 2H), δ 1.43-1.54 (m, 4H), δ 1.28-1.63 (m, 14H); ^{13}C ($CDCl_3$, 100 MHz) δ 75.69, 33.67, 29-14-28.02, 25.63, 24.23.

***tert*-butyl ((11-mercaptoundecyl) oxy) carbamate (8).** The procedure mentioned under compound **4** synthesis was followed to afford 6.483 g, (92%) of compound **8** as a yellow

liquid. FT-IR 2565, 1725, 1114 cm^{-1}; ^{1}H NMR ($CDCl_3$, 400 MHz,): δ 7.13 (s, 1H), δ 3.83-3.79 (m, 2H), δ 2.52-2.46 (m, 2H), δ 1.61-1.56 (m, 4H), δ 1.46 (s, 9H), δ 1.34-1.24 (m, 14H); ^{13}C ($CDCl_3$, 100 MHz) δ 157.18, 81.79, 34.03, 29.73-28.49, 26.13, 24.91.

5.4.2. Functionalized Thiol Capped Au MPCs Synthesis

Synthesis of Metal-ion Functionalized Au MPCs from the *N*-Boc Protected Thiol Compound 4 and 8 (Chapter 3, Scheme 3.1.)

5.4.2.1. Synthesis of *N*-Boc Protected Au MPCs (9).

N-Boc protected hexanethiolate-functionalized Au MPCs (**9**, Scheme 3.3) were synthesized according to the Brust-Shiffrin method[55] using a 3:1 thiol:$HAuCl_4 \cdot 3H_2O$ ratio. A solution of $HAuCl_4 \cdot 3H_2O$ (0.460 g, 1.171 mmol) in nanopure water (37.0 mL) was added to a solution of tetraoctylammonium bromide (TOAB) (0.735 g, 1.341 mmol) in toluene (184.0 mL) at rt. The reaction mixture was stirred vigorously for 30 min at rt under nitrogen. Once the aqueous layer became colorless, the layers were separated by removal of the aqueous layer using a pipette. To the remaining toluene solution at rt was added the synthesized thiol **4** (0.873 g, 3.500 mmol) and the mixture was stirred 2 h at rt. The mixture then was cooled to 0 °C and a solution of $NaBH_4$ (0.441 g, 11.70 mmol) in nanopure water (37.0 mL) was added dropwise followed by vigorous stirring for 30 min at 0 °C and then 12 h at rt. The black toluene layer was separated and evaporated under reduced pressure to near dryness. Acetonitrile (30.0 mL) was added to the black residue and the resultant suspension was stored at 0 °C for 24 h to precipitate the Au MPCs **9**. The Au MPCs was collected by centrifugation and then washed with acetonitrile several times to remove any

TOAB or unreacted thiol. The isolated Au MPCs **9** was characterized by ^{1}H NMR spectroscopy, FT-IR, UV–vis, TEM, and TGA.

5.4.2.2. Synthesis of Aryl Ester-Functionalized Au MPCs (**11**).

Deprotection of Au MPCs **9** (step *a*, Scheme 3.3) was accomplished by modification of literature procedure.[56] Au MPCs **9** (0.580 g, 0.820 mmol *N*-Boc, determined by TGA analysis of **9** indicating 35% organic composition) were dissolved in CH_2Cl_2 (2.0 mL) and cooled to 0 °C. To the solution was added dropwise a solution of trifluoroacetic acid (0.25 mL, 3.27 mmol) in CH_2Cl_2 (0.25 mL). The reaction mixture was stirred 15 mins at 0 °C, whereupon stirring was ceased to allow the deprotected Au MPCs to settle. The solvents were then carefully decanted to collect the black precipitate. The precipitates were washed with CH_2Cl_2 (10 x 3.0 mL) until neutral to pH paper. To the isolated Au MPCs (0.390 g, 0.520 mmol) in a 2:1 mixture of MeOH:DCM (3.0 mL) at 0 °C was added triethylamine (0.72 mL, 5.21 mmol) dropwise. The reaction mixture was stirred 3 h at rt and then concentrated under reduced pressure to near dryness. Without any delay, the crude aminooxy Au MPCs so obtained were suspended in solution by addition of acetonitrile (5.0 mL). Excess triethylamine was removed by washing the isolated Au MPCs successively with nanopure water (2 x 2.0 mL) followed by MeOH (5 x 2.0 mL) to afford aminooxy Au MPCs **10** (0.280 g), which were used directly in the next step without further purification.

To a solution of Au MPCs **10** (0.280 g, 0.660 mmol –ONH_2) in CH_2Cl_2 (1.00 mL) at 0 °C was added dropwise (step *c*, Scheme 3.3) a solution of methyl 4-formylbenzoate (0.543 g, 3.310 mmol, 5 eq.) in CH_2Cl_2 (1.00 mL). The reaction mixture was stirred 17 h

at rt whereupon the solvents were removed by rotary evaporation. The residue was washed with MeOH (10 x 3.0 mL) to remove unreacted benzoate and then air dried to afford Au MPCs **11** (0.250 g). Oximation was confirmed by characterization using ^{1}H and ^{13}C NMR and FTIR.

5.4.2.3. Synthesis of Alkali Metal-Functionalized Au MPCs (12).

Alkali metal cations were introduced (step *d*, Scheme 3.3) by saponification of the aryl ester-functionalized Au MPCs **11** using corresponding hydroxide salts. To prepare the potassium and sodium sensors, a 0.1 M solution of alkali metal hydroxide (0.290 mmol) in MeOH was added slowly to a solution of Au MPCs **11** (0.080 g, 0.100 mmol $–CO_2Me$) in a 9:1 mixture of CH_2Cl_2: MeOH (1.00 mL) at 0 °C. The reaction was allowed to warm to rt and stirred 17 h, whereupon the solvents were concentrated by rotary evaporation and the resultant Au MPCs suspended by addition of acetonitrile (5.00 mL). The particles were isolated by centrifugation and then washed several times using methanol (10 x 3.00 mL).

To prepare the lithium sensor, a 0.1M solution of lithium hydroxide (0.290 mmol) in MeOH was added slowly to a solution of Au MPCs **11** (0.080 g) in a 2:1 mixture of THF:H_2O (1.00 mL) at 0 °C. The reaction was allowed to warm to rt and stirred 17 h, whereupon the solvents were concentrated by rotary evaporation and the resultant Au MPCs suspended by addition of acetonitrile (5.0 mL). The lithium carboxylate functionalized Au MPCs was isolated by centrifugation and then washed several times with nanopure water (10 x 3.0 mL).

Using the same synthetic route in Scheme 3.1. *n*-alkane C11 length Na^+-functionalized Au MPCs were synthesized **(12-Na^+/C11)**.

5.4.2.4. Synthesis of K^+-Functionalized Au MPCs Using Commercially Available Thiols.

As shown in the Chapter 3, Table 3.1, 5 different types of Au MPCs were synthesized using the commercially available thiols. Place-Exchanged Au MPCs were synthesized according to the method described by Murray *et. al.*[57]

Synthesis of 4-Mercaptobenzoic Acid Functionalized Au MPCs (a). 4-mercaptobenzoic acid functionalized Au MPCs (Sensor **a** or Au(4-MBA) were synthesized according to the one-phase method described by Brust *et al.*[58] with several modifications using a 3:1 thiol:$HAuCl_4 \cdot 3H_2O$ ratio. A solution of 4-mercaptobenzoic acid (0.587 g, 3.800 mmol) in methanol (170.0 mL) was added to a solution of $HAuCl_4 \cdot 3H_2O$ (0.500 g, 1.270 mmol) in methanol (30.0 mL) at rt. The reaction mixture was stirred vigorously for 2.5 h at rt under nitrogen. Once the mixture became colorless, it was cooled to 0 °C and a methanolic solution (30.0 mL) of freshly prepared $NaBH_4$ (0.480 g, 12.69 mmol) was added drop wise while stirring the solution vigorously. After 30 min string at 0 °C, the mixture was stirred overnight at rt. The formed Au MPCs were isolated by removal of the methanolic layer using a pipette. The isolated precipitate was washed with methanol several times to remove the excess $NaBH_4$ or unreacted thiol. Na^+ salt of 4-mercaptobenzoic acid functionalized Au MPCs were collected as a black precipitate. To prepare the 4-mercaptobenzoic acid functionalized Au MPCs, the Na^+ functionalized Au MPCs were dissolved in nanopure water and cooled down to 0 °C followed by addition of 0.1 M aqueous H_2SO_4 dropwise until a precipitate was formed. The Au MPCs of 4-MBA were isolated by centrifugation and the precipitate was washed with nanopure water several times (until the solution pH neutral to pH papers) to remove the excess acid.

Synthesis of K^+ Salt of 4-Mercaptobenzoic Acid Functionalized Au MPCs (b). To a methanolic solution of the prepared Au MPCs of sensor **a** in an ice-bath, 24% (w/v%) KOH in methanol was added drop wise until a precipitate was formed in the solution. The formed precipitate was isolated by centrifugation, and it was washed with methanol several times removing times (until the solution pH neutral to pH papers) to remove the base.

Synthesis of Hexanethiol / K^+ Salt of 4-Mercaptobenzoic Acid Functionalized Au MPCs (c). Mixed monolayer Au MPCs were prepared from hexanethiol and the K^+ salt of 4-mercaptobenzoic acid according to the Au MMPCs place-exchange protocol.[57] Initially, hexanethiolated Au MPCs were synthesized using the two-phase Brust-Shiffrin method[55] using a 3:1 thiol:$HAuCl_4 \bullet 3H_2O$ ratio. A solution of $HAuCl_4 \bullet 3H_2O$ (1.000 g, 2.540 mmol) in nanopure water (80.0 mL) was added to a solution of tetraoctylammonium bromide (TOAB) (1.597 g, 0.920 mmol) in toluene (400.0 mL) at rt. The reaction mixture was stirred vigorously for 30 min at rt under nitrogen. Once the aqueous layer became colorless, the layers were separated by removal of the aqueous layer using a pipette. To the remaining toluene solution at rt was added the hexanethiol (1.080 mL, 7.620 mmol) and the mixture was stirred 2 h at rt. The mixture then was cooled to 0 °C and a solution of $NaBH_4$ (0.961 g, 25.39 mmol) in nanopure water (80.0 mL) was added dropwise followed by vigorous stirring for 30 min at 0 °C and then 12 h at rt. The black toluene layer was separated and evaporated under reduced pressure to near dryness. Acetonitrile (30.0 mL) was added to the black residue and the resultant precipitate was isolated by removing the organic layer. The obtained Au MPCs were washed with acetonitrile several times to remove any TOAB or unreacted thiol to afford hexanethiolated Au MPCs.

The following calculation was used to calculate the weight of 4-mercaptobenzoic acid needed to have 1:1 thiol exchange. 1-Hexanethiol (C6SH) was used as the non-linker thiol and 4-mercaptobenzoic acid was utilized as the linker thiol.

$Au_{144}(C_6S)_{53}X$ is the molecular formula for place-exchanged Au MPCs (mixed monolater Au MPCs or Au MMPCs) confirmed by Murray *et al.,*[57] when 1-hexanethiol is used as the non-linker ligand, where X = linker thiol or a 2nd thiol.

SR = 1- hexanethiol SR′ = linker ligand (4-MBA)

Molecular weight of Au = 196. 97 g/mol

Molecular weight of 1-Hexanethiol = 118 g/mol

Total molecular weight of the = MW of $Au_{144}(C_6S)_{53}X$

place-exchanged Au MPCs = (196.97/mol x 144) + (117 g/mol x 53)

= 34569 g/mol[57]

If the weight of 1-Hexanethiol coated Au MPCs is m g,

moles of Au MPCs for m grams of MPCs = m g / 34569 g mol^{-1} = y mol

moles of SR for y moles of clusters = y mol x 53 = z mol

- multiply by 53 because there are 53 moles of SR for every 1 mole of Au MPCs

If the linker thiol is SR′ and non-linker thiol is SR,

1:1 ratio of SR′: SR, (for 50 % of ligand exchange)

moles of SR’ = 2 (moles of SR)

= 2 x z mol (moles of SR′ want to add to m grams of clusters)

Weight SR′ = 2 z mol x $MW_{SR'}$ g/mol

(1:1 means, approximately, about 26 SR′ and 26 SR ligands for 53 total)

To prepare the Au MMPCs, hexanethiolated Au MPCs (0.251 g, 0.390 mmol) were dissolved in dry CH_2Cl_2 (2.00 mL) and purged with argon for 10 min. To the solution of hexanetiolated Au MPCs, 4-mercaptobenzoic acid (0.119 g, 0.770 mmol) was added and stirred at rt for 4 days. The solvent was removed by rotary evaporation and the place-exchanged Au MPCs were precipitated by adding CH_3CN (5.0 mL) followed by centrifugation. Isolated Au MPCs were washed with CH_3CN several times to remove the excess thiols in the medium and to obtain the mixed monolayer of hexanethiol(C6)/4-mercaptobenzoic acid functionalized Au MPCs. The isolated Au MPCs (0.100 g) were dissolved in ethanol (4.00 mL) and cooled to 0 °C. 24% (w/v%) KOH in ethanol was added drop wise to the black Au MPCs solution until precipitate form in the solution. The precipitate was isolated by centrifugation and washed the particles with ethanol (until the solution pH neutral to pH papers) to afford hexanethiol / K^+ salt of 4-mercaptobenzoic acid functionalized Au MPCs (c).

Synthesis of Dodecanethiol / K^+ Salt of 4-mercaptobenzoic Acid Functionalized Au MPCs (d). The experimental procedure described under the "Synthesis of 1-hexanethiol / K^+ salt of 4-mercaptobenzoic acid functionalized Au MPCs (c)" was followed. 1-dodecanethiol was used as the non-linker ligand.

Synthesis of K^+ Salt of 16-Mercaptohexadecanoic Acid Functionalized Au MPCs (e)
Initially, the experimental procedure described under the "Synthesis of 4-mercaptobenzoic acid functionalized Au MPCs (a)" was used to synthesize the Na^+-salt of 16-mercaptohexadecanoic acid functionalized Au MPCs using the 16-mercaptohexadecanoic acid and the experimental procedure of "Synthesis of K^+ salt of 4-mercaptobenzoic acid

functionalized Au MPCs (b)" was followed to prepare K^+ salt of 16-mercaptohexadecanoic acid functionalized Au MPCs **(e).**

5.4.3. Microsensor Design and Fabrication

The microsensor was designed using L-edit software. The dimension of the sensor chip is 1 cm x 1 cm. The microsensor chip features four circularly shaped (diameter 2 mm) sensing areas containing interdigitated electrodes (line width = 20 µm, spacing = 10 µm) connected to Cr/Pt contact pads. A similar design was placed in an arrangement to fit onto

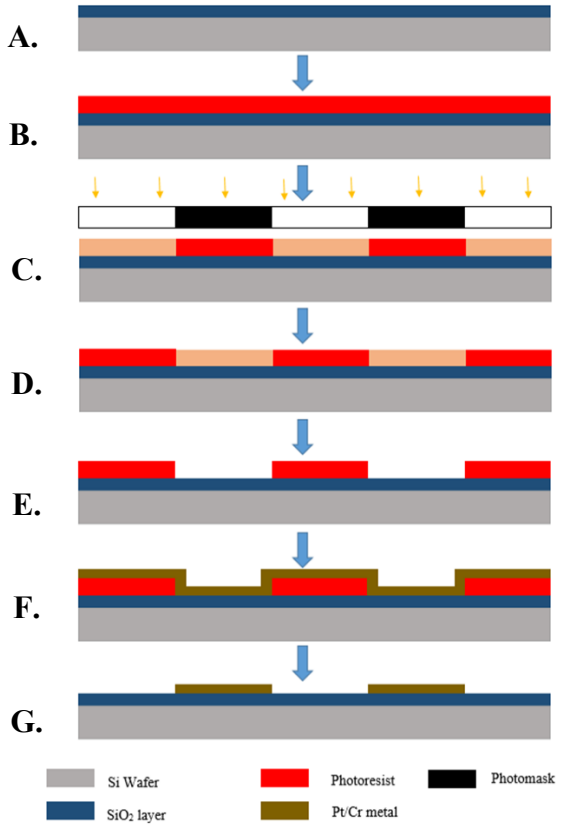

Figure 3.11. Fabrication process flow diagram: **A.** oxidized silicon wafer; **B.** photoresist coating; **C.** UV light exposure; **D.** YES Image Reversal; **E.** Development; **F.** metal sputtering; and **G.** lift-off.

a standard 4-inch wafer where a total of 52 chips were obtained. A clear field photomask was used to pattern the interdigitated electrodes and contact pads on a silicon wafer. For the fabrication of the microsensors, a single-side polished 4″ oxidized 500 μm-thick silicon wafer was used (Figure 3.11 A) where the oxide layer serves as an electrical insulation. After cleaning the wafer by successively washing with acetone, methanol, and deionized (DI) water, the surface of the wafer was exposed to a stream of nitrogen to remove any trace contaminations, such as dust or any ionic or metallic compounds. A positive photoresist (Shipley 1813) then was coated on the wafer (Figure 3.11 B). The wafer was soft baked at 115 °C for two minutes and then exposed (contact exposure method using Karl Suss Mask Aligner MA6/BA6) to UV light for 12 seconds at 12W/cm^2 through a clear field photomask (Figure 3.11 C). Next, the wafer was treated with ammonia (g) at 90 °C in YES Image Reversal oven followed by flood exposure for 25 seconds (Figure 3. 11 D), which improved re-entrant sidewalls for metal sputtering. The wafer was developed (Microposit MF319) for 90 seconds followed by rinsing in a DI water bath, dried by N_2, and hard baked for 2 minutes using a hotplate at 115 °C (Figure 3.11 E). The silicon wafer surface was treated with O_2 plasma (March RIE CS1701) for 15 seconds to remove any organics to promote better adhesion of metal to the substrate surface. Chromium (Cr) and platinum (Pt) metals were sputtered (Kurt J. Lesker PVD 75, 300W DC power) on the wafer for 2 and 6 minutes, respectively, to create a 180 nm thick metal layer (Cr adhesion layer ~30 nm, Pt layer ~150 nm; Figure 3.11 F). The wafer then was placed in an ultrasonic bath containing acetone to complete the lift-off process, where the sacrificial layer of photoresist is removed (Figure 3.11 G). Finally, the wafer was diced into 1 cm x 1 cm sensor chips (Figure 3.12).

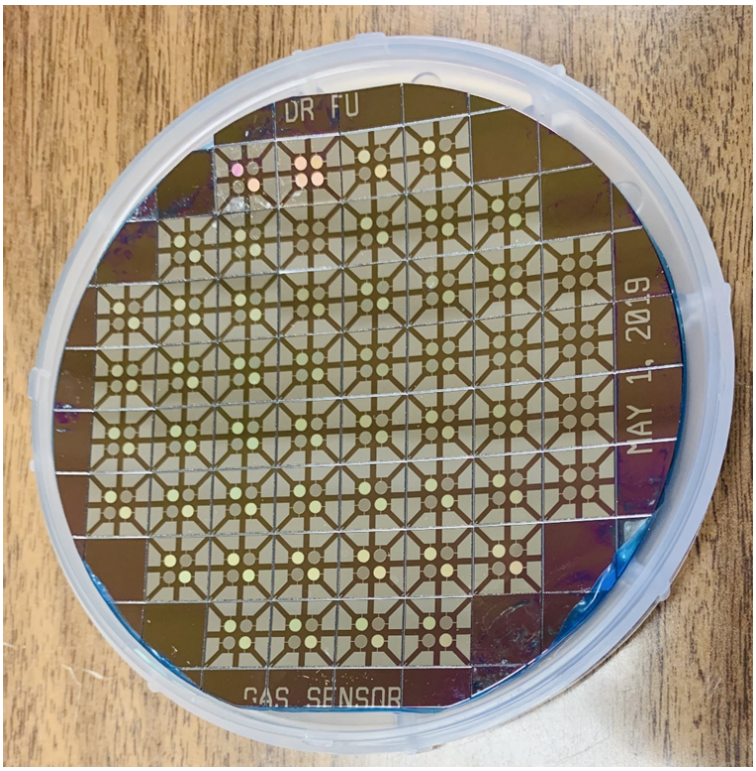

Figure 3.12. Diced wafer into 1 cm x 1 cm sensor chips.

5.4.4. Sensor Evaluation

The microsensor chip was wire-bonded on a 24-pin dual in-line package (DIP) Round Solder IC Socket by 200 μm in diameter aluminium (Al) wire. Au MPCs were dispersed in nanopure water by sonication for 5 mins and then drop-cast onto the four different IDE areas of the microchip by dropwise addition. The solvent was evaporated to afford a flat, roughly circular film of AuNPs. The chip was kept in an oven at 40 °C overnight to ensure removal of solvent from the film. The microsensor chip carrier was placed in a 4-way standard cross stainless-steel test chamber (C-0275, Kurt J. Lesker Company) fitted with inlet and outlet tubing. Sensing film resistances were measured and recorded by a multi-channel multimeter (Keithley DAQ 6510) and a single channel

multimeter (Keithley 2400). In a typical experiment of a particular gas sample (for a lab set-up schematic, Figure 3.13), sensor response was measured over 5 mins under a vacuum of 28 inches Hg to remove VOCs adsorbed on the Au MPCs sensor film, followed by gas sample exposure at atmospheric pressure, and then again for 5 minutes under vacuum of 28 inches Hg. The cycles were repeated at least three times to check reproducibility. Each sensor material was exposed to 100 ppb, 500 ppb, 1 ppm, and 5 ppm of benzene, toluene, ethylbenzene, xylene, nitrobenzene, cyclohexane, ethanol, and acetone single analyte samples.

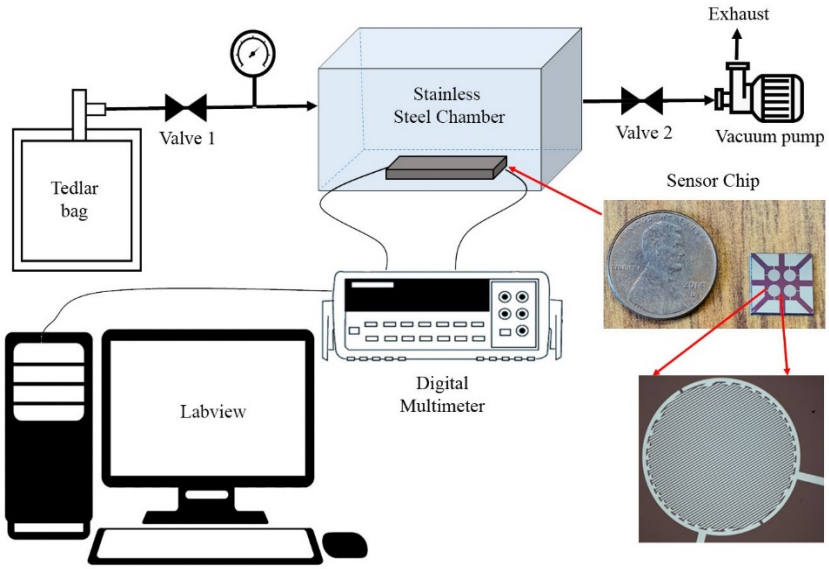

Figure 3.13. Laboratory setup showing test chamber for measuring chemiresistor responses to VOCs

All the analyte samples were prepared using Tedlar bags. A 1000 ppm concentration of benzene vapor was produced by injecting 3.7 µL of benzene into a Tedlar bag containing 1 L dry air. In similar fashion, 1000 ppm of toluene, ethylbenzene, xylene,

nitrobenzene, cyclohexane, ethanol, and acetone were made by injecting corresponding amounts of the solvents. Then, 100 mL of the above gas samples were removed from the Tedlar bag using an air-tight syringe and injected into a new Tedlar bag containing 900 mL of dry air, resulting in a concentration of 100 ppm. The 10 ppm samples were prepared in a similar way and the 5 ppm, 1 ppm, 500 ppb and 100 ppb of analyte samples were then produced by dilution processes using the 10 ppm sample. A small KNF diaphragm vacuum pump was then used to evacuate the test chamber followed by introduction of the analyte sample directly from the sample bag attached to the test chamber. All the experiments were performed under ambient conditions (at 22 °C).

5.4.5. Sensor Data Measurement.

The sensor response is defined by the following equation:

$$\text{Response} = \frac{R_o - R_{gas}}{R_{gas}} = \frac{R_o}{R_{gas}} - 1 \qquad (1)$$

where R_o and R_{gas} are the resistances of the sensor in synthetic air and in the presence of the analyte, respectively.[41] The response and recovery times are defined as the time taken by the sensors to achieve 90% of the total resistance change in either the adsorption or desorption case.

5.5. EXPERIMENTAL PROCEDURES OF CHAPTER 4

5.5.1. Functionalized Thiol Ligand Synthesis

Synthesis of an *N*-Boc Protected Aminooxy Hexane Thiol Ligand

n-Alkane (C6) *N*-Boc protected aminooxy thiol ligand (**4**) synthesized according to the experimental procedure described under 5.4.1.

Synthesis of an Oxy Benzoic Acid Thiol Ligand

The oxy benzoic acid thiol ligand was synthesized according to the reported synthetic route of Iqbal P. *et al*.[57]

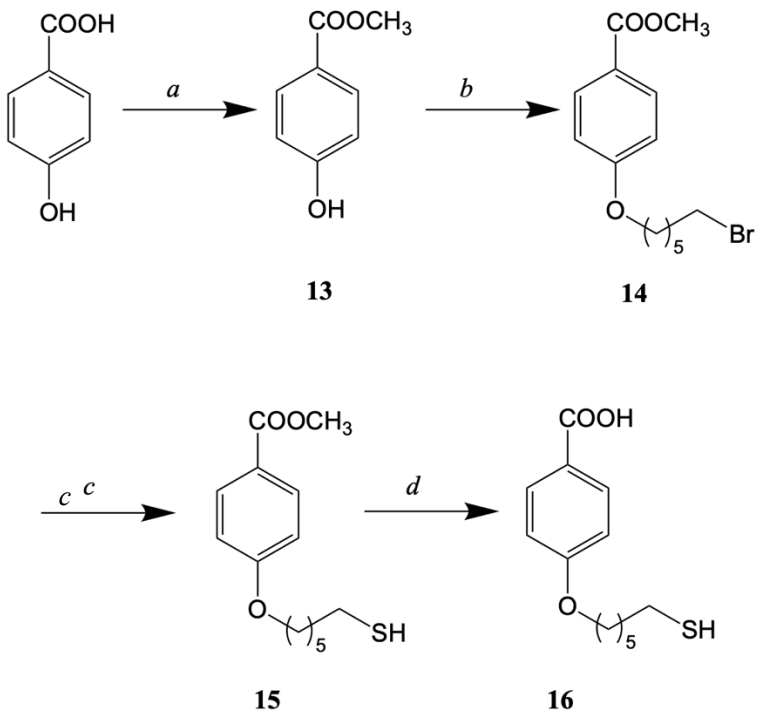

Scheme 4.2. Synthesis of an oxy benzoic acid thiol ligand; Reagents and conditions: a. cat. Conc. H_2SO_4, dry MeOH, reflux, 20 h; b. K_2CO_3, $Br(CH_2)_6Br$, dry CH_3CN, reflux, 20 h; c. Thiourea ($H_2NC(S)NH_2$), dry ethanol, reflux, 20 h; d. NaOH, THF, reflux, 20 h.

Methyl 4-hydroxybenzoate (13). 4-Hydroxybenzoic acid (7.038 g, 50.96 mmol) was dissolved in dry MeOH (100 mL) and conc. H_2SO_4 (0.55 mL, 10.2 mmol) was added dropwise while stirring the solution. The mixture was heated at reflux for 20 h and then allowed to cool to room temperature followed by concentration to ~10 mL using rotary evaporation. The crude solution was diluted with water (100.0 mL) and the aqueous layer was extracted with Et_2O (4 × 25.0 mL). The combined organic layer was washed with sat. NaCl solution (50.0 mL), dried (Na_2SO_4) and then filtered. The solvent was removed *in vacuo* to afford 6.970 g (90%) of compound **13** as white solid. ^{1}H NMR ($CDCl_3$, 400 MHz,): δ 7.96-7.94 (d, 2H), δ 6.90-6.86 (d, 2H), δ 3.90 (s, 3H).

Methyl 4-((6-bromohexyl) oxy) benzoate (14). To a solution of compound **13** (5.250 g, 34.54 mmol) in dry CH_3CN (150.0 mL) was added K_2CO_3 (9.547 g, 69.08 mmol) and 1,6-dibromohexane (10.6 mL, 69.1 mmol). The reaction mixture was heated at reflux with a $CaCl_2$ guard connected to reflux condenser for 20 h. The mixture then was allowed to cool to rt and the solvent was removed by rotary evaporation to a volume of ~10 mL. The crude mixture was diluted by addition of water (100.0 mL) and the crude product was extracted by washing with EtOAc (4 × 30.0 mL). The collected organic layers were combined and washed with sat. NaCl and dried over Na_2SO_4. Afterward, the mixture was concentrated using rotary evaporation and the obtained crude product was purified by SiO_2 column chromatography using 100 % CH_2Cl_2 to yield 7.940 g (73 %) of compound **14** as a white solid. TLC, R_f = 0.42 (100% CH_2Cl_2); ^{1}H NMR ($CDCl_3$, 400 MHz,): δ 7.99-7.97 (d, 2H), δ 6.91-6.89 (d, 2H), δ 4.03-4.00 (m, 2H), δ 3.88 (s, 3H), δ 3.44-3.41 (m, 2H), δ 1.91-1.08 (m, 4H), δ 1.59-1.51 (m. 4H).

Methyl 4-((6-mercaptohexyl) oxy) benzoate (15). To a solution of compound **14** (5.000 g, 15.87 mmol) in dry ethanol (100.0 mL) was added thiourea (1.312 g, 17.46 mmol). The reaction mixture was heated at reflux under argon for 20 h. After 20 h, 5 M aqueous NaOH (3.17 mL, 15.9 mmol) was added dropwise, and the mixture was refluxed for another 20 h. The mixture was allowed to cool to rt and concentrated to 10 mL by rotary evaporation. The remained solution was diluted with water (50.0 mL) and the mixture was acidified by adding 1 M HCl to yield a white precipitate. The crude precipitate was extracted to CH_2Cl_2 (5 × 40.0 mL) and combined CH_2Cl_2 layers were concentrated by rotary evaporation to yield a white precipitate. The obtained residue was purified by SiO_2 column chromatography using 100 % CH_2Cl_2 to yield 3.488 g (82 %) of compound **15** as a white solid. TLC, R_f = 0.33 (100% CH_2Cl_2); ^{1}H NMR ($CDCl_3$, 400 MHz,): δ 7.98-7.96 (d, 2H), δ 6.90-6.88 (d, 2H), δ 4.02-4.00 (m, 2H), δ 3.88 (s, 3H), δ 2.54-2.50 (m, 2H), δ 1.82-1.79 (m, 2H), δ 1.64-1.58 (m. 2H). δ 1.47 (m. 4H).

4-((6-Mercaptohexyl) oxy) benzoic acid (16). The thiol ester **15** (1.688 g, 6.298 mmol) was dissolved in THF (25.0 mL) and an aqueous solution (15.0 mL) of NaOH (0.504 g, 12.59 mmol) was added to the solution followed by heating at 95 °C for 3 h. The reaction mixture was cool to the room temperature and further to 0 °C. 1 M aqueous (HCl) was added to acidify the mixture and the white precipitate was extracted using CH_2Cl_2. The combined organic layers were dried over Na_2SO_4 and concentrated under reduced pressure to afford 1.360 g (85 %) of oxy-benzoic acid thiol **16** as a white solid. ^{1}H NMR ($CDCl_3$, 400 MHz): δ 8.06-8.04 (d, 2H), δ 6.93-6.92 (d, 2H), δ 4.04-4.01 (m, 2H), δ 2.56-2.54 (m,

2H), δ 1.82 (m, 2H), δ 1.66 (m. 2H). δ 1.49-1.47 (m. 4H); ^{13}C NMR ($CDCl_3$, 100 MHz) δ 171.28, 162.73, 132.49, 121.51, 114.35, 68.23, 34.00, 29.12-24.68.

5.5.2. Functionalized Thiol Capped Au MPCs Synthesis

Synthesis of 12-Cs^+/C6 Au MPCs Chemiresistive Film

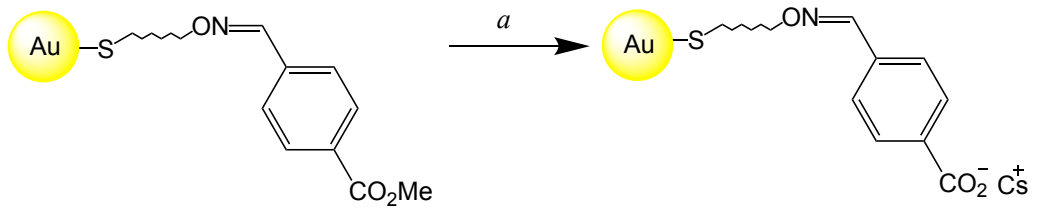

11 **12-Cs^+/C6**

Scheme 4.3. Synthesis of 12-Cs^+/C6 Au MPCs from Au MPCs 11. Only one ligand is emphasized. Reagents and conditions: a. $CsOH.H_2O$, THF, 0 °C to rt, 18 h.

To prepare the cesium sensor **12-Cs^+/C6**, a 0.5 M solution of cesium hydroxide monohydrate (0.459 mmol) in THF was added slowly to a solution of Au MPCs 11 (0.045 g) in THF (1.00 mL) at 0 °C. The reaction was allowed to warm to rt and stirred 18 h, whereupon the solvent was concentrated by rotary evaporation and the resultant Au MPCs suspended by addition of acetonitrile (6.00 mL). The cesium carboxylate-functionalized Au MPCs were isolated by centrifugation and then washed several times with acetonitrile (10 x 3.0 mL) and THF (5 x 3.0 mL) until the color of the pH paper changed to neutral.

Synthesis of an Oxy Benzoic Acid Thiolate Coated Au MPCs and Its Cesium Salt Chemiresistor

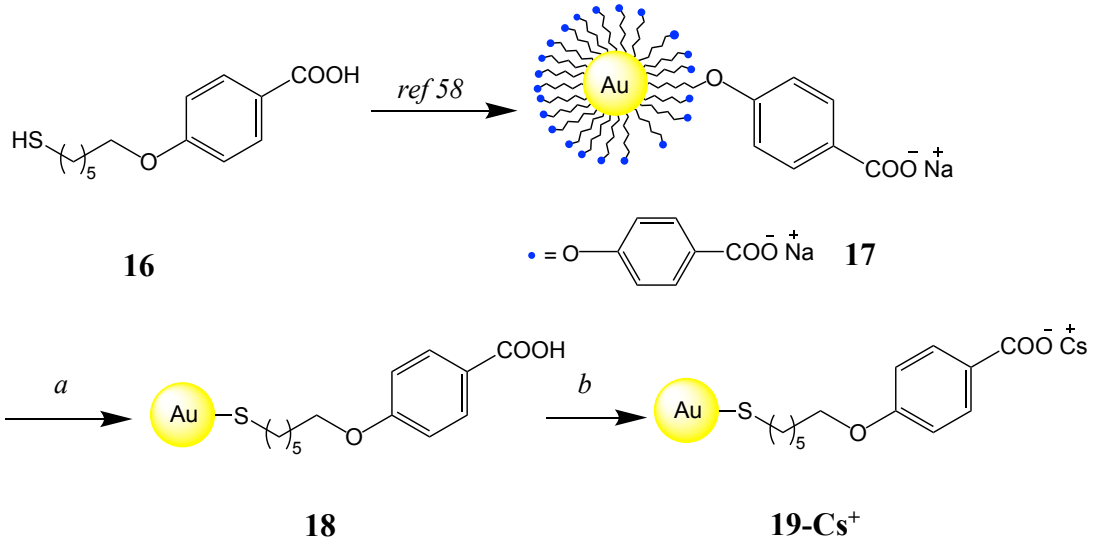

Scheme 4.4. Synthesis of cesium ion-functionalized *p*-oxybenzoate Au MPCs. Only one ligand is emphasized in MPCs **17-19**. Reagents and conditions: *a*. 0.5 M HCl, H_2O, 0 °C, 10 min.; *b*. 0.1 M CsOH.H_2O, THF, 0 °C, 10 min.

Synthesis of cesium salt of *p*-alkoxybenzoic acid functionalized Au MPCs (19-Cs^+). *p*-alkoxybenzoic acid-functionalized Au MPCs were synthesized according to the one-phase method described by Brust *et al.*[58] with several modifications using a 3:1 thiol:$HAuCl_4$•$3H_2O$ ratio. A solution of synthesized thiol benzoic acid **16** (0.423 g, 1.670 mmol) in THF (20.0 mL) was added to a solution of $HAuCl_4$•$3H_2O$ (0.219 g, 0.555 mmol) in methanol (180.0 mL) at rt. The reaction mixture was stirred vigorously for 2.5 h at rt under nitrogen. Once the mixture became colorless, it was cooled to 0 °C and a methanolic solution (30.0 mL) of freshly prepared $NaBH_4$ (0.210 g, 5.550 mmol) was added drop wise while stirring the solution vigorously. After 30 min string at 0 °C, the mixture was stirred

overnight at rt. The formed Au MPCs were isolated by removal of the methanolic layer using a pipette. The isolated precipitate was washed with methanol and THF several times to remove the excess $NaBH_4$ or unreacted thiol. The corresponding sodium carboxylate preparation of the *p*-alkoxybenzoic acid functionalized Au MPCs **17** was collected as a black precipitate.

To prepare the *p*-alkoxybenzoic acid functionalized Au MPCs, the Na^+-functionalized Au MPCs were dissolved in nanopure water and cooled to 0 °C followed by addition of 0.5 M aqueous HCl dropwise until a precipitate formed. The functionalized Au MPCs **18** were isolated by centrifugation and the precipitate was washed with nanopure water several times (until the solution pH was neutral to pH paper) to remove any remaining acid.

To a solution of the *p*-alkoxybenzoic acid functionalized Au MPCs **18** in THF at 0 °C was added dropwise 0.1 M cesium hydroxide monohydrate in THF until a precipitate formed. The formed precipitate was isolated by centrifugation and washed with THF several times (until the solution pH was neutral to pH paper) to afford the Au MPCs **19-Cs^+.**

<u>Synthesis of Cesium Carboxylate-Functionalized Au MPCs from Commercially Available Thiols</u>

Synthesis of Au MMPCs coated by 1-dodecanethiol and 11-mercaptoundecanoic acid: C12/Cs^+-MUA (21). The mixed monolayer Au MPCs **21** were synthesized according to the place-exchanged experimental procedure described under the "Synthesis of hexanethiol / K^+ salt of 4-mercaptobenzoic acid functionalized Au MPCs (c) in section **5.5.2.4.**" by

using 1-dodecanethiol as the non-linker ligand and 11-mercaptoundecanoic acid (MUA) as the linker ligand.

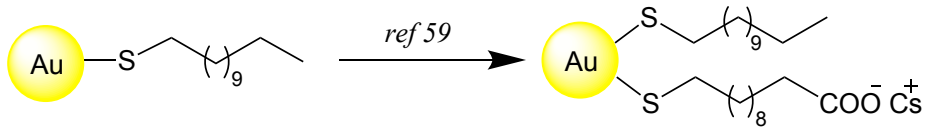

21

Scheme 4.5. Synthesis of Au MMPCs using 1-dodecanethiol and 11-mercaptoundecanoic acid.

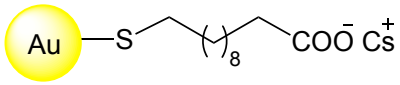

Synthesis of Cesium Salt of 11-Mercaptoundecanoic Acid Functionalized Au MPCs: Cs^+-MUA (22). The experimental procedure described under the "Synthesis of Au MPCs **19** in Section **5.5.2.**" was followed by using 11-mercaptoundecanoic acid as the thiol.

5.5.3. Microsensor Design and Fabrication

The experimental procedure mentioned under the section 5.4.3. was followed.

5.5.4. Sensor Evaluation

The experimental procedure mentioned under the section 5.4.4. was followed. Methanol, trichloroethylene, perchloroethylene, 1,2-dichloroethane, chloroform, DCM, 1,2-dichlorobenzene, cyclohexene, 1,1-dichloroethene, *trans*-1,2-dichloroethylene, *cis*-1,2-dichloroethylene, and 1,1-dichloroethane were used as the vapor analytes. All the analytes were dried using 48 hr oven dried (300°C) 4°A molecular sieves prior to analysis.

5.5.5. Sensor Data Measurement.

The experimental procedure mentioned under the section 5.4.5. was followed.

REFERENCES

R.1. CHAPTER 1 REFFERENCES

1. Gründler, P. *Chemical Sensors: An Introduction for Scientists and Engineers,* 1st ed.; Berlin Heidelberg: New York, 2007; pp 1-126.
2. Bănică, F.-G. *Chemical Sensors and Biosensors: Fundamentals and Applications,* 1st ed.; John Wiley & Sons: United Kingdom, 2012; pp 1-245.
3. Janata, J. *Principles of Chemical Sensors*, 2nd ed.; Springer: New York, 2009; pp 1-258.
4. What is a Sensor? https://www.electronicshub.org/different-types-sensors/ (accessed 11/29/2021).
5. Passive vs Active Sensing, https://www.nrcan.gc.ca/maps-tools-publications/satellite-imagery-air-photos/remote-sensing-tutorials/introduction/passive-vs-active-sensing/14639 (accessed 11/30/21).
6. Yan, J. *Machinery Prognostics and Prognosis Oriented Maintenance Management*, 1st ed.; Wiley & Sons: Singapore, 2015; pp 107-108.
7. Kenny, T. Chemical Sensors. In *Sensor Technology Handbook*; Wilson, J. S., Eds.; Newnes: USA, 2002; pp 181-191.
8. Sinclair, I. R. Sensors and transducers, 3rd ed.; Newnes: Boston, 2001; pp xi-xiv.
9. Fu, Z.; Lu, Y.-C.; Lai, J. J. *Chonnam Med J.* **2019**, *55(2)*, 86-98.
10. Khanna, V. K. *Nanosensors: Physical, Chemical, and Biological,* 2nd ed.; CRC Press: Florida, 2021; pp 100 - 556.
11. Ibañez, F. J.; Zamborini, F. P. *Small* **2012**, *8*, 174–202.
12. *Wohltjen, H.; Barger, W.R.; Snow, A.W.; Jarvis, N.L. IEEE Trans. Electron Devices.* **1985,** *32(7),* 1170–1174.
13. Panes-Ruiz, L. A.; Shaygan, M.; Fu, Y.; Liu, Y.; Khavrus, V.; Oswald, S.; Gemming, T.; Baraban, L.; Bezugly, V.; Cuniberti, G. *ACS Sens.* **2018,** *3,* 79-86.
14. Behi, S.; Bohli, N.; Casanova-Cháfer, J.; Llobet, E.; Abdelghani, A. *Sensors* **2020**, *20*, 3413.
15. Mirzaei, A.; Leonardi, S G.; Neri, G. *Ceram.* **2016**, *42(14),* 15119-15141.
16. Liu, Y.; Antwi-Boampong, S.; BelBruno, J. J.; Crane, M. A.; Tanski, S. E. *Nicotine & Tobacco Research* **2013**, *15(9),* 1511–1518.

17. Azzarelli, J. M.; *Mirica, K. A.*; Ravnsbæk, J. B.; Swager, T. M. *Proceedings of the National Academy of Sciences* **2014,** *111(51),* 18162–18166.

18. Van Gerwen, P.; Laureyn, W.; Laureys, W.; Huyberechts, G.; Op De Beeck, M.; Baert, K.; Suls, J.; Sansen, W.; Jacobs, P. *Sens. Actuators B Chem.* **1998**, *49(1–2),* 73–80.

19. Ahmad, W. R. W.; Mamat, M. H.; Zoolfakar, A. S.; Khusaimi, Z.; Rusop, M. A. *IEEE Student Conference on Research and Development (SCOReD)*, **2016**, pp. 1-6.

20. a. An Introduction to MEMS, https://engineeringproductdesign.com/mems-micro-electro-mechanical-system/ (accessed 12/20/2021) b. MEMES and Nanotechnology Exchange https://www.mems-exchange.org/MEMS/what-is.html (accessed 03/20/2022)

21. Adams, T. M.; Layton, R. A. Introductory MEMS Fabrication and Applications; 1st ed.; Springer, USA, 2010, pp 3-12.

22. Franke, M.E.; Koplin, T. J.; Simon, U. *Small* **2006***, 2(1),* 36–50.

23. Dovgolevsky, E.; Konvalina, G.; Tisch, U.; Haick, H. *J. Phys. Chem. C*. **2010,** *114,* 14042.

24. Ibañez, F. J.; Zamborini, F. P. *ACS Nano* **2008**, *2*, 1543.

25. Kim, J. K.; Yang, Y. S.; Ha, S. C.; Cho, S. M.; Kim, Y. S.; Kim, H. Y.; Yang, H.; Kim, Y. T. *Sens. Actuators B Chem.* **2005**, *106*, 189.

26. Han, L.; Daniel, D. R.; Maye, M. M.; Zhong, C.-J. *Anal. Chem.* **2001**, *73*, 4441

27. Liu, J.; Legros, S.; Ma, G.; Veinot, J. G. C.; Kammer, F.; Hofmann, T. *Chemosphere,* **2012**, *87(8),* 918–24.

28. Raguse, B.; Barton, C. S.; Müller, K.-H.; Chow, E.; Wieczorek, L. *J. Phys. Chem.* C. **2009,** *113(34),* 15390–15397.

29. Terrill, R.H.; Postlethwaite, T. A.; Chen, C.; Poon, C.-D.; Terzis, A.; Chen, A.; Hutchison, J. E.; Clark, M. R.; Wignall, G. *J. Am. Chem. Soc.* **1995,** *117(50),* 2537–48.

30. Wuelfing, W.P.; Murray, R. W. *J. Phys. Chem. B.* **2002,** *106(12),* 3139–3145

31. Wuelfing, W.P.; Green, S. J.; Pietron, J. J.; Cliffel, D. E.; Murray, R. W. *J. Am. Chem. Soc.* **2000**, *122(46),* 11465–11472.

32. https://commons.wikimedia.org/wiki/File:Circular_interdigitated_electrodes_with_and_without_gold_nanoparticle_chemiresistor_film.jpg (accessed12/01/2021).
33. Yan, H.; Choe, H.; Nam, S. S.; Hu, Y.; Das, S.; Klemic, J. F.; Ellenbogen, J. C.; Lieber, C. M. *Nature* **2010,** *470*, 240.
34. Yurko, G.; Roostaei, J.; Dittrich, T.; Xu, L.; Ewing, M.; Zhang, Y.; Shreve, G. *Chemosensors* **2019,** *7,* 40.
35. Li, H.-Y.; Zhao, S.-N.; Zang, S.-Q.; Li, J. *Chem. Soc. Rev.***, 2020**,49, 6364-6401.
36. Wilson, D. M.; Hoyt, S.; Janata, J.; Booksh, K.; Obando, L. *IEEE Sensors Journal* **2001**, *1(4),* 256–274.
37. Khanna, V.K. (2012). Nanosensors: Physical, chemical, and biological. Boca Raton, FL: CRC Press, pp 637.
38. Kong, J.; Franklin, N. R.; Zhou, C.; Chapline, M. G.; Peng, S.; Cho, K.; Dai, H. *Science* **2000,** *287(5453),* 622–625.
39. Bradley, K.;*Gabriel, J.-C. P.; Star, A.; Grüner, G. Appl. Phys. Lett*. **2003,** *83(18),* 3821–3823.
40. Helbling, T.; Hierold, C.; Durrer, L.; Roma, C.; Pohle, R.; Fleischer, M. *Physica. status Solidi B.* **2008,** *245(10),* 2326–30.
41. Maeng, S.; Moon, S.; Kim, S.; Lee, H.-Y.; Park, S.-J.; Kwak, J.-H.; Park, K.-H.; Park, J.; Choi, Y.; Udrea, F.; Milne, W. I.; Lee, B. Y.; Lee, M.; Hong, S. *Appl. Phys. Lett.* **2008**, *93(11),* 113111.
42. Penza, M.; Rossi, R.*;* Alvisi, M.; Signore, M. A.; Serra, E. *J. Phys. D: Appl. Phys.* **2009**, *42(7),* 072002.
43. Wang, F.; Swager, T. M. *J. Am. Chem. Soc.* **2011**, *133(29),* 11181–11193.
44. Bekyarova, E.; Davis, M.; Burch, T.; Itkis, M. E.; Zhao, B.; Sunshine, S.; Haddon, R. C. *J. Phys. Chem. B.* **2004**, *108(51),* 19717–19720.
45. Li, Y.; Wang, H.-C.; Yang, M.-J. *Sens. Actuators B Chem.* **2007,** *121(2),* 496–500.
46. Wang, F.; Gu, H.; Swager, T. M. et al. *J. Am. Chem. Soc.* **2008**, *130(16),* 5392–5393.
47. Wei, C.; Dai, L.; Roy, A.; Tolle, T. B. *J. Am. Chem. Soc.* **2006**, *128(5),* 1412–1413.

48. a. Norizan, M. N.; Moklis, M. H.; Demon, S. Z. N.; Halim, N. A.; Samsuri, A.; Mohamad, I. S.; Knight, V. F.; Abdullah, N. *RSC Adv.,* **2020**, *10,* 43704-43732. b. Zhang, W.-D.; Zhang, W.-H. *Journal of Sensors,* **2009**, 160698. c. Liu, Y.; Antwi-Boampong, S.; BelBruno, J. J.; Crane, M. A.; Tanski, S. E. *Nicotine Tob. Res.* **2013**, *15(9),* 1511–1518.
49. Tang, R.; Shi, Y.; Hou, Z.; Wei, L. *Sensors* **2017**, *17(4),* 882-889.
50. Huang, J.; Wei, Z.; Chen, J. *Sens. Actuators B Chem.* **2008**, *134(2),* 573–578.
51. Antwi-Boampong, S.; Mani, K. S.; Carlan, J.; BelBruno, J. J. *Journal of Molecular Recognition* **2014**, *27(1),* 57–63.
52. Cooper, J. S.; Myers, M.; Chow, E.; Hubble, L. J.; Pejcic, B.; Müller, K.-H.; Wieczorek, L.; Raguse, B. *J. Nanoparticle Res.* **2014**, *16(1),* 1–13.
53. Rao, C.N.R.; Govindaraj, A. Carbon Nanotubes. In Nanotubes and nanowires, The Royal Society of Chemistry, Cambridge, UK, 2005; pp 1-44. DOI: 10.1039/9781849732840
54. Schedin, F.; Geim, A. K.; Morozov, S. V.; Hill, E. W.; Blake, P.; Katsnelson, M. I.; Novoselo, K. S. *Nature Materials* **2007**, *6(9),* 652–655.
55. Joshi, R. K.; Gomez, H.; Farah, A.; Kumar, A. *Journal of Physical Chemistry C.* **2007**, *114(14),* 6610–6613.
56. Dan, Y.; Lu, Y.; Kybert, N. J.; Luo, Z.; Johnson, A. T. C. *Nano Letters*. **2009**, *9 (4)*, 1472–1475.
57. Ohno, Y.; Maehashi, K.; Yamashiro, Y.; Matsumoto, K. *Nano Letters*. **2009**, *9(9),* 3318–3322.
58. a. Robinson, J. T.; Perkins, F. K.; Snow, E. S.; Wei, Z.; Sheehan, P. E. Nano Letters. **2008**, *8(10),* 3137–3140. b. Lee, C. W.; Suh, J. M.; Jang, H. W. *Front.Chem*. **2019**, *7*, 708.
59. Turkevich, J.; Stevenson, P. C.; Hiller, J. Discuss. *Faraday Soc.* **1951**, 55.
60. Murphy, C.J.; Sau, T. K.; Gole, A. M.; Orendorff, C. J.; Gao, J.; Gou, L.; Hunyadi, S. E.; Li, T.; *J. Phys. Chem. B* **2005**, *109*, 13857.
61. Huang, X.; Neretina, S.; El-Sayed, M. A. *Adv. Mater.* **2009**, *21*, 4880.
62. Jana, N. R.; Gearheart, L.; Murphy, C. J. *J. Phys. Chem. B,* **2001**, *105*, 4065.
63. Gittins, I.; Caruso, F.; *J. Phys. Chem. B,* **2001**, *105*, 6846.

64. Ibañez, F. J.; Zamborini, F. P. *J. Am. Chem. Soc.* **2008**, *130*, 622.

65. Brust, M. Walker, D. Bethell, D. J. Schiffrin, R. Whyman, J. *Chem. Soc., Chem. Commun.* **1994**, *7*, 801.

66. Hostetler, M. J.; Wingate, J. E.; Zhong, C.-J.; Harris, J. E.; Vachet, R. W.; Clark, M. R.; Londono, J. D.; Green, S. J.; Stokes, J. J.; Wignall, G. D.; Glish, G. L.; Porter, M. D.; Evans, N. D.; Murray, R. W. *Langmuir,* **1998**, *14*, 17.

67. Wohltjen, H.; Snow, A. W. *Anal. Chem.* **1998**, *70*, 2856.

68. Zamborini, F. P.; Leopold, M. C.; Hicks, J. F.; Kulesza, P. J.; Malik, M. A.; Murray, R. W. *J. Am. Chem. Soc.* **2002**, *124*, 8958.

69. Joseph, Y.; Besnard, I.; Rosenberger, M.; Guse, B.; Nothofer, H.-G.; Wessels, J. M.; Wild, U.; Knop-Gericke, A.; Su, D.; Schlogl, R.; Yasuda, A.; Vossmeyer, T.; *J. Phys. Chem. B,* **2003**, *107*, 7406.

70. Briglin, S. M.; Gao, T.; Lewis, N. S. *Langmuir,* **2004**, *20*, 299.

71. Joseph, Y.; Guse, B.; Yasuda, A.; Vossmeyer, T. *Sens. Actuators B,* **2004**, *98*, 188.

72. Ibañez, F. J.; Zamborini, F. P. *J. Am. Chem. Soc.* **2008**, *130*, 622.

73. Templeton, A. C.; Hostetler, M. J.; Warmoth, E. K.; Chen, S.; Hartshorn, C. M.; Krishnamurthy, V. W.; Forbes, M. D. E.; Murray, R. W. *J. Am. Chem. Soc.* **1998**, *120*, 4845.

74. Hostetler, M. J.; Templeton, A. C.; Murray, R. W. *Langmuir* **1999**, *15*, 3782.

75. Brewer, S. H.; Glomm, W.R.; Knag, M. K.; Johonson, M. C.; Franzen, S. *Langmuir* **2005**, *21*, 9303.

76. Shiigi, H.; Tokonami, S.; Yakabe, H.; Nagaoka, T. J. *J. Am. Chem. Soc.* **2005**, *127*, 3280.

77. Ibañez, F. J.; Zamborini, F. P. *Langmuir* **2006,** *22*, 9789.

78. Zhang, H.-L.; Evans, S. D.; Henderson, J. R.; Miles, R. E.; Shen, T.-H. *Nanotechnology* **2002**, *13*, 439.

79. Ahn, H.; Chandekar, A.; Kang, B.; Sung, C.; Whitten, J. E. *Chem. Mater.* **2004**, *16*, 3274.

80. Tokonami, S.; Shiigi, H.; Nagaoka, T. *J. Electrochem. Soc.* **2008**, *115*, 105.

81. Krasteva, N.; Besnard, I.; Guse, B.; Bauer, R. E.; Mullen, K.; Yasuda, A.; Vossmeyer, T. *Nano Lett.* **2002**, *2*, 551.

82. Leopold, M. C.; Donkers, R. L.; Georganopoulou, D.; Fisher, M.; Zamborini, F. P.; Murray, R. W. *Faraday Discuss.* **2004**, *125*, 63.

83. Joseph, Y.; Krasteva, N.; Besnard, I.; Guse, B.; Rosenberger, M.; Wild, U.; Knop-Gericke, A.; Schlogl, R.; Krustev, R.; Yasuda, A.; Vossmeyer, T. *Faraday Discuss.* **2004**, *125*, 77-97.

84. Leibowitz, F. L.; Zheng, W.; Maye, M. M.; Zhong, C.-J. *Anal. Chem*. **1999**, *71*, 5076.

85. Harnack, O.; Raible, I.; Yasuda, A.; Vossmeyer, T. *Appl. Phys. Lett.* **2005**, *86,* 034108.

86. Covington, E.; Bohrer, F. I.; Xu, C.; Zellers, E. T.; Kurdak, C. *Lab Chip,* **2010**, *10*, 3058.

87. Raguse, B.; Christopher, E. C.; Barton, C. S.; Wieczorek, L. *Anal. Chem.* **2007,** *79*, 7333

88. Ibañez, F. J.; Growrishetty, U.; Crain, M. M.; Walsh, K. M.; Zamborini, F. P. *Anal. Chem.* **2006,** *78*, 753.

89. Erkoc, P.; Ulucan-Karnak, F. *Prosthesis* **2021**, *3*, 25-52.

90. Sheng, P.; Abeles, B. *Phys. Rev. Lett.* **1972**, *28*, 34.

91. Culligan Water https://www.culligannation.com/vocs-impact-drinking-water/ (accessed 12/30/2021).

92. ThermoFisherScientific https://www.thermofisher.com/us/en/home/industrial/environmental/environmental-learning-center/contaminant-analysis-information/volatile-organic-compounds-analysis.html (accessed 12/30/2021).

93. United States environmental protection Agency https://www.epa.gov/laws-regulations/summary-occupational-safety-and-health-act (accessed 12/31/2021).

94. United States department of Labor https://www.osha.gov/annotated-pels (accessed 12/31/2021).

95. Awe International https://www.aweimagazine.com/article/voc-detection-and-measurement-techniques/ (accessed 12/31/2021).

96. Montes-García, V.; Squillaci, M. A.; Diez-Castellnou, M.; Ong, Q. K.; Stellacci, F.; Samorì, P. *Chem. Soc. Rev.* **2021**, *50*, 1269−1304.

97. Potyrailo, R. A. *Chem. Soc. Rev*. **2017,** *46*, 5311−5346.

98. Ingram, R. S.; Hostetler, M. J.; Murray, R. W. *J. Am. Chem. Soc.* **1997**, *119*, 9175-9178.

99. Evans, S. D.; Johnson, S. R.; Cheng, Y. L.; Shen, T.; *J. Mater. Chem.* **2000**, *10*, 183.

100. Zhang, H.-L.; Evans, S. D.; Henderson, J. R.; Miles, R. E.; Shen, T.-H. *Nanotechnology* **2002**, *13*, 439–444.

101. Han, Li.; Shi, X.; Wu, W.; Kirk, F. L.; Luo, J.; Wang, L.; Mott, D.; Cousineau, L.; Lim, S. I. I.; Lu, S.; Zhong, C. J. *Sens. Actuators B Chem.* **2005,** *106*, 431-441.

102. Foos, E. E.; Snow, A. W.; Twigg, M. E.; Ancona, M. G. *Chem. Mater.* **2002**, *14*, 2401.

103. Garg, N.; Mohanty, A.; Lazarus, N.; Schultz, L.; Rozzi, T. R.; Santhanam, S.; Weiss, L.; Snyder, J. L.; Fedder, G. K.; Jin, R. *Nanotechnology* **2010**, *21*, 405501.

104. Cai, Q.-Y.; Zellers, E. T.; *Anal. Chem.* **2002,** *74*, 3533.

105. Peng, G.; Hakim, M.; Broza, Y. Y.; Billan, S.; Abdah-Bortnyak, R.; Kuten, A.; Tisch, U.; Haick, H.; Brit. J. *Cancer,* **2010,** *103*, 542.

106. Peng, G.; Tisch, U.; Adams, O.; Hakim, M.; Shehada, N.; Broza, Y. Y.; Billan, S.; Abdah-Bortnyak, R.; Kuten, A.; Haick, *Nat. Nanote chnol.* **2009**, *4*, 669.

107. García-Berríos, E.; Brunschwig, B. S.; Gao, T.; Woodka, M. D.; Ellsworth, M. W.; Maldonado, S.; Lewis, N. S. *J. Phys. Chem. C*. **2010,** *114*, 21914.

108. Wang, L.-S.; Xiajing, K.; Karuiki, N. N.; Schadt, M.; Wang, G. R.; Rendeng, Q.; Choi, J.; Luo, J.; Lu, S.; Zhong, J C.-J. *Am. Chem. Soc.* **2007**, *129*, 2161.

109. Guo, J.; Pang, P.; Cai, Q. *Sens. Actuators B Chem.* **2007**, *120*, 52.

110. Joseph, Y.; Guse, B.; Vossmeyer, T.; Yasuda, A. *J. Phys. Chem. C* **2008**, *112*, 212507.

R.2. CHAPTER 2 REFFERENCES

1. United States Department of Labor, https://www.osha.gov/chemicaldata/476 (accessed 1/16/2022)
2. State of New Jersey Department of Health, https://nj.gov/health/workplacehealthandsafety/right-to-know/ (accessed 1/16/2022).
3. Miekisch, W.; Schubert, J. K.; Gabriele, F. E.; Schomburg, N. *Clin. Chim. Acta*. **2004**, *347*, 25-39.
4. Rooth, G.; Östenson, S. *Lancet* **1966,** *288*, 1102-1105.
5. Kim, K. H.; Jahan, S. A.; Kabir, E. *Trends Analyt. Chem.* **2012**, *33*, 1-8.
6. a. Ivanco, J.; Luby, Š.; Jergel, M.; Šiffalovic, P.; Benkovicová, M.; Halahovets, Y.; Majková, E.; Rella, R.; Manera, M. G. *Sensor Lett*. **2013**, *11*, 1–5. b. Alizadeh, N.; Jamalabadi, H.; Tavoli, F. *IEEE Sens. J*. **2020**, *20(1),* 5-31.
7. Wang, L.; Yun, X.; Stanacaevic, M.; Gouma, P. I. An Acetone Nanosensor for Non-invasive Diabetes Detection, AIP Conference Proceedings, **1137**, 206, 2009.
8. Jia, Q. Q.; Ji, H. M.; Wang, D. H.; Bai, X.; Sun, X. H.; Jin, Z. G. *J. Mater. Chem. A.* **2014**, *2*, 13602-13611.
9. a. Xiao, T.; Wang, X. Y.; Zhao, Z. H.; Li, L.; Zhang, L.; Yao, H. C.; Wang, J. S.; Li, Z. J. *Sens. Actuators B: Chem.* **2014**, *199*, 210-219. b. Righettoni, M.; Tricoli, A.; Pratsinis, S. E. *Chem. Mater*. **2010**, *22*, 3152-3157. c. Bai, X.; Ji, H. M.; Gao, P.; Zhang, Y.; Sun, X. H. *Sens. Actuators B:* **2014**, *193*, 100- 106. d. Choi, S. J.; Fuchs, F.; Demadrille, R.; Grévin, B.; Jang, B. H.; Lee, S. J.; Lee, J. H.; Tuller, H. L.; Kim, I. D. *ACS Appl. Mater. Interfaces* **2014**, *6*, 9061-9070.
10. Wang, C.; Zhu, J. W.; Liang, S. M.; Bi, H. P.; Han, Q. F.; Liu, X. H.; Wang, X. J. Mater. *Chem. A*. **2014**, *2*, 18635-18643.
11. Singkammo, S.; Wisitsoraat, A.; Sriprachuabwong, C.; Tuantranont, A.; Phanichphant, S.; Liewhiran, C. *ACS Appl. Mater. Interfaces*. **2015**, *7*, 3077-3092.
12. Shellaiah, M.; Sun, K. W. *Sensors*, **2021**, *21*, 633.
13. Nemufulwi, M. I.; Swart, H. C.; Mhlongo, G. H. *Mater. Res. Bull*. **2021**, *142*, 111395.

14. Patel, S. V.; Hobson, S.; Cemalovic, S.; Tolley, W. K. *ACS Appl. Nano Mater*. **2018,** *1(8),* 4092–4100.
15. Chen, L.; Huang, L.; Lin, Y.; Sai, L.; Chang, Q.; Shi, W.; Chen, Q. *Sens. Actuators B: Chem.* **2018**, *255(2),* 1482-1490.
16. Young, S. J.; Lin, Z. D. *Microsyst. Technol*. **2018**, *24(10)*, 3973–3976.
17. Hwang, S. I.; Chen, H.-Y.; Fenk, C.; Rothfuss, M. A.; Bocan, K. N.; Franconi, N. G.; Morgan, G. J.; White, D. L.; Burkert, S. C.; Ellis, J. E.; Vinay, M. L.; Rometo, D. A.; Finegold, D. N.; Sejdic, E.; Cho, S. K.; Star, A. *ACS Sens.* **2021**, *6*, 871−880.
18. a. Tu, M.-C.; Svm, H. K.; Thilini, A; Wallace, L. T. L.; Moochhala, S.; Yildiz, U. H.; Palaniappana, A.; Liedberg, B. *Sens. Actuators B Chem.* **2017**, *247*, 916– 922. b. Baysak, E.; Yuvayapan, S.; Aydogan, A.; Hizal, G. *Sens. Actuators B Chem.* **2018***, 258*, 484–491.
19. Ellis, J. E.; Star, A. *ChemPlusChem*. **2016**, *81*, 1248 – 1265.
20. Luo, J.; Luo, J.; Wang, L.; Shi, X.; Yin, J.; Crew, E.; Lu, S.; Lesperance, L. M.; Zhong, C.-J. *Sens. Actuators B Chem*. **2012**, *161*, 845-854.
21. a. Pavluchenko, A. S.; Mamykin, A. V.; Kukla, A. L.; Konoshchuk, N. V.; Posudievsky, O. Y.; Koshechko, V. G. *Sens. Actuators B Chem*. **2016**, *232*, 203-218. b. Mallya, A. N.; Kottokkaran, R.; Ramamurthy, P. C. *Sens. Actuators B Chem*. **2014,** *201*, 308-320.
22. a. Kang, E.; Kim, M.; Oh, J. S.; Park, D. W.; Shim, S. E. *Macromol. Res*. **2012**, *20(4),* 372-378. b. Choi, J.; Leea, J.; Choi, J.; Jung, D.; Shim, S. E. *Synthetic Metals* **2010**, *160*, 415–1421. c. Jeong, Y. J.; Koo, W.-T.; Jang, J.- S.; Kim, D.-H.; Cho, H.-J; Kim, I.-D. *Nanoscale* **2018**, *10,* 13713-13721.
23. Yang, J.; Shih, Y.-R.; Chen, I.-C.; Kuo, C.-I.; Huang, Y.-S. *Appl. Spectrosc.* **2005**, *59(8),* 1002-1008.
24. Meng, Z.; Stolz, R. M.; Mendecki, L. M.; Mirica, K. A. *Chem. Rev.* **2019**, *119*, 478−59.
25. Konvalina, G.; Haick, H. *Acc. Chem. Res.* **2014**, *47(1),* 66-76.
26. Wang, H.L.; Li, B.; Wu, H.; Hu, T.L.; Yao, Z. Z.; Zhou, W.; Xiang, S.C.; Chen, B.L. *J. Am. Chem. Soc.* **2015**, *137(31),* 9963-9970.

27. Luo, X.Z.; Jia, X.J.; Deng, J.H.; Zhong, J.L.; Liu, H.J.; Wang, K.J.; Zhong, D.C. *J. Am. Chem. Soc*. **2013**, *135(32),* 11684-11687.

28. Kaftory, M.; Kapon, M.; Botoshanksy, M. *Chem. Mater.* **1994**. *6(8),* 1245-1249.

29. a. Hooper, A.E.; Kennedy, S.R.; Jones, C.D.; Steed, J.W. *ChemComm.* **2016**, *52(1),* 198-201. b. Wilcox, C. S.; Kim, E.; Romano, D.; Kuo, L. H.; Burt, A. L.; Curran, D. P. *Tetrahedron* **1995**, *51*, 621.

30. a. Howlader, P.; Das, P.; Zangrando, E.; Mukherjee, P.S. *J. Am. Chem. Soc*. **2016**, *138(5),* 1668- 1676. b. Amendola, V.; Fabbrizzi, L.; Mosca, L. *Chem. Soc. Rev.* **2010**, *39(10),* 3889-3915.

31. Bregovic, V.B.; Basaric, N.; Mlinaric-Majerski, K. *Coord. Chem. Rev.* **2015**, *295*, 80-124. b. Yabuuchi, K.; Marfo-Owusu, E.; Kato, T. *Organic & Biomolecular Chemistry* **2003**, *1(19)*, 3464-3469.

32. Zheng, W.; Fu, Y.; Liu, L.; Guo, Q. *Acta Phys. -Chim. Sin*. **2007**, *23(7)*, 1018−1024.

33. Xie, Z.; Raju, M. V. R.; Stewart, A. C.; Nantz, M. H.; Fu, X.-F. *RSC Adv.* **2018**, *8*, 35618–35624.

34. Xie, Z.; Raju, M. V. R.; Adhihetty, P. K.; Fu, X.-F.; Nantz, M. H. *Sensors* **2020**, *20*, 7024.

35. Hosseini, M.W.; Blacker, A.J.; Lehn, J.M. *J. Am. Chem. Soc*. **1990**, *112(10),* 3896-3904.

36. Zie, Z. Electronic nose for analysis of volatile organic compounds in air and exhaled breath. Ph. D. Thesis, University of Louisville, May 2017.

37. a. Güntner, A.T.; Koren, V.; Chikkadi, K.; Righettoni, M.; Pratsinis, S.E. *ACS Sens*. **2016**, *1*, 528–535. b. K.J.; Jang, H.W. *Sensors* **2010**, *10*, 4083–4099.

38. Master Organic Chemistry, https://www.masterorganicchemistry.com/2014/07/01/substituted-cyclohexanes-a-values/ (2/27/2022).

39. Boiadjiev, S. E.; Lightner, D. A. *J. Am. Chem. Soc.* **2000**, *122*, 11328-11339.

40. Edwards, J.O.; Pearson, R. G. *J. Am. Chem. Soc.* **1962**, *84*, 16-21.

41. Grekov, A.P.; Veselov, V. Y. *Chem. Rev*. **1978**, 47, 631-648.

42. a. Bordwell, F.G.; Ji, G.Z. *J. Am. Chem. Soc*. **1991**, *113(22),* 8398-8401. b. Bordwell, F.G.; Fried, H.E.; Hughes, D.L.; Lynch, T.Y.; Satish, A.V.; Whang, Y.E. Journal of Organic Chemistry **1990**, *55(10),* 3330-3336.

43. a. Bordwell, F.G. *Acc. Chem. Res.* **1988**, *21(12),* 456-463. b. Bordwell, F.G.; Algrim, D.J.; Harrelson, J.A. *J. Am. Chem. Soc*. **1988**, *110(17),* 5903-5904.

44. Brust, M.; Walker, M.; BethellD.; Schiffrin, D. J.; Whyman, R. *J. Chem. Soc., Chem. Commun.* **1994**, 801-802

R.3. CHAPTER 3 REFFERENCES

1. Queensland Government, Department of Environment and Science, https://environment.des.qld.gov.au/management/activities/non-mining/fraccing/btex-chemicals (accessed 3/12/22).
2. Chromatography Today, https://www.chromatographytoday.com/article/gas-chromatography/64/pollution-analytical-equipment/why-do-you-need-to-measure-btex-in-ambient-air/2552 (accessed 3/13/22).
3. KORE Technology, https://kore.co.uk/applications/environment/btex-in-ambient-air/ (accessed 3/12/22).
4. United States Department of Labor, https://www.osha.gov/annotated-pels/table-z-1 (accessed 3/13/22).
5. ENVIROTECH online, Detection of BTEX in Environmental Air, https://www.envirotech-online.com/news/air-monitoring/6/ametek-mocon/detection-of-btex-in-ambient-air/31095 (accessed 3/12/22).
6. AMETEMOCON, BTEX in Ambient Air, https://www.thomasnet.com/catalogs/item/10067547-6982-1026-1007/ametek-mocon/br-btex-in-ambient-air-application/ (accessed 3/12/22).
7. Aeroqual, Real-Time BTEX / Benzene Monitor, https://www.aeroqual.com/products/aqm-stations/btex-benzene-monitor (accessed 3/13/22).
8. Kerchich, Y.; Kerbachi, R. *J. Air Waste Manag. Assoc.* **2012,** *62(12),* 1370-1379.
9. Finlayson-Pitts, B.J.; Pitts, J.N. *J. Air Waste Manag. Assoc.* **1993**, *43*, 1091–1100.
10. a. Soleimani, E. *Rev. Anal. Chem*. **2020,** *39*, 168–187. b. Alloucha, A.; Calvéa, S.L.; Serra, C. A. *Sens. Actuators B Chem.* **2013,** *182*, 446–452. c. Spinelle, L.; Gerboles, M.; Kok, G.; Persijn, S.; Sauerwald, T. *Sensors*. **2017**, *17*, 1520.
11. a. Majhi, S.M.; Mirzaei, A.; Kim, H.W.; Kim, S.S.; Kim, W. *Nano Energy*. **2021**, *79* ,105369. b. Mirzaei, A.; Kim, J.-H.; Kim, H. W.; Kim, S. S. *J. Mater. Chem. C* **2018**, *6,* 4342-4370.
12. Badjagbo, K.; Picard, P.; Moore, S.; Sauvé, S. *J. Am. Soc. Mass. Spectrom.* **2009**, *20(5),* 829-836.

13. a. Baimatova, N.; Kenessov, B.; Koziel, J. A.; Carlsen, L.; Bektassov, M.; Demyanenko, O. P. *Talanta* **2016**, *1(154),* 46-52. b. Bahrami, M.; Pirmohammadi, Z.; Bahrami, A. *Biomed. Chromatogr.* **2021**, *35(9),* 5131. c. Baimatova, N.; Koziel, J. A.; Kenessov, B.; *Anal. Chim. Acta.* **2015**, *11(873),* 38-50.
14. a. Tumbiolo, S.; Gal, J.-F.; Maria, P.-C.; Zerbinati, O. *Anal. Bioanal. Chem.* **2004**, *380*, 824-30. b. Riboni, N.; Trzcinski, J. W.; Bianchi, F.; Massera, C.; Pinalli, R.; Sidisky, L.; Dalcanale, E.; Careri, M. *Analytica. Chimica. Acta.* **2016**, *905*, 79-84.
15. Lara-lbeas, I.; Rodríguez-Cuevas, A.; Andrikopoulou C.; Persona, V.; Baldas, L.; Colin, S.; Calve, S. L. *Micromachines (Basel).* **2019**, *10(3),* 187.
16. Rodríguez-Cuevas, A.; Lara-Ibeas, I.; Leprince, A.; Wolf, M.; Calv´e, S. L. *Sens. Actuators B Chem*. **2020**, *324*, 128690.
17. Rebordão, G.; Susana I C J Palma, S. I. C. J.; Roque, A. C. A. *Sensors (Basel)* **2020,** *9(20),* 5742.
18. Ueno, Y.; Horiuchi, T.; Morimoto, T.; Niwa, O. *Anal. Chem*. **2001**, *73*, 4688-4693.
19. Iyer, A.; Mitevska, V.; Samuelson, J.; Campbell, S.; Bhethanabotla, V. R. *Sensors (Basel)* **2021**, *21(16),* 5667.
20. Wang, Z.; Liu, K.; Chang, X.; Qi, Y.; Shang, C.; Liu, T.; Liu, J.; Ding, L.; Fang**,** Y. *ACS Appl. Mater. Interfaces* **2018**, *10(41),* 35647–35655.
21. a. Patil, K.; Jeong, S.; Lim, H.; Byun, H.; Han, S. *Environ Eng Res*. **2019**, *24(4),* 600-607. b. Saha, D.; Mirando, N.; Levchenko, A. *J. Clean. Prod*. **2018**, *182*, 372-378. c. Baytar, O.; Sahin, O.; Horoz, S.; Kutluay, S. *Environ Sci Pollut Res.* **2020**, *27*, 26191-26210.
22. Megías-Sayagoa, C.; Lara-Ibeasb, I.; Wang, Q.; Calvé, S.L.; Louis, B. *J. Environ. Chem. Eng.* **2020***, 8*, 103724.
23. Gura, S.; Tarifa, A.; Mulloor, J.; Torres, M. N.; Almirall, J. R. *Analytica Chimica Acta.* **2018,** *1014*, 27-40.
24. a. Khan, S.; Newport, D.; Calve, S.L. *Spectrochimica Acta Part A: Molecular and Biomolecular Spectroscopy* **2020**, *243*, 118727. b. Crystal Kou, D.; Ma, W.; Zhang, S.; Li, R.; Zhang, Y. *ACS Appl. Mater. Interfaces* **2020**, *12(10),* 11955–11964. c.

Alloucha, A.; Calvéa, S.L.; Serra, C.A. *Sens. Actuators B Chem***. 2013**, *182*, 446–452.

25. Sekharz, P. K.; Subramaniyam, K. *ECS Electrochemistry Letters* **2014**, *3(2),* B1-B4.
26. a. Favard, A.; Aguir, K.; Contaret, T.; Dumas, A.; Bendahan, M. *Mater. Today*, **2019**, *6(3),* 323-327. b. Caoa, J.; Wang, S.; Li, J.; Xing, Y.; Zhao, X.; Li, D. *Sens. Actuators B Chem***. 2020**, *315*, 128120.
27. a. Wang, D.; Yin, Y.; Xu, P.; Wang, F.; Wang, P.; Xu, J.; Wang, X.; Li, X. *J. Mater. Chem. A* **2020**, *8*, 11188-11194. b. Thangamani, J.G.; Pasha, S.K.K. *Chemosphere* **2021,** *277*,130237.
28. Behi, S.; Bohli, N.; Casanova-Cháfer, J.; Llobet, E.; Abdelghani, A. *Sensors*. **2020**, *20*, 3413.
29. Luo, S.L.; Lin, C.; Ku, K.H.; Yoshinaga, K.; Swager, T.M. *ACS Nano.* **2020**, *14(6),* 7297–7307.
30. Hodul, J.N.; Murray, A.K.; Carneiro, N.F.; Meseke, J.R.; Morris, J.; He, X.; Zemlyanov, D.; Chiu, G.T.; Braun, J.E.; Rhoads, J.F.; Boudouris, B.W. *ACS Applied Nano Materials* **2020**, *3(10),* 10389-10398.
31. a. Cooper, J. S.; Myers, M.; Chow, E.; Hubble, L. J.; Cairney, J. M.; Pejcic, B.; Muller, K. H.; Wieczorek, L.; Raguse, B. *J. Nanopart. Res*. **2014**, *16*, 2173. b. Dilonardo, E.; Alvisi, M.; Rossi, R.; Cassano, G.; Di Palo, F.; Palazzo, G.; Penza, M., *MRS Advances*, **2017**, *2(18),* 1009-1014.
32. a. Cooper, J. S.; Kiiveri, H.; Hubble, L. J.; Chow, E.; Webster, M. S.; Muller, K.-H.; Sosa-Pintos, A.; Bendavid, A.; Raguse, B.; Wieczorek, L. *Analyst (Cambridge, United Kingdom)* **2015**, *140(9),* 3233-3238. b. Clément, P.; Korom, S.; Struzzi, C.; Parra, E.J.; Bittencourt, C.; Ballester, P.; Llobet, E. *Adv. Funct. Mater.* **2015**, *25*, 4011–4020.
33. Alkilany, M. A.; Murphy, C. J. *J. Nanopart. Res*. **2010,** *12*, 2313–2333.
34. Motes–Garca, V.; Squillaci, M. A.; Diez-Castellnou, M.; Ong, Q. K.; Stellacci, F.; Samorì, P. *Chem. Soc. Rev.* **2021**, *50*, 1269–1304,

35. a. Ibañez, F. J.; Growrishetty, U.; Crain, M. M.; Walsh, K. M.; Zamborini, F. P. *Anal. Chem.* **2006**, *78*, 753–761. b. Steinecker, W. H.; Rowe, M. P.; Zellers, E. T. *Anal. Chem.* **2007**, *79*, 4977–4986.

36. a. Hamwell, M. D.; Heriot, S. Y.; Richardson, T. H.; Cowlama, N.; Ross, I. N. *Colloids Surf. A: Physicochem. Eng. Asp.* **2006**, *284-285*, 379–383. b. Joseph, Y.; Peić, A.; Chen, X.; Michl, J.; Vossmeyer, T.; Yasuda, A. *J. Phys. Chem. C.* **2007**, *111*, 12855–12859.

37. Wohltjen, H; Snow, A. W. *Anal.Chem.* **1998**, *70*, 2856-259.

38. Han, L.; Shi, X.; Wu, W.; Kirk, F. L.; Luo, J.; Wang, L.; Mott, D.; Cousineau, L.; Lim, S. I.-I.; Lu, S.; Zhong, C. J. *Sens. Actuators B Chem.* **2005,** *106*, 431-441.

39. Huang, R-X.; Lu, C.-J.; Tian, W.-C. *Chemosensors* **2014**, *2(1),* 85-96.

40. Kim, Y. J.; Pyo, H.-B.; Park, S. H. In *Response Properties of the Gold Nanoparticle Sensors toward Benzene and Toluene Vapors,* IEEE SENSORS, EXCO, Daegu, Korea, October 22-25, 2006.

41. Xie, Z.; Raju, M. V. R.; Stewart, A. C.; Nantz, M. H.; Fu, X.-A. *RSC Adv*. **2018**, *8*, 35618–35624.

42. Kimura, M.; Yokokawa, M.; Sato, S.; Fukawa, T.; Mihara, T. *Chem. Lett*. **2011**, *40*, 1402–1404.

43. Ma, J. C.; Dougherty, D. A. *Chem. Rev*. **1997**, *97*, 1303–1324.

44. a. Mecozzi, S.; West, A. P.; Dougherty, D. A. *J. Am. Chem. Soc.* **1996,** *118*, 2307–2308. b. Raju, R. K.; Bloom, J. W. G.; An, Y.; Wheeler, S. E. *Chem. Phys. Chem.* **2011**, *12,* 3116–30. c. Gapeev, A.; Yang, C.-N.; Klippenstein, S. J.; Dunbar, R. C. *J. Phys. Chem. A.* **2000,** *104***,** 3246–3256.

45. Gallivan, J. P.; Dougherty, D. A. *J. Am. Chem. Soc.* **2000**, *122***,** 870–874.

46. Marshall, M. S.; Steele, R. P.; Thanthiriwatte, K. S.; Sherrill, C. D. *J. Phys. Chem. A*. **2009**, *113*, 13628–32.

47. Kumpf, R. A.; Dougherty, D. A. *Science* **1993**, *261*, 1708–1710.

48. a. Yi, H.-B.; Lee, H. M.; Kim, K. S. *J. Chem. Theory Comput.* **2009**, *5*, 1709–1717. b. Anslyn, E. V.; Dougherty, D. A. Solutions and non-covalent binding forces, Modern Physical Organic Chemistry, University Science Books: Sausalito, California, 2004, pp. 180-186.

49. a. Mecozzi, S.; West Jr, A. P.; Dougherty, D. A. *Proc. Natl. Acad. Sci. USA*, **1996**, *93*, 10566–10571, b. Hunter, C. A.; Low, C. M. R.; Rotger, C.; Vinter, J. G.; Zonta, C. *Proc. Natl. Acad. Sci. USA*, **2002**, *99*, 4873–4876.

50. a. Heemstra, J. M.; Moore, J. S. *Chem. Commun.* **2004**, *13*, 1480–1481. b. Schneider, H.-J. Prof., *Angew. Chem. Int. Ed.* **2009,** *48*, 3924–3977.

51. a. Yamada, S.; Morita, C. *J. Am. Chem. Soc.* **2002**, *124*, 8184–8185. b. Yamada, S.; Yamashita, K. *Tetrahedron Lett.* **2008**, *49*, 32–35. c. Kennedy, C. R.; Lin, S.; Jacobsen, E. N. *Angew. Chem. Int. Ed.* **2016**, *55*, 2-31.

52. a. Chen, W.; Elfeky, S. A.; Nonne, Y.; Male, L.; Ahmed, K.; Amiable, C.; Axe, P.; Yamada, S.; James, T. D.; Bull, S. D.; Fossey, J. S. *Chem. Commun.* **2011**, *47*, 253–255. b. Meyer, E. A.; Castellano, R. K.; Diederich, F. *Angew. Chem., Int. Ed.* **2003**, *42*, 1210-1250.

53. Leopold, M. C.; Donkers, R. L.; Georganopoulou, D.; Fisher, M.; Zamborini, F. P.; Murray, R. W. *Faraday Discuss.* **2004**, *125*, 63–76.

54. Zamborini, F. P.; Leopold, M. C.; Hicks, J. F.; Kulesza, P. J.; Malik, M. A.; Murray, R. W. *J. Am. Chem. Soc.* **2002,** *124*, 8958–8964.

55. Brust, M.; Walker, M.; Bethell, D.; Schiffrin, D. J.; Wyman, R. *J. Chem. Soc. Chem. Commun.* **1994***, 7*, 801–802.

56. Dasog, M.; Kavianpour, A.; Paige, M. F.; Kraatz, H.-B.; Scott, R. W. J. *Can. J. Chem.* **2008,** *86*, 368-375.

57. Hostetler, M. J.; Templeton, A. C.; Murray, R. W. *Langmuir* **1999**, *15*, 3782-3789.

58. Brust, M.; Fink, J.; Bethell, D.; Schiffrin, D. J.; Kiely, C. J. *Chem. Soc., Chem. Commun.* **1995**, 1655-1656.

59. Park, S.; Yousaf, M. N. An interfacial oxime reaction to immobilize ligands and cells in patterns and gradients to photoactive surfaces, *Langmuir* **2008**, *24*, 6201-6207.

60. Sibakoti, T. R.; Stinger, C. R.; Adhihetty, P. K.; Zamborini, F. P.; Nantz, M. H. *Part. Part. Syst. Charac.* **2019**, *36*, 1900093.

61. Bjorgo, J.; Boyd, D. R.; Watson, C. G. *J. Chem. Soc. Perkin Trans.* **1974**, *II*, 757–762.

62. Hine, J.; Yeh, C. Y. *J. Am. Chem. Soc.* **1967**, *89*, 2669-2676.
63. Mallinson, C. F.; Castle, J. E.; Watts, J. F. *Surf. Sci. Spectra*, **2013**, *20*, 113–127.
64. Xie, Z.; Raju, M. V. R.; Adhihetty, P. K.; Fu, X.-A.; Nantz, M. H. *Sensors,* **2020**, *20*, 7024.
65. Ibañez, F. J.; Zamborini, F. P. *Small*, **2012**, *8*, 174–202.
66. Bania, K. K.; Guha, A. K.; Bhattacharyya, P. K.; Sinha, S. *Dalton Trans.* **2014**, *43*,1769-1784.
67. Sthoer, A.; Hladílková, J.; Lund, M.; Tyrode, E. *Phys. Chem. Chem. Phys*. **2019**, *21*, 11329–11344.
68. Fukin, G. K.; Lindeman, S. V.; Kochi, J. K. *J. Am. Chem. Soc.* **2011**, *123*, 3092-3107.
69. Deakyne, C. A.; Meot-Ner, M. *J. Am. Chem. Soc.* **1985**, *107*, 474–479.
70. France, M. R.; Pullins, S. H.; Duncan, M. A. *J. Chem. Phys.* **1998**, *108*, 7049-7 051.
71. Yamada, S.; Misono, T.; Tsuzuki, S. *J. Am. Chem. Soc.* **2004**, *126*, 9862–9872.

R.4. CHAPTER 4 REFFERENCES:

1. Schaumburg, F. D. *Environ. Sci. Technol*. **1990**, *24(1),* 17-22.
2. Waters, E. M.; Gerstner, H. B.; Huff, J. E. *J. Toxicol. Environ*. **1977**, *2(3),* 671-707.
3. Wypych, G. *19-toxic effects of solvent exposure: Handbook of Solvents*, 3rd ed.; ChemTec Publishing: ON, Canada, 2019; Vol. 2, pp 1347-1454.
4. Agency for Toxic Substances and Disease Registry. https://www.atsdr.cdc.gov/tox-tool/trichloroethylene/01/how_can_i_be_exposed.html (accessed 1/15/22).
5. a. Dick, R B. *Neurotoxicol Teratol.* **1988**, *10(1),* 39-50. b. Lash, L. H.; Fisher, J. F.; Lipscomb, J. C.; Parker, J. C. *Environ. Health Perspect*. **2000**, *108*, 177-200.
6. Bronley-DeLancey, A.; McMillan, D. C.; McMillan, J. M.; Jollow, D. J.; Mohr, L. C.; Hoel, D. G. *Environ. Health Perspect*. **2006,** *114(8),* 1237-1242.
7. National Cancer Institute. https://www.cancer.gov/about-cancer/causes-prevention/risk/substances/trichloroethylene (accessed 1/15/22).
8. Trichloroethene (TCE) in Indoor and Outdoor Air; Bureau of Toxic Substance Assessment New York State Department of Health: NY, 2015.
9. a. Smith, G. F. *Brit. J. industr. Med.* **1966**, *23(4),* 249-262. b. Bonvallot, N.; Harrison, P.; Loh, M. *Trichloroethylene. In: WHO Guidelines for Indoor Air Quality: Selected Pollutants* (Online); World Health Organization, Geneva, 2010; pp-377-400. https://www.euro.who.int/__data/assets/pdf_file/0009/128169/e94535.pdf (accessed 1/16/22).
10. a. Lawrence, S.J. *Description, properties, and degradation of selected volatile organic compounds detected in ground water— A Review of Selected Literature*; Open-File Report 2006-1338: U. S. Geological Survey, Atlanta, Georgia, 2006; 10-25. b. Cathles, L.; Deschere, K.; Dunn, R.; Gillett, J. W.; Harpold, A.; Morales, V.; Shannon, R.; Smith, B.; Smith, J.; Toevs, I.; Steenhuis, T. A Historical and Technical Review and Analysis of TCE Contamination in the South Hill Area of Ithaca, New York; A report to the Citizens of South Hill:

Ithaca, 2006. c. Gist, G. L.; Burg, J. A. R. *Toxicol. Ind. Health,* **1995**, *11(3),* 1995, 253-307.

11. United state department of Labor, Ocuupational safety and health Administration. https://www.osha.gov/annotated-pels/table-z-2 (accessed 1/20/22).
12. Castello, G. *J. Chromatogr*. **1971**, *58(1),* 117-125. b. Humbert, B. E.; Fernández, B. E. *Int. Arch. Occup. Environ. Heath.* **1976**, *36*, 235–241.
13. Zoccolillo, L.; Amendola, L.; Cafaro, C.; Insogna, S. *J. Chromatogr. A,* **2005,** *1077*, 181–187. b. United States Environmental Protection Agency. https://clu-in.org/contaminantfocus/default.focus/sec/trichloroethylene_(tce)/cat/Detectiona nd_Site_Characterization/ (accessed 01/23/22).
14. a. Plummer, L. N.; Busenberg, E.; Eberts, S. M.; Bexfield, L. M.; Brown, C. J.; Fahlquist, L. S.; Katz, B. G.; Landon, M. K. *J. Hydrol. Eng.* **2008**, *13*, 1049-1068. b. Omrane, F. Gargouri, I.; Khadhraoui, M. *Per- and Trichloroethylene Air Monitoring in Dry Cleaners in the City of Sfax (Tunisia). In Solvents, Ionic Liquids and Solvent Effects* (Online); 2020. https://www.intechopen.com/chapters/67601 (accessed 01/23/22).
15. Cooper, C. V., White, L. D.; Kupel, R. E. *Am. Ind. Hyg. Assoc. J.* **1971**, *32(6),* 383-386.
16. Delinsky, A. D.; Bruckner, J. V.; Bartlett, M. G.; *Biomed. Chromatogr.* **2005**, *19*, 617–639.
17. a. Stewart, R. D.; Hake, C. L.; Peterson, J. E. *Arch. Environ. Health* **1974**, *29(1),* 6-13. b. Bangalore, A. S.; Small, G. W.; Combs, R. J.; Knapp, R. B.; Kroutil, R. T.; Traynor, C. A.; Ko, J. D. *Anal. Chem*. **1997**, *69*, 118-129.
18. a. Fan, J.; Yates, J. T. Jr. *J. Am. Chem. Soc*. **1996,** *118(19),* 4686-4692. b. Hammer, C. L.; Small, G. W. *Anal. Chem.* **2000**, *72*, 1680-1689.
19. Pal, T.; Vo-Dinh T., *J. Indian Chem. Soc.* **1998**, *75*, 470-473.
20. Stack, V. T., Jr.; Forrest, D. E.; Wahl, K. K. Am. *Ind. Hyg. Assoc. J.* **1961**, *22*, 184-186.

21. a. Getty, D.; Westre, S. G.; Bezabeh, D. Z.; Barrall, G. A.; Burmeister, M. J.; Kelly, P. B. *Appl. Spectrosc*. **1992**, *46(4),* 620-625. b. Ewing, K. J.; Bilodeau, T.; Nau, G.; Schneider, I.; Aggarwal, D. *Appl. Opt*. **1994**, *33(27),* 6323-6327.
22. Yu, Z.; Smith, M. E.; Zhang, J.; Zhou, Y.; Zhan, P. *Mikrochim. Acta*. **2018***, 185*, 330.
23. Ho, C. K; McGrath, L. K; Davis, C. E; Thomas, M. L; Wright, J. L; Kooser, A. S; Hughes, R. C. Chemiresistor Microsensors for In-Situ Monitoring of Volatile Organic Compounds: Final LDRD Report. SAND2003-3410. 2003:17–20.
24. Karellas, N. S.; Chen, Q. *Journal of Environmental Protection* **2013**, *4(8A),* 99-105.
25. Deyl, Z.; Effenberger, M. *Voda.* **1958**, *37*. 90-92.
26. Lai, W.-C.; Chakravarty, S.; Zou, Y.; Chen, R. T. *Opt. Lett*. **2013**, *38(19),* 3799-3802.
27. Chen, M.-H.; Chou, T.-C. *J. Electrochem. Soc.* **2003**, *150(9),* H214-H219.
28. Hoffman, F.; Ronen, D.; Rosin, H.; Milanovich, F. *Talanta* **1996**, *43*, 681-689.
29. a. Han, T. S.; Sasaki, S.; Yano, K.; Ikebukuro, K.; Kitayama, A.; Nagamune, T.; Karube, I. *Talanta* **2002**, *57(2),* 271-276. b. Lei, Y.; Chen, W.; Mulchandani, A. *Anal. Chim. Acta*, **2006**, *568*, 200–210. c. Hnaien, M.; Bourigua, S.; Bessueille, F.; Bausells, J.; Errachid, A.; Lagarde, F.; Jaffrezic-Renault, N. *Electrochim. Acta,* **2011**, *56*, 10353–10358.
30. Ho, C. K.; Lindgren, E. R.; Rawlinson, K. S.; McGrath, L. K.; Wright, J. L. *Sensors* **2003**, *3*, 236-247.
31. Ho, C. K.; Hughes, R. C. *Senso*r **2002**, *2*, 23-34.
32. a. Chang, H.; Kim, S. K.; Sukaew, T.; Bohrer, F.; Zellers, E. T. *Procedia Eng*. **2010**, *5,* 973–976.
33. Kim, S. K.; Burris, D. R.; Bryant-Genevier, J.; Gorder, K. A.; *Environ. Sci. Technol.* **2012**, *46*, 6073−6080.
34. Fatah, A. A.; Arcilesi, R. D., Jr.; Peterson, J. C.; Lattin, C. H.; Wells, C. Y.; McClintock, J. A. *Guide for the Selection of Chemical Detection Equipment for Emergency First Responders*; 3rd ed. U.S. Department of Homeland Security: NW Washington, DC, 2007; C-170-C171.

35. CleanAir https://www.cleanair.com/product/inficon-hapsite-er-portable-gc-ms/ (accessed 01/24/22).

36. Ho, C.K., Wright, J.; McGrath, L. K.; Lindgren, E. R.; Rawlinson, K. S.; Lohrstorfer, C. F. *Field Demonstrations of Chemiresistor and Surface Acoustic Wave Microchemical Sensors at the Nevada Test Site*, SAND2003-0799, Sandia National Laboratories Report, Albuquerque, NM, 2003.

37. a. Rivera, D.; Alam, M. K.; Davib, C. E.; Ho, C. K. *Sens. Actuators B Chem.* **2003**, *92*, 110–120. b. Ho, C. K.; Lohrstorfer, C. F. *Ground Water Monit. Remediat.* **2003**, *23(4),* 85-90. c. Lei, H.; Pitt, W. G.; McGrath, L. K.; Ho, C. K. *Sens. Actuators B Chem*. **2007**, *125*, 396–407.

38. Wohltjen, H.; Snow, A.W. *Anal. Chem*. **1998**, *70*, 2856-2859.

39. Joseph, Y.; Krasteva, N.; Besnard, I.; Guse, B.; Rosenberger, M.; Wild, U.; Knop-Gericke, A.; Schlo¨gl, R.; Krustev, R.; Yasudaa, A.; Vossmeyer, T. *Faraday Discuss.* **2004**, *125,* 77–97.

40. a. Kim, S. K.; Burris, D. R.; Chang, H.; Bryant-Genevier, J.; Zellers, E. T. *Environ. Sci. Technol.* **2012**, *46*, 6065−6072. b. Kim, S. K.; Chang, H.; Zellers, E. T. *Anal. Chem.* **2011**, *83*, 7198−7206. c. Lu, C. J.; Whiting, J.; Sacks, R. D.; Zellers, E. T. *Anal. Chem.* **2003**, *75(6),* 1400-1409.

41. a. Zhong, Q.; Steinecker, W. H.; Zellers, E. T. *Analyst*, **2009**, *134***,** 283-293. b. Lu, C.-J.; Steinecker, W. H.; Tian, W.-C.; Oborny, M. C.; Nichols, J. M.; Agah, M.; Potkay, J. A.; Chan, H. K. L.; Driscoll, J.; Sacks, R. D.; Wise, K. D.; Pang, S. W.; Zellers, E. T. *Lab Chip* **2005**, *5*, 1123−1131.

42. Bryan, J. C.; Kavallieratos, K.; Sachleben, R. A.; *Inorg. Chem.* **2000**, *39*, 1568-1572.

43. Levitskaia, T. G.; Bryan, J. C.; Sachleben, R. A.; Lamb, J. D.; Moyer, B. A. *J. Am. Chem. Soc.* **2000**, *122*, 554-562.

44. Cametti, M.; Nissinen, M.; Cort, A. D.; Rissanen, K.; Mandolini, L. *Inorg. Chem.* **2006**, *45*, 6099−6101.

45. Smith, G. *Acta Cryst*. **2013**, *E69*, m22–m23.

46. a. Smith, G. *Acta Cryst.* **2015**, *E71*, 931–933. b. Smith, G.; O'Reilly, E. J.; Kennard, C. H. L. *Cryst. Struct. Commun.* **1981*b*,** *10*, 1277–1282.

47. a. Smith, G.; O'Reilly, E. J.; Kennard, C. H. L. *Aust. J. Chem.* **1981*a*,** *34*, 891–896. b. O'Reilly, E. J.; Smith, G.; Kennard, C. H. L.; White, A. H. *Aust. J. Chem.* **1983**, *36*, 183–190.

48. Aggarwal, V.; Li, H.; Boyd, S. A.; Teppen, B. T. *Environ. Sci. Technol.* **2006**, *40*, 894-899.

49. Vayssilov, G. N.; Lercher, J. A.; Rösch, N. *J. Phys. Chem. B* **2000**, *104*, 35, 8614–8623.

50. a. Smith, R. P.; Mortensen, E. M. *J. Am. Chem. Soc.* **1956**, *78(16),* 3932–3936. b. Breysse, P. N.; Cappabianca, A. M.; Hall, T. A.; Risby, T. *Carbon* **1987**, *25(6),* 803-808.

51. a. Chen, X.; Hojo, M.; Chen, Z.; Kobayashi, M. *J. Mol. Liq.* **2016**, *214*, 369-377. b. Carlos, J.; Ruiz, G.; Nöth, H.; Warchhold, M. *Eur. J. Inorg. Chem.* **2008**, 251–266. c. Steed, *Coord. Chem. Rev*. **2001**, *215,* 171–221.

52. a. Smith, A. G.; Tasker, P. A.; White, D. J. *Coord. Chem. Rev.* **2003**, *241*, 61-85. b. Kukushkin, V. Y.; Pombeiro, A. J. L. *Coord. Chem. Rev.* **1999**, *181*, 147–175. c. Boone, L. L.; Mroz, A. E.; VanDerveer, D. G.; Hancock, R. D.; *Eur. J. Inorg. Chem.* **2011**, 2706–2711. d. Bolotin, D. S.; Bokach, N. A.; Demakova, M. Y.; Kukushkin, V. Y. *Chem. Rev.* **2017,** *117(21),* 13039–13122.

53. R. I. Kulawiec and R. H. Crabtree, *Coord. Chem. Rev.* **1990**, 99, 89.

54. a. Takemura, H.; Nakashima, S.; Kon, N. *Tetrahedron Letters* **2000**, *41,* 6105-6109. b. Inazu, T.; Yang Z.; Rodgers, M. T. *J. Am. Chem. Soc.* **2004**, *126*, 16217-16226. c. Parra, R. D. *Chem. Phys. Lett.* **2015**, *637*, 177–181.

55. a. Takemura, H.; Nakashima, S.; Kon, N.; Yasutake, M.; Shinmyozu, T.; Inazu, T. *J. Am. Chem. Soc.* **2001**, *123*, 9293-9298. b. Takemura, H.; Kon, N.; Kotoku, M.; Nakashima, S.; Otsuka, K.; Yasutake, M.; Shinmyozu, T.; Inazu, T. *J. Org. Chem.* **2001**, *66*, 2778-2783.

56. Periodic Trends in Electronegativity https://www.ck12.org/book/ck-12-chemistry-second-edition/r15/section/9.5/ (accessed 19/3/2022).

57. Iqbal, P.; Critchley, K.; Bowen, J.; Attwood, D.; Tunnicliffe, D.; Evans, S. D.; Preece, J. A. *J. Mater. Chem.* **2007**, *17*, 5097–5110.

58. Brust, M.; Walker, M.; Bethell, D.; Schiffrin, D. J.; Wyman, R. *J. Chem. Soc. Chem. Commun.* **1994***, 7*, 801–802.

59. Hostetler, M. J.; Templeton, A. C.; Murray, R. W. *Langmuir*, **1999**, *15*, 3782-3789.

APPENDIX A

CHARACTERIZATION DATA

A.1. Index of NMR spectra and other characterization data

A.2. Selected NMR spectra, TEM images, and TGA curves from Chapter 2

A.3. Selected NMR spectra, FT-IR spectra, X-Ray photoelectron spectroscopy spectra, and slectron microscope SEM/EDX spectra, FT-IR spectra, UHPLC-MS spectra, UV-Vis. spectra, TEM images, and TGA curves from Chapter 3

A.4. Selected NMR spectra, and electron microscope SEM/EDX spectra, and UV-Vis. spectra from Chapter 4

A.1. Index of NMR Spectra and Other Characterization Data

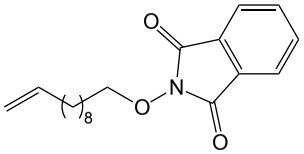

Compound **1**: ^{1}H NMR ($CDCl_3$, 400 MHz)

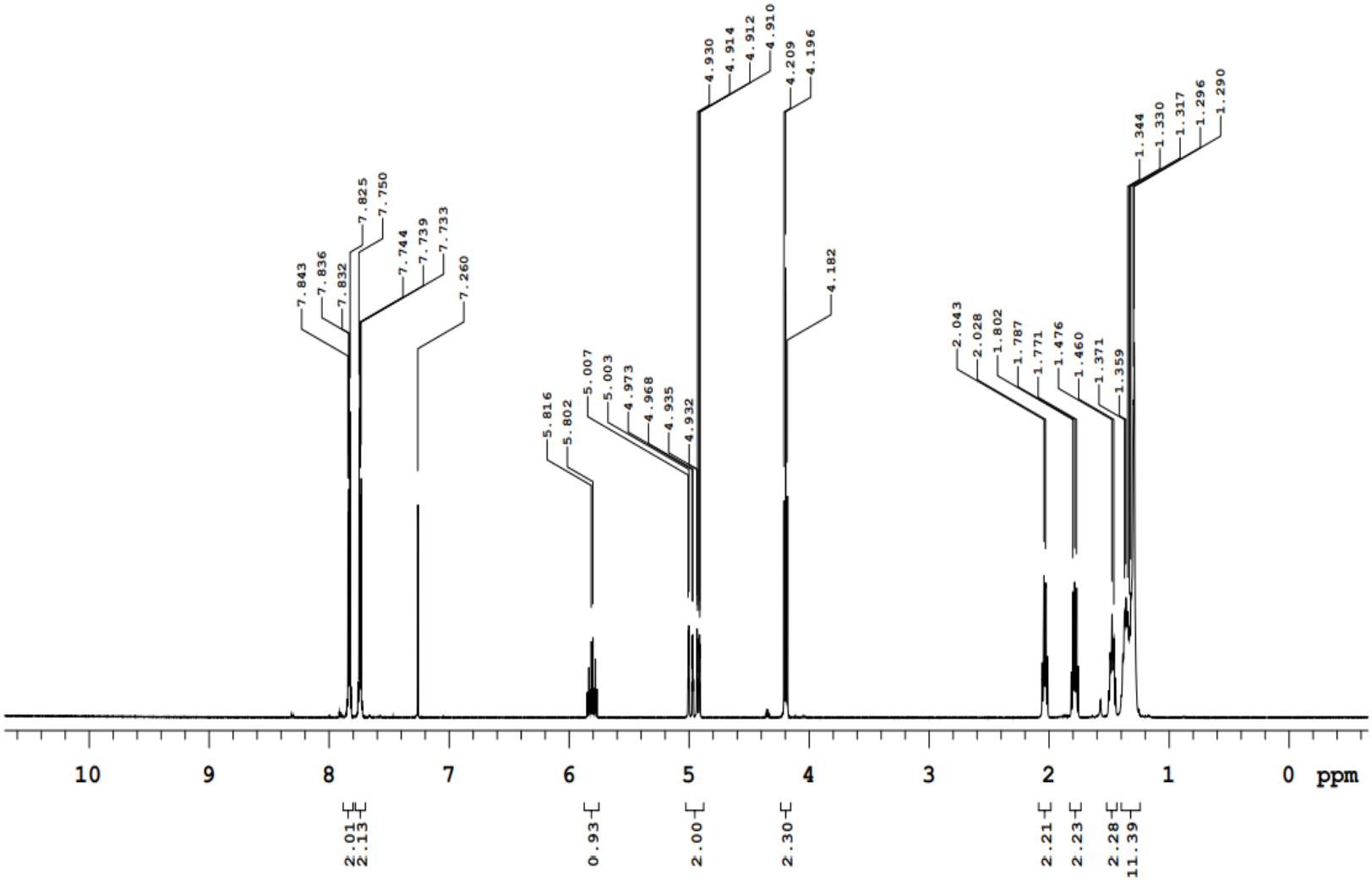

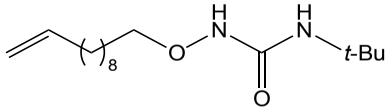

Compound **3.1**: ^{1}H NMR ($CDCl_3$, 400 MHz)

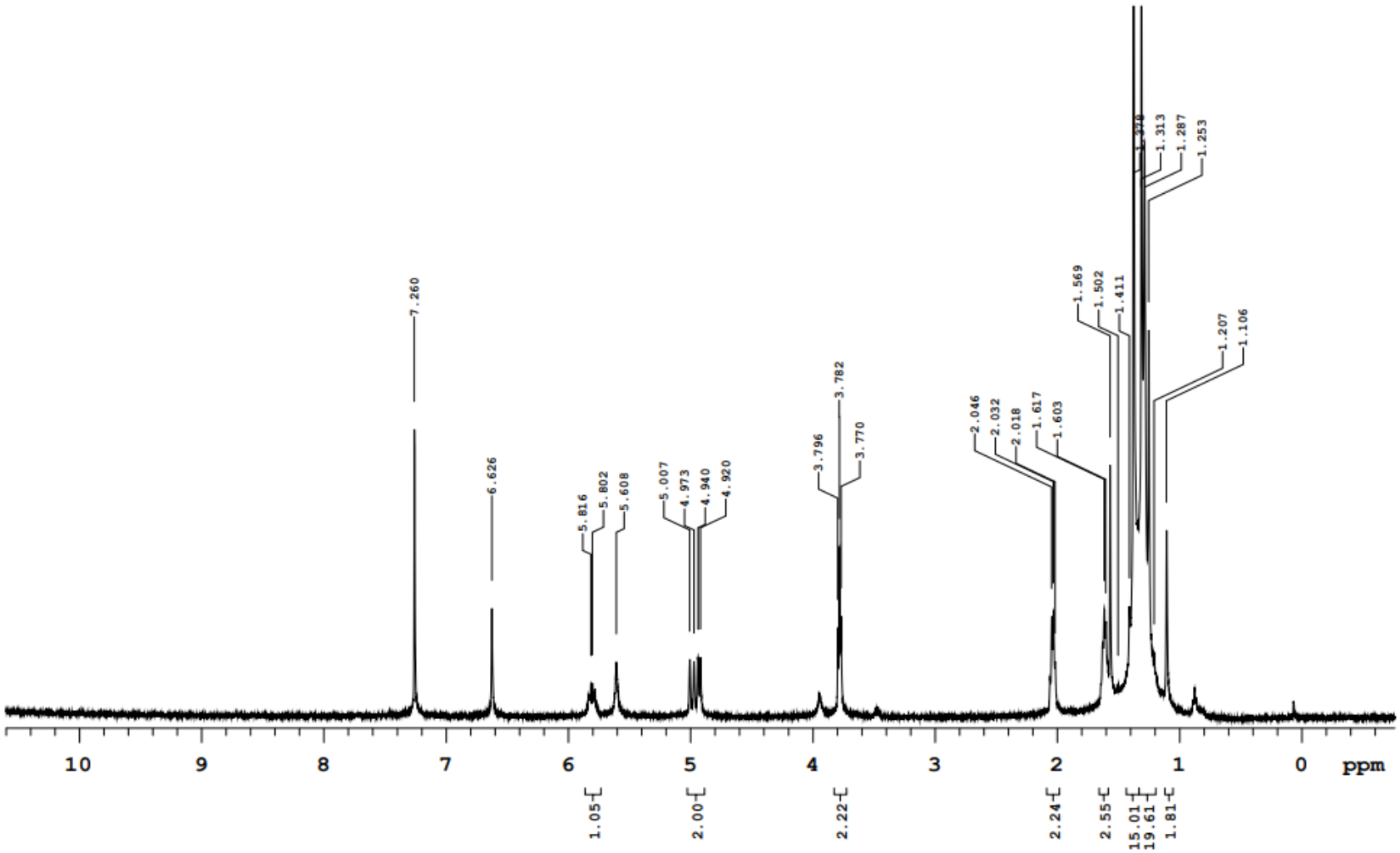

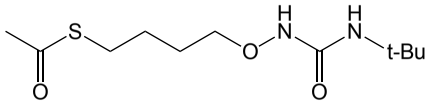

Compound **4.1**: ^{1}H NMR ($CDCl_3$, 400 MHz)

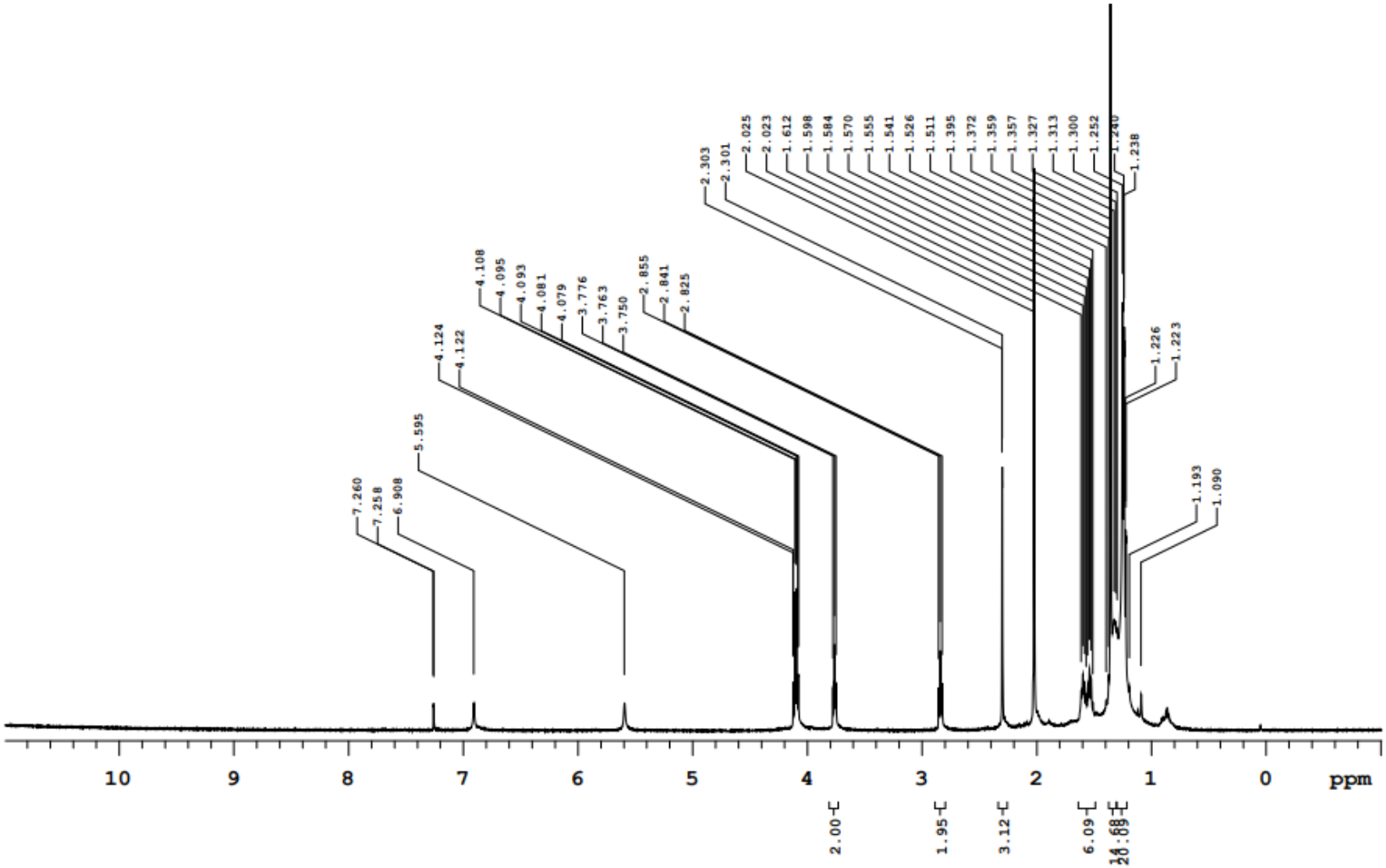

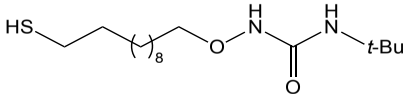

Compound **5.1**: ^{1}H NMR ($CDCl_3$, 500 MHz)

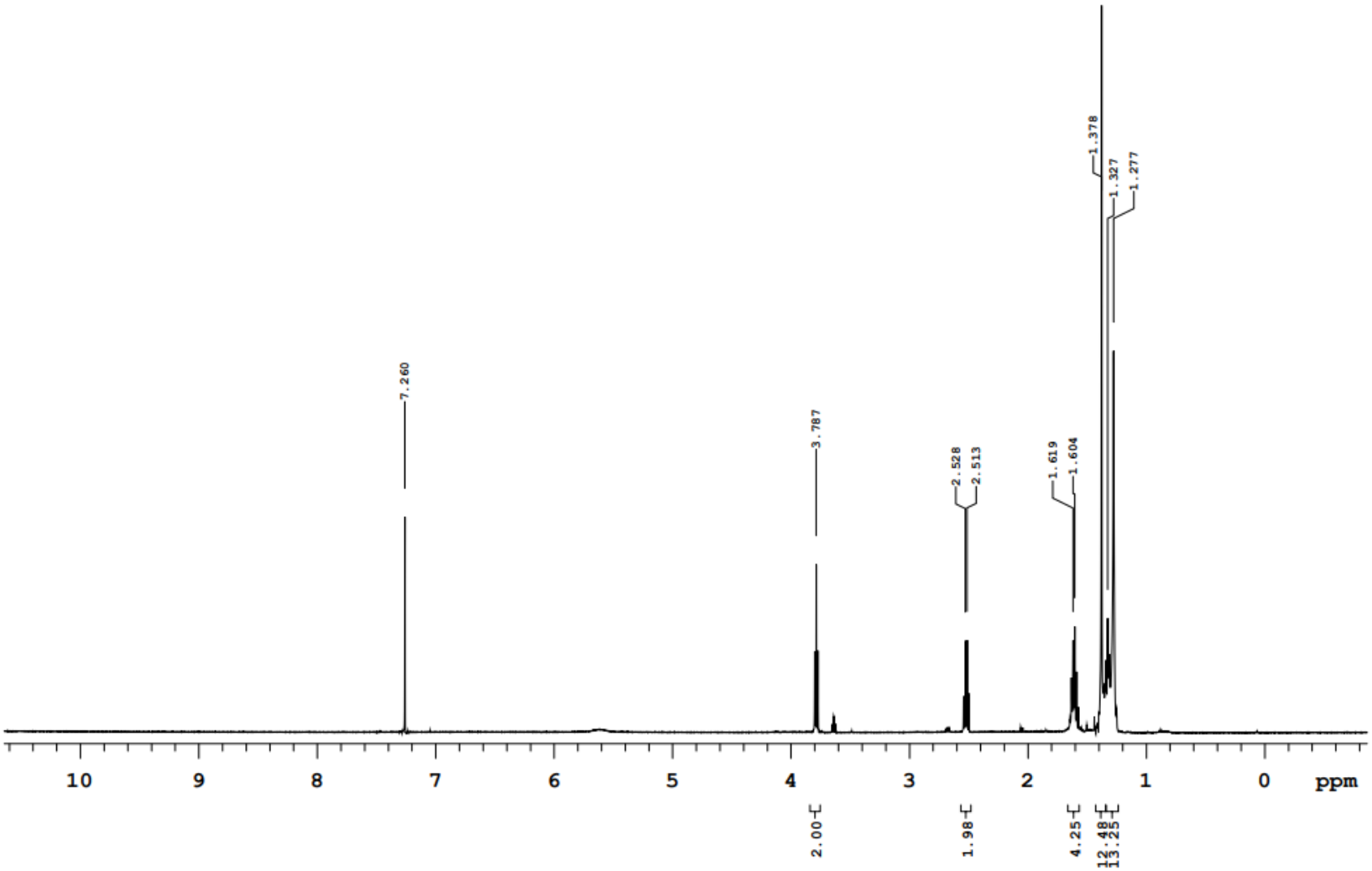

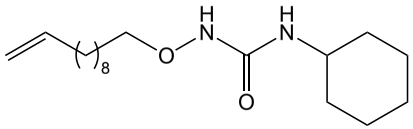

Compound **3.2**: ^{1}H NMR ($CDCl_3$, 400 MHz)

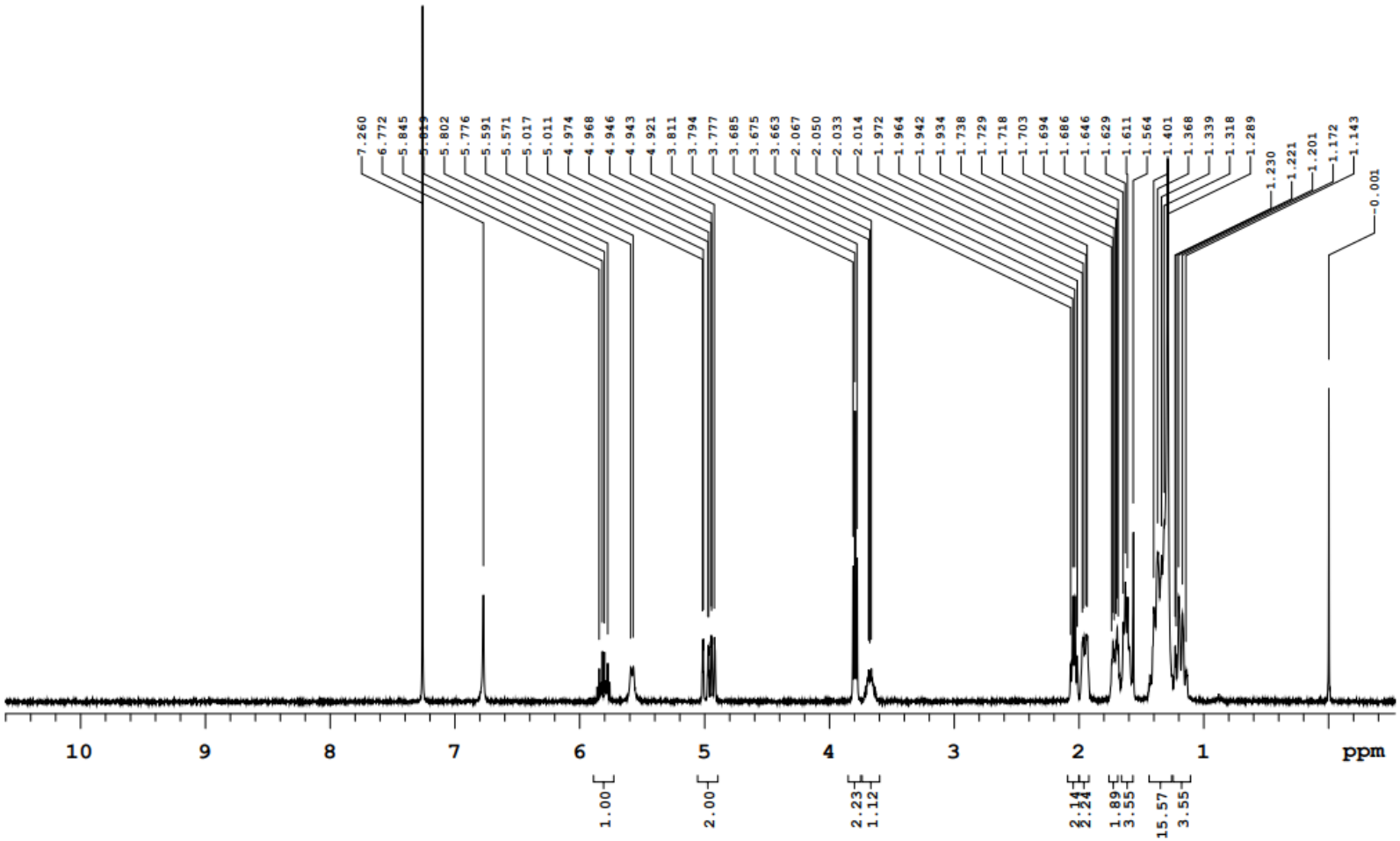

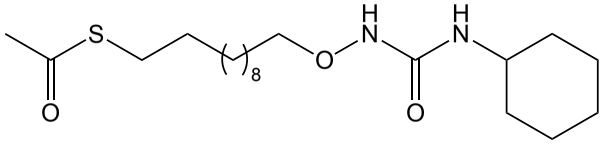

Compound **4.2**: ^{1}H NMR ($CDCl_3$, 400 MHz)

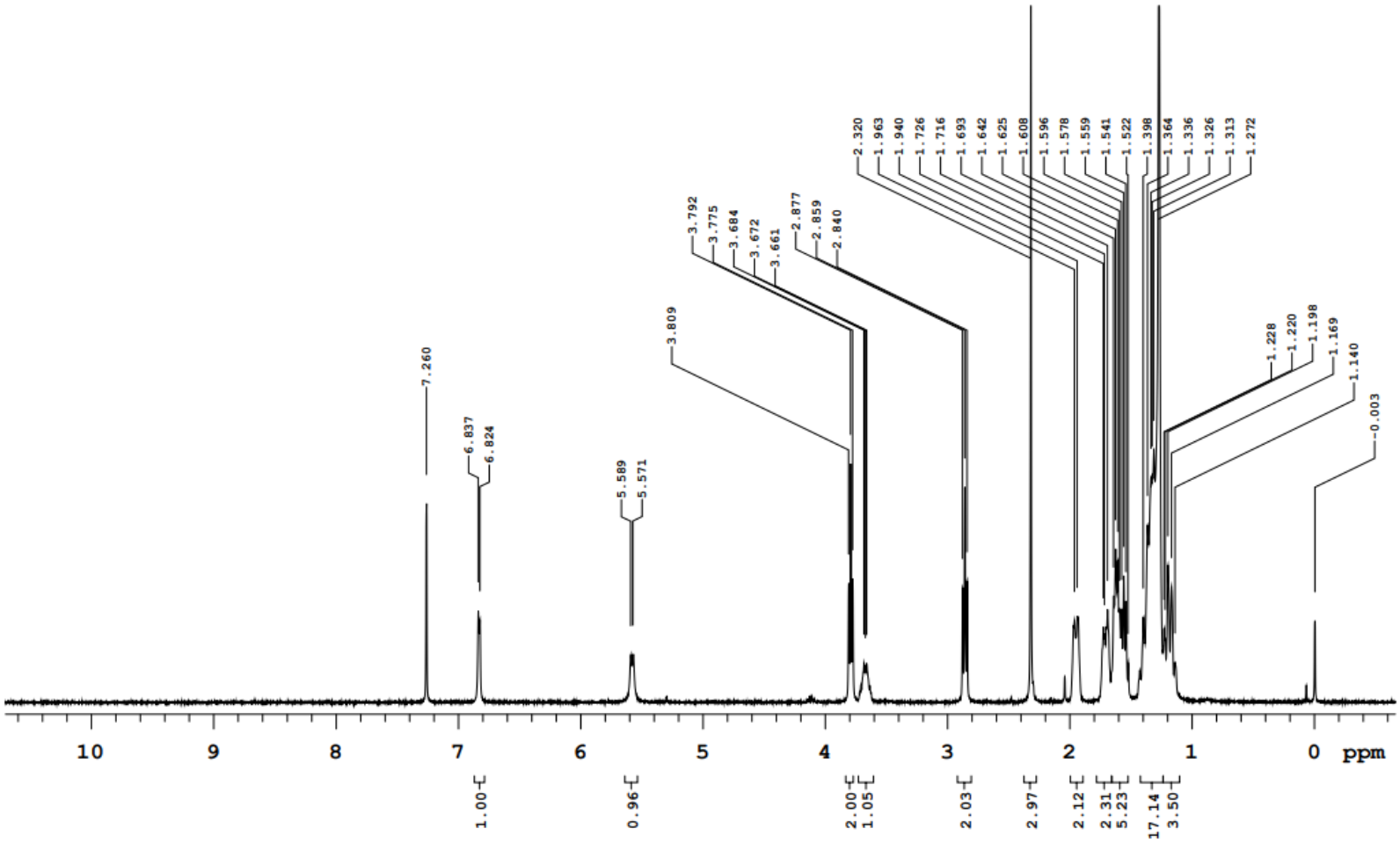

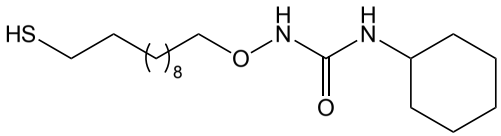

Compound **5.2**: ^{1}H NMR ($CDCl_3$, 400 MHz)

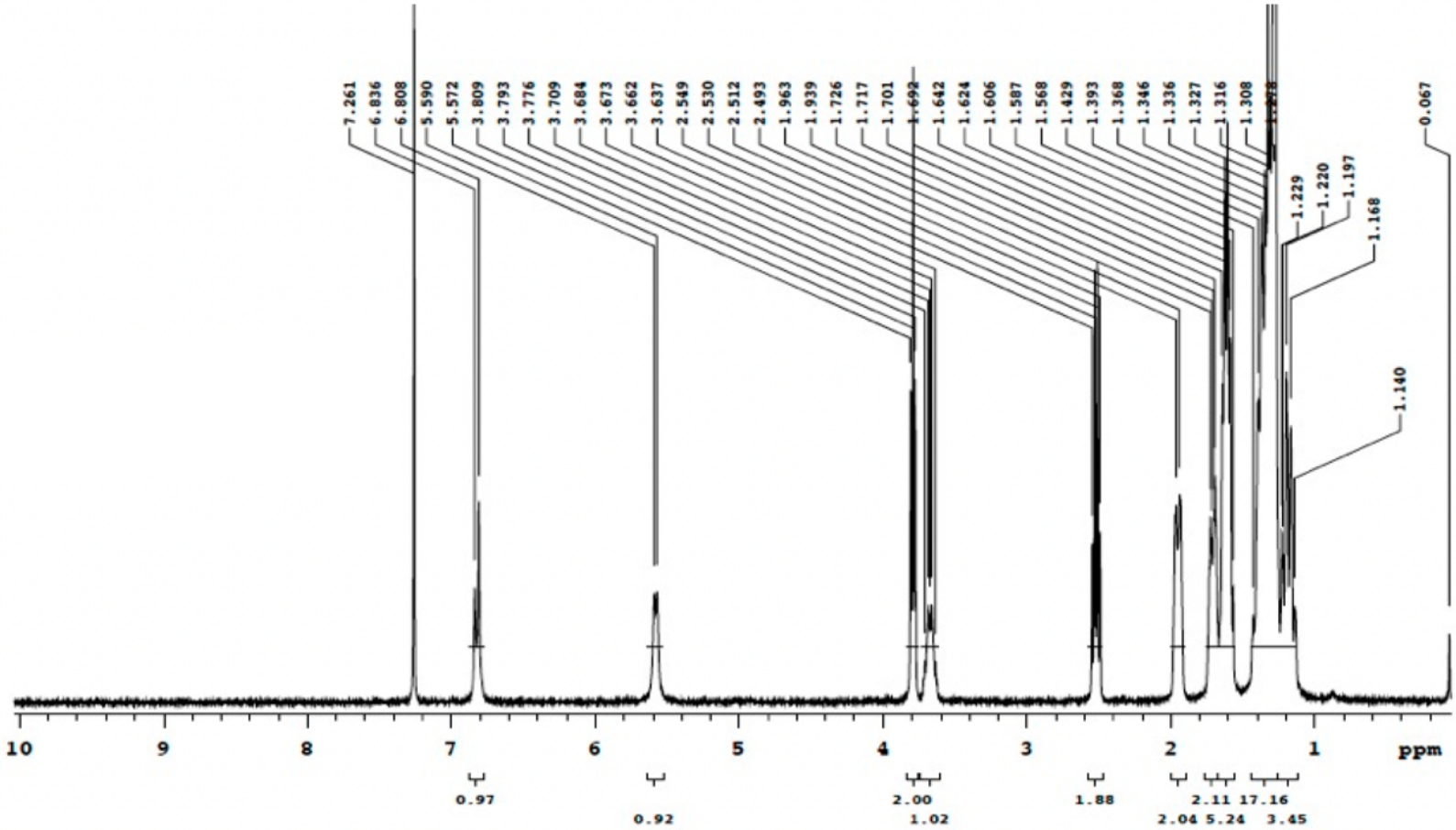

Compound **5.2**: ^{13}C NMR ($CDCl_3$, 100 MHz)

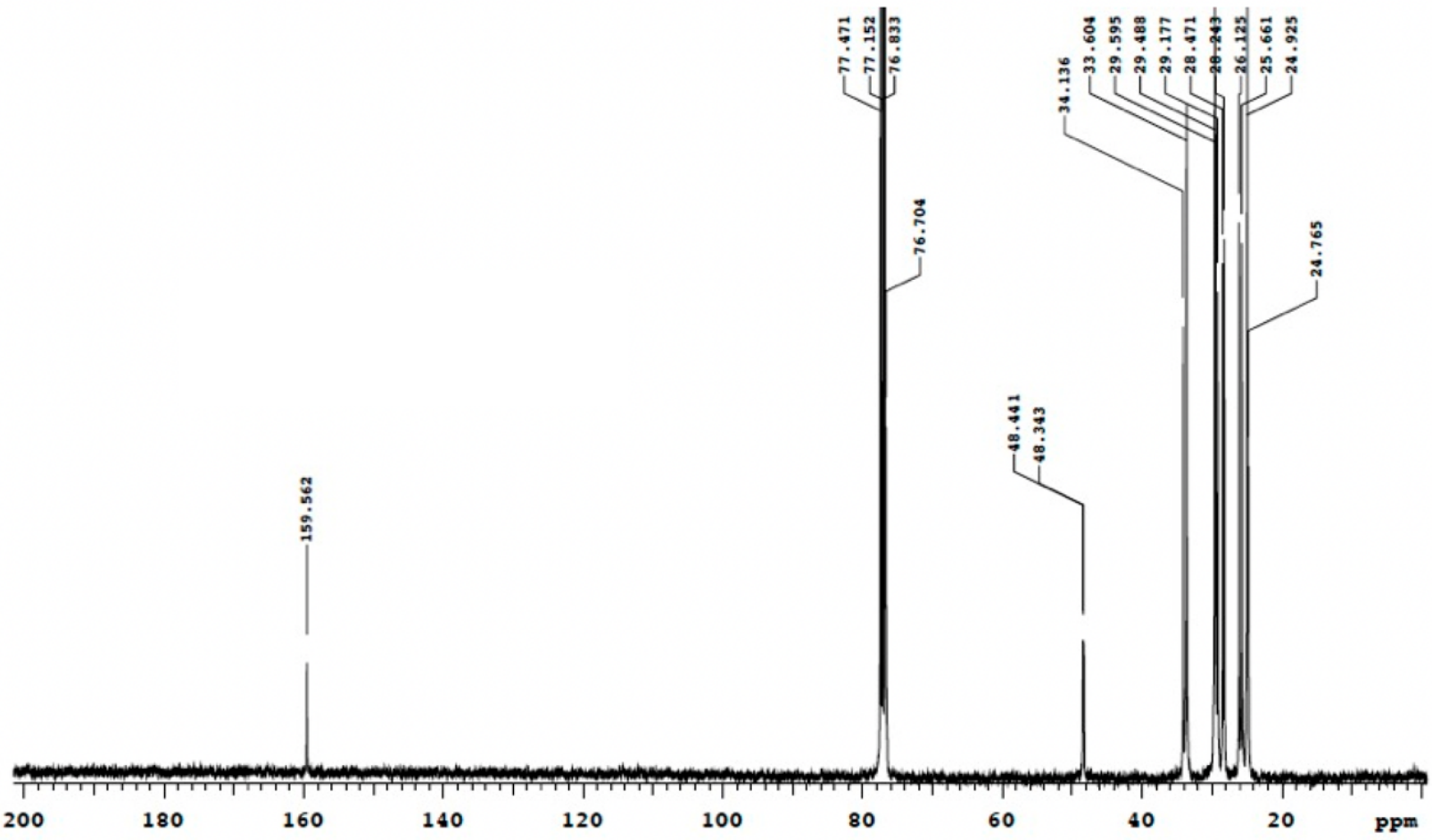

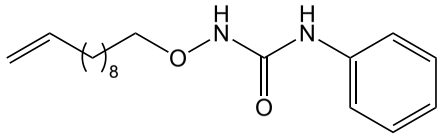

Compound **3.3**:^{1}H NMR ($CDCl_3$, 500 MHz)

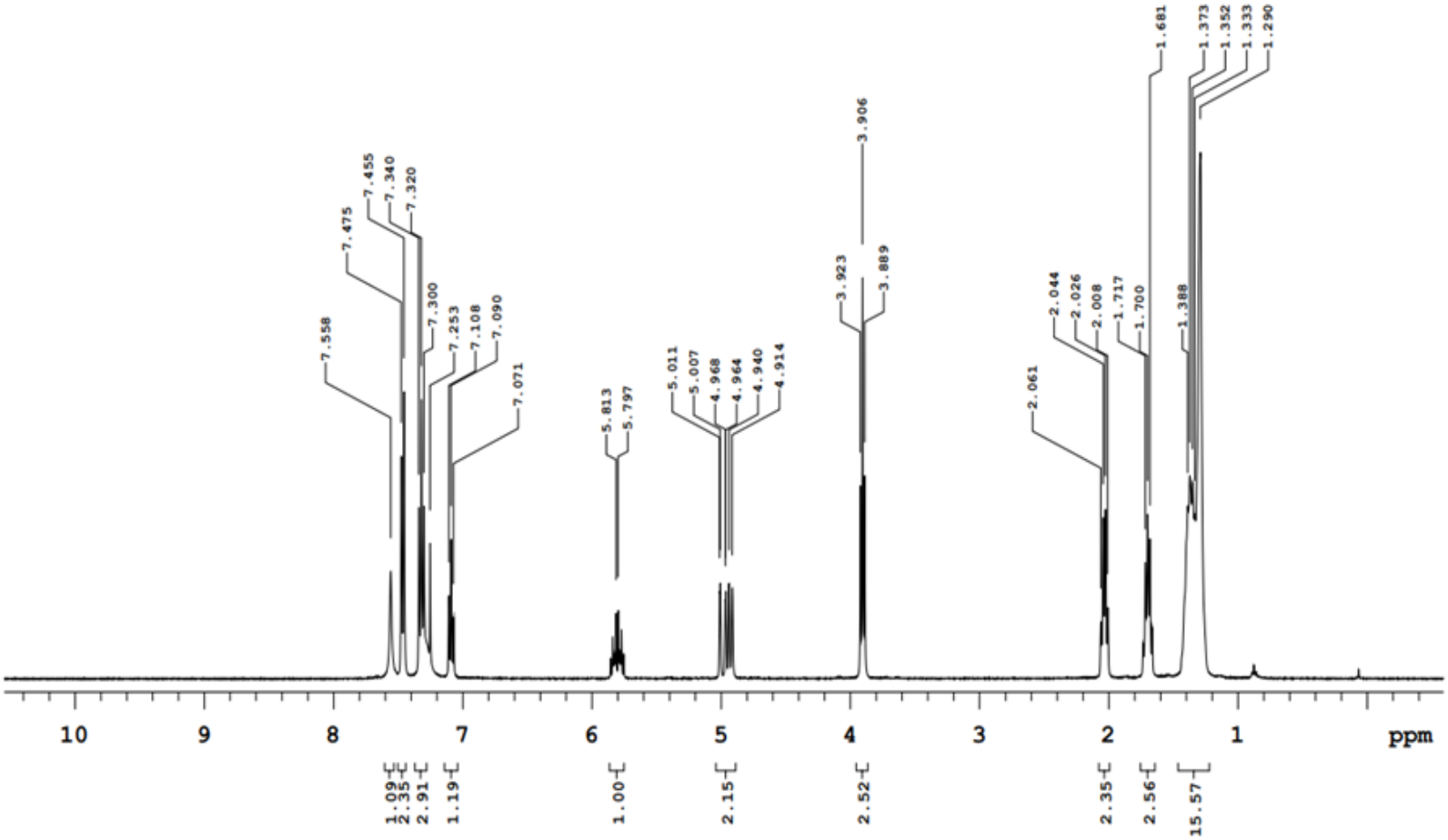

Compound **4.3**: ^{1}H NMR ($CDCl_3$, 400 MHz)

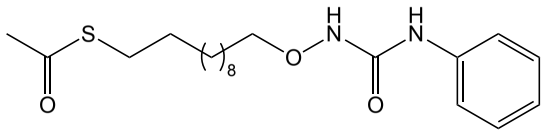

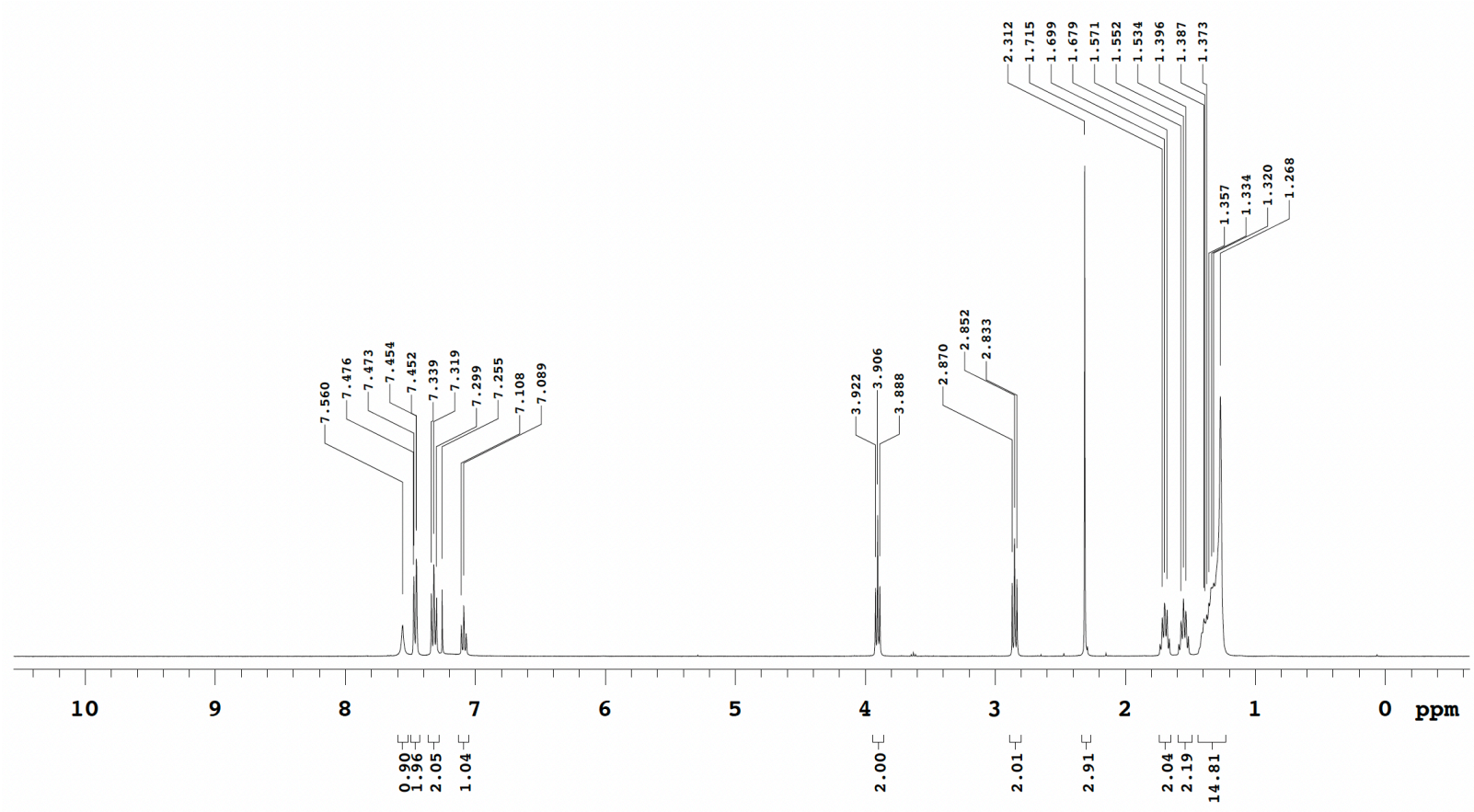

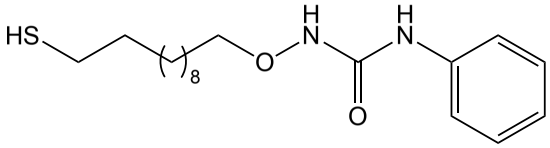

Compound **5.3**: ^{1}H NMR ($CDCl_3$, 400 MHz)

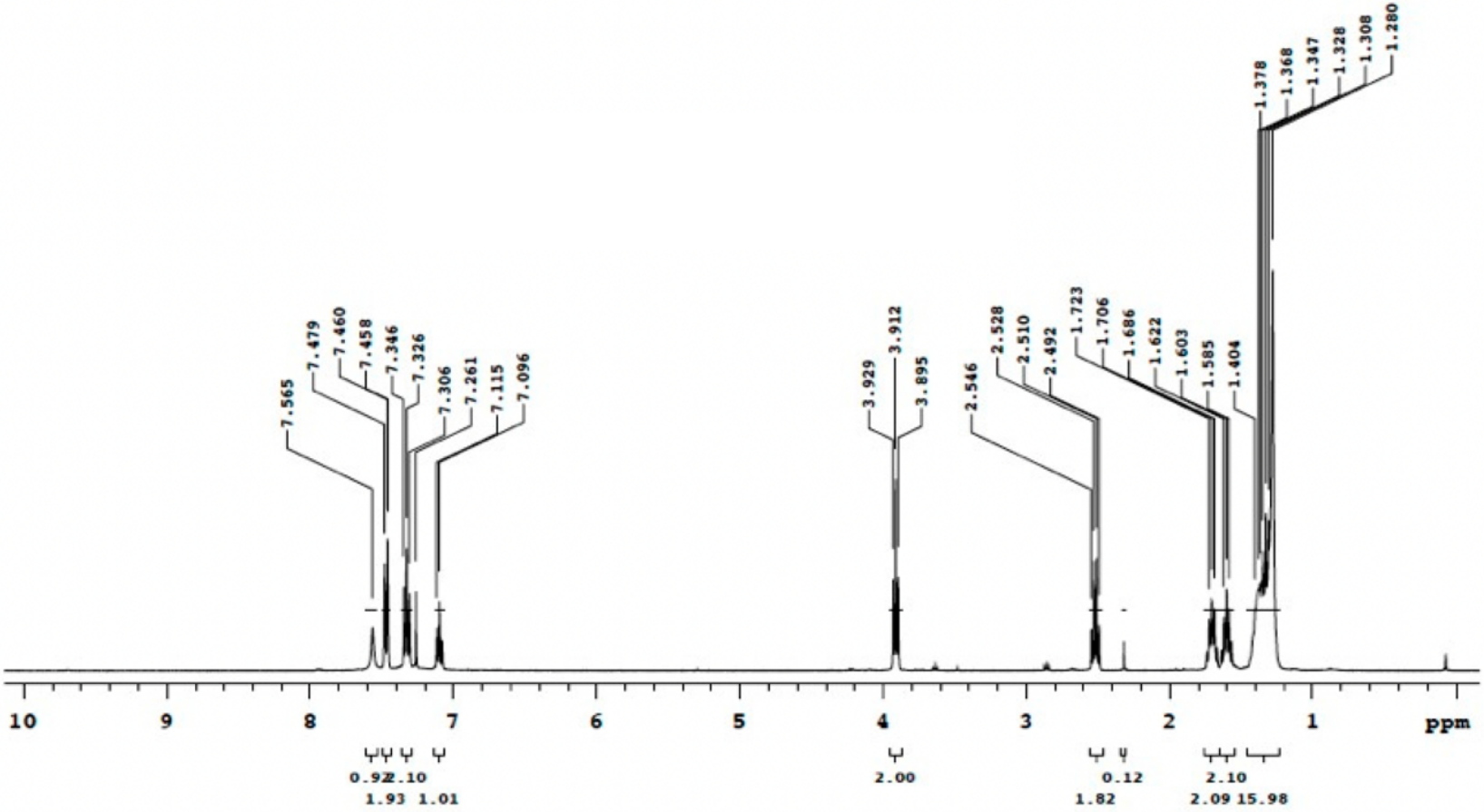

Compound **5.3**: ^{13}C NMR ($CDCl_3$, 100 MHz)

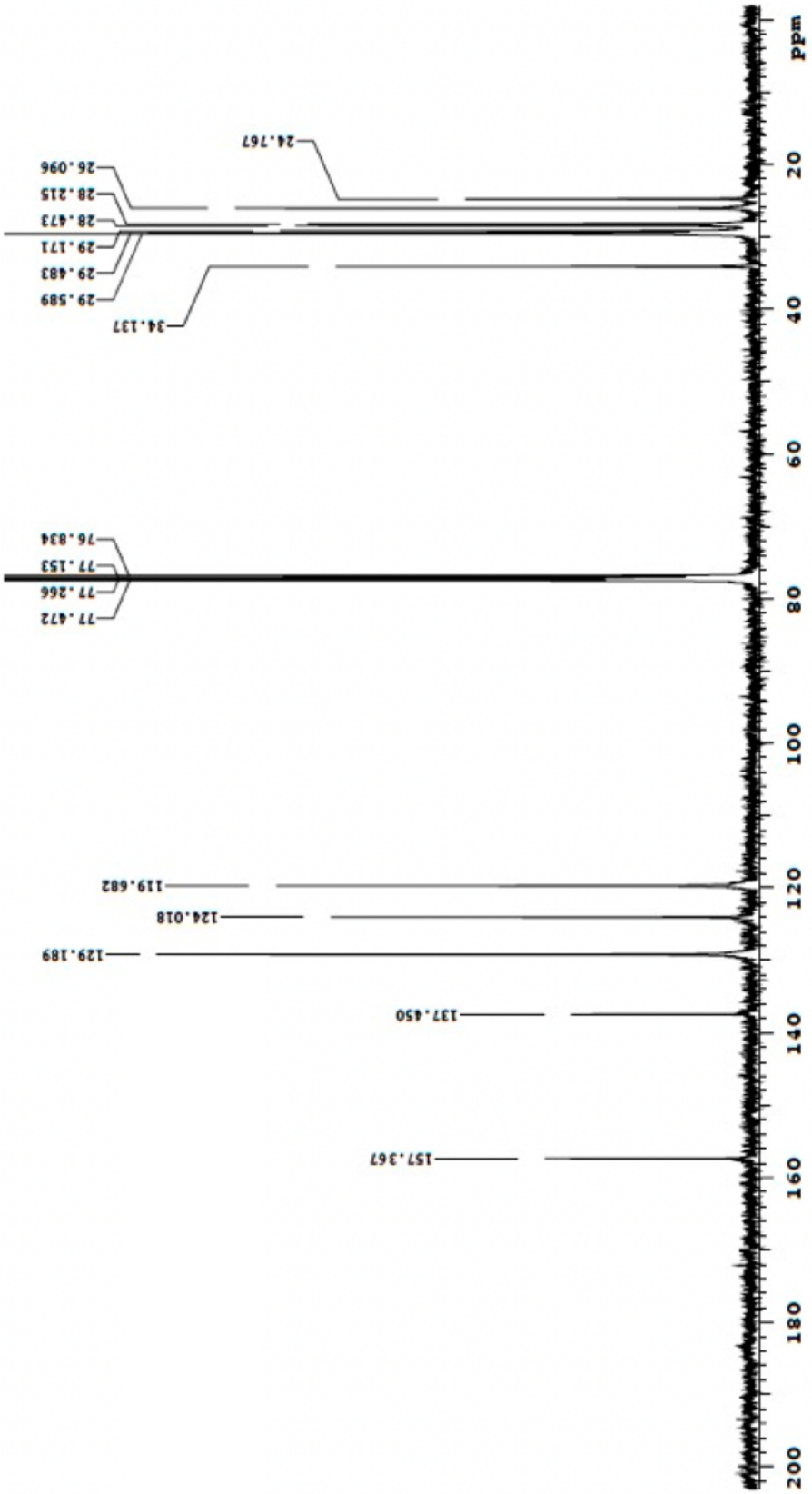

Compound **4.4**: ^{1}H NMR ($CDCl_3$, 500 MHz)

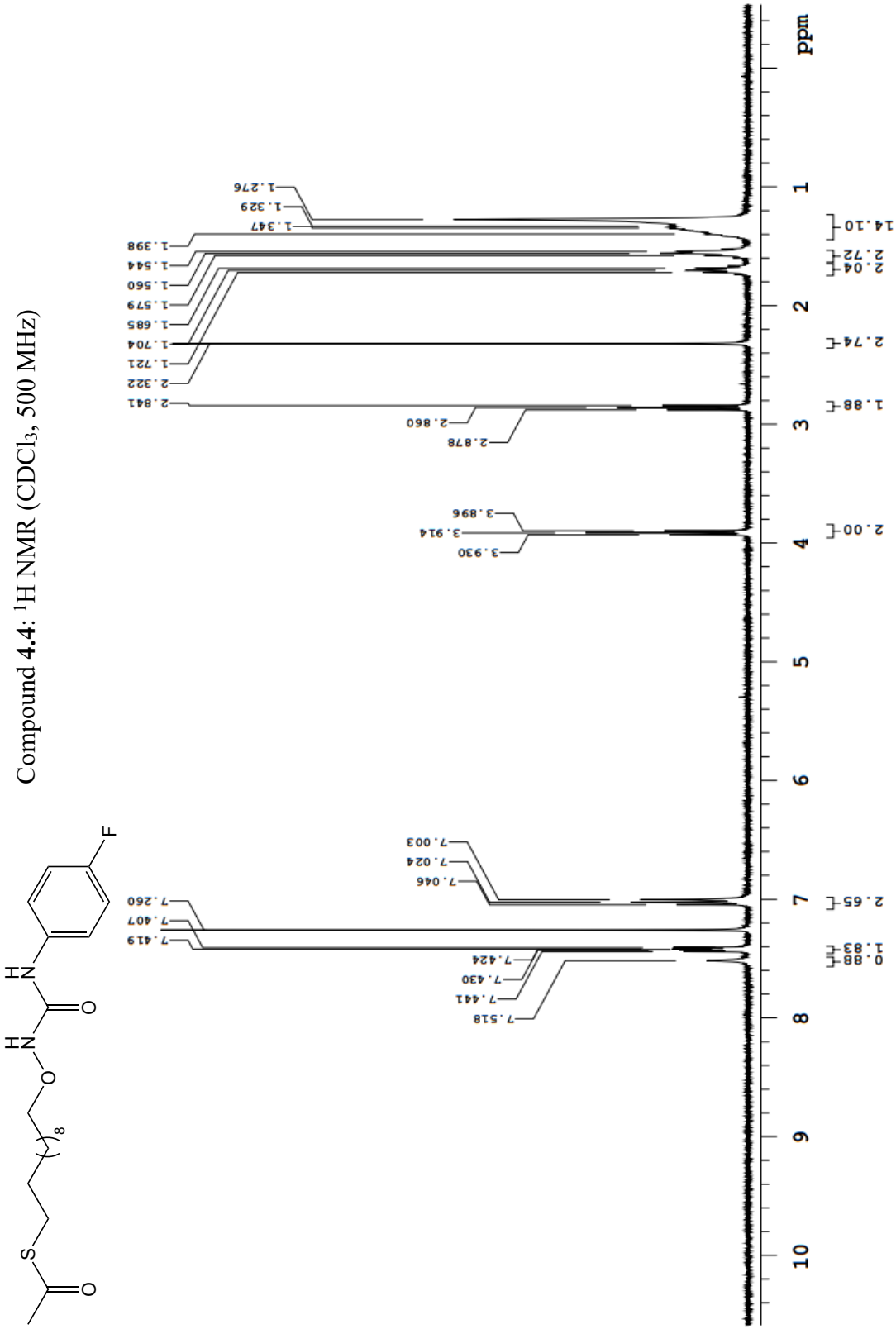

Compound **5.4**: ^{1}H NMR ($CDCl_3$, 400 MHz)

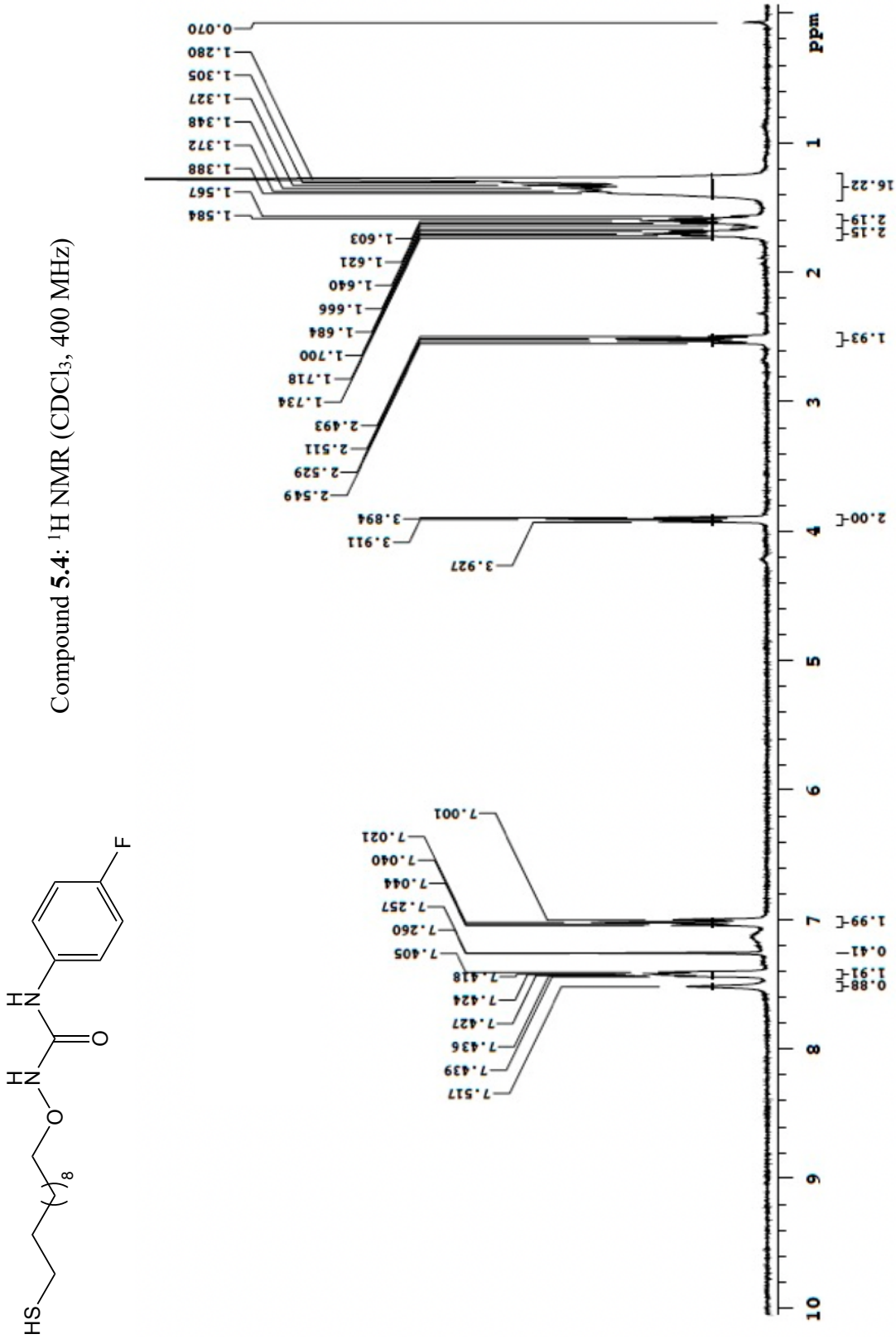

Compound **5.4**: ^{13}C NMR ($CDCl_3$, 100 MHz)

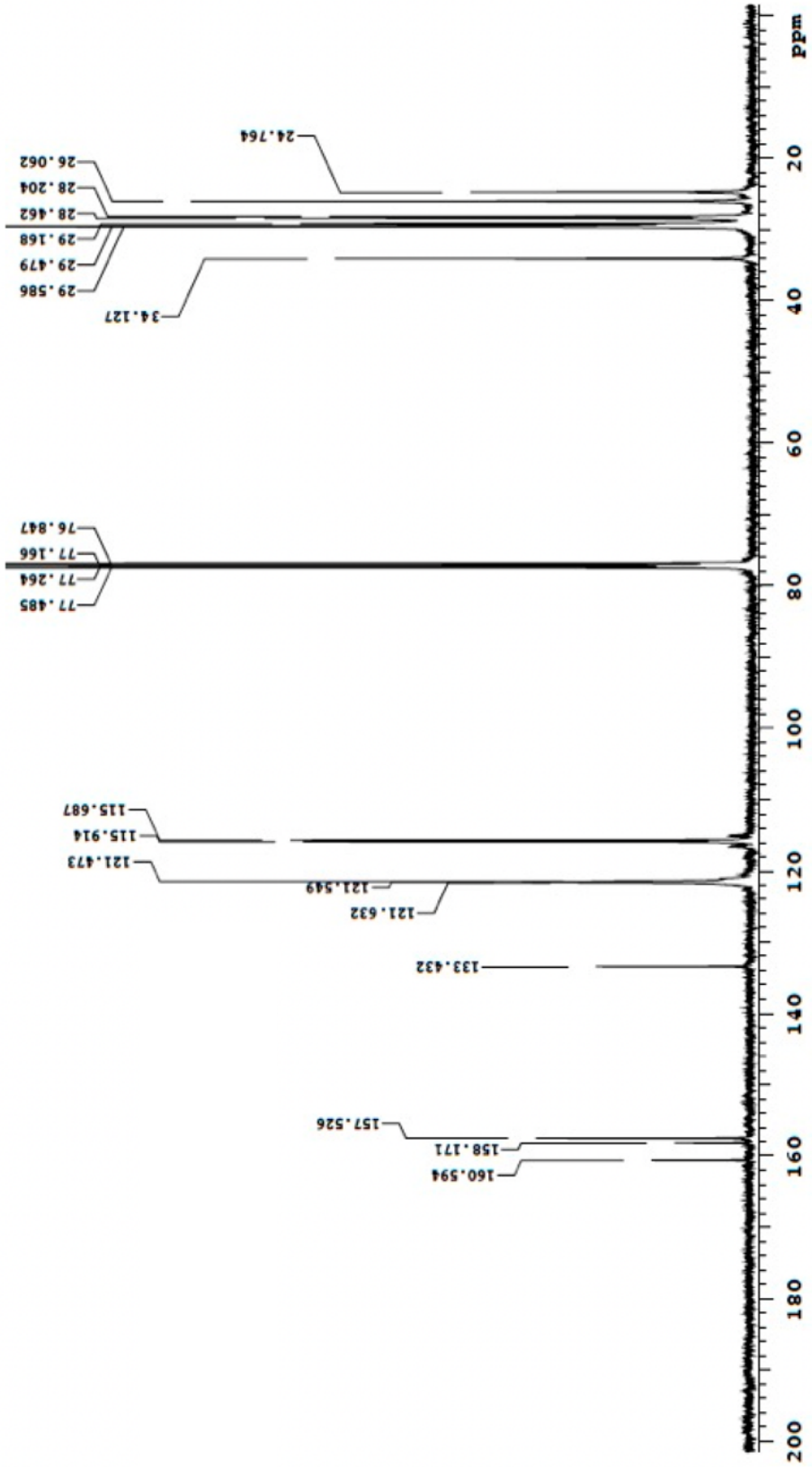

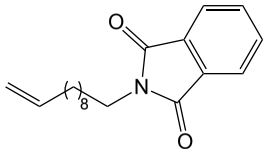

Compound **6**: ^{1}H NMR ($CDCl_3$, 500 MHz)

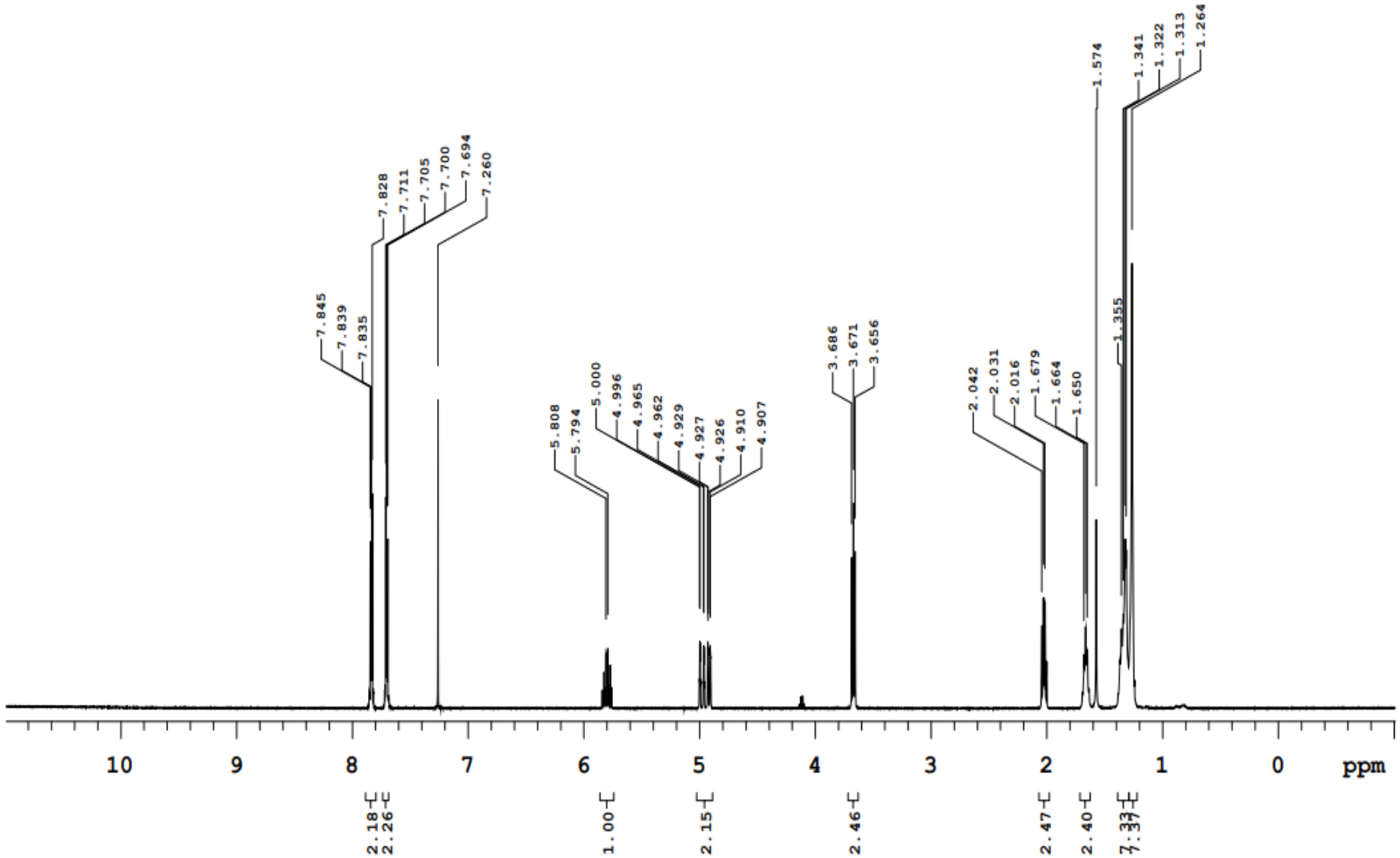

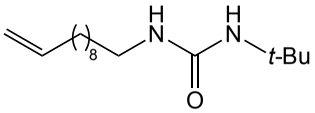

Compound **8.1:** ^{1}H NMR ($CDCl_3$, 500 MHz)

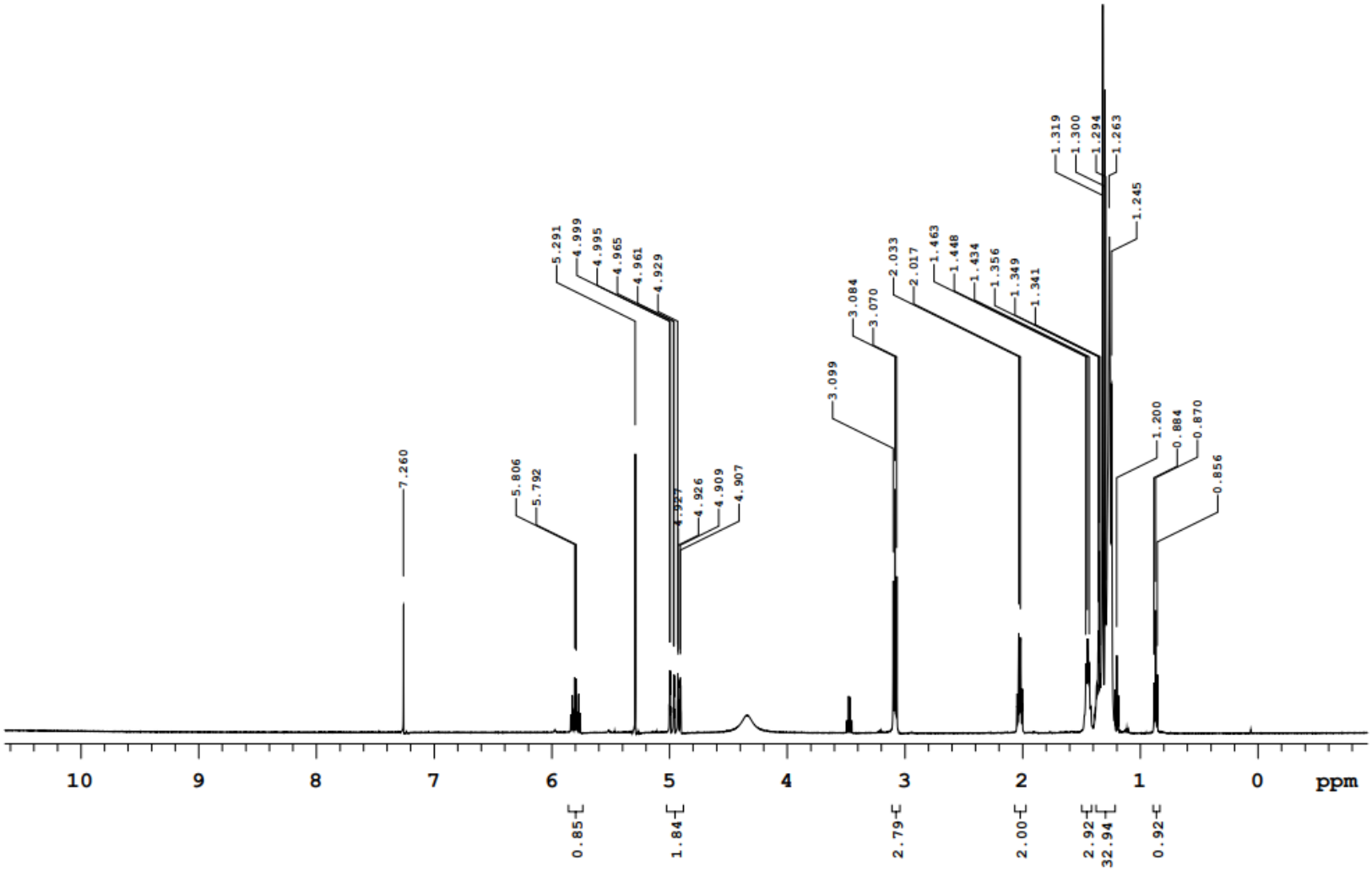

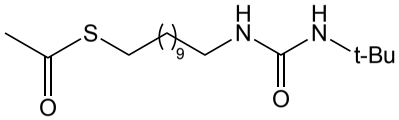

Compound **9.1**: ^{1}H NMR ($CDCl_3$, 500 MHz)

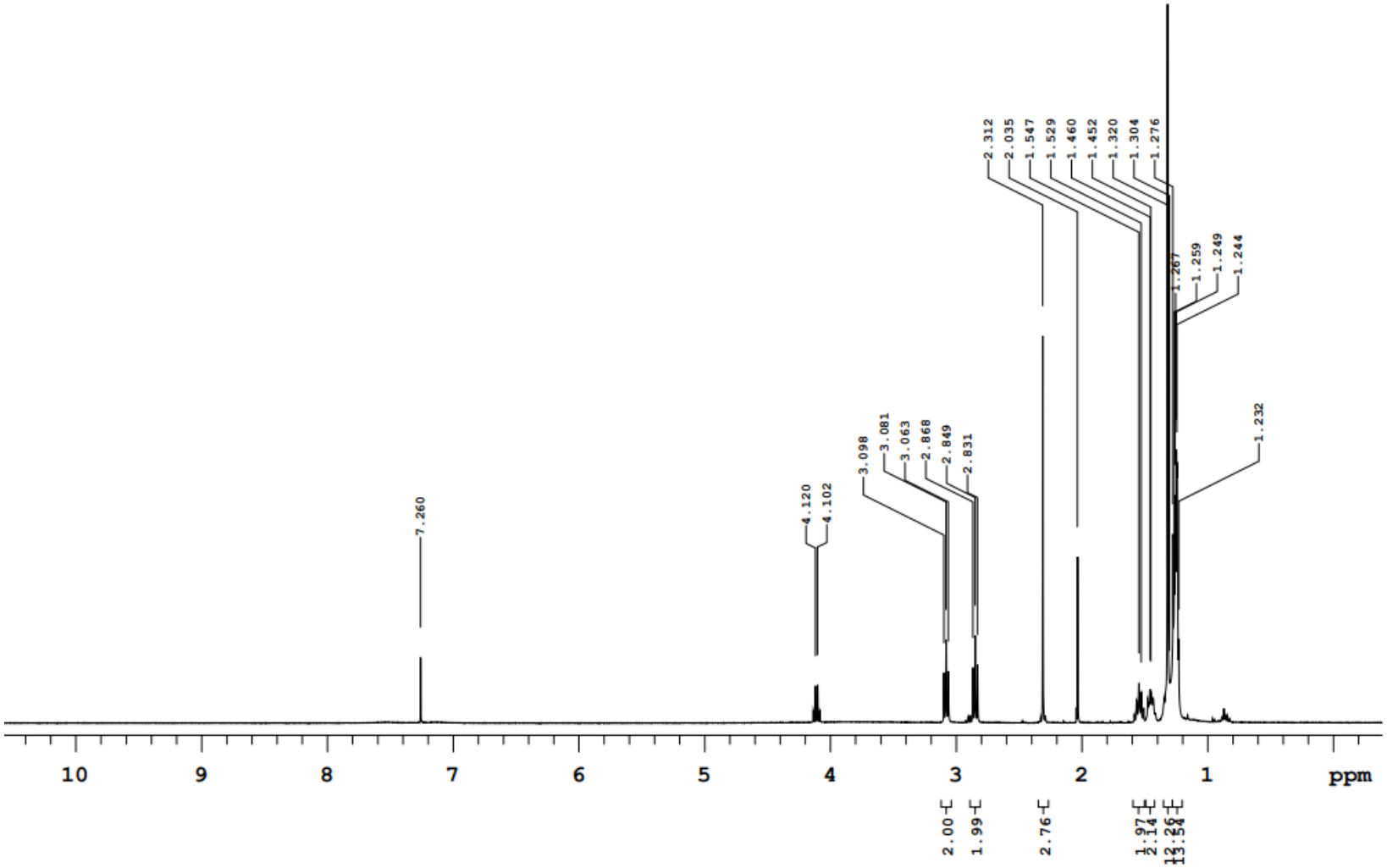

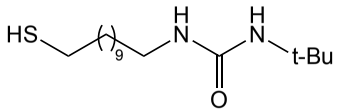

Compound **10.1**: ^{1}H NMR ($CDCl_3$, 500 MHz)

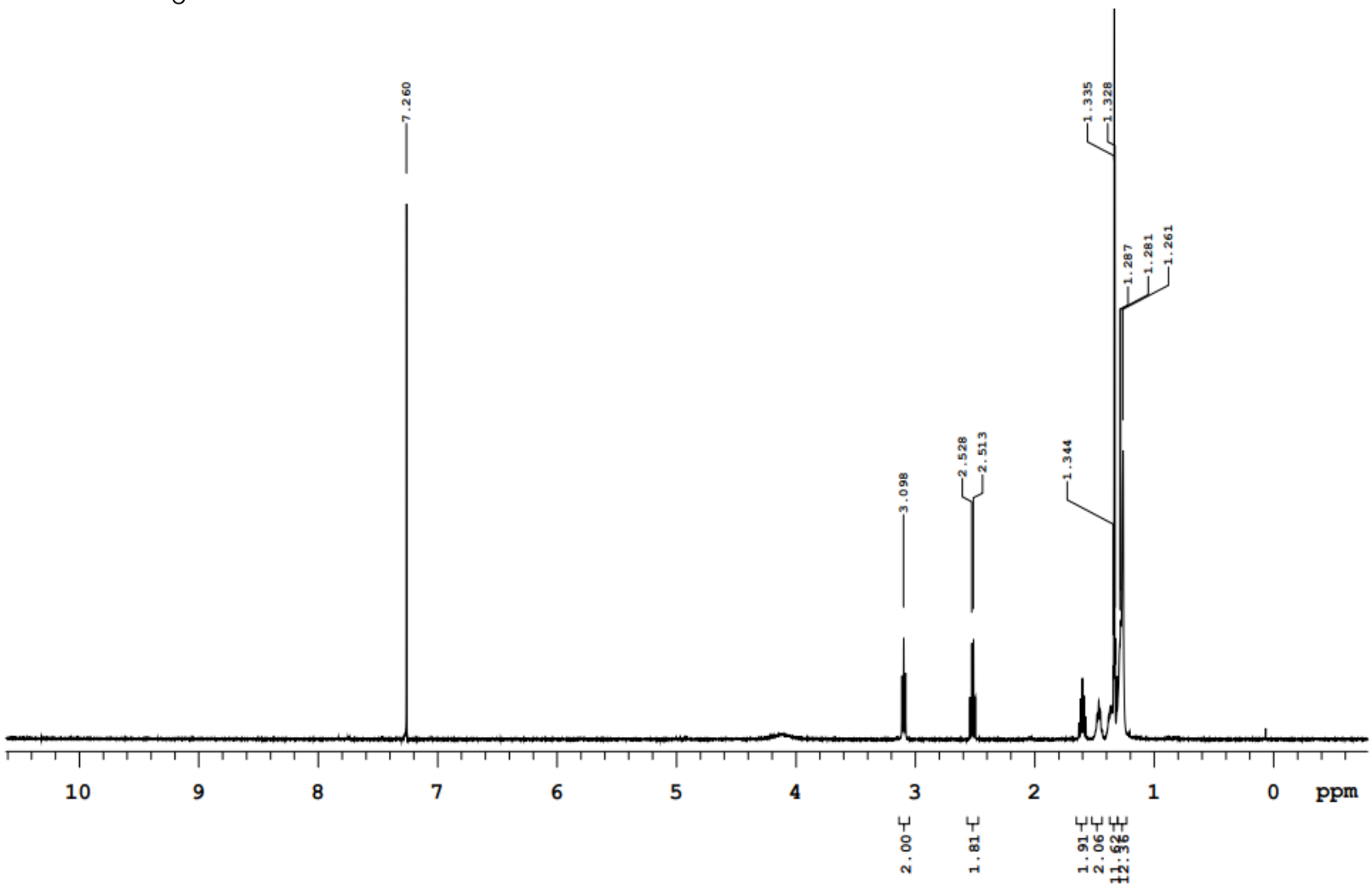

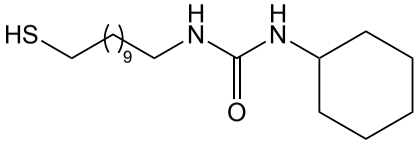

Compound **10.2**: ^{1}H NMR ($CDCl_3$, 400 MHz)

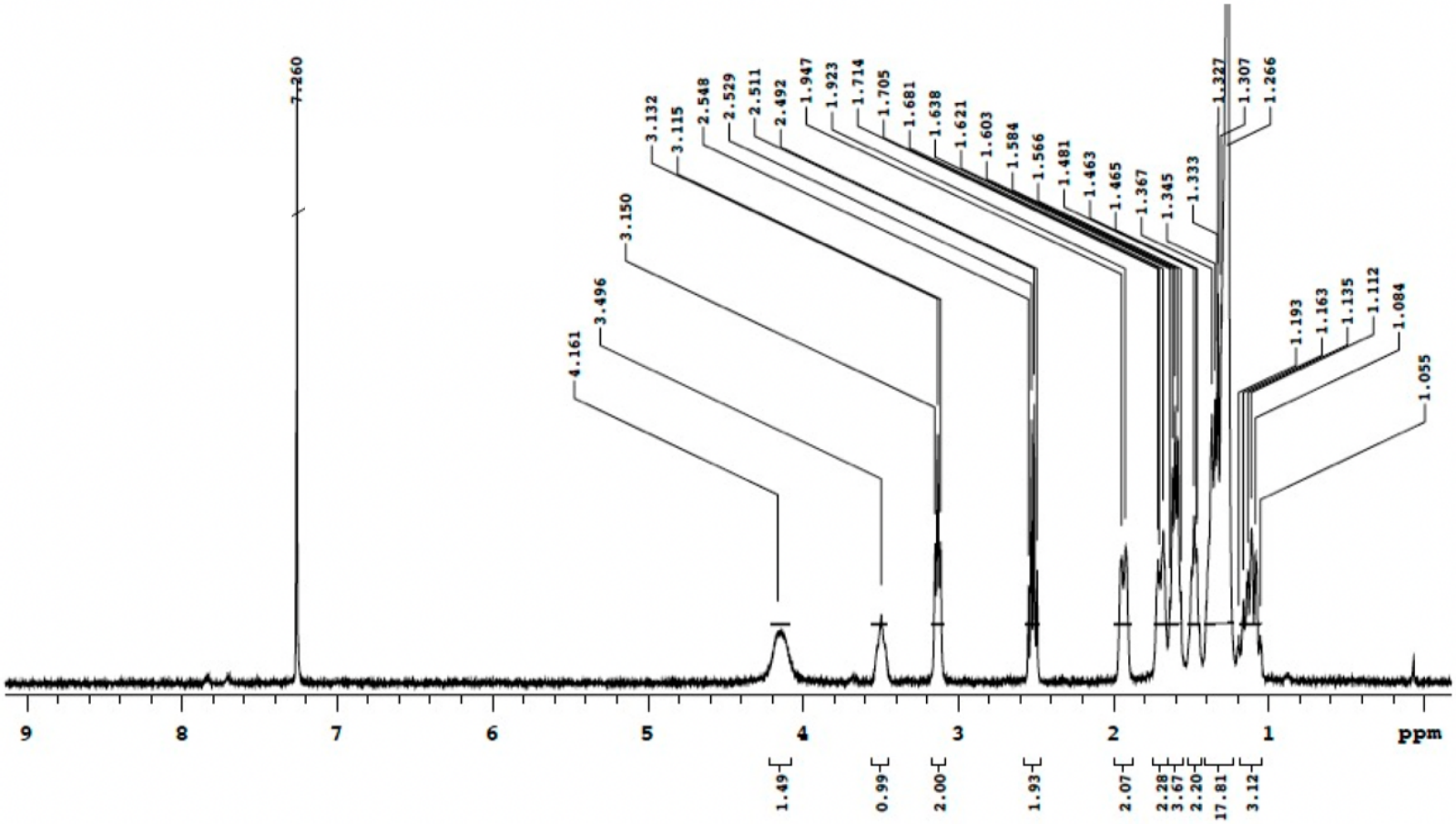

Compound **10.2**: ^{13}C NMR ($CDCl_3$, 100 MHz)

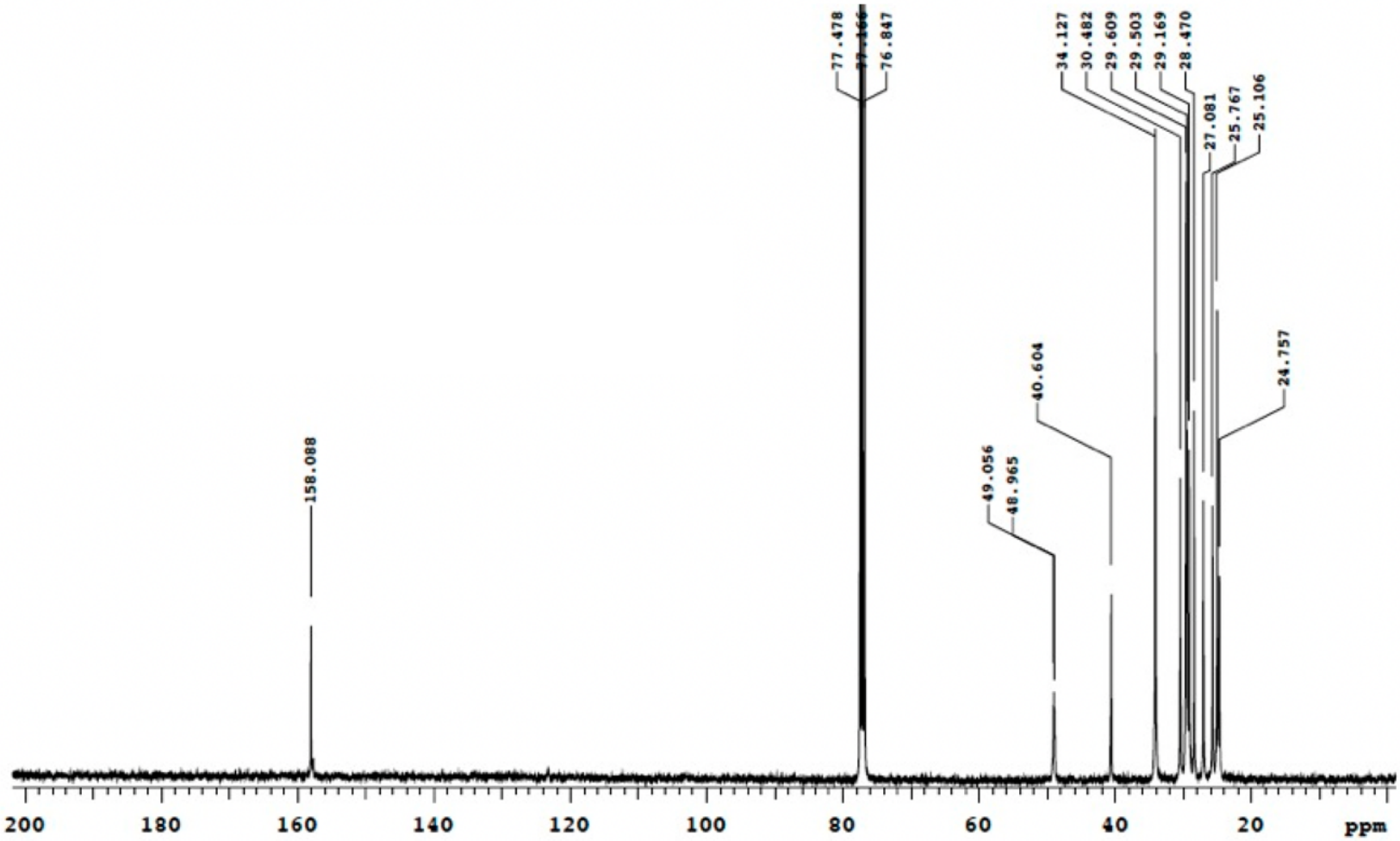

Compound **10.3**: ^{1}H NMR ($CDCl_3$, 400 MHz)

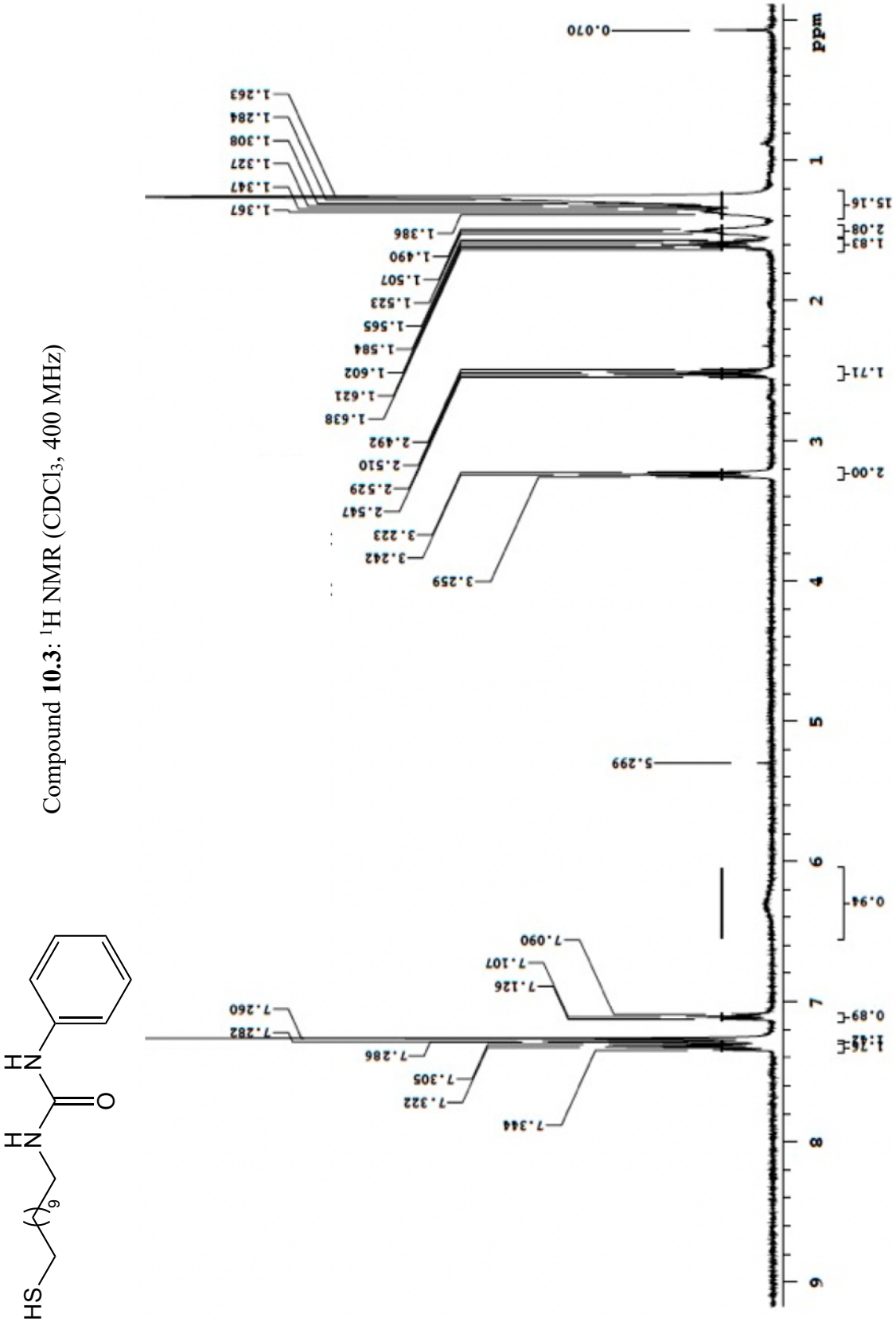

Compound **10.3**: ^{13}C NMR ($CDCl_3$, 100 MHz)

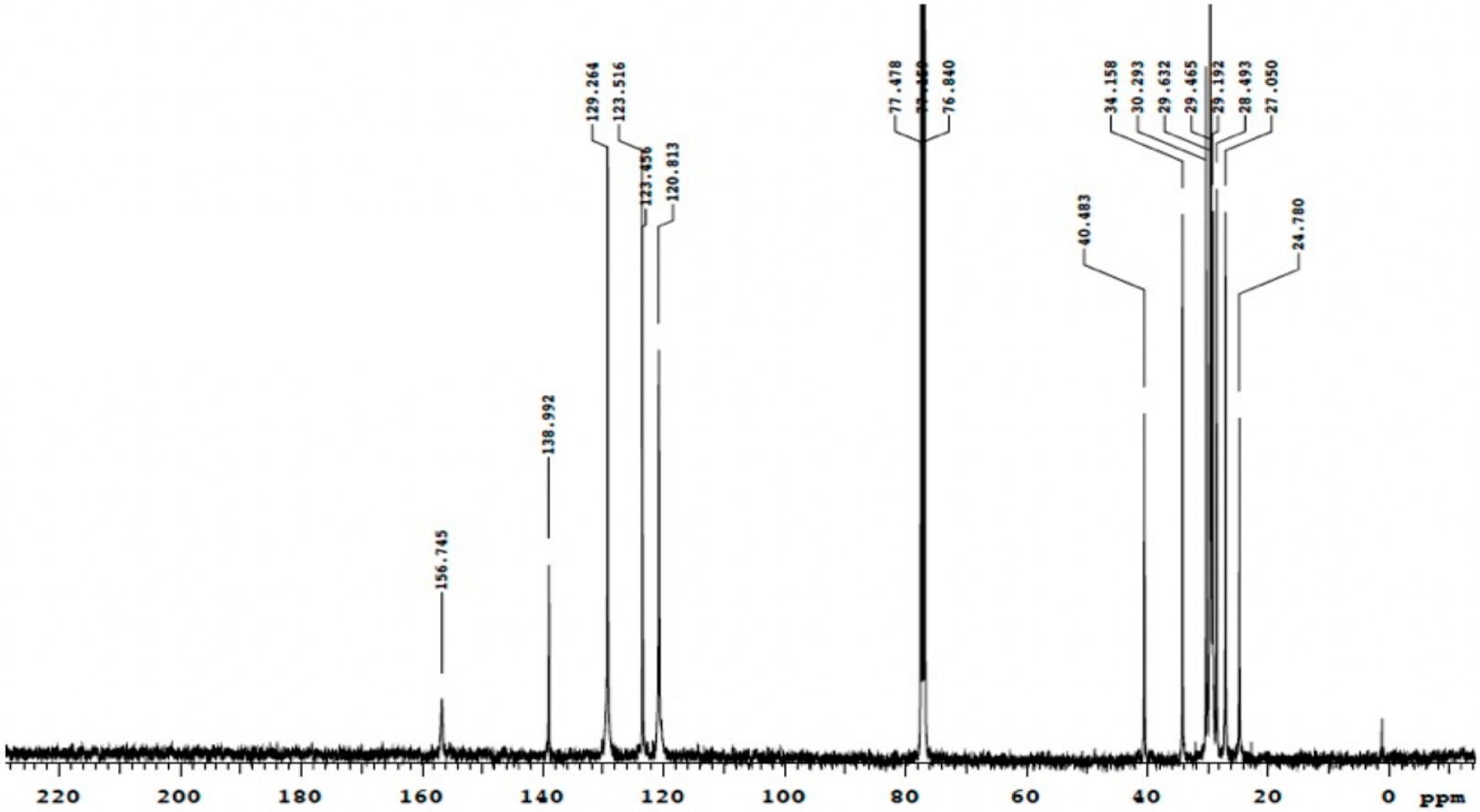

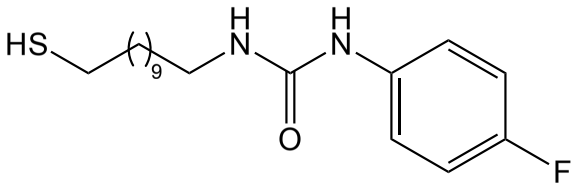

Compound **10.4**: ^{1}H NMR ($CDCl_3$, 400 MHz)

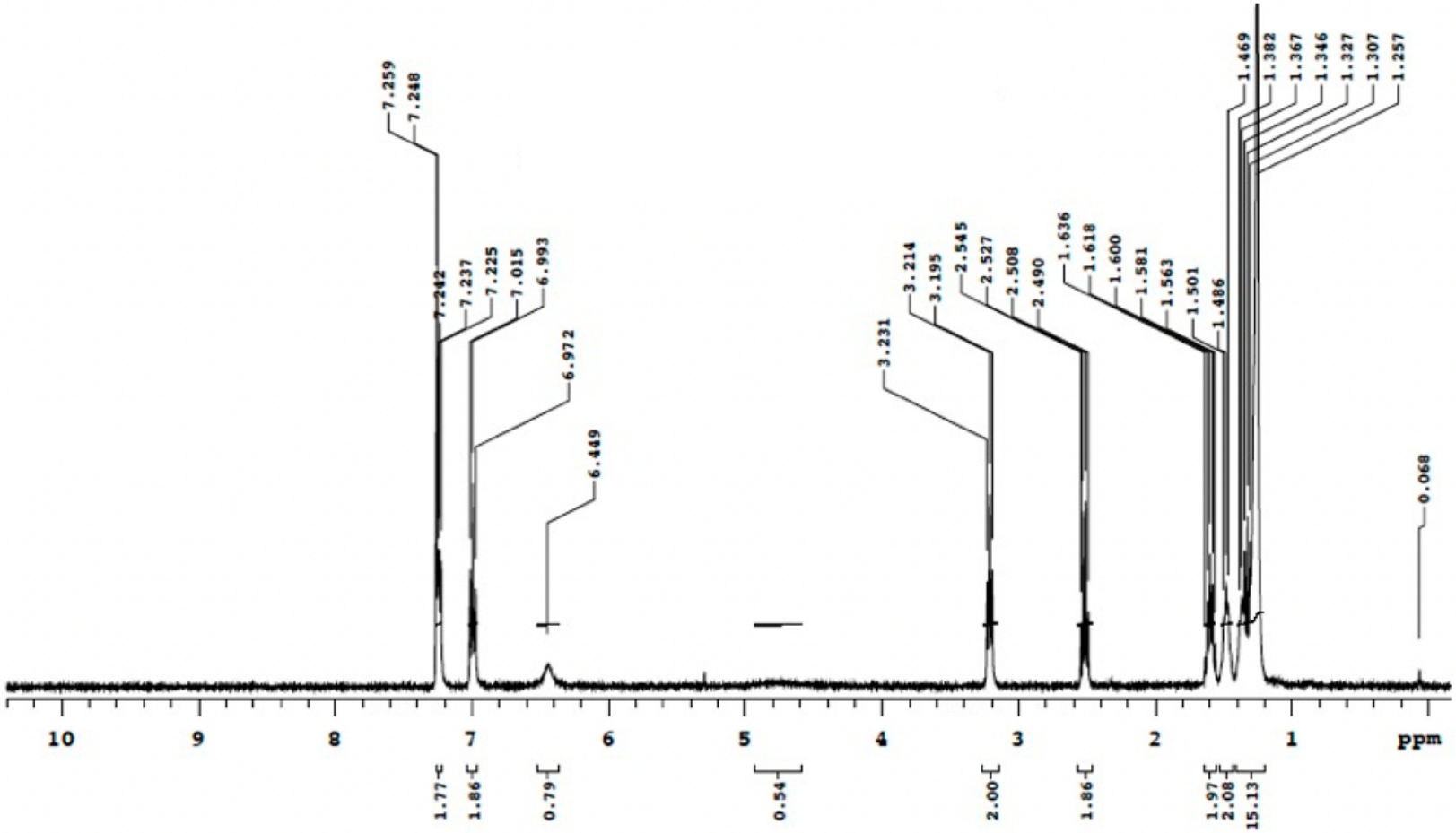

Compound **10.4**: ^{13}C NMR ($CDCl_3$, 100 MHz)

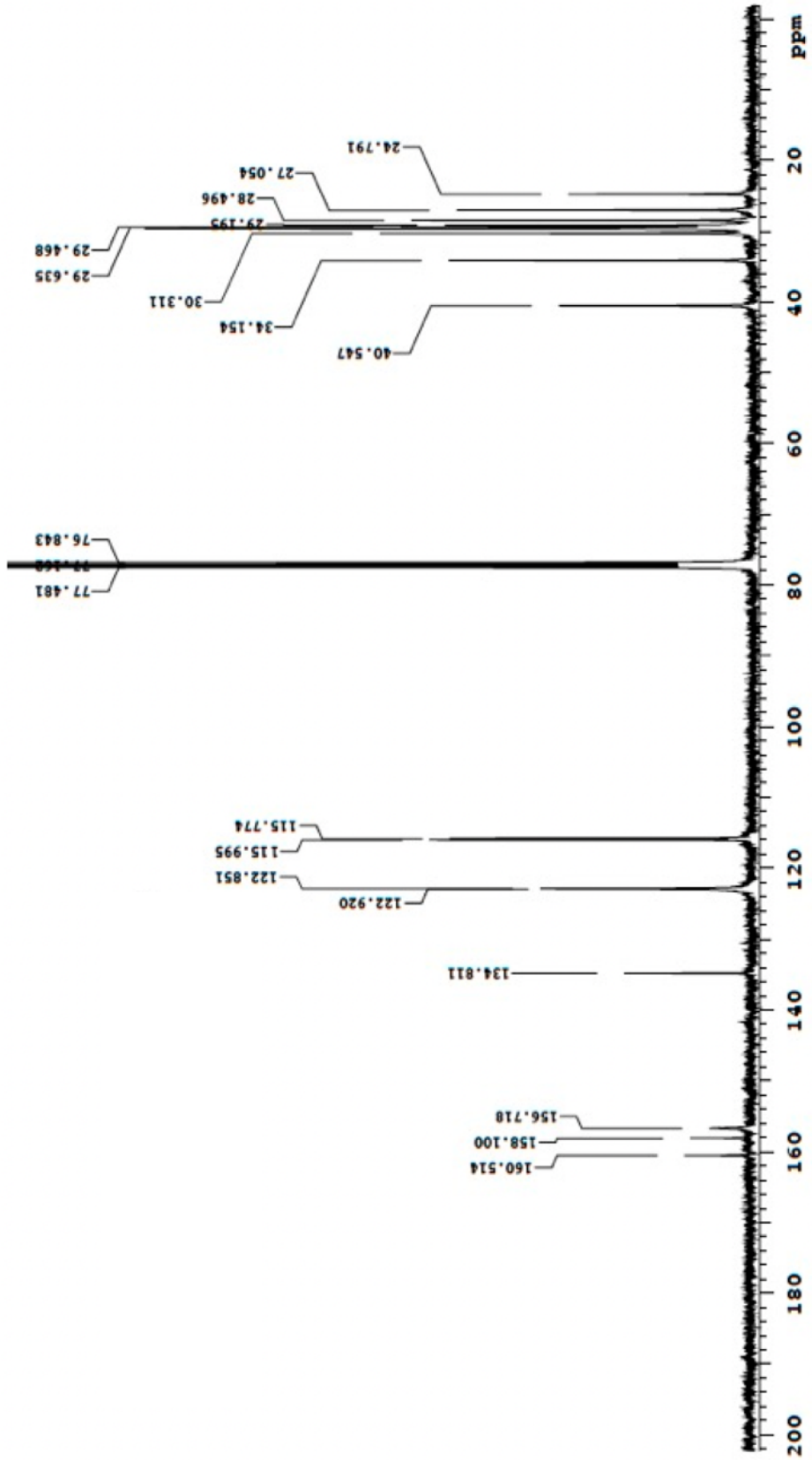

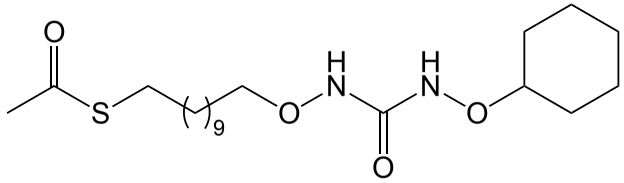

Compound **12.2 a**: ^{1}H NMR ($CDCl_3$, 400 MHz)

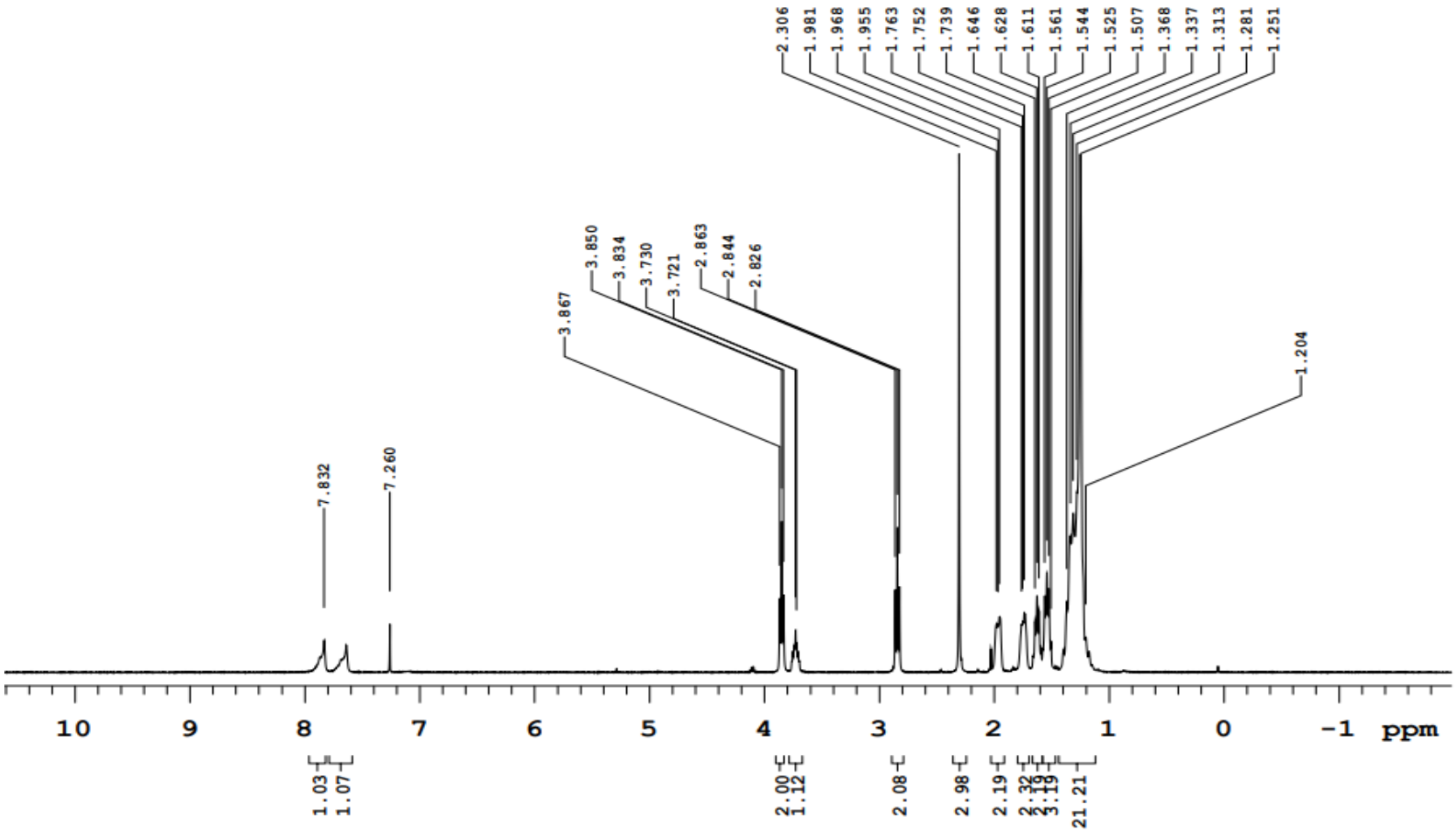

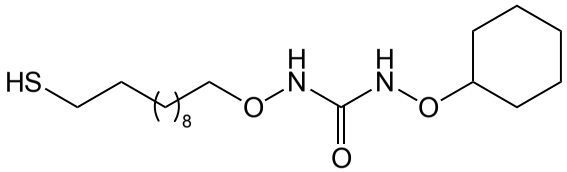

Compound **13.2**: ^{1}H NMR ($CDCl_3$, 400 MHz)

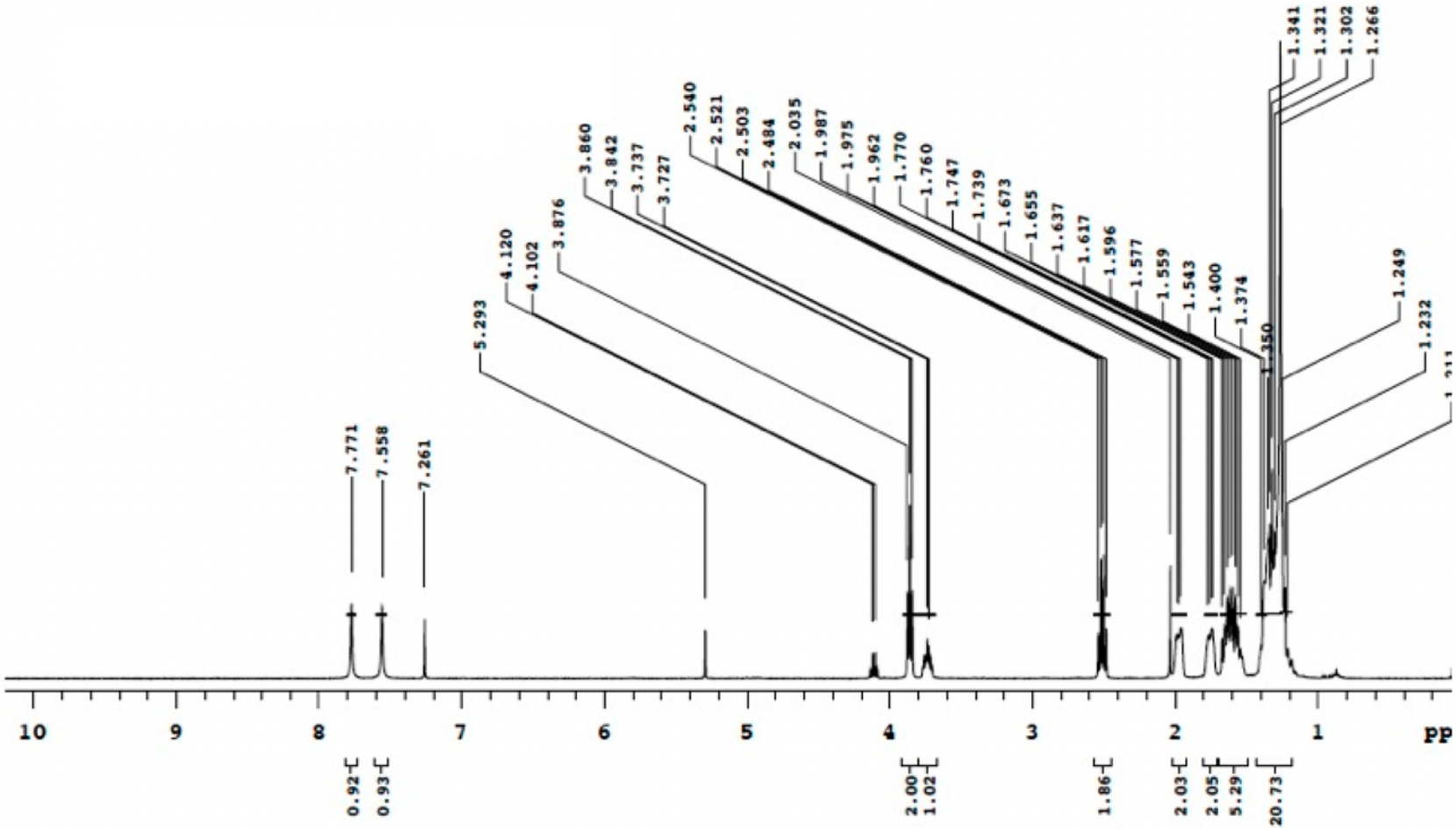

Compound **13.2**: ^{13}C NMR ($CDCl_3$, 100 MHz)

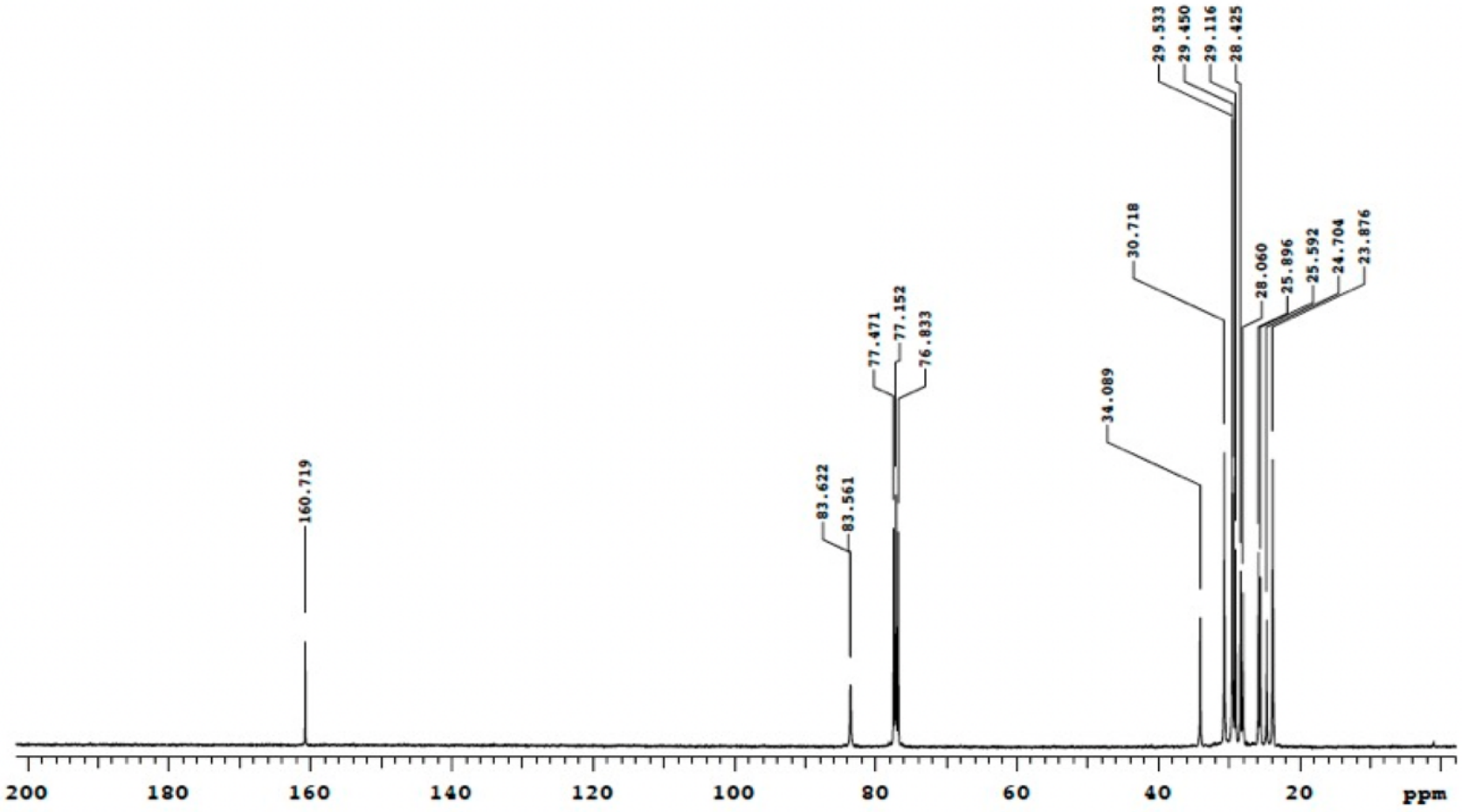

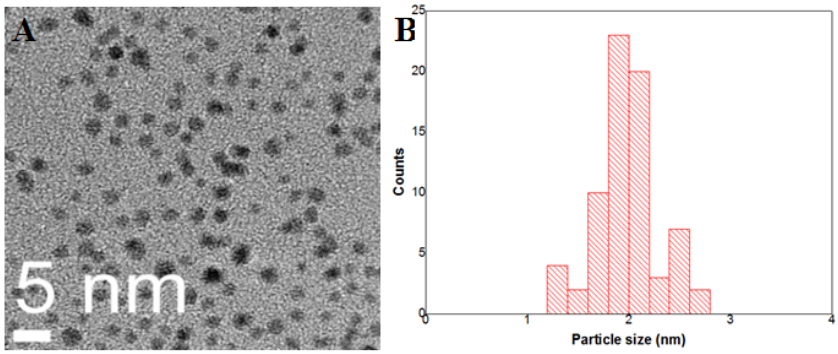

Figure 2. 18. A. TEM image and **B.** Histogram of **5.1** monoalkoxyurea thiol functionalized Au MPCs.[33]

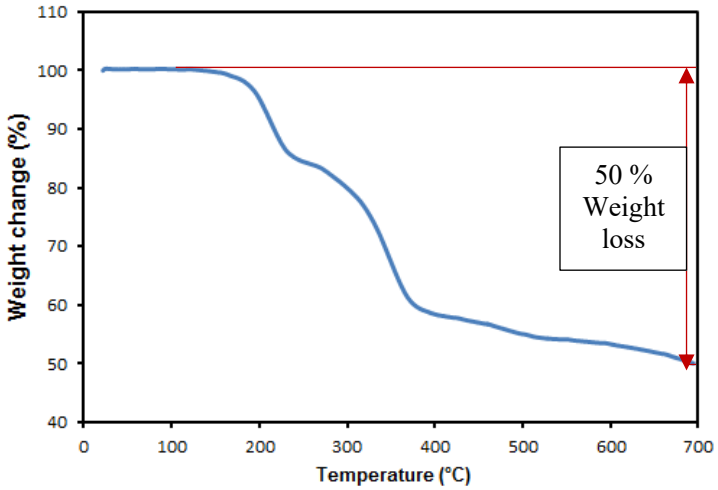

Figure 2.20. TGA curve of **5.1** monoalkoxyurea thiol functionalized Au MPCs.[33]

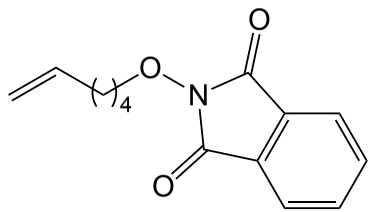

Compound **1**: ^{1}H NMR ($CDCl_3$, 400 MHz)

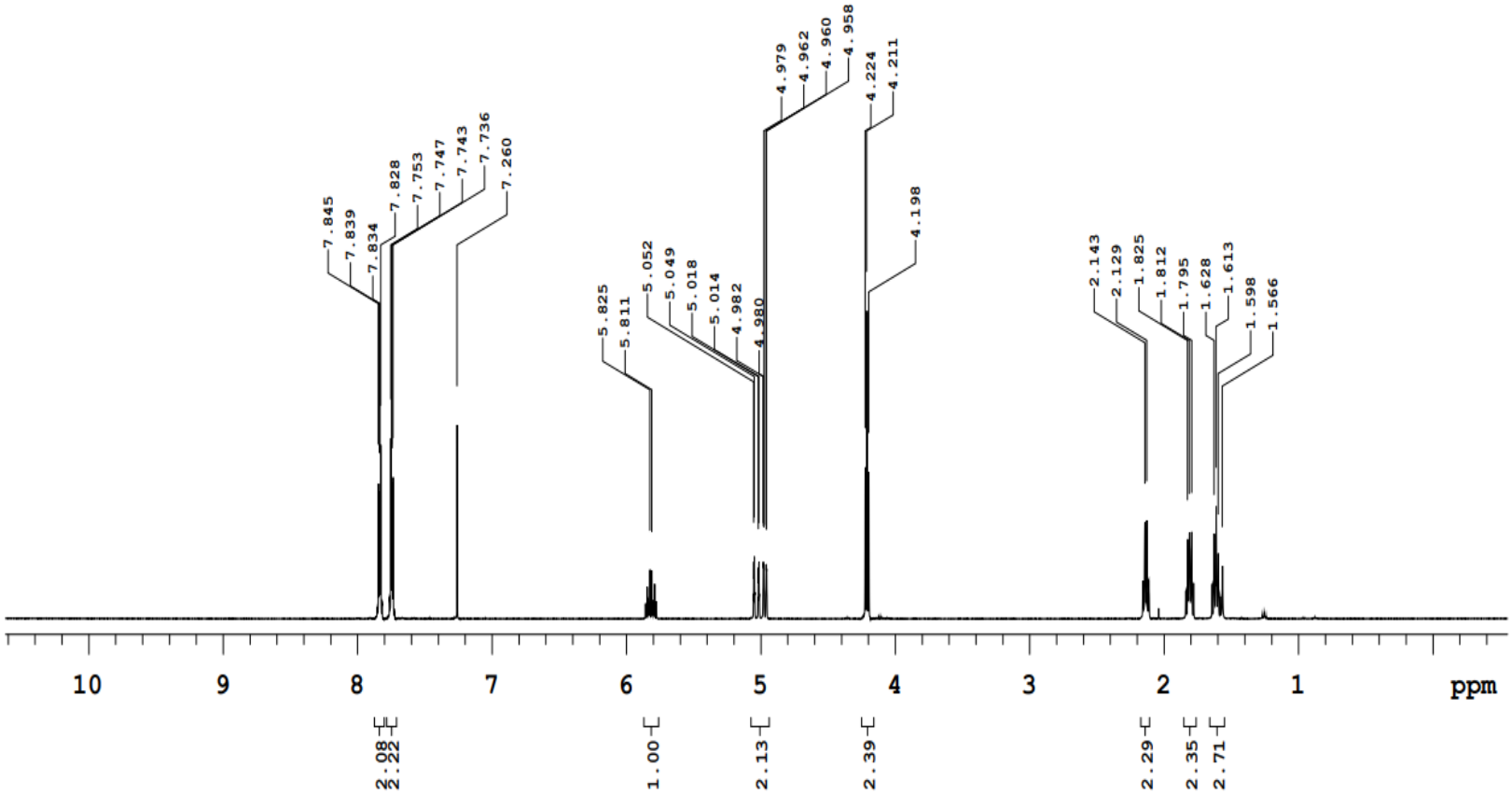

Compound **1**: ^{13}C NMR ($CDCl_3$, 100 MHz)

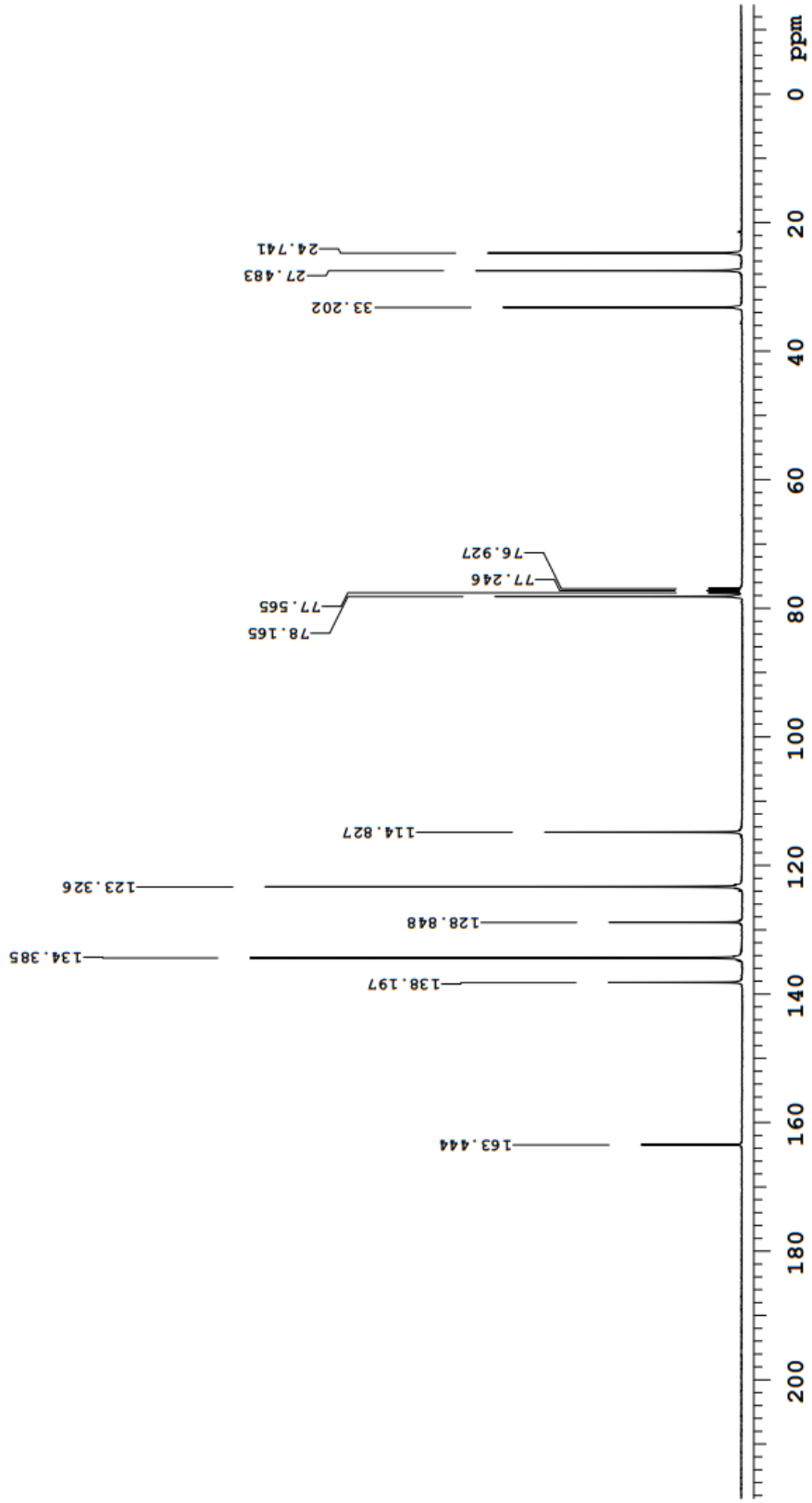

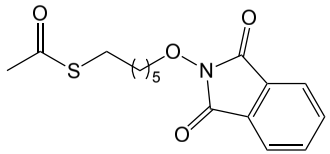

Compound **2**: ^{1}H NMR ($CDCl_3$, 400 MHz)

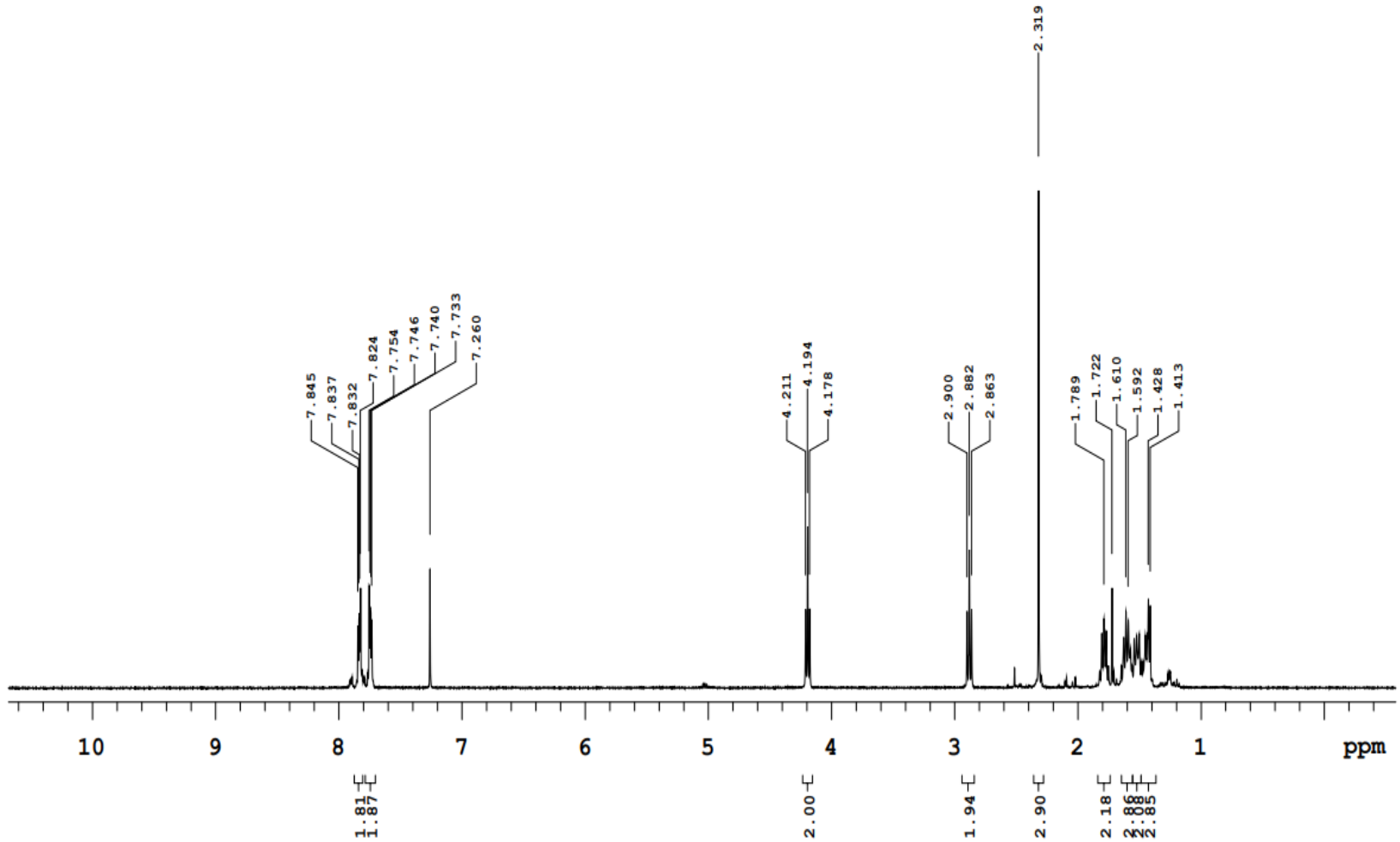

Compound **2**: ^{13}C NMR ($CDCl_3$, 100 MHz)

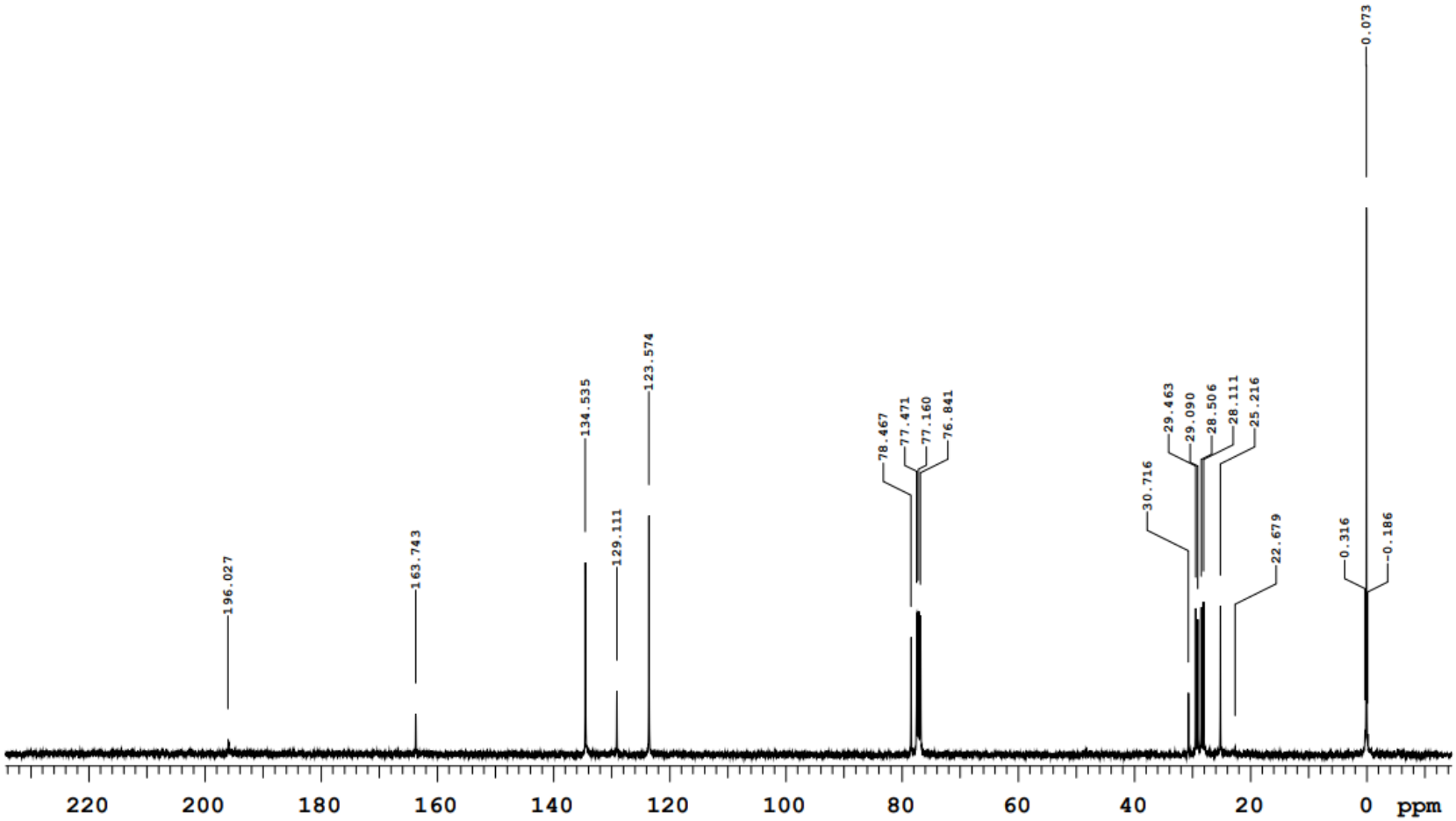

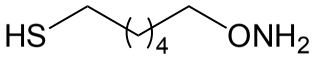

Compound **3**: ^{1}H NMR ($CDCl_3$, 400 MHz)

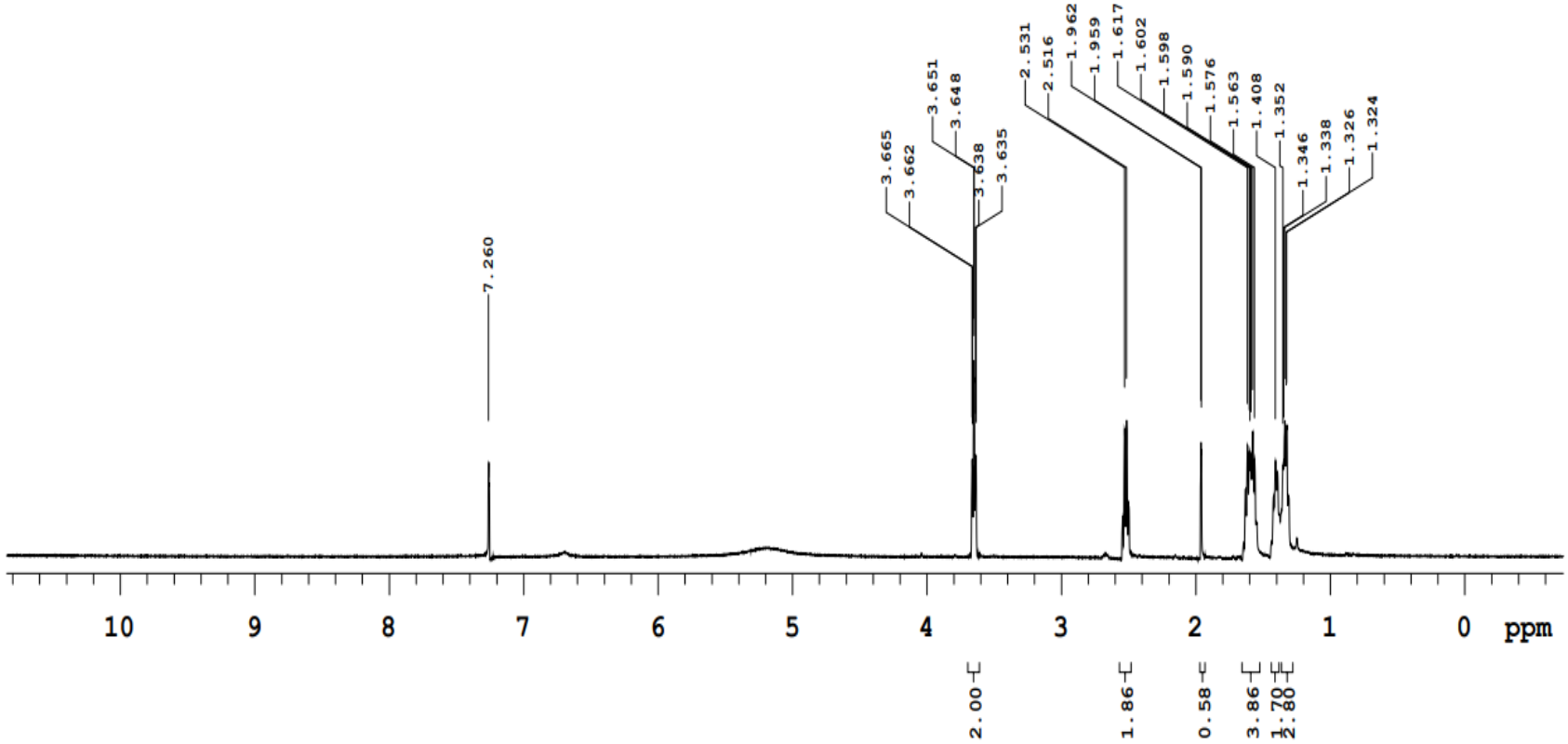

Compound **3**: ^{13}C NMR ($CDCl_3$, 100 MHz)

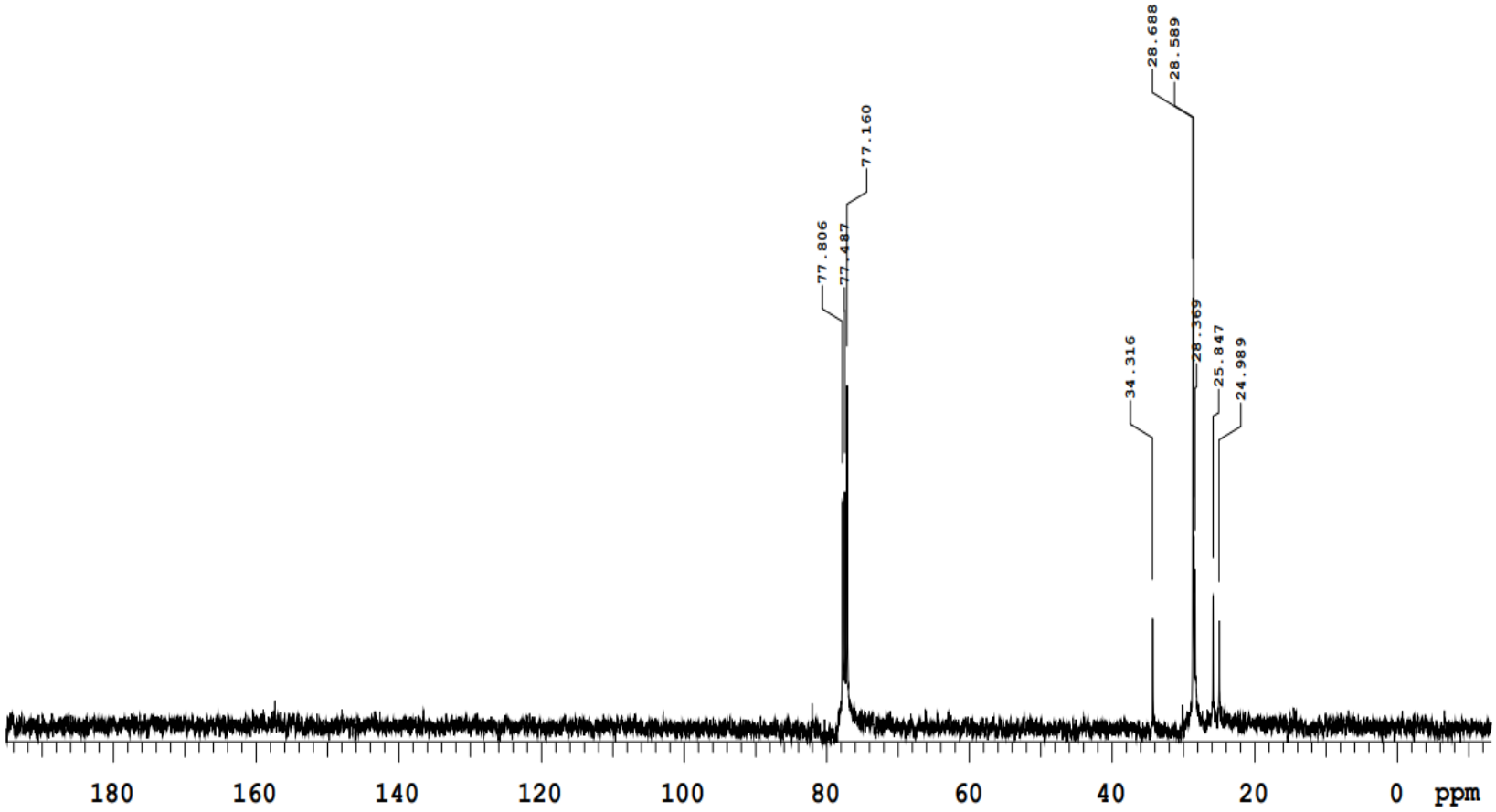

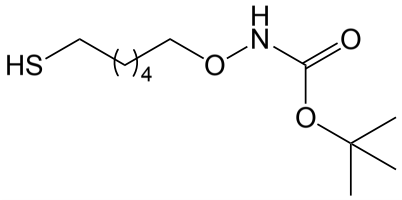

Compound **4**: ^{1}H NMR ($CDCl_3$, 400 MHz)

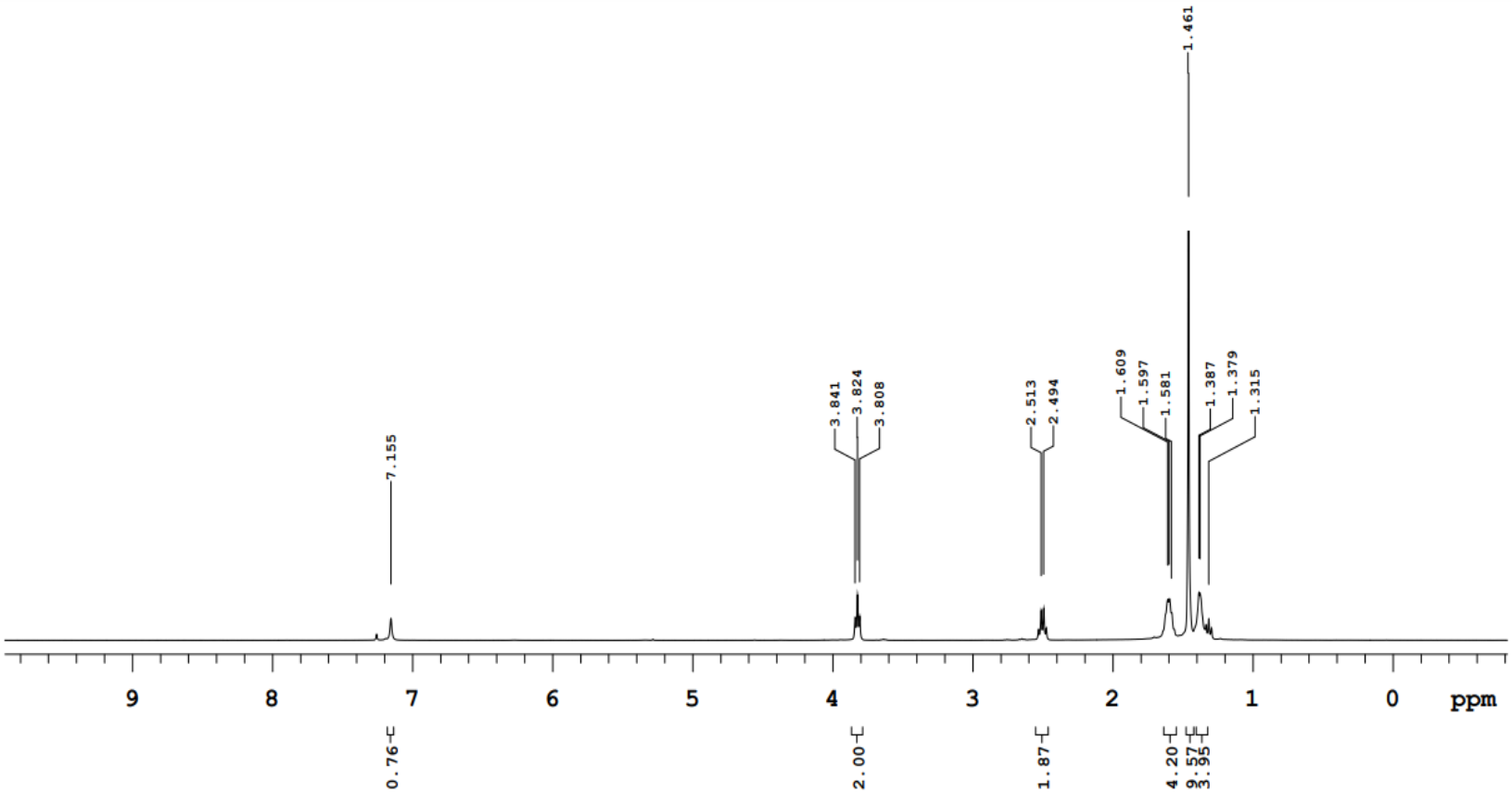

Compound **4**: ^{13}C NMR ($CDCl_3$, 100 MHz)

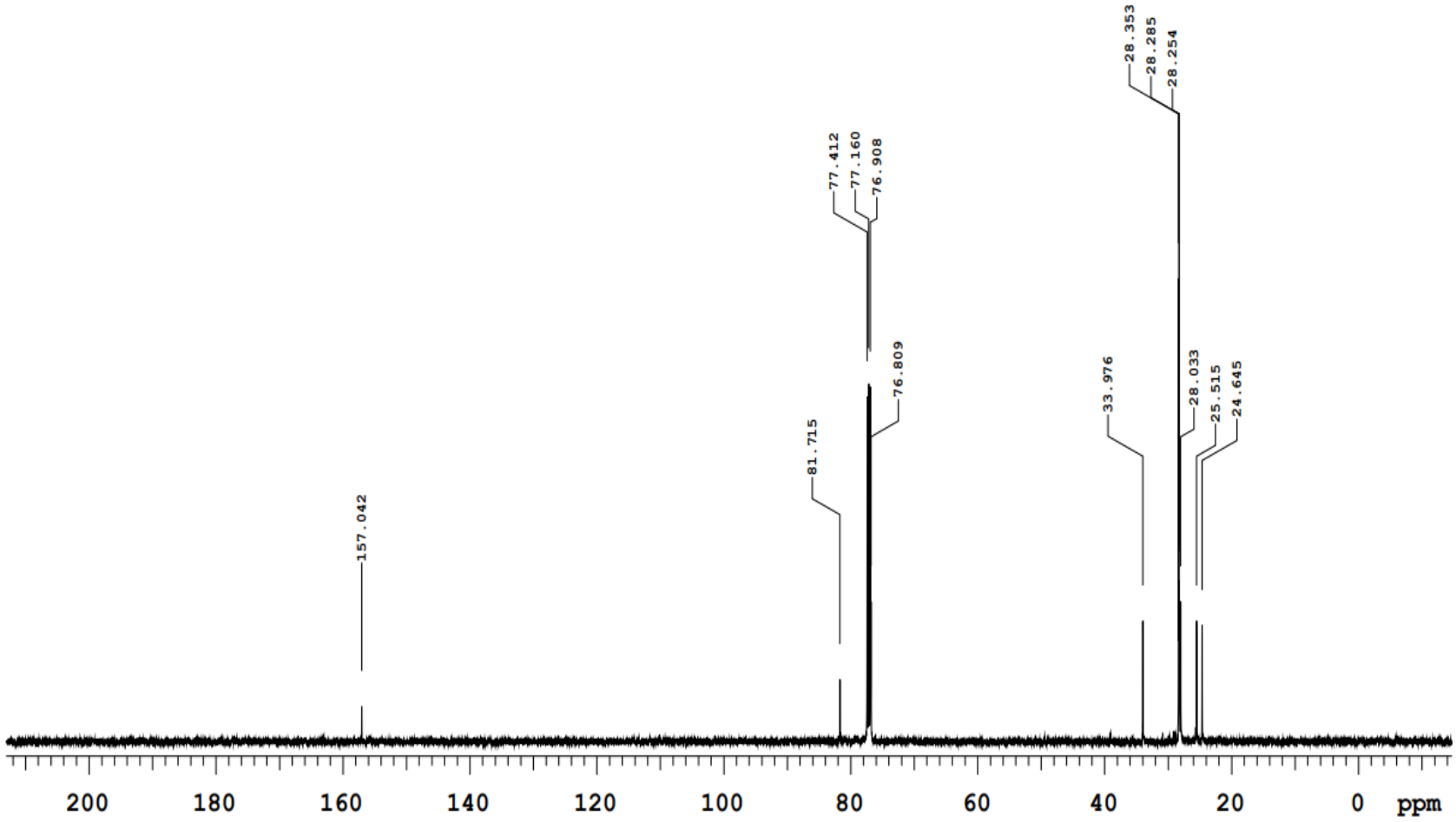

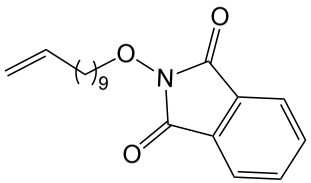

Compound **5**: ^{1}H NMR ($CDCl_3$, 400 MHz)

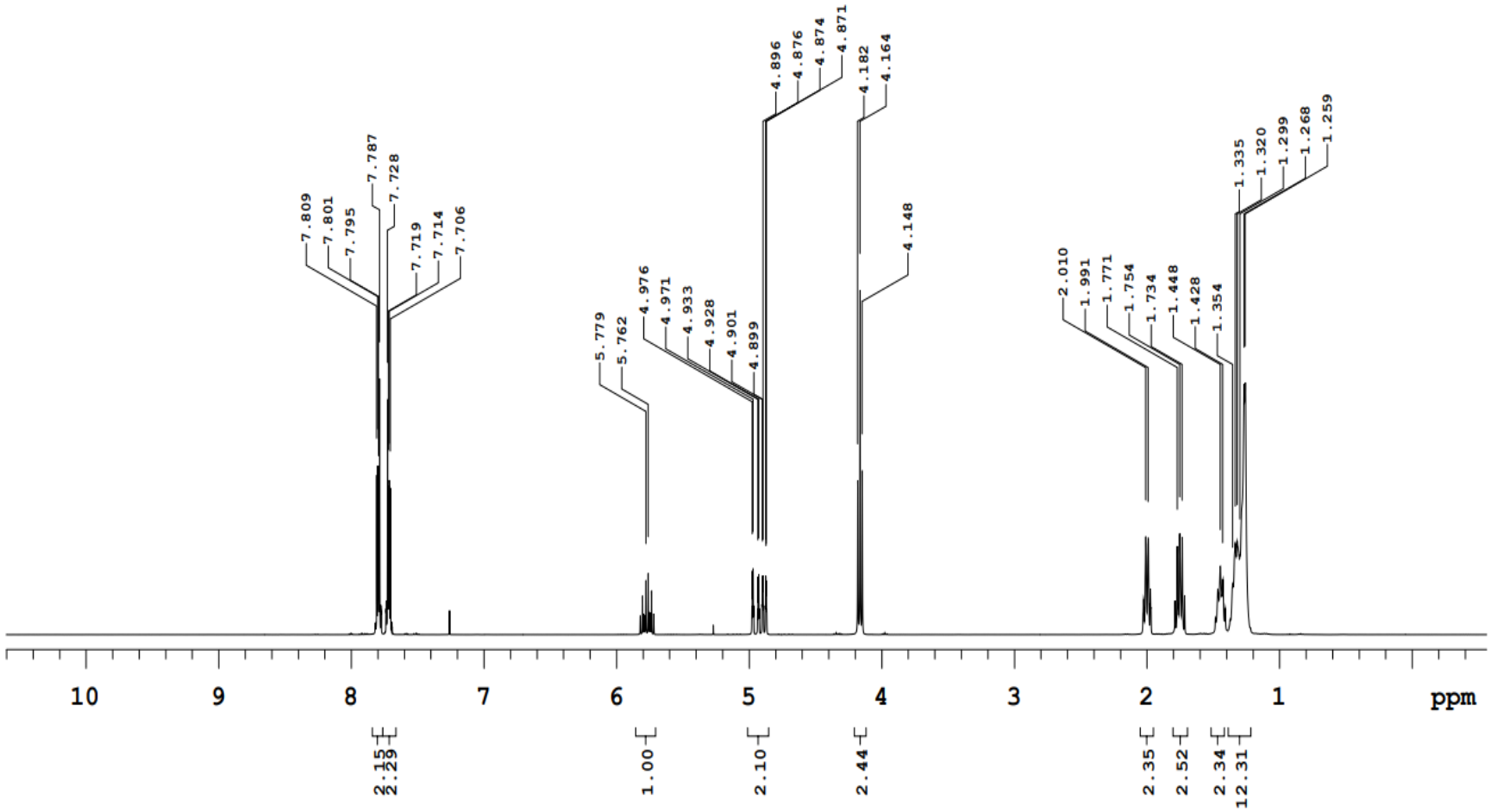

Compound **5**: ^{13}C NMR ($CDCl_3$, 100 MHz)

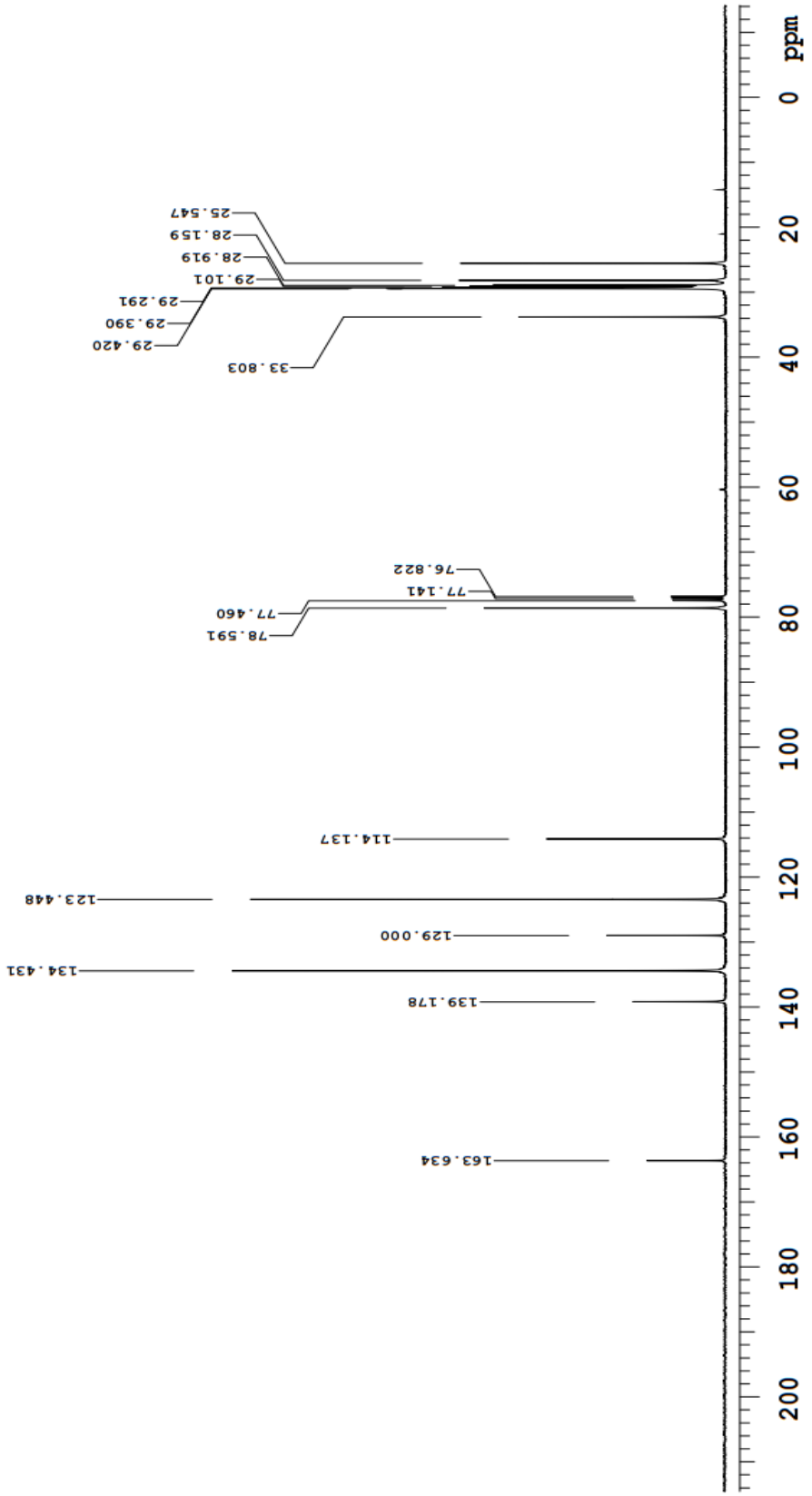

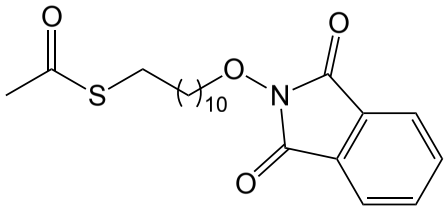

Compound **6**: ^{1}H NMR ($CDCl_3$, 400 MHz)

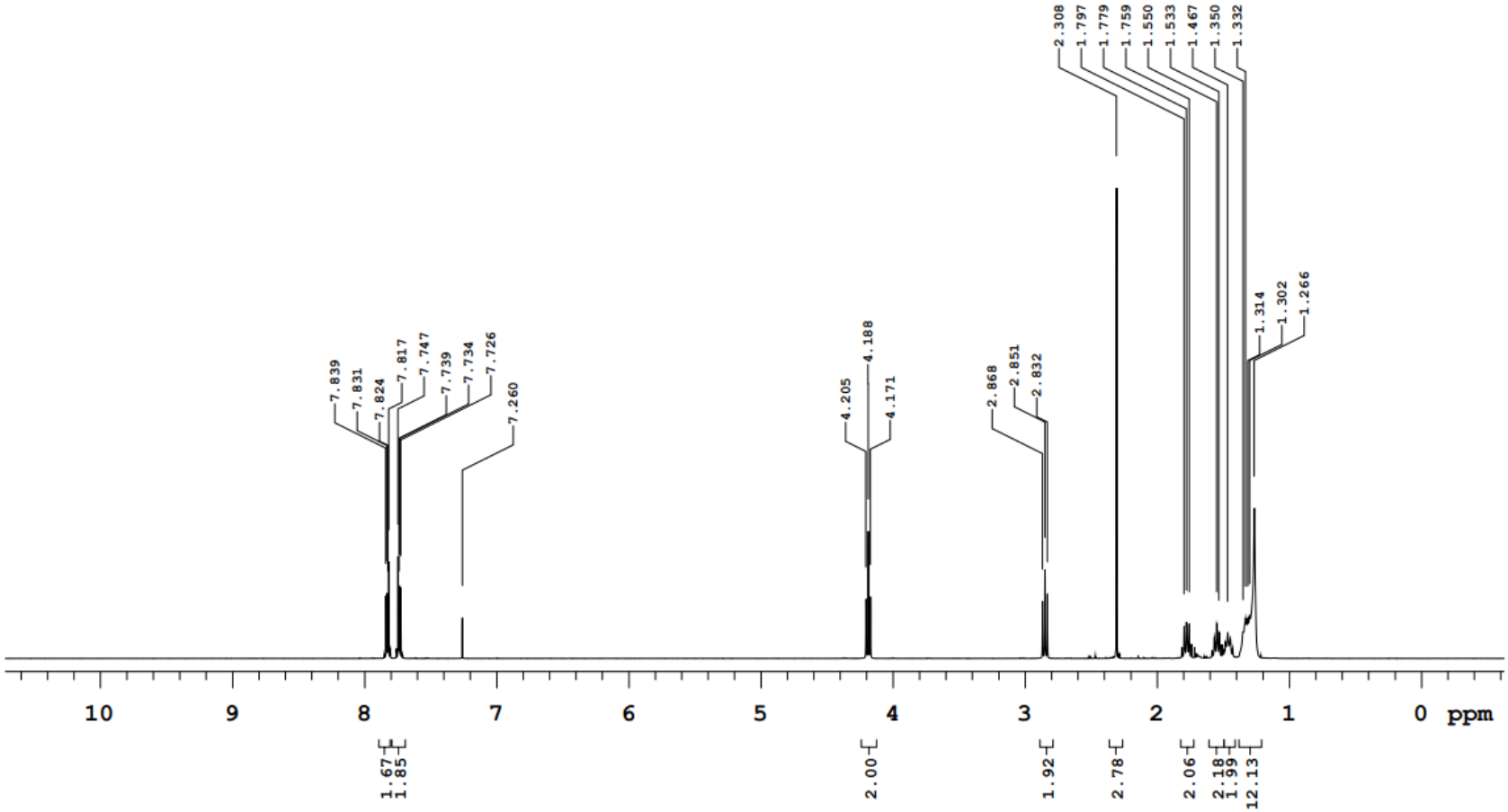

Compound **6:** ^{13}C NMR ($CDCl_3$, 100 MHz)

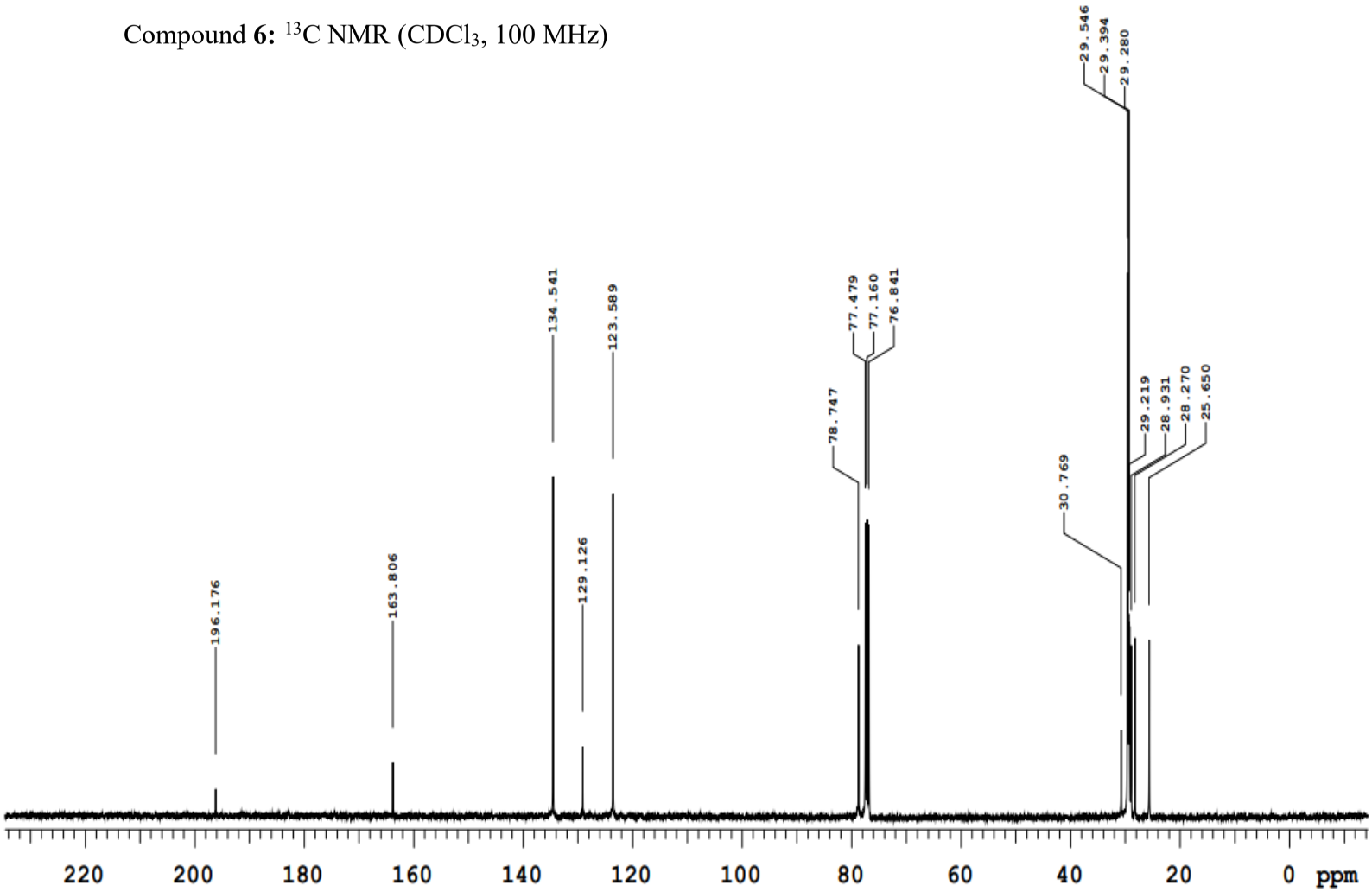

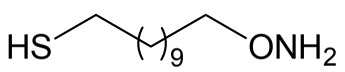

Compound **7:** ^{1}H NMR ($CDCl_3$, 400 MHz)

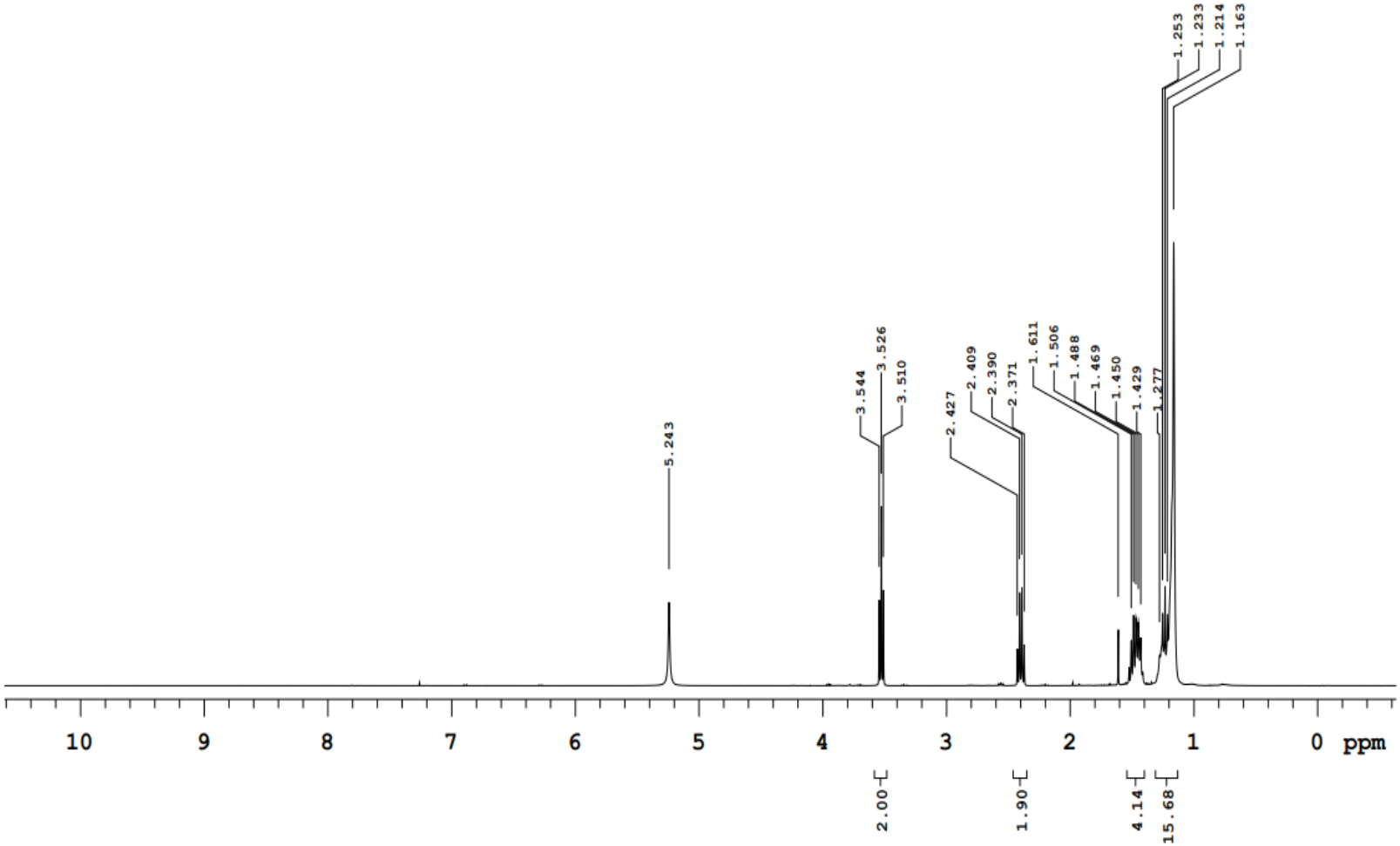

Compound **7:** ^{13}C NMR ($CDCl_3$, 100 MHz)

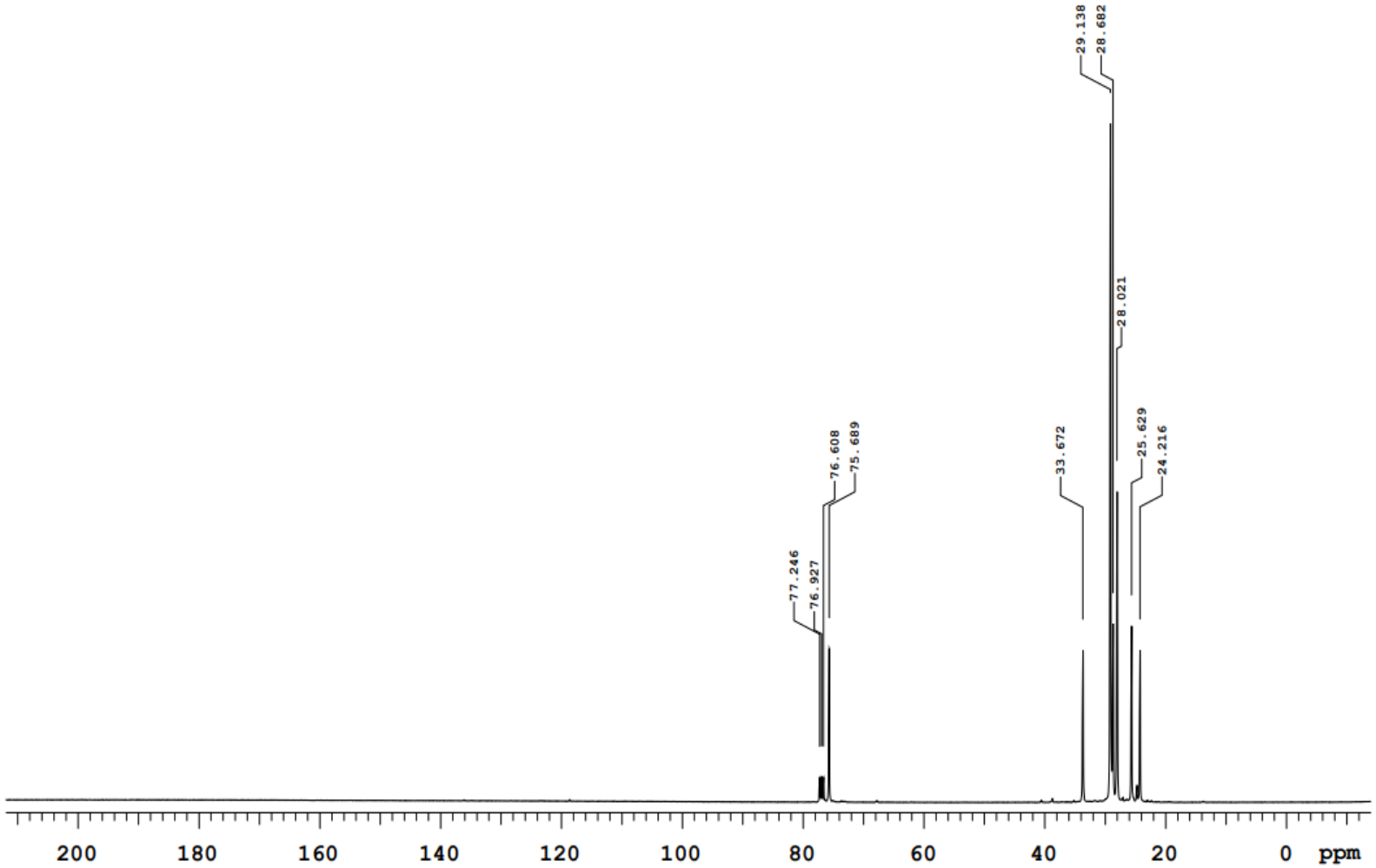

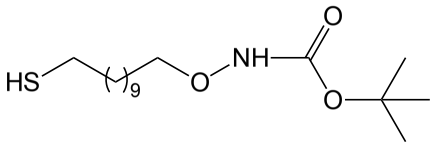

Compound **8**: ^{1}H NMR ($CDCl_3$, 400 MHz)

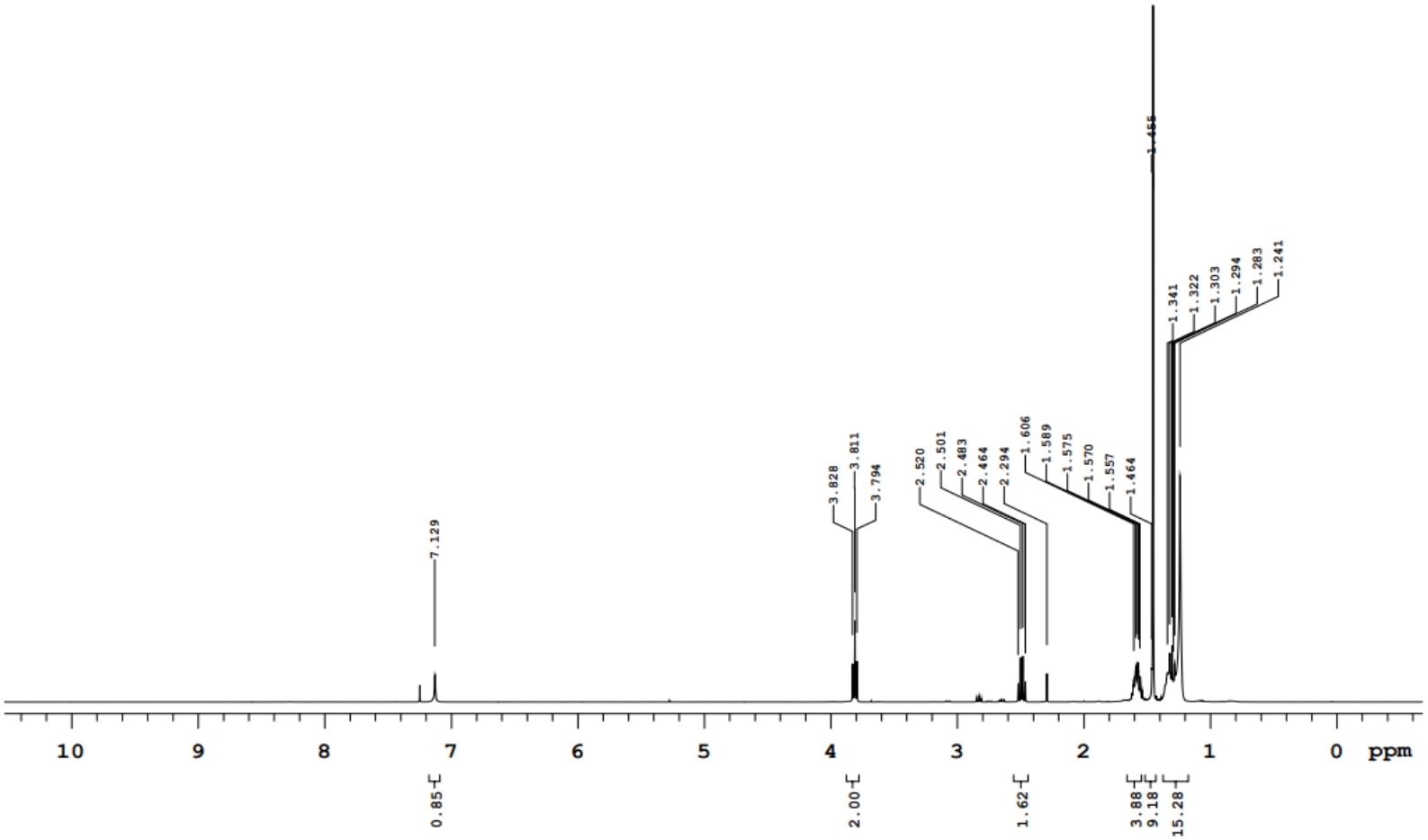

Compound **8**: ^{13}C NMR ($CDCl_3$, 100 MHz)

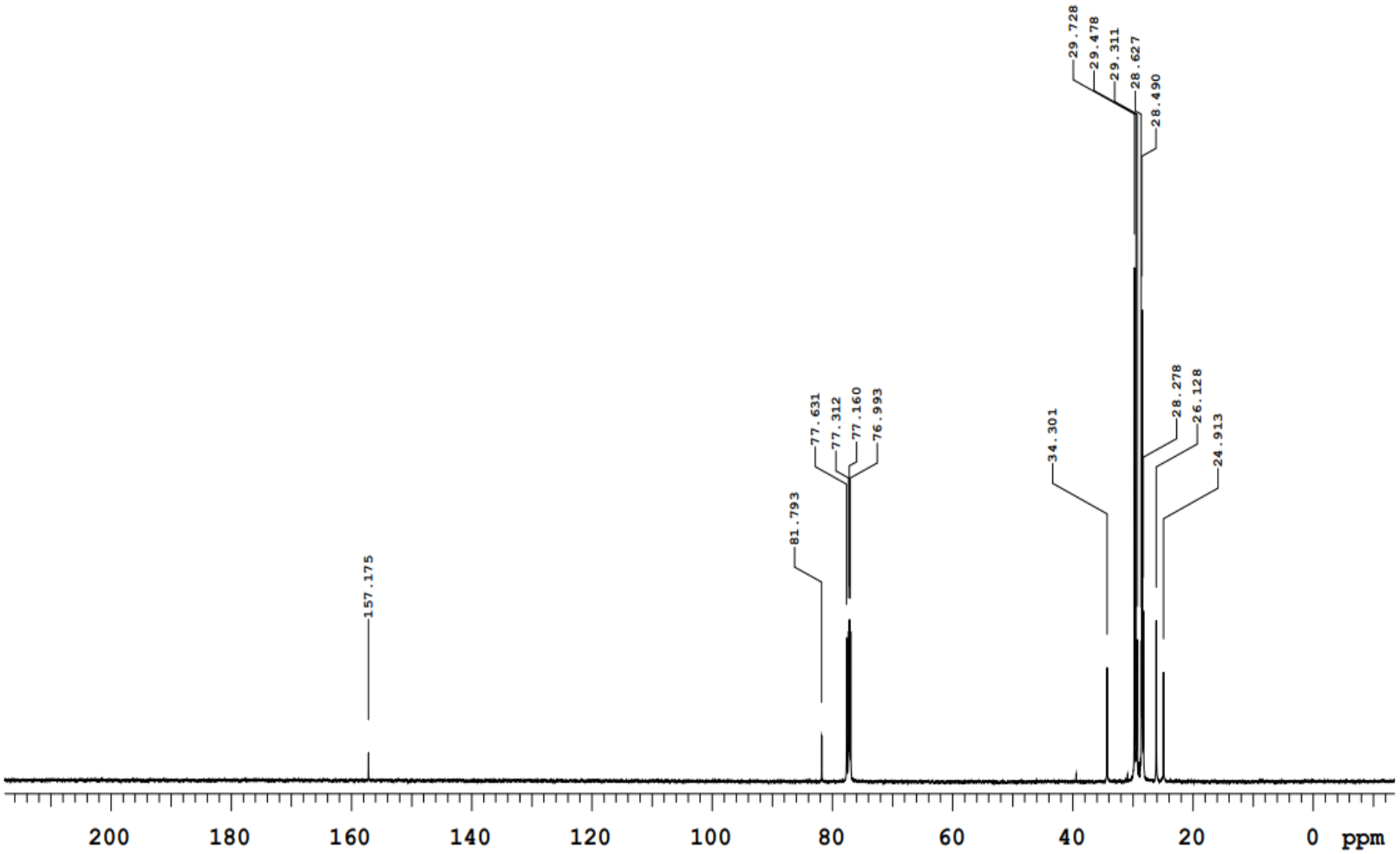

N-Boc protected **Au MPCs 9/C6** : ^{1}H NMR ($CDCl_3$, 400 MHz)

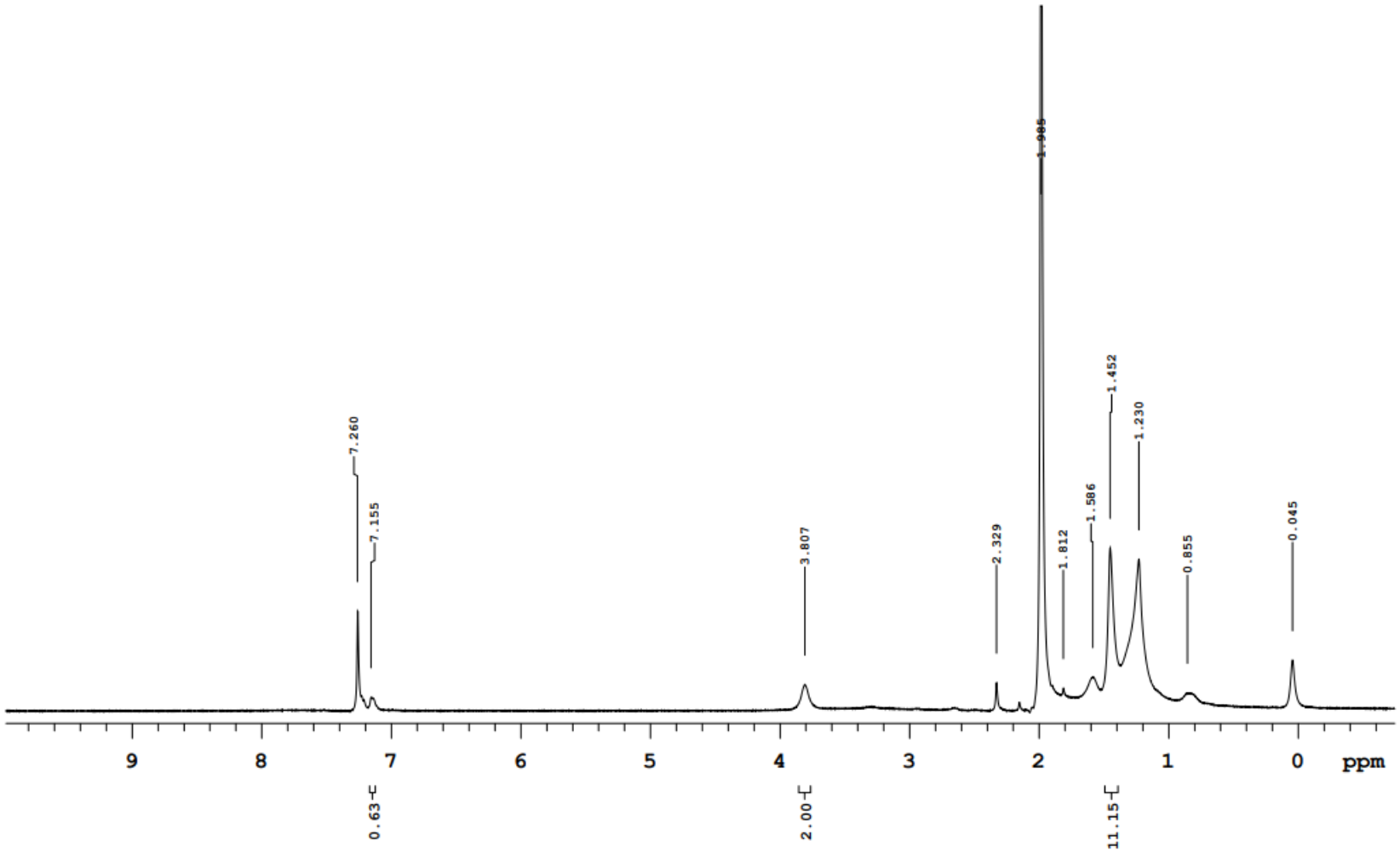

Au MPCs 10/C6 step a; Oxy-ammonium triflate salt of Au MPCs: ^{1}H NMR ($CDCl_3$, 400 MHz)

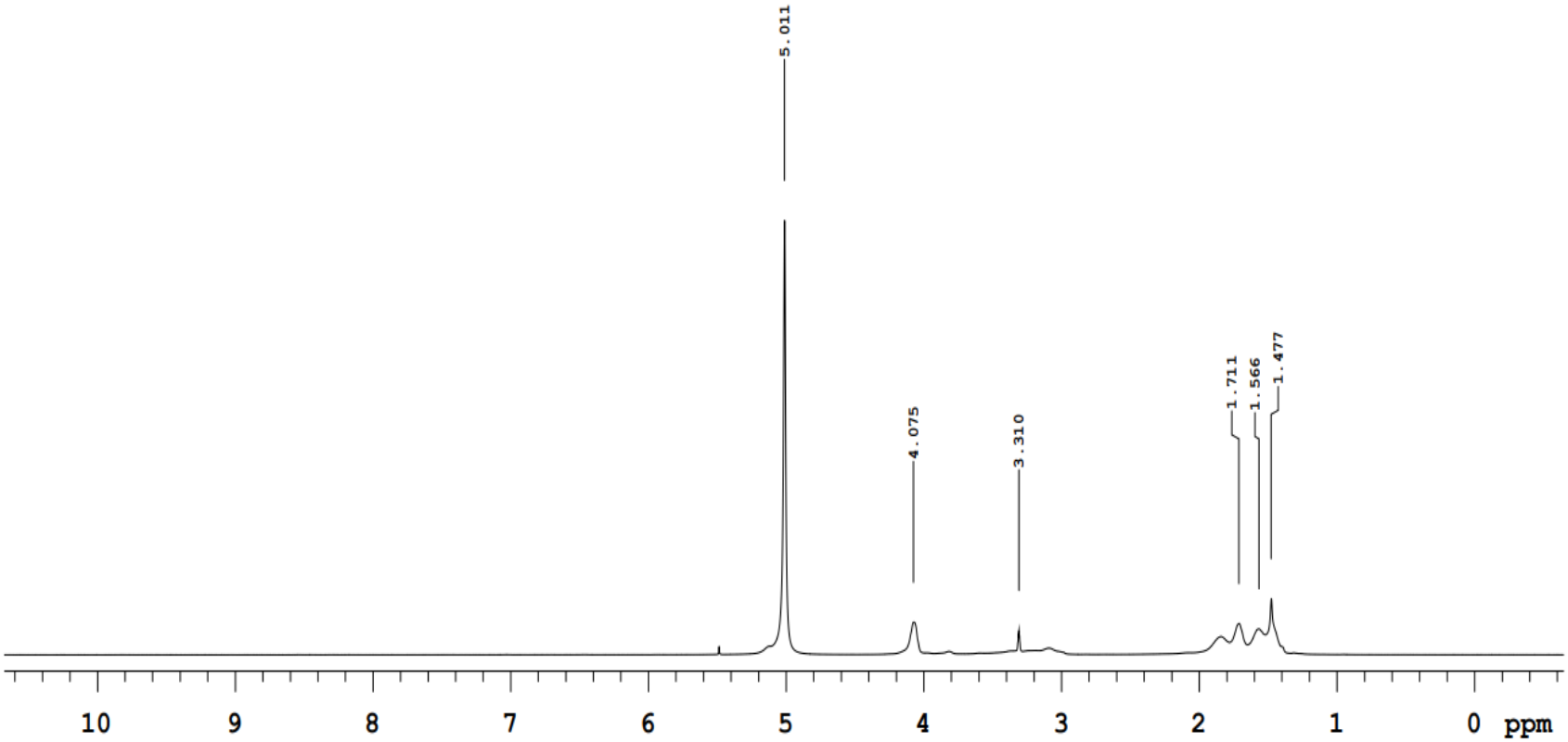

Au MPCs 10/C6 step b; Aminooxy Au MPCs ^{1}H NMR ($CDCl_3$, 400 MHz)

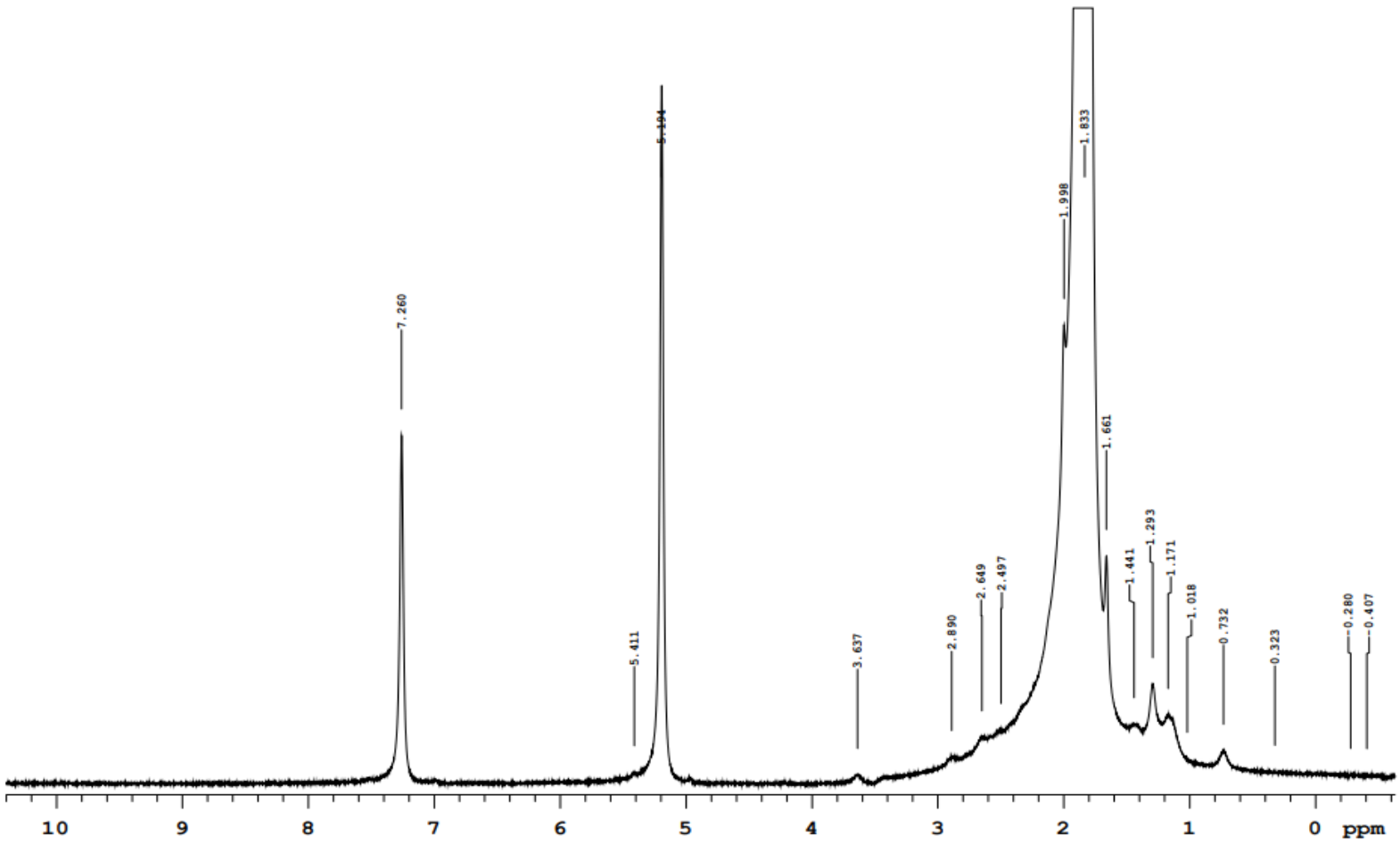

Au MPCs 11/C6; Oxime ether adduct: ^{1}H NMR ($CDCl_3$, 400 MHz)

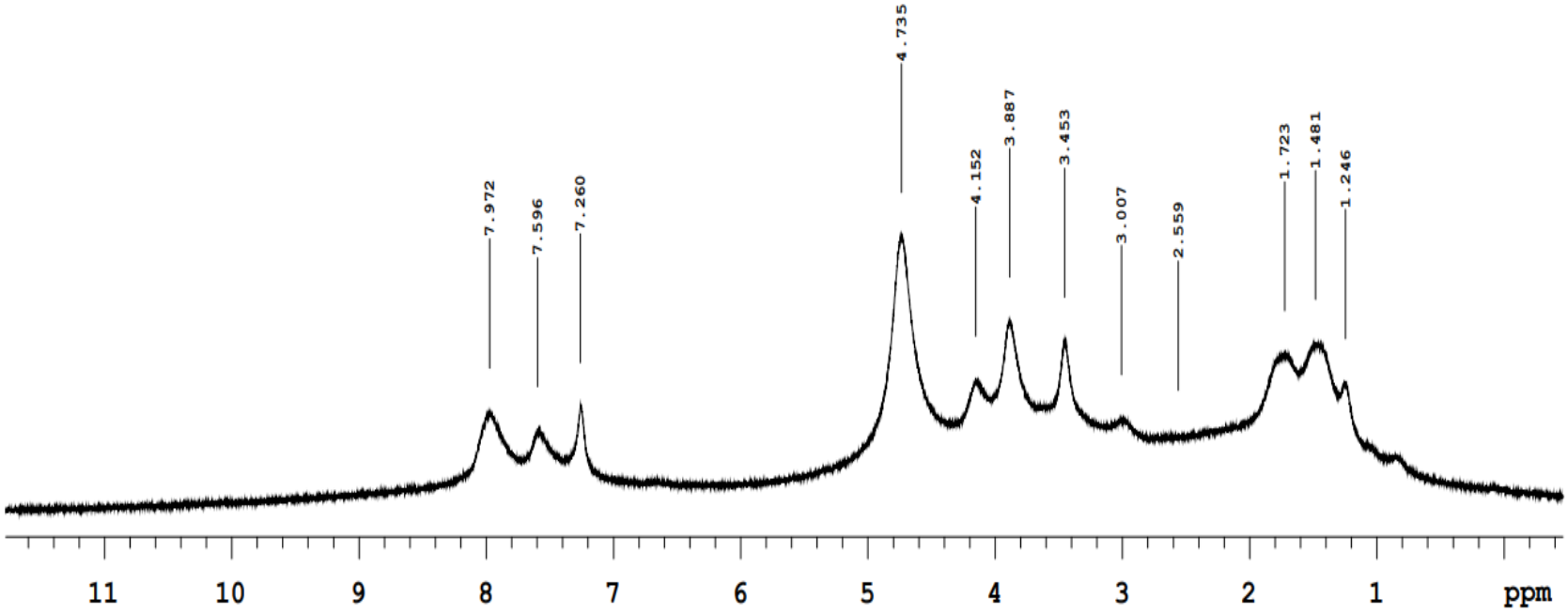

Au MPCs 11/C6; Oxime ether adduct: ^{13}C NMR ($CDCl_3$, 100 MHz)

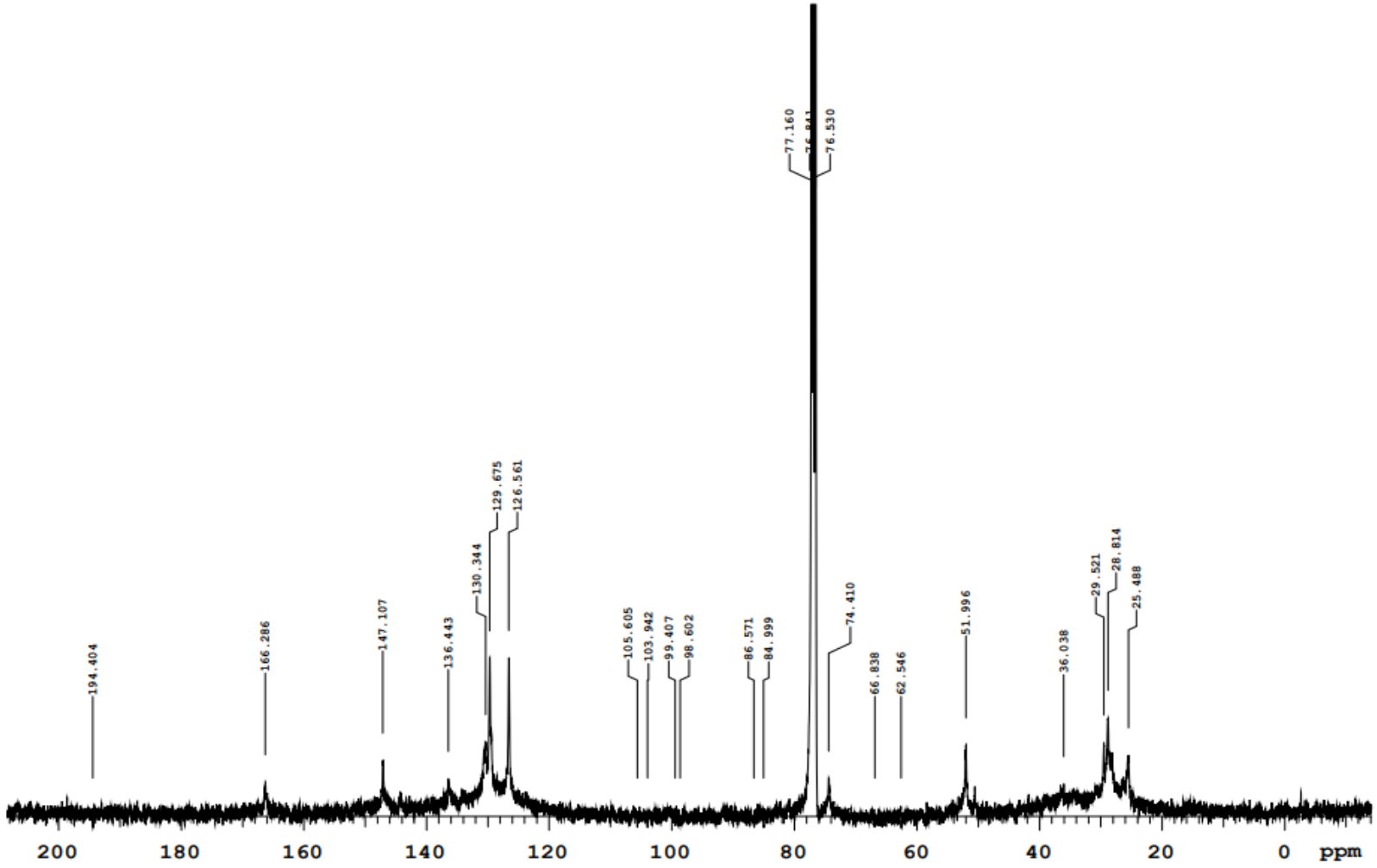

Au MPCs 9/C12; *N*-Boc protected Au MPCs: ^{1}H NMR ($CDCl_3$, 400 MHz)

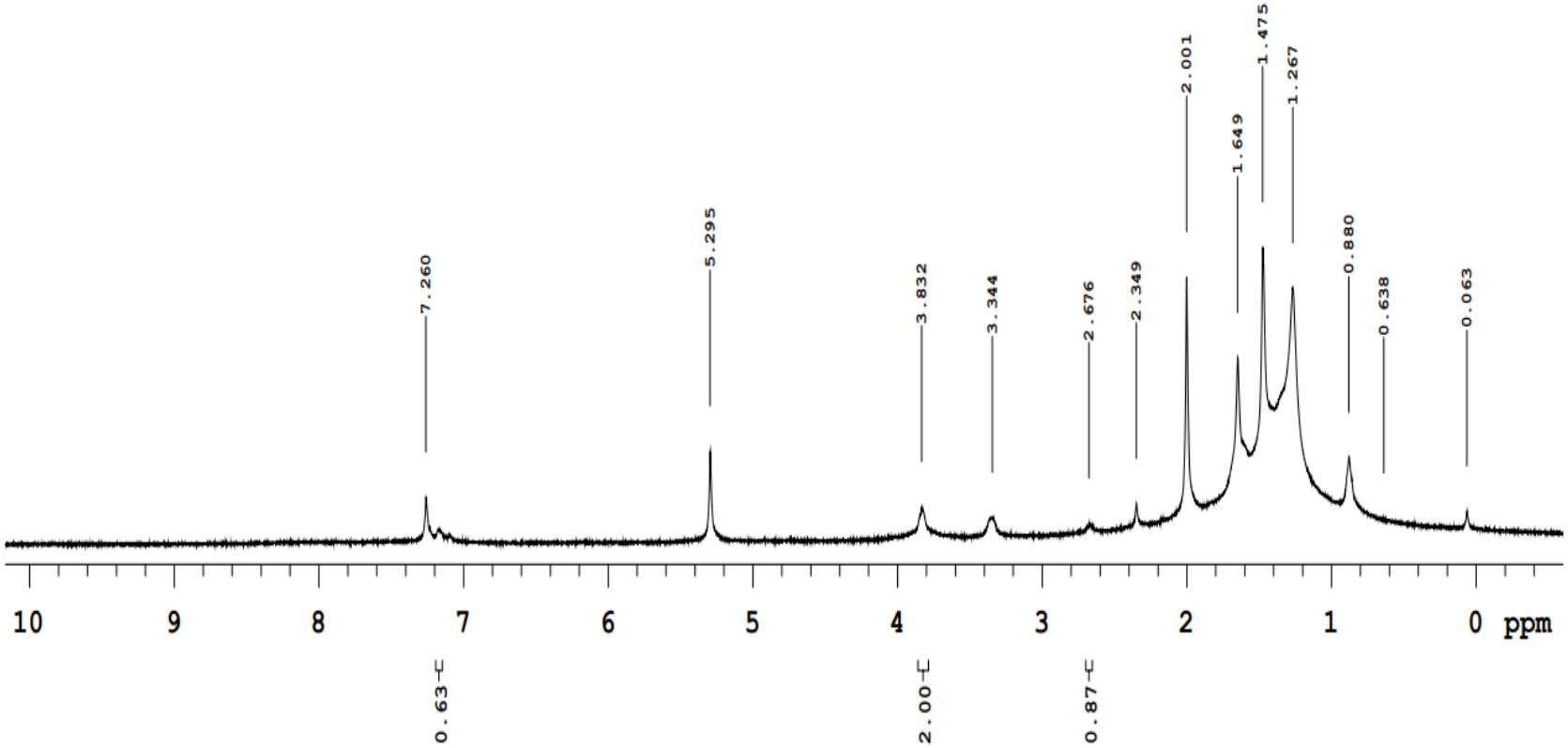

Au MPCs 10/C12 step a; Oxy-ammonium triflate salt of Au MPCs: ^{1}H NMR ($CDCl_3$, 400 MHz)

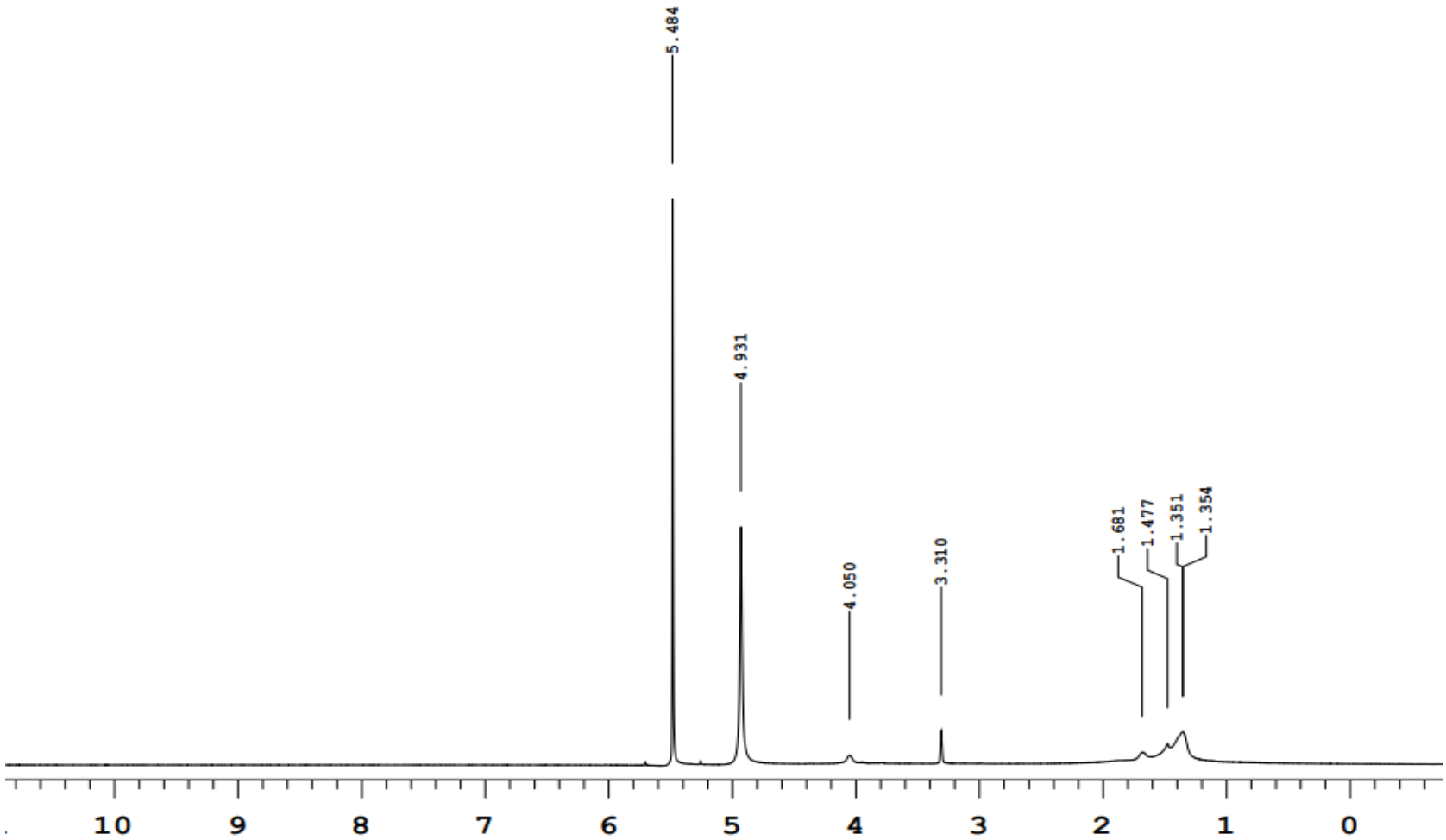

Au MPCs 10/C12 step b; Aminooxy Au MPCs ^{1}H NMR ($CDCl_3$, 400 MHz)

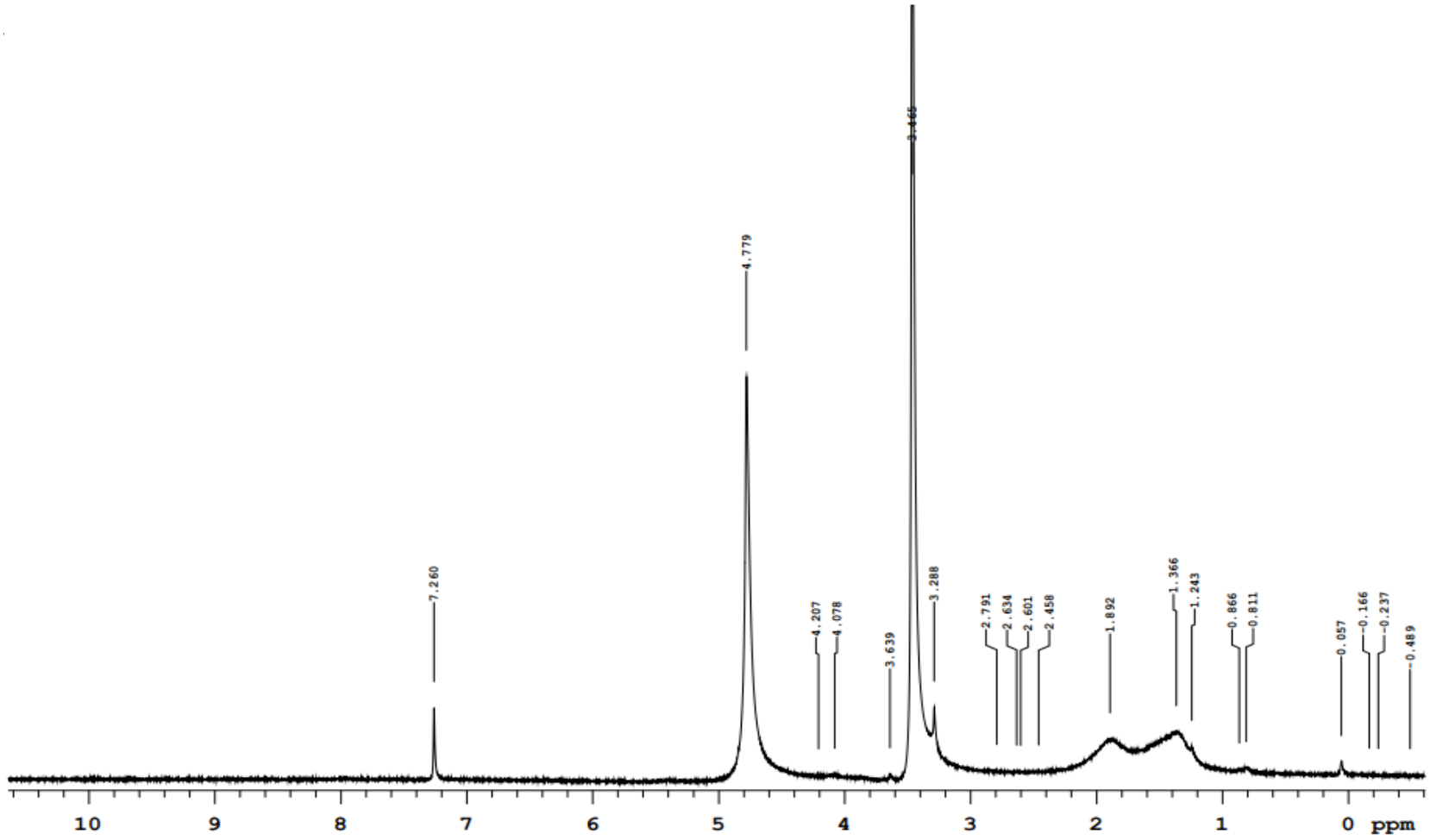

Au MPCs 11/C12; Oxime ether adduct: ^{1}H NMR ($CDCl_3$, 400 MHz)

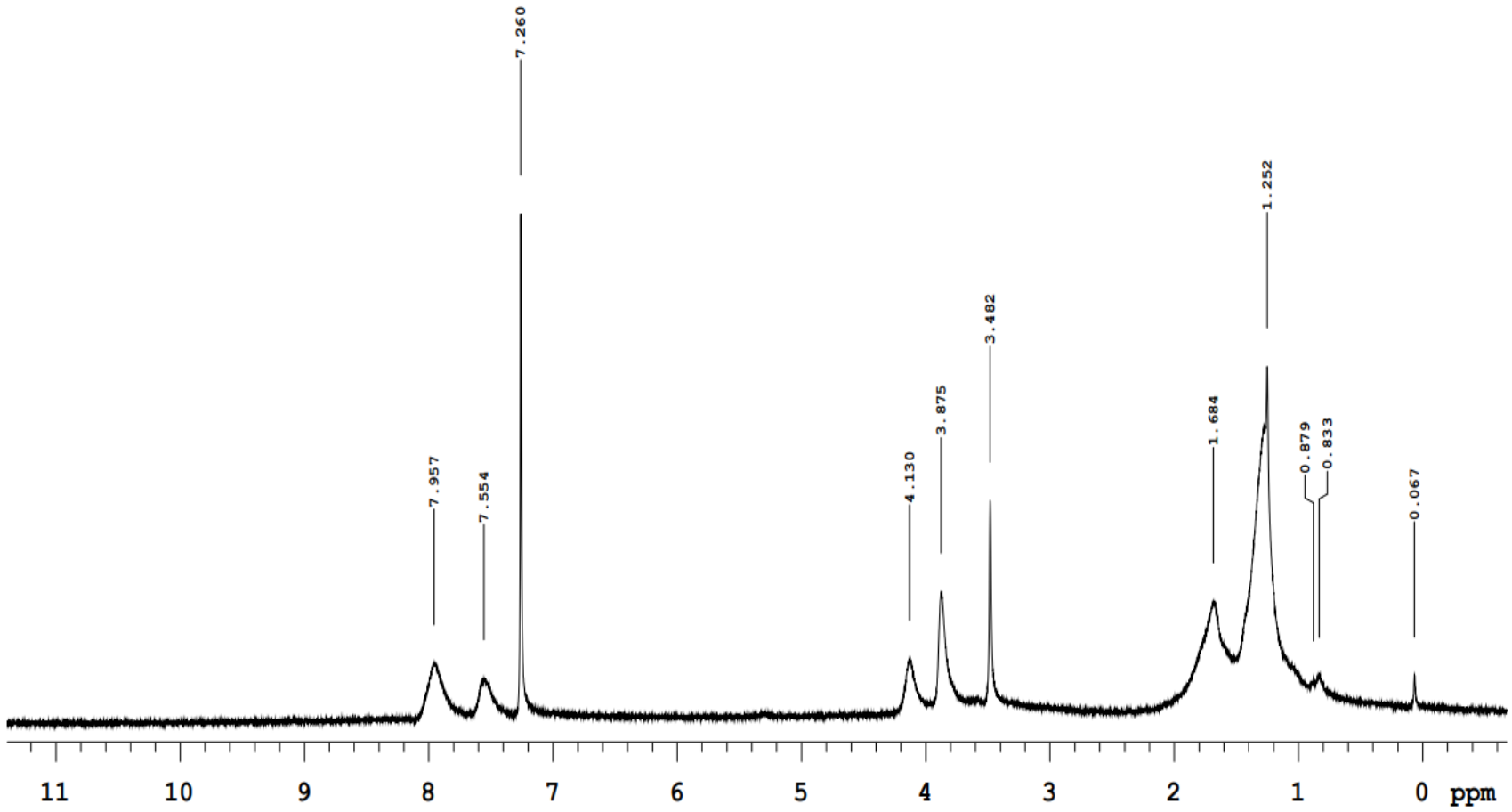

Au MPCs 11/C12; Oxime ether adduct: ^{13}C NMR ($CDCl_3$, 100 MHz)

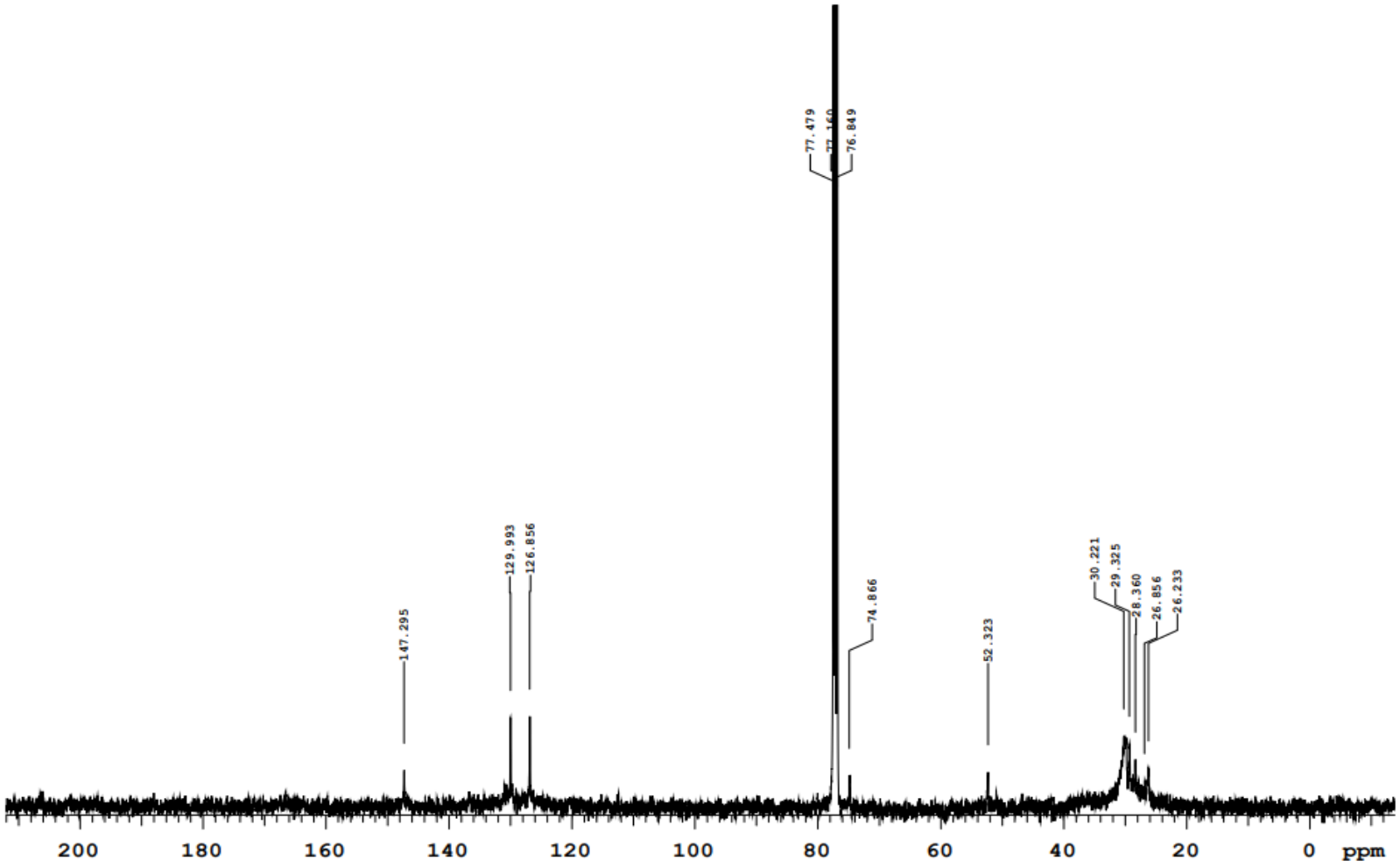

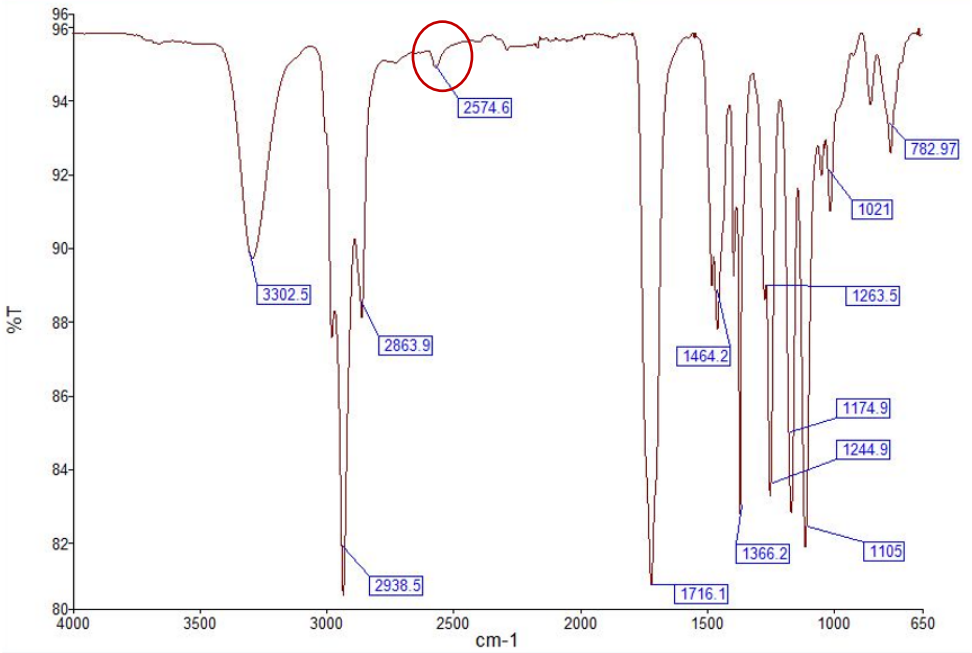

Figure 3.14. FT-IR spectrum of compound **4**. Circled absorption corresponds to RS-H stretching.

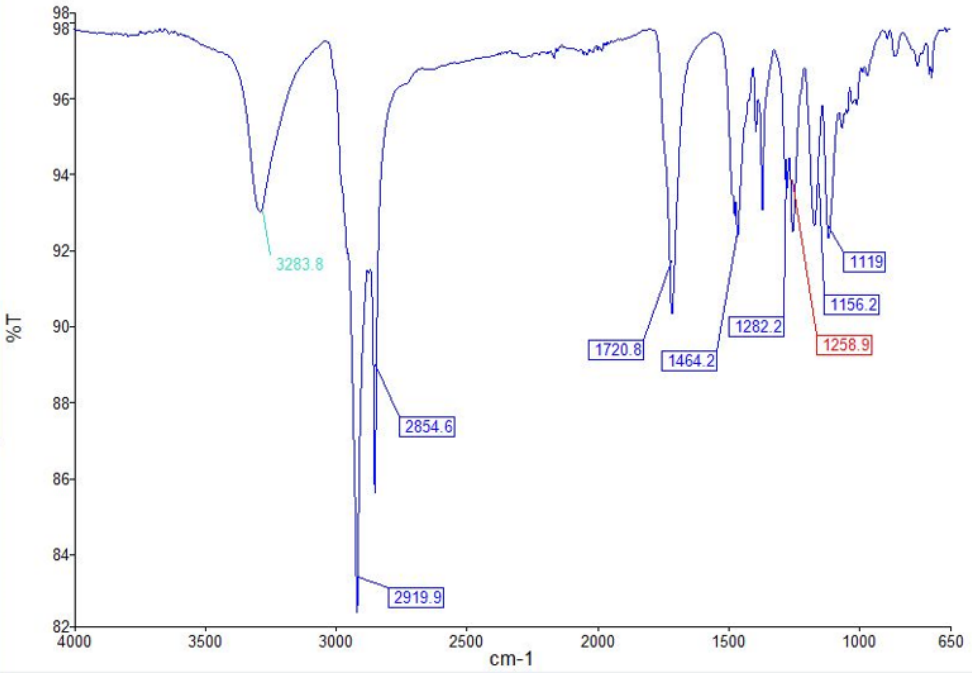

Figure 3.15. FT-IR spectrum of Au MPCs **9/C6**.

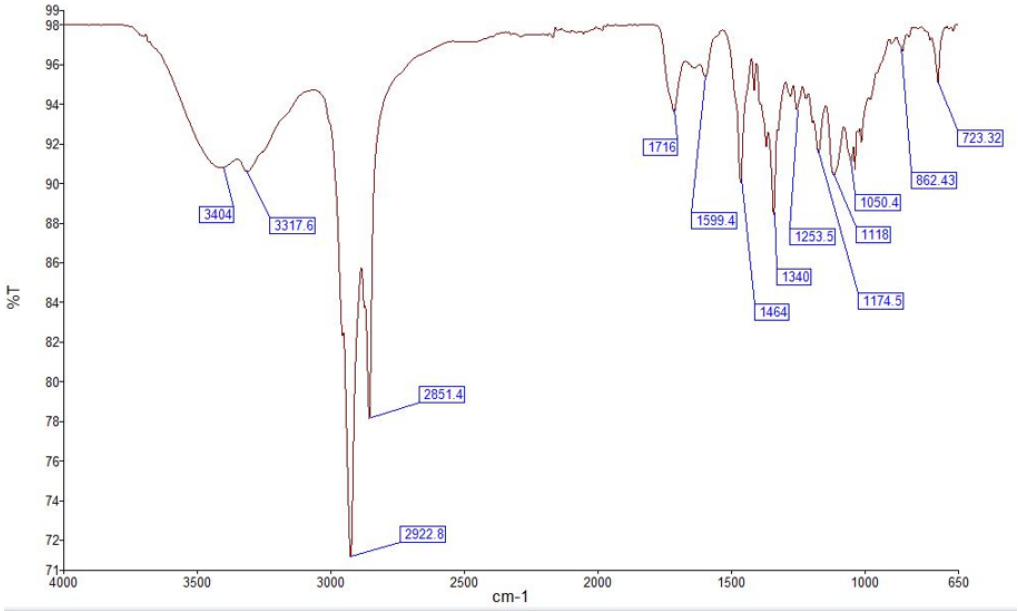

Figure 3.16. FT-IR spectrum of Au MPCs **10/C6**.

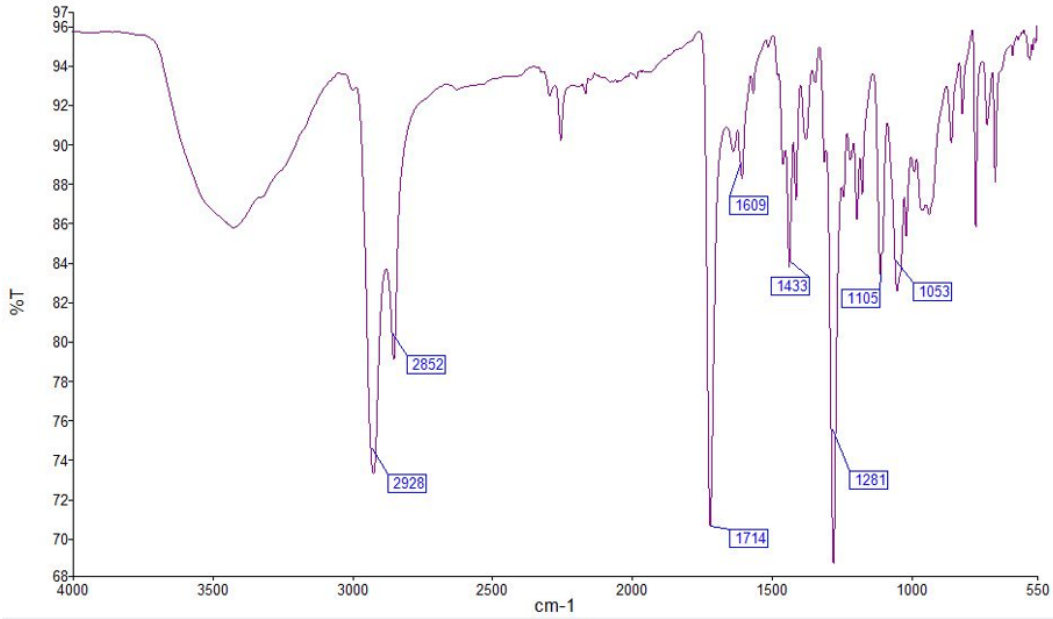

Figure 3.17. FT-IR spectrum of aryl ester Au MPCs **11/C6**.

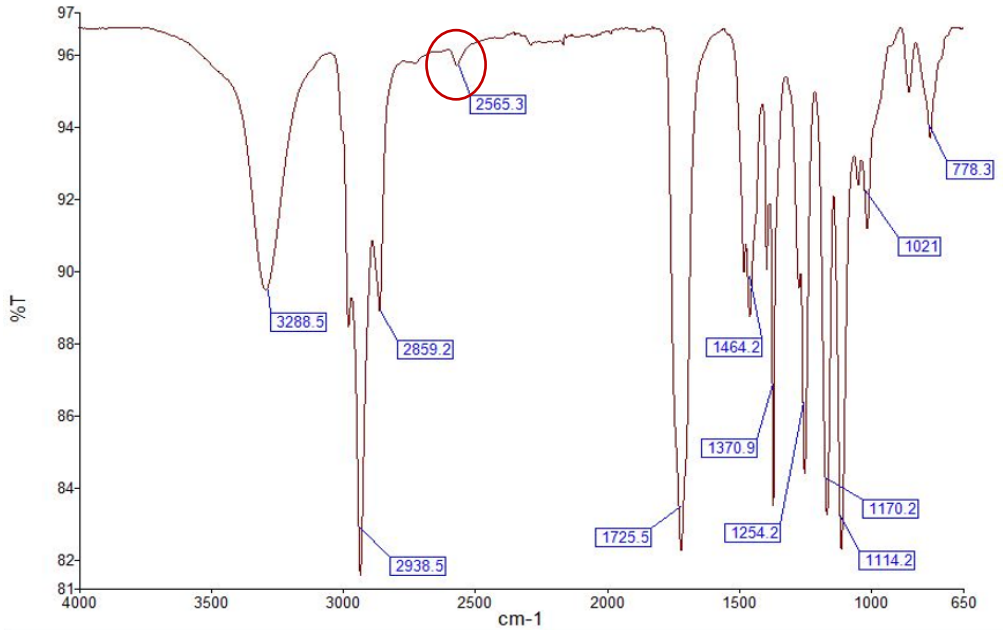

Figure 3.18. FT-IR spectrum of compound **8**. Circled absorption corresponds to RS-H stretching.

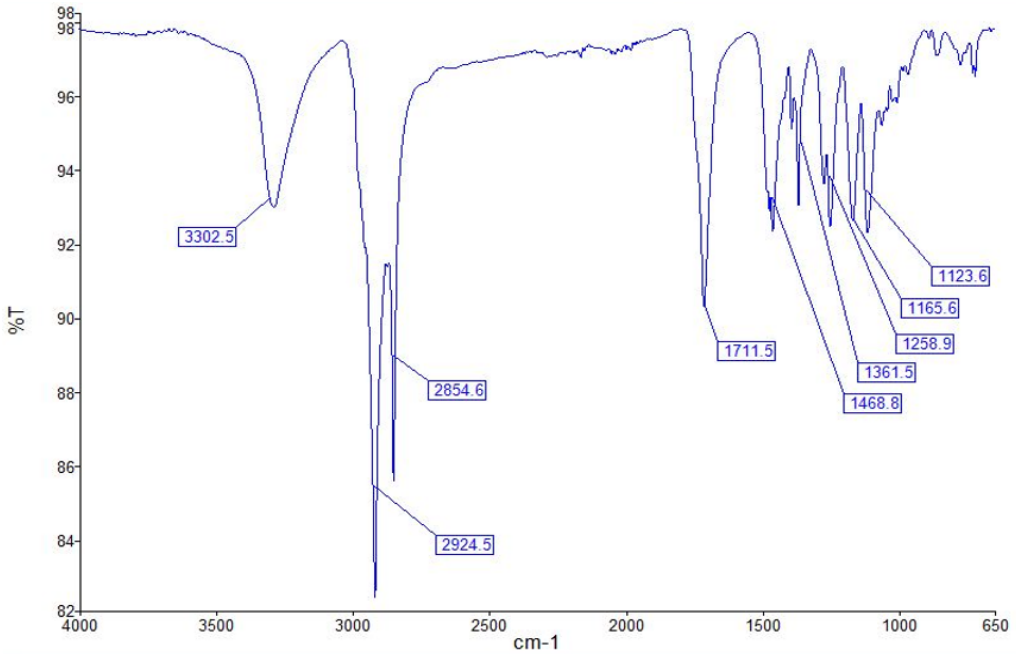

Figure 3.19. FT-IR spectrum of Au MPCs **9/C12**.

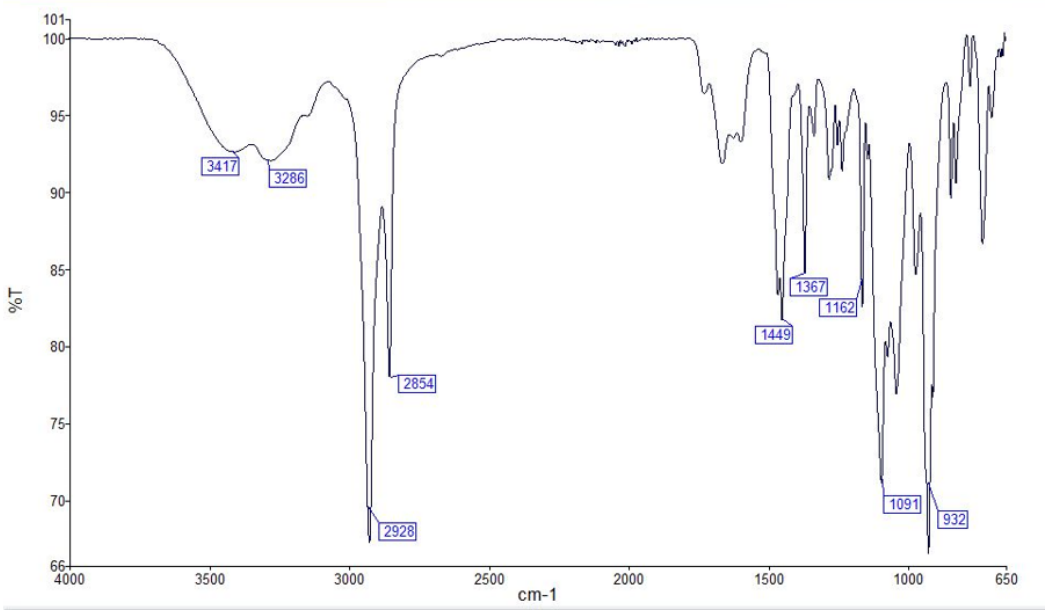

Figure 3.20. FT-IR spectrum of Au MPCs **10/C12**.

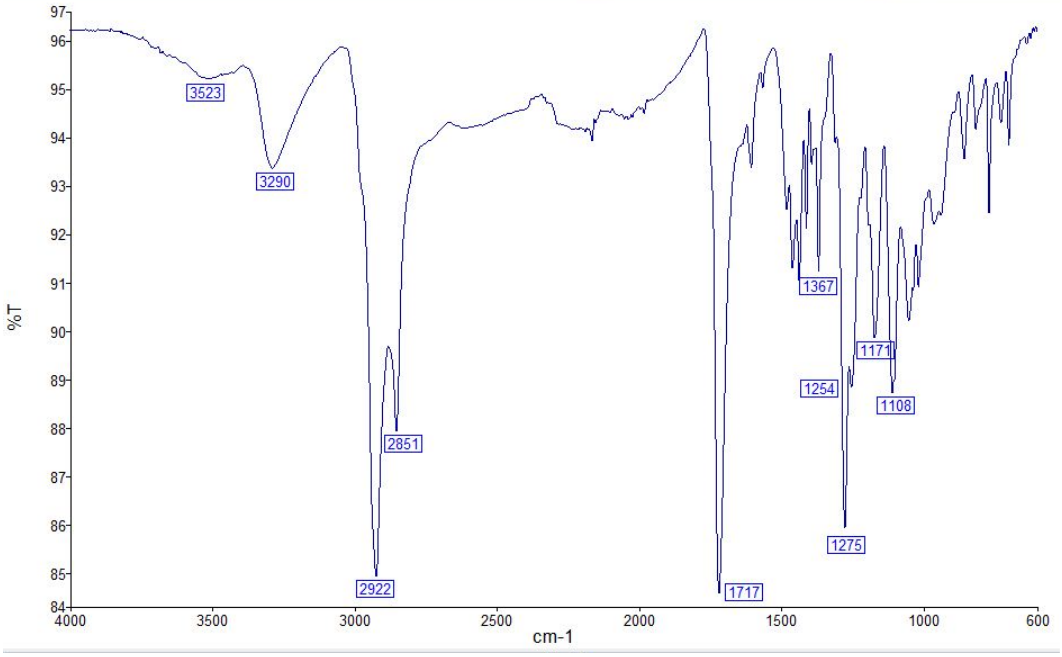

Figure 3.21. FT-IR spectrum of aryl ester Au MPCs **11/C12**.

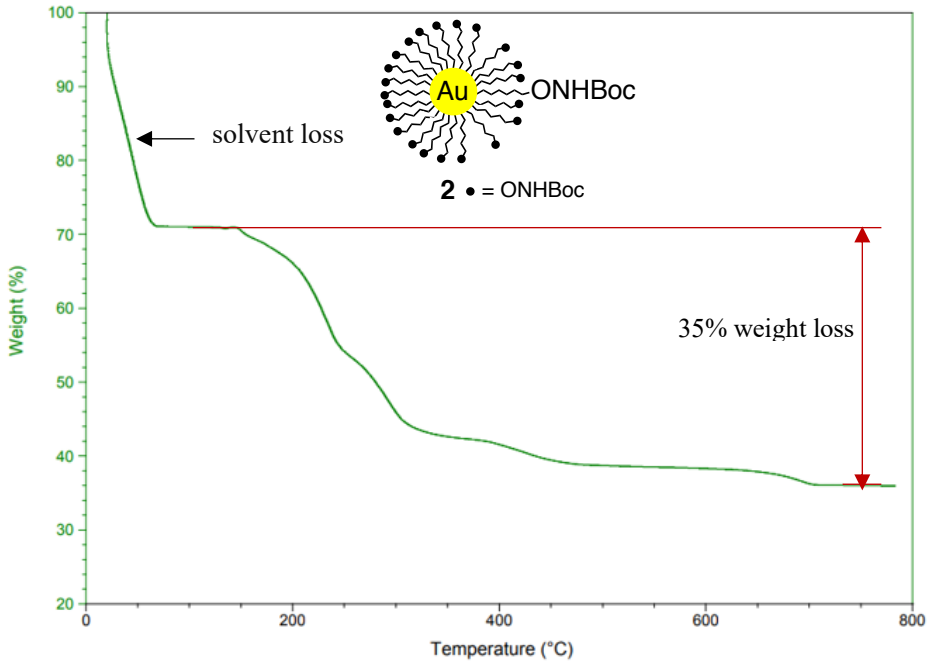

Figure 3.22. TGA of *N*-Boc Au MPCs **9/C6.**

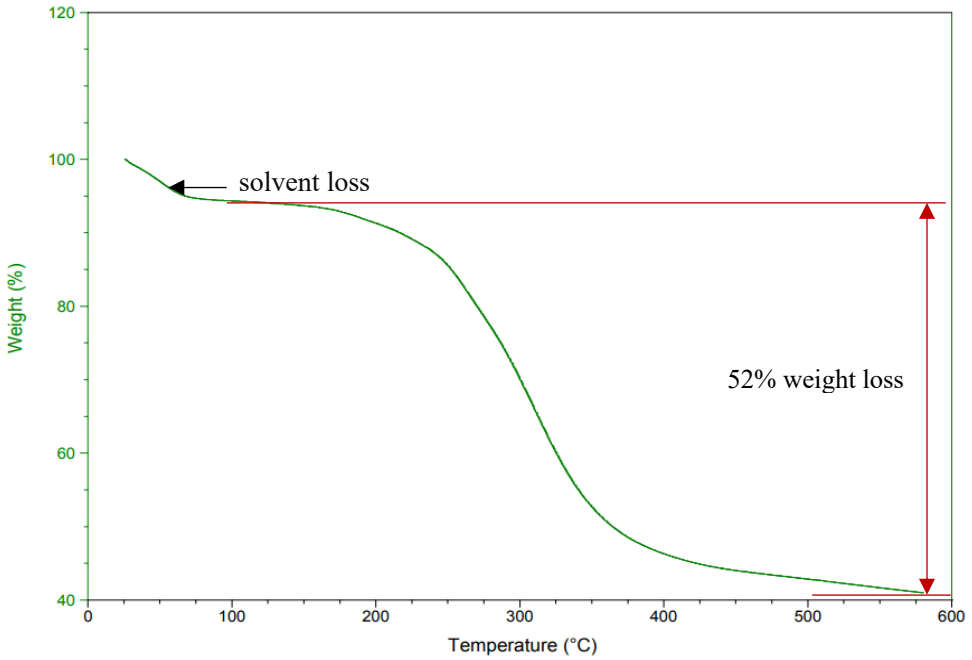

Figure 3.23. TGA of *N*-Boc Au MPCs **9/C12.**

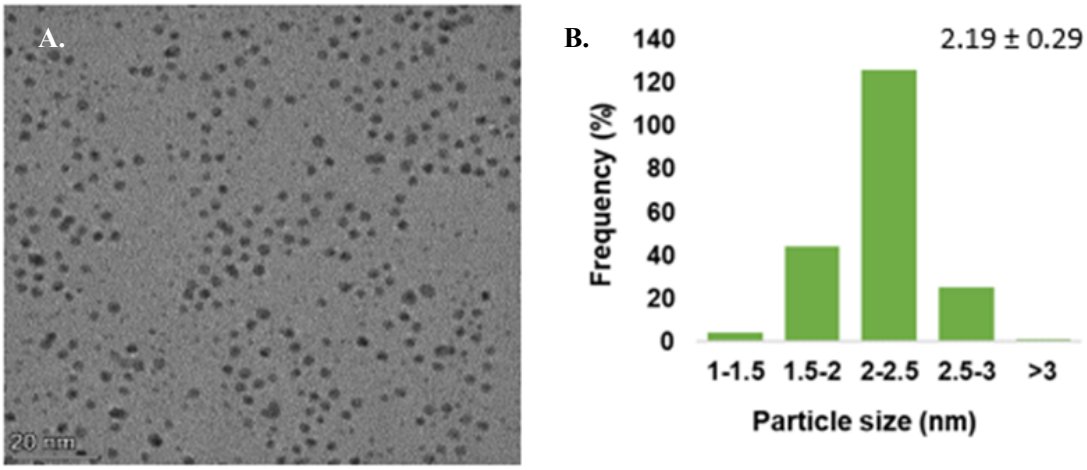

Figure 3.24. A. TEM image of *N*-Boc Au MPCs **9/C6** and **B.** histogram of the particle size distribution.

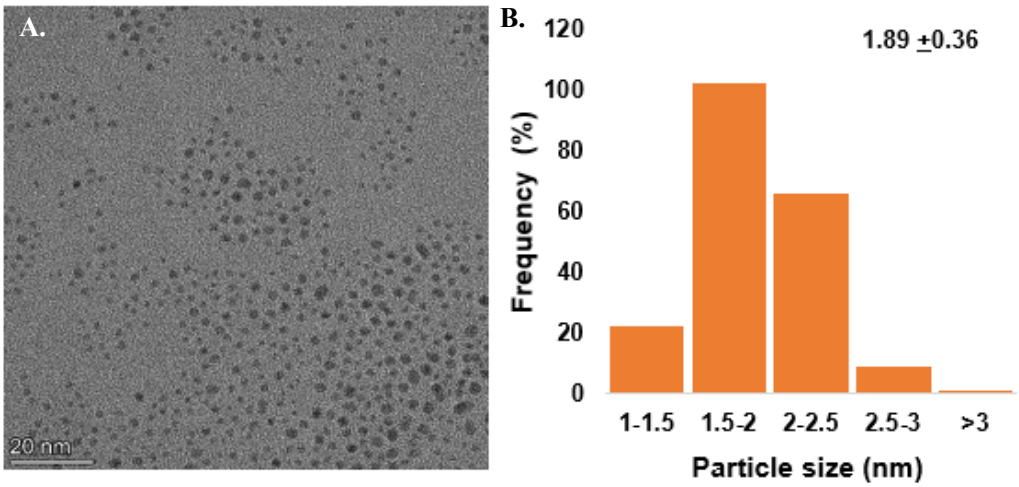

Figure 3.25. A. TEM image of *N*-Boc Au MPCs **9/C12** and **B.** histogram of the particle size distribution.

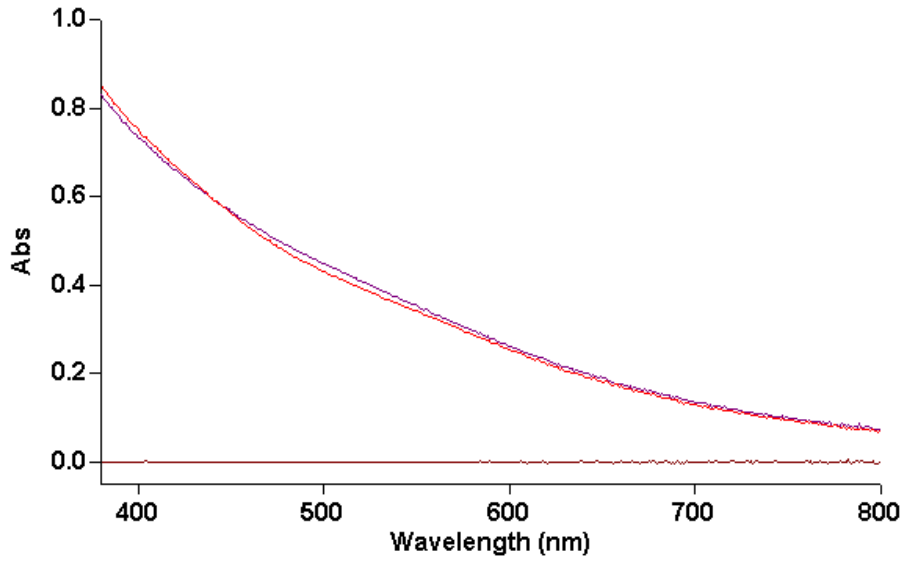

Figure 3.26. UV-Vis *N*-Boc Au MPCs **9/C6** (red line) and aryl ester Au MPCs **11/C6** (purple line). (CH_2Cl_2 – blank, 8.5 x 10^{-4} g ml^{-1} particle concentration)

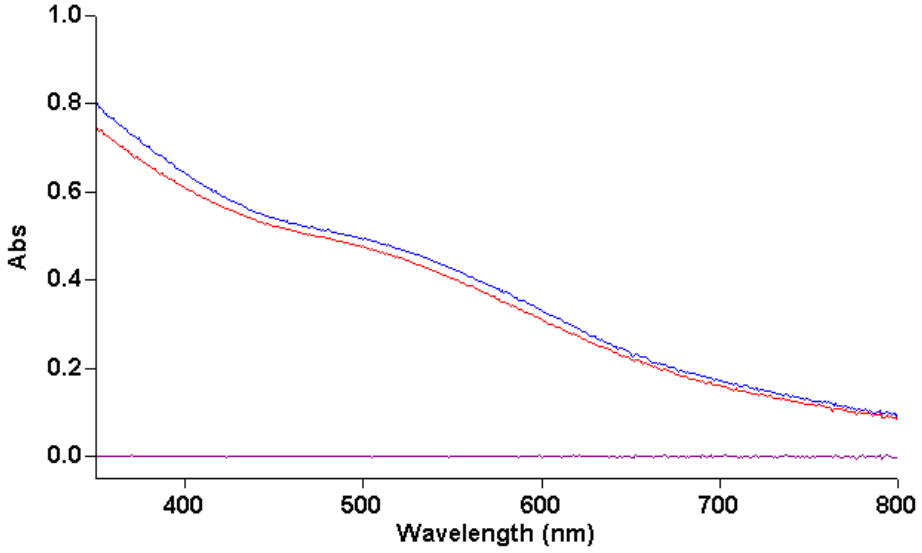

Figure 3.27. UV-Vis *N*-Boc Au MPCs **9/C12** (red line) and aryl ester Au MPCs **11/C12** (blue line). (CH_2Cl_2 – blank, 8.0 x 10^{-4} g ml^{-1} particle concentration)

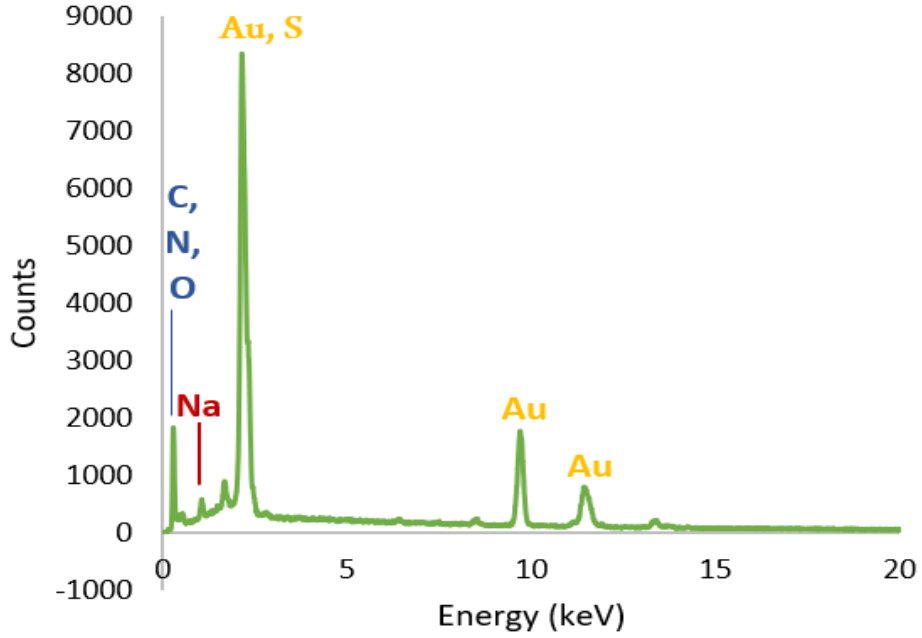

Figure 3.28. EDS spectrum of Au MPCs **12-Na**$^{+}$/C6.

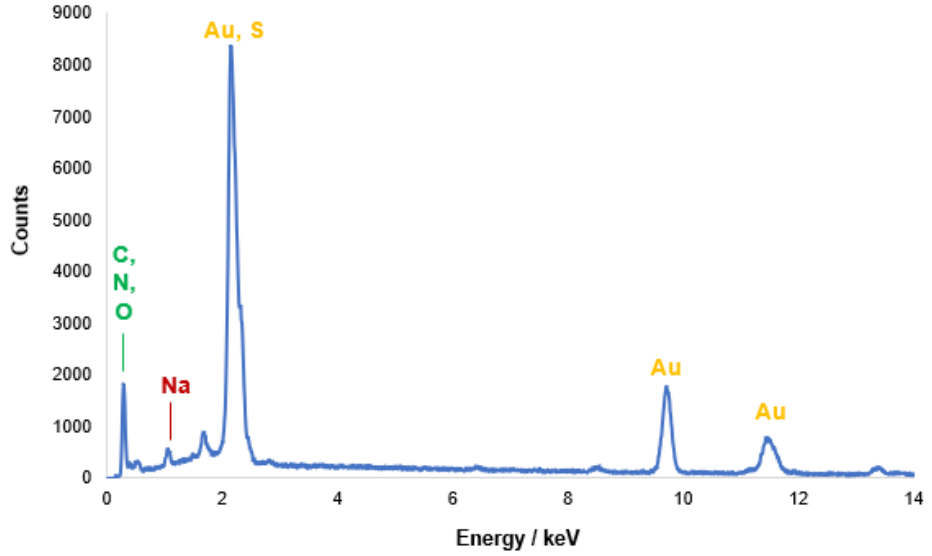

Figure 3.29. EDS spectrum of Au MPCs **12-Na**$^{+}$/C12.

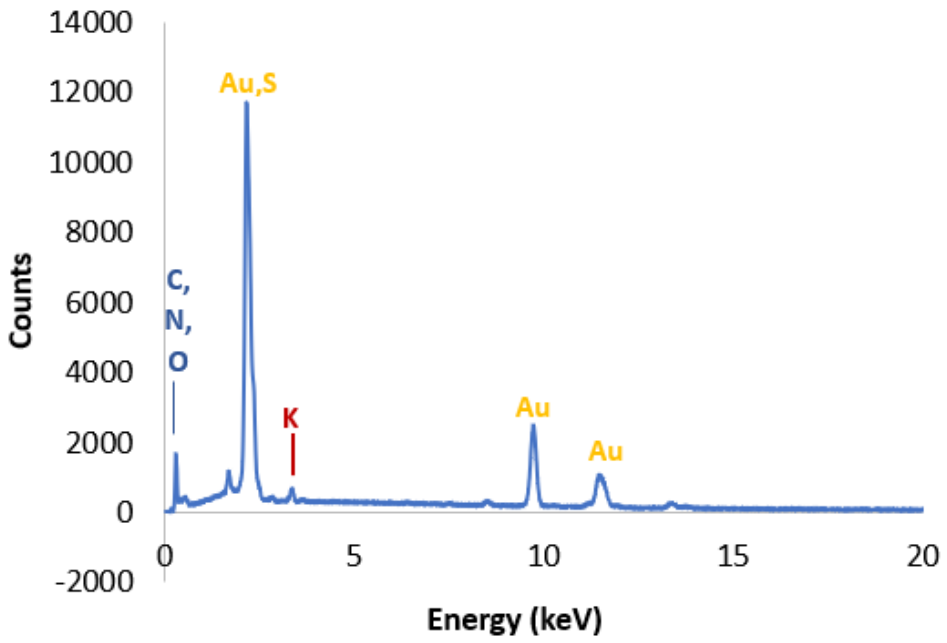

Figure 3.30. EDS spectrum of Au MPCs **12-K**$^{+}$/C6.

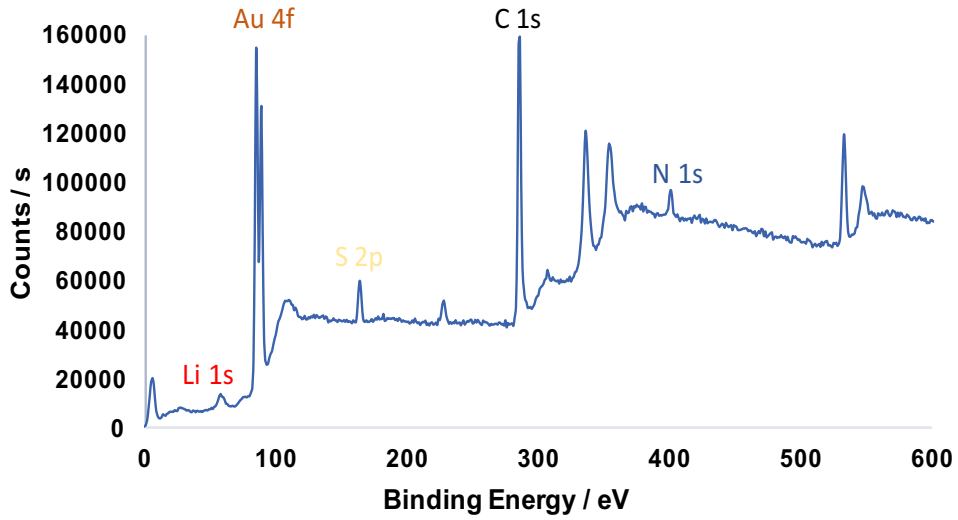

Figure 3.31 XPS survey spectrum of Au MPCs **12-Li**$^{+}$**/C6**.

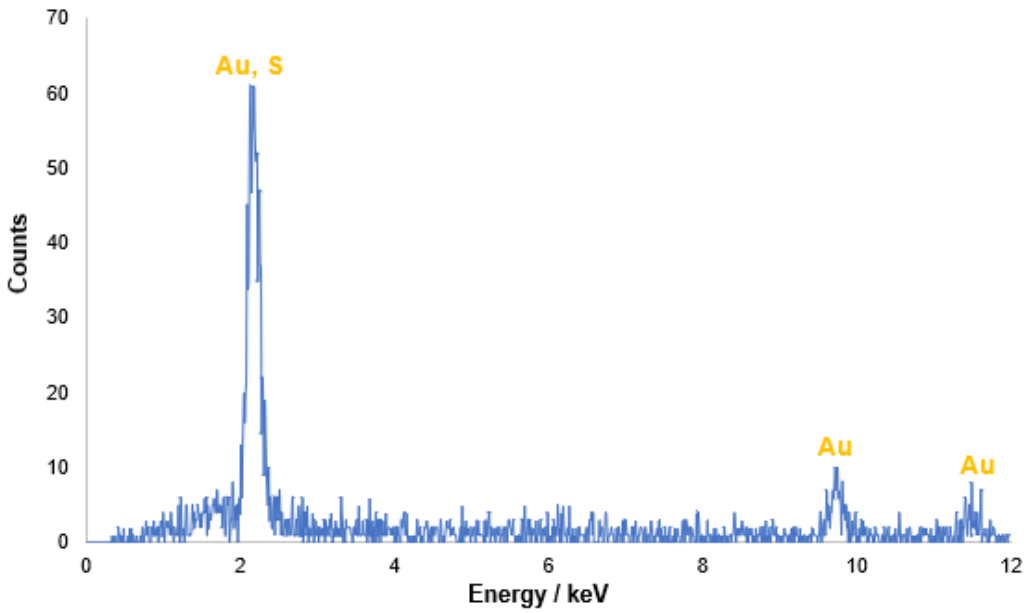

Figure 3.32. EDS spectrum of dodecanethiolate coated Au MPCs treated with 0.1 M KOH

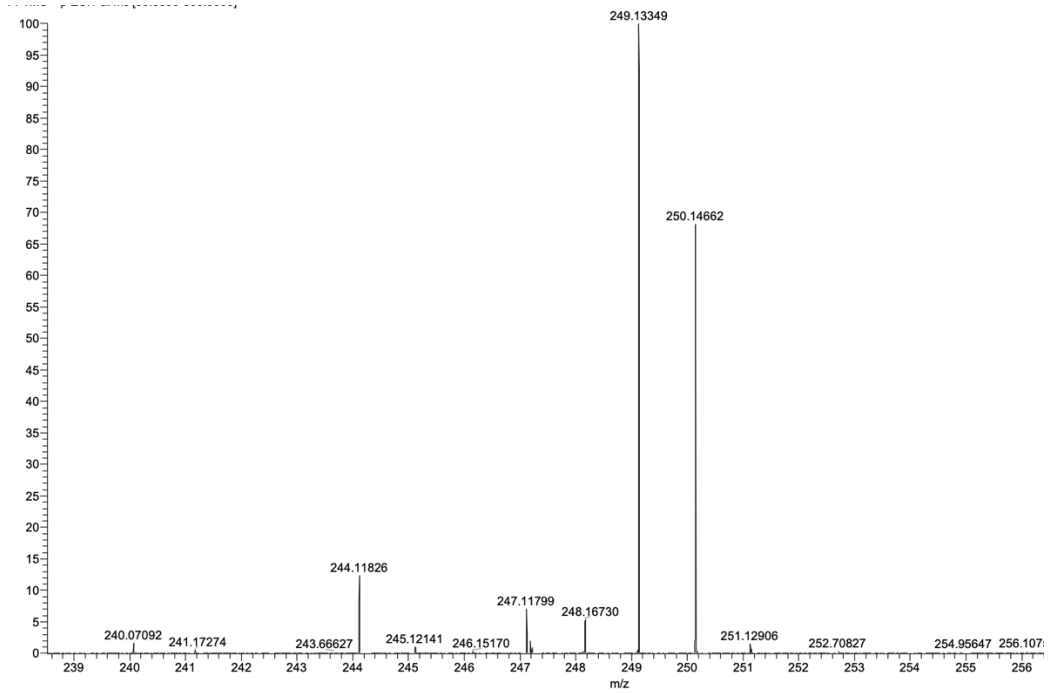

Figure 3.33. UHPLC-MS spectrum of compound **4.** (*N*-Boc protected hexane thiol)

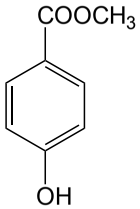

Compound **13**: ^{1}H NMR ($CDCl_3$, 400 MHz)

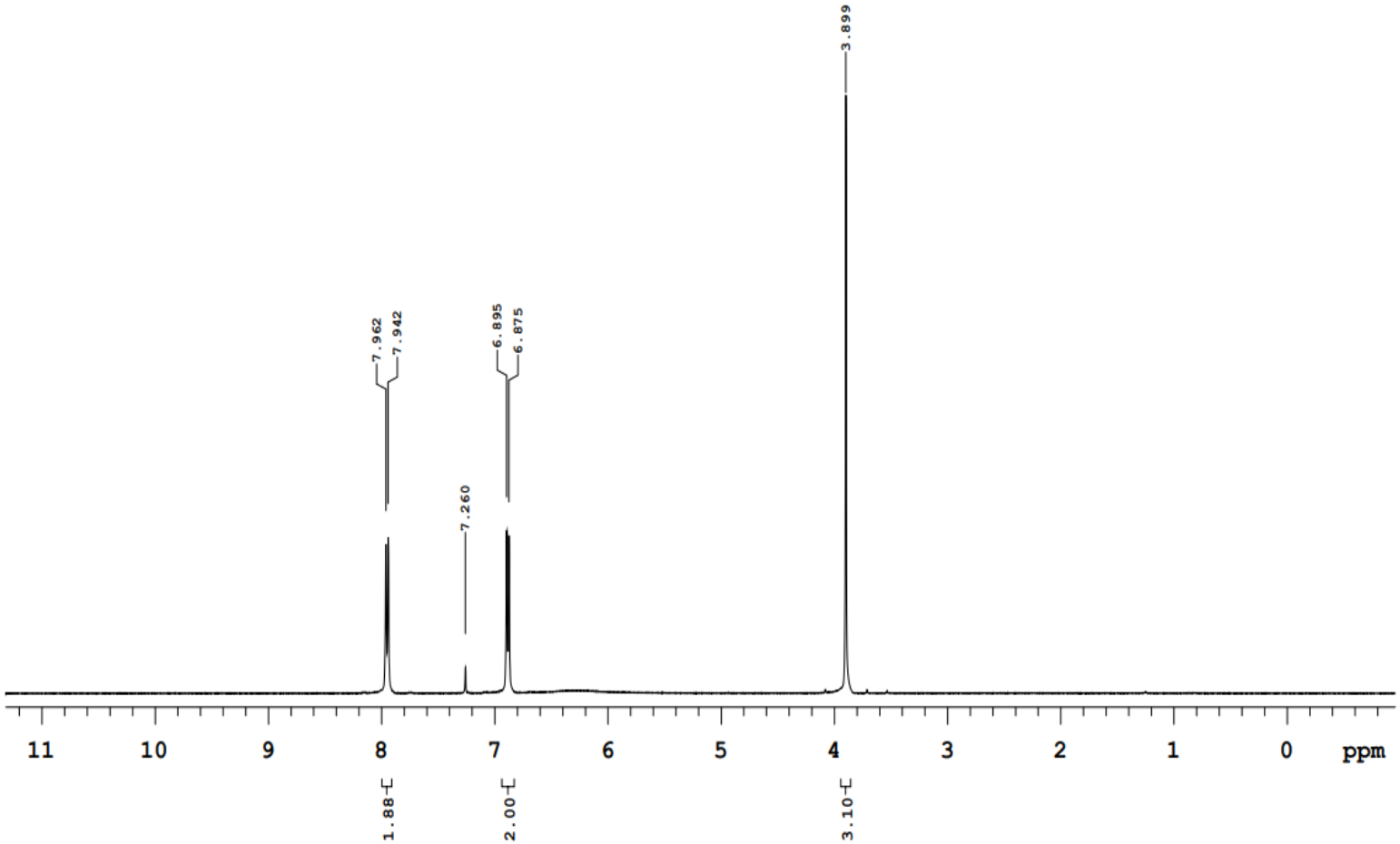

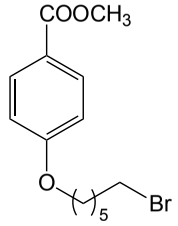

Compound **14**: ^{1}H NMR ($CDCl_3$, 400 MHz)

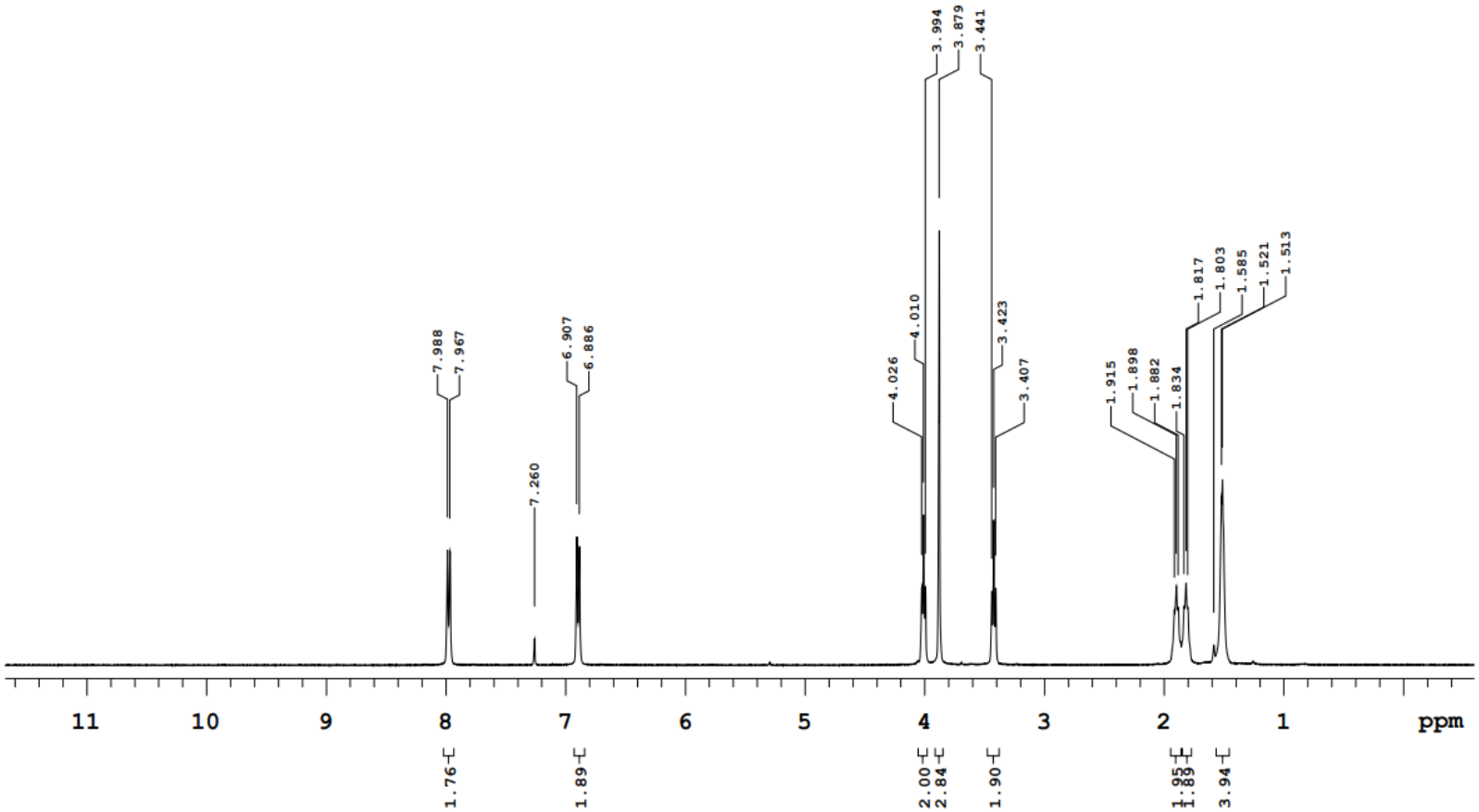

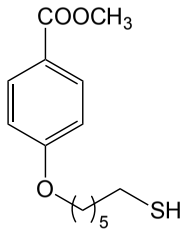

Compound **15**: ^{1}H NMR ($CDCl_3$, 400 MHz)

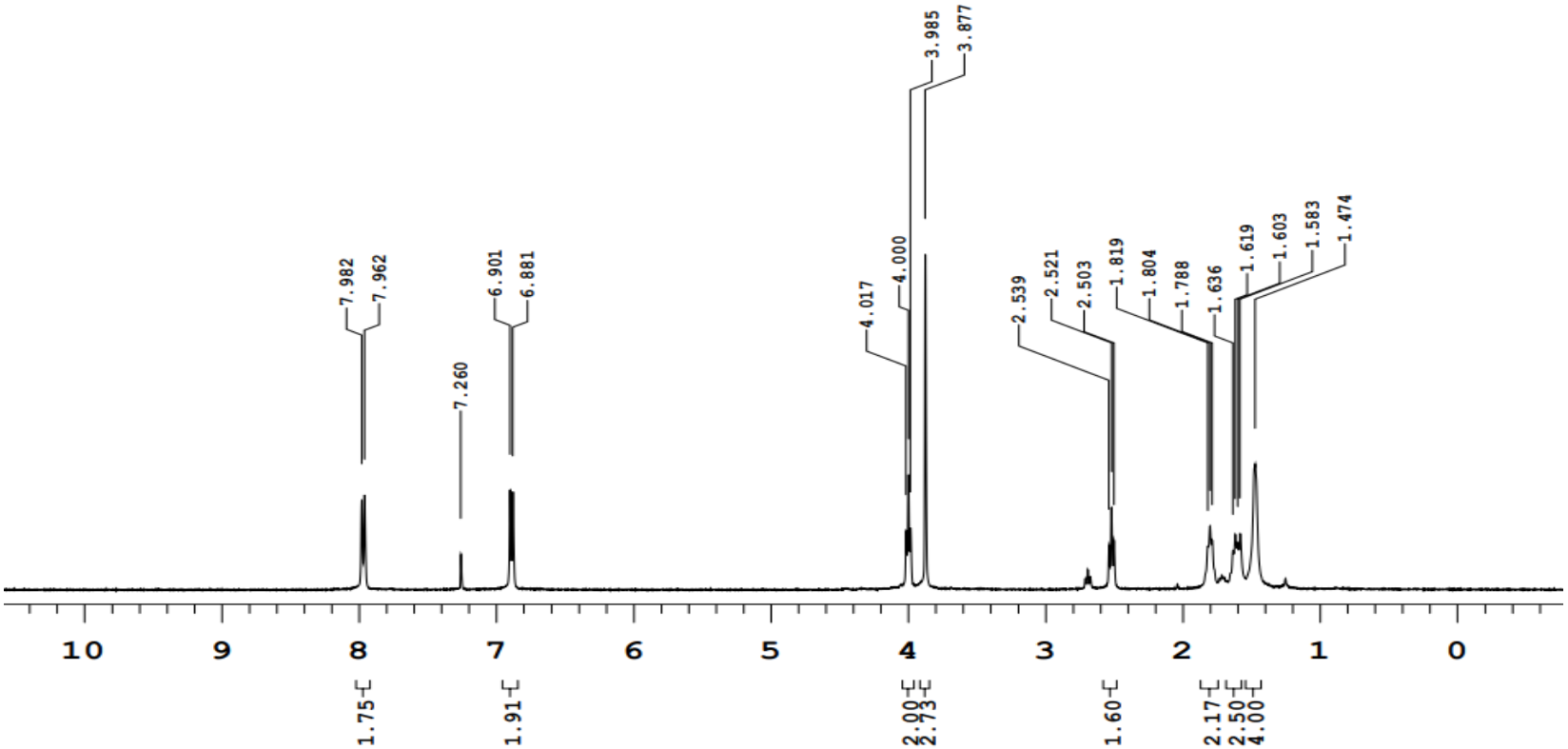

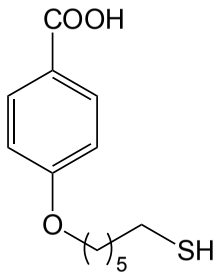

Compound **16**: ^{1}H NMR ($CDCl_3$, 400 MHz)

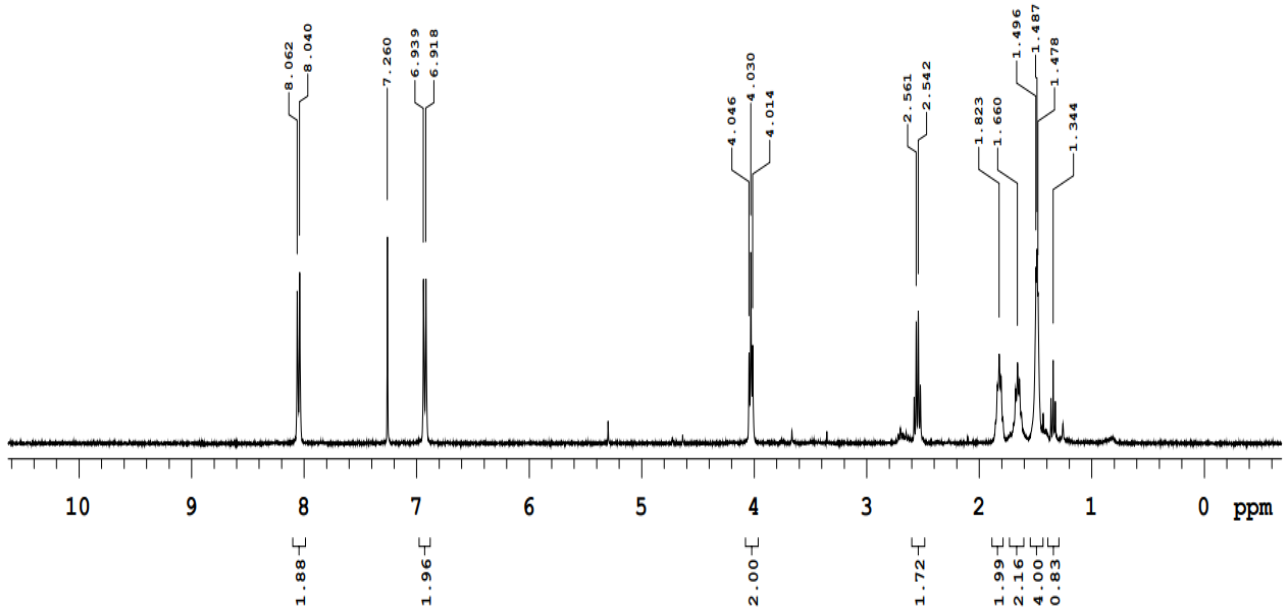

Compound **16**: ^{13}C NMR ($CDCl_3$, 400 MHz)

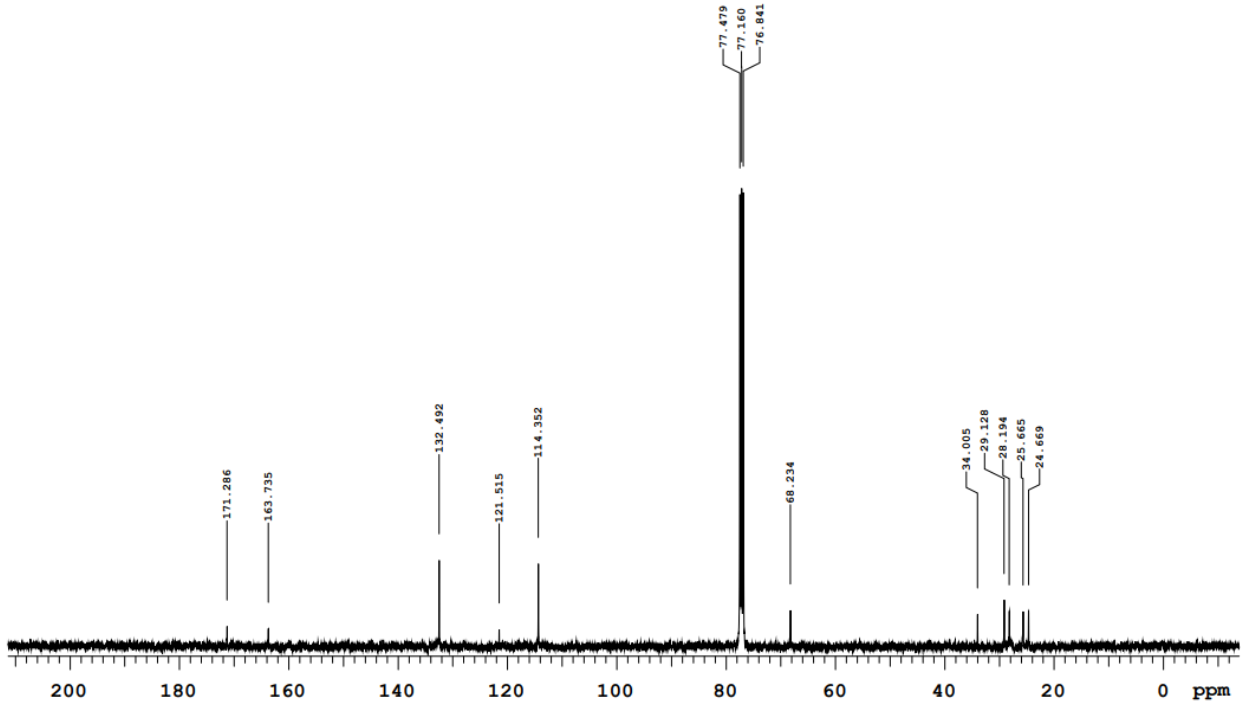

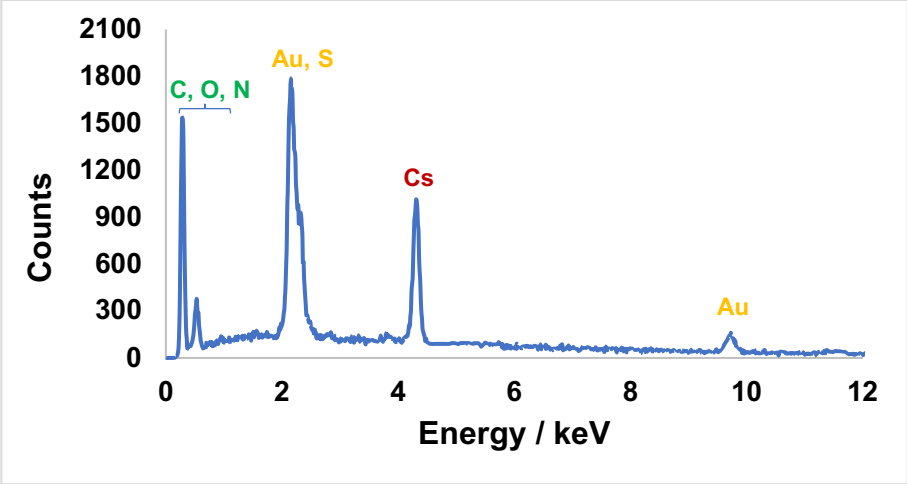

Figure 4.14. EDS spectrum of Au MPCs **12-Cs**$^{+}$/C6.

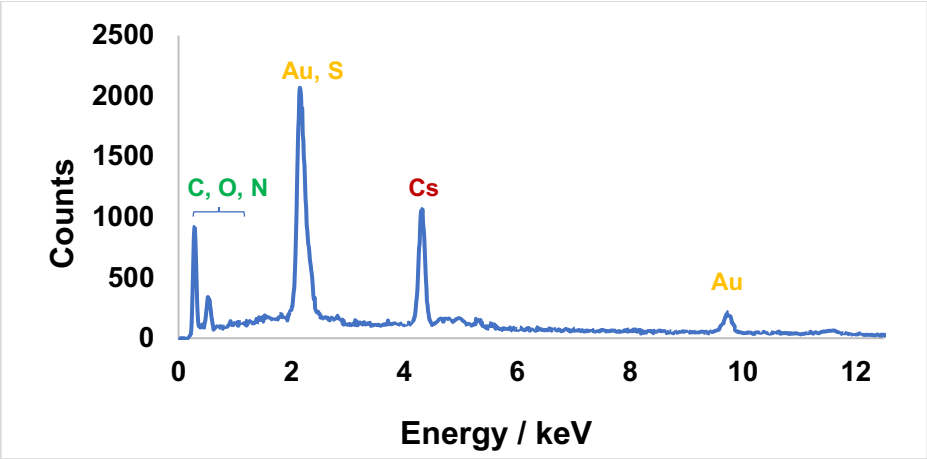

Figure 4.15. EDS spectrum of cesium ion-functionalized oxy benzoate Au MPCs **19**.

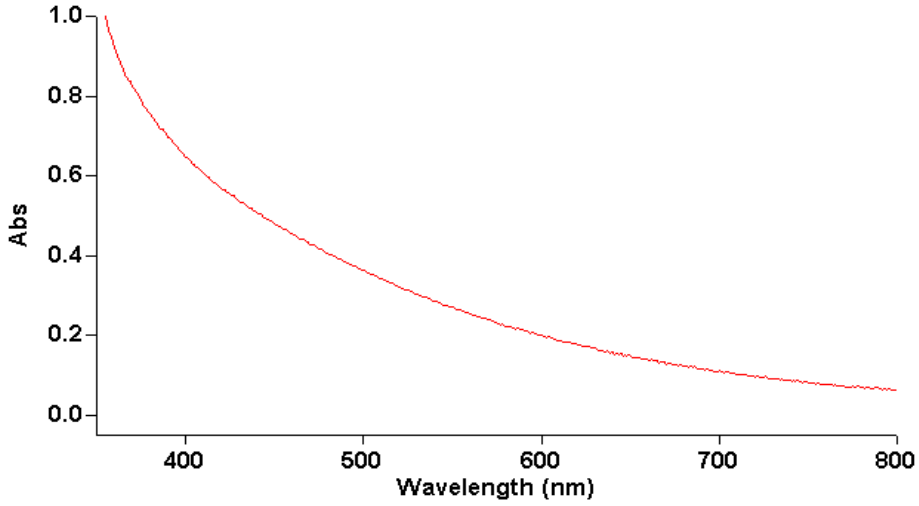

Figure 4.16. UV-Vis spectra of Au MPCs **12-Cs**$^{+}$/C6. (H_2O – blank, 9.7 x 10^{-4} g ml^{-1} particle concentration).

APPENDIX B

LIST OF PUBLICATIONS

B.1. List of Publications

B.2. Manuscript Title Pages

B.3. Copyright Permissions

B.1. List of Publications:

1. Xie, Z.; Raju, M. V. R.; Adhihetty, P. K.; Fu, X.; Nantz, M. H. Effect of Thiol Molecular Structure on the Sensitivity of Gold Nanoparticle-Based Chemiresistors toward Carbonyl Compounds. *Sensors* **2020**, *20(24)*, 7024. [Chapter 2]

2. Sibakoti, T. R.; Stinger, C. R.; Adhihetty, P. K.; Zamborini, F. P.; Nantz, M. H. Tunable Aminooxy-Functionalized Monolayer-Protected Gold Clusters for Nonpolar and Aqueous Oximation Reactions. *Particle & Particle Systems Characterization* **2019***, 36(7),* 1900093. [cited in Chapter 3]

3. Adhihetty, P. K.; Halder, S.; Jasinski, J. B.; Fu, X.-A.; Nantz, M. H. (2022). Harnessing the Cation-π Interactions of Metalated Gold Monolayer-Protected Clusters to Detect Aromatic Volatile Organic Compounds. (In Review *Talanata*) [Chapter 3]

4. Adhihetty, P. K.; Halder, S.; Fu, X.-A.; Nantz, M. H. (2022). Introducing a New Approach for Sensing Trichloroethylene (TCE) in Air. (Manuscript preparing) [Chapter 4]

B.2. Manuscript Title Pages

sensors

MDPI

Letter

Effect of Thiol Molecular Structure on the Sensitivity of Gold Nanoparticle-Based Chemiresistors toward Carbonyl Compounds

Zhenzhen Xie [1,†], Mandapati V. Ramakrishnam Raju [2,†], Prasadanie K. Adhihetty [3], Xiao-An Fu [1] and Michael H. Nantz [3,*]

1 Department of Chemical Engineering, University of Louisville, Louisville, KY 40208, USA; zhenzhen.xie@louisville.edu (Z.X.); xiaoan.fu@louisville.edu (X.-A.F.)
2 Department of Chemistry, University of Minnesota, Minneapolis, MN 55455, USA; smandapa@umn.edu
3 Department of Chemistry, University of Louisville, Louisville, KY 40208, USA; prasadi.adhihetty@louisville.edu
* Correspondence: michael.nantz@louisville.edu
† These authors contributed equally.

Received: 2 November 2020; Accepted: 4 December 2020; Published: 8 December 2020

check for updates

Abstract: Increasing both the sensitivity and selectivity of thiol-functionalized gold nanoparticle chemiresistors remains a challenging issue in the quest to develop real-time gas sensors. The effects of thiol molecular structure on such sensor properties are not well understood. This study investigates the effects of steric as well as electronic effects in a panel of substituted thiol-urea compounds on the sensing properties of thiolate monolayer-protected gold nanoparticle chemiresistors. Three series of urea-substituted thiols with different peripheral end groups were synthesized for the study and used to prepare gold nanoparticle-based chemiresistors. The responses of the prepared sensors to trace volatile analytes were significantly affected by the urea functional motifs. The largest response for sensing acetone among the three series was observed for the thiol-urea sensor featuring a tert-butyl end group. Furthermore, the ligands fitted with N, N′-dialkyl urea moieties exhibit a much larger response to carbonyl analytes than the more acidic urea series containing N-alkoxy-N′-alkyl urea and N, N′-dialkoxy urea groups with the same peripheral end groups. The results show that the peripheral molecular structure of thiolate-coated gold nanoparticles plays a critical role in sensing target analytes.

Keywords: molecular selectivity; carbonyl sensing; urea; alkoxy urea; bis(alkoxy) urea

---

1. Introduction

Monolayer protected gold clusters (MPCs) have attracted wide attention due to their unique electronic, electrochemical and biochemical properties [1–5] as well as their broad applications in materials science and biomedical diagnostics, where MPCs have been used as sensors [6–8], catalysts [9,10], biological imaging agents [11], and in studies on optics [12]. Many materials, including metal oxide nanoparticles and nanowires [13–17] and composites [18–20], semiconductors [21], carbon nanotubes [22,23], and polymer nanofibers [24,25], have been studied for the detection of a variety of volatile organic compounds (VOCs). However, these materials have encountered several challenges, including poor sensitivity and selectivity, lack of reproducibility, and large power consumption. Continued development of MPCs fitted with novel surface functionality has the potential to overcome these problems. The important characteristics of MPCs include operation at ambient temperature, variability in functional thiolate ligands, and the radial nature of the ligand monolayer arising from the faceted surface of the metal core [3,26,27].

Particle & Particle Systems Characterization
www.particle-journal.com

Tunable Aminooxy-Functionalized Monolayer-Protected Gold Clusters for Nonpolar and Aqueous Oximation Reactions

Tirtha R. Sibakoti, Colton R. Stinger, Prasadanie K. Adhihetty, Francis P. Zamborini, and Michael H. Nantz**

Aminooxy (–ONH$_2$) groups are well known for their chemoselective reactions with carbonyl compounds, specifically aldehydes and ketones. The versatility of aminooxy chemistry has proven to be an attractive feature that continues to stimulate new applications. This work describes application of aminooxy click chemistry on the surface of gold nanoparticles. A trifunctional amine-containing aminooxy alkane thiol ligand for use in the functionalization of gold monolayer-protected clusters (Au MPCs) is presented. Diethanolamine is readily transformed into an organic-soluble aminooxy thiol (AOT) ligand using a short synthetic path. The synthesized AOT ligand is coated on ≤2-nm-diameter hexanethiolate-(C$_6$S)-capped Au MPCs using a ligand-exchange protocol to afford organic-soluble AOT/C$_6$S (1:1 ratio) Au mixed monolayer-protected clusters (MMPCs). The synthesis of these Au(C$_6$S)(AOT) MMPCs and representative oximation reactions with various types of aldehyde-containing molecules is described, highlighting the ease and versatility of the chemistry and how amine protonation can be used to switch solubility characteristics.

1. Introduction

Aminooxy-based click[1] chemistry has proven to be a versatile means of ligation, as evidenced by broad application in the fields of material science, biology, biochemistry, analytical chemistry, and nanoscience.[2–4] Aminooxy groups (RONH$_2$) react chemoselectively with aldehydes and ketones under mild conditions to form highly stable oxime ether adducts. The chemoselectivity of the oximation reaction has stimulated efforts to exploit oxime ether formation not only as a straightforward, efficient coupling approach, but also as a means for identification and quantification of carbonyls in complex mixtures. For example, aminooxy derivatization reagents have been used to selectively tag and/or sequester carbonyl substrates in biological extracts,[5,6] environmental air and water,[7,8] exhaled breath,[9,10] and even living organisms.[11]

As the usefulness of oximation chemistry has become apparent, several approaches exploiting nanoparticles fitted with aminooxy surfaces have been reported.[12–14] The ease of functionalization of gold surfaces, clusters, and nanoparticles with a monolayer of thiol- or dithiol-containing molecules[15,16] has guided some efforts toward developing and applying thiol ligands containing aminooxy functionality.[17] For example, Nagahori et al. prepared aminooxy-functionalized gold nanoparticles (NPs) for capture and enrichment of glycosphingolipid (GSL)-generated aldehydes as a means to characterize whole GSLs in living cells.[18] Thygesen et al. developed a bifunctional thiol–aminooxy oligo(ethylene glycol) ligand for preparation of aminooxy-conjugated gold glycanoparticles.[19] Maynard and co-workers synthesized a photocaged aminooxy alkane thiol for conjugating carbonyl substrates to gold surfaces following photolysis.[20] Given the rapidly growing interests in using gold monolayer-protected clusters (Au MPCs) and Au NPs for applications in catalysis,[21–23] sensing volatile organic compounds,[24,25] analyzing small molecule mixtures using NP-mediated Raman and laser desorption/ionization spectroscopy,[26] and drug delivery,[27,28] the development of aminooxy-functionalized thiol ligands to improve ease of carbonyl ligation as well as to provide flexibility in addressing solubility and adduct loading considerations would enable new applications. With this in mind, we designed a trifunctional amine-containing aminooxy thiol (**AOT**) ligand for use in monolayer functionalization of hexanethiolate (C$_6$S)-protected Au MPCs to produce Au(C$_6$S)(**AOT**) mixed monolayer protected clusters (MMPCs) (**Figure 1**). Incorporation of the amine group was motivated by several considerations: (a) The solubility properties of the cluster may be adjusted by control over the amine protonation or alkylation state; (b) the amine moiety enables convenient structural bifurcation to increase pendant aminooxy density; and (c) an ammonium NH could potentially accelerate oximation reactions.[29] Herein, we describe the synthesis of such a trifunctional thiol ligand and its use in the formation of Au MMPCs. We also present our findings on representative

T. R. Sibakoti, C. R. Stinger, P. K. Adhihetty, Prof. F. P. Zamborini, Prof. M. H. Nantz
Department of Chemistry
University of Louisville
Louisville, KY 40208, USA
E-mail: f.zamborini@louisville.edu; michael.nantz@louisville.edu
The ORCID identification number(s) for the author(s) of this article can be found under https://doi.org/10.1002/ppsc.201900093.

DOI: 10.1002/ppsc.201900093

B.3. Copyright Permissions

Crystal Structure of a CsF–Uranyl–Salen Complex. An Unusual Cesium–Chlorine Coordination

Author: Massimo Cametti, Maija Nissinen, Antonella Dalla Cort, et al

Publication: Inorganic Chemistry

Publisher: American Chemical Society

Date: Aug 1, 2006

Copyright © 2006, American Chemical Society

PERMISSION/LICENSE IS GRANTED FOR YOUR ORDER AT NO CHARGE

This type of permission/license, instead of the standard Terms and Conditions, is sent to you because no fee is being charged for your order. Please note the following:

- Permission is granted for your request in both print and electronic formats, and translations.
- If figures and/or tables were requested, they may be adapted or used in part.
- Please print this page for your records and send a copy of it to your publisher/graduate school.
- Appropriate credit for the requested material should be given as follows: "Reprinted (adapted) with permission from {COMPLETE REFERENCE CITATION}. Copyright {YEAR} American Chemical Society." Insert appropriate information in place of the capitalized words.
- One-time permission is granted only for the use specified in your RightsLink request. No additional uses are granted (such as derivative works or other editions). For any uses, please submit a new request.

If credit is given to another source for the material you requested from RightsLink, permission must be obtained from that source.

Enhanced Sorption of Trichloroethene by Smectite Clay Exchanged with Cs

Author: Vaneet Aggarwal, Hui Li, Stephen A. Boyd, et al

Publication: Environmental Science & Technology

Publisher: American Chemical Society

Date: Feb 1, 2006

Copyright © 2006, American Chemical Society

PERMISSION/LICENSE IS GRANTED FOR YOUR ORDER AT NO CHARGE

This type of permission/license, instead of the standard Terms and Conditions, is sent to you because no fee is being charged for your order. Please note the following:

- Permission is granted for your request in both print and electronic formats, and translations.
- If figures and/or tables were requested, they may be adapted or used in part.
- Please print this page for your records and send a copy of it to your publisher/graduate school.
- Appropriate credit for the requested material should be given as follows: "Reprinted (adapted) with permission from {COMPLETE REFERENCE CITATION}. Copyright {YEAR} American Chemical Society." Insert appropriate information in place of the capitalized words.
- One-time permission is granted only for the use specified in your RightsLink request. No additional uses are granted (such as derivative works or other editions). For any uses, please submit a new request.

If credit is given to another source for the material you requested from RightsLink, permission must be obtained from that source.

Unusual Ligand Coordination for Cesium

Author: Jeffrey C. Bryan, Konstantinos Kavallieratos, Richard A. Sachleben

Publication: Inorganic Chemistry

Publisher: American Chemical Society

Date: Apr 1, 2000

Role of Hydrogen Bonding in Determining the Crystal Structures of the Adducts between Acetone and Urea Derivatives

Author: Menahem Kaftory, Moshe Kapon, Mark Botoshansky

Publication: Chemistry of Materials

Publisher: American Chemical Society

Date: Aug 1, 1994

A Surprising Host–Guest Relationship between 1,2-Dichloroethane and the Cesium Complex of Tetrabenzo-24-crown-8

Author: Tatiana G. Levitskaia, Jeffrey C. Bryan, Richard A. Sachleben, et al

Publication: Journal of the American Chemical Society

Publisher: American Chemical Society

Date: Feb 1, 2000

Colloidal Metal–Insulator–Metal Ensemble Chemiresistor Sensor

Author: Hank Wohltjen, Arthur W. Snow

Publication: Analytical Chemistry

Publisher: American Chemical Society

Date: Jul 1, 1998

Dual-Chemiresistor GC Detector Employing Monolayer-Protected Metal Nanocluster Interfaces

Author: Qing-Yun Cai, Edward T. Zellers

Publication: Analytical Chemistry

Publisher: American Chemical Society

Date: Jul 1, 2002

Chemiresistive Sensing of Volatile Organic Compounds with Films of Surfactant-Stabilized Gold and Gold−Silver Alloy Nanoparticles

Author: Francisco J. Ibañez, Francis P. Zamborini

Publication: ACS Nano

Publisher: American Chemical Society

Date: Aug 1, 2008

Thank you for your order!

Dear Dr. Prasadanie Adhihetty,

Thank you for placing your order through Copyright Clearance Center's RightsLink® service.

Order Summary

Licensee:	University of Louisville
Order Date:	Apr 20, 2022
Order Number:	5293201030588
Publication:	Sensors and Actuators B: Chemical
Title:	Nanoparticle-structured sensing array materials and pattern recognition for VOC detection
Type of Use:	reuse in a thesis/dissertation
Order Ref:	N/A
Order Total:	0.00 USD

View or print complete details of your order and the publisher's terms and conditions.

Sincerely,

Copyright Clearance Center

This Agreement between University of Louisville -- Prasadanie Adhihetty ("You") and Elsevier ("Elsevier") consists of your license details and the terms and conditions provided by Elsevier and Copyright Clearance Center.

License Number	5293201030588
License date	Apr 20, 2022
Licensed Content Publisher	Elsevier
Licensed Content Publication	Sensors and Actuators B: Chemical
Licensed Content Title	Nanoparticle-structured sensing array materials and pattern recognition for VOC detection
Licensed Content Author	Li Han,Xiajing Shi,Wendy Wu,F. Louis Kirk,Jin Luo,Lingyan Wang,Derrick Mott,Lisa Cousineau,Stephanie I-Im Lim,Susan Lu,Chuan-Jian Zhong
Licensed Content Date	Apr 29, 2005
Licensed Content Volume	106
Licensed Content Issue	1

APPENDIX C

LIST OF ABBREVIATIONS

BTEX	–	benzene, toluene, ethylbenzene, xylenes
DCM	–	dichloromethane
DMSO	–	dimethylsulfoxide
EtOAc	–	ethylacetate
EDS	–	Energy Dispersive X-Ray Spectroscopy
EPA	–	Environmental Protection Agency
g	–	gram
h	–	hour
HCl	–	hydrogen chloride
HRMS	–	High Resolution Mass Spectroscopy
IDE	–	Interdigitated Electrodes
IR	–	Infra Red
LoD	–	Limit of Detection
MHz	–	mega hertz
M	–	molar
min	–	minute
mL	–	mililiter
mmol	–	millimole
MEMS	–	Micro Electromechanical System

MPCs – Monolayer Protected Clusters

MMPCs – Mixed Monolayer Protected Clusters

MS – Mass Spectroscopy

MUA – 11-mercaptoundecanoic acid

NPs – nanoparticles

NMR – Nuclear Magnetic Resonance

NaCl – sodium chloride

$NaHCO_3$ – sodium bicarbonate

OSHA – Occupational Safety and Health Administration

PEL – Permissible Exposure Limit

ppm – parts per million

ppb – parts per billion

ppt – parts per trillion

PCE – perchloroethylene

SAM – Self Assembled Monolayer

tert – tertiary

TLC – Thin Layer Chromatography

TFA – trifluoroacetic acid

TEM – Transmission Electron Microscope

TGA – Thermo Gravimetric Analysis

TCE – trichloroethylene

THF – tetrahydrofuran

UV – Ultraviolet

VOCs – Volatile Organic Compounds

XPS – X-Ray Photoemission Spectroscopy

CURRICULUM VITAE

Prasadanie Karunarathna Adhihetty

785, Eastern Parkway, Apt 04,
Louisville, KY, USA, 40217
Phone (+1) 502 298 4102 (Mobile)
Email: pkadhi01@louisville.edu, prasadi.kln@gmail.com

HIGHER EDUCATION

Ph. D. Chemistry, University of Louisville, Louisville, Kentucky, USA (2022)

- U*of*L and NIEHS/SRP-funded research on "Surface-Functionalized Chemiresistive Films that Exploit H-Bonding, Cation-π, and Metal-halide Interactions".
  Supervisor: Dr. Michael H. Nantz, Professor, Department of Chemistry, University of Louisville, USA.

M.S. Chemistry, University of Louisville, Louisville, Kentucky, USA (2019)

B.Sc. [Second Class (Upper Division) Honors] Chemistry, University of Kelaniya, Kelaniya, Sri Lanka (2014)

- Research on "Computational Study of Bergman Cyclization of Cyclic Enediynes".
  Supervisor: Dr. Dinesh R. Pandithavidana, Professor, Department of Chemistry, University of Kelaniya, Sri Lanka.

PENDING PATENT APPLICATIONS

M.H. Nantz, F. Ibrahim and P. K. Adhihetty
Boron Compounds, Related Lipid Particles, Compositions, and Methods of Use
US Provisional Application **63/363,716**; Filed April 28, 2022

WORK EXPERIENCE

Graduate Fellow (January 2022 – May 2022); Department of Chemistry, University of Louisville, Louisville, Kentucky, USA

Graduate Research Assistant (August 2019 – December 2021); Department of Chemistry, University of Louisville, Louisville, Kentucky, USA

Graduate Teaching Assistant (August 2017 – April 2019); Department of Chemistry, University of Louisville, Louisville, Kentucky, USA

Teaching Assistant (January 2016 – September 2016); Department of Chemistry, The Open University of Sri Lanka, Nawala, Sri Lanka

Teaching Assistant (January 2014 – December 2015); Department of Chemistry, University of Kelaniya, Kelaniya, Sri Lanka

Professional placement (May 2013 – August 2013); Industrial Technology Institute, Herbal Technology Section, Bauddhaloka Mawatha, Colombo 07, Sri Lanka

- Comparative pharmacognostic evaluation of *Munronia pinnata* (Wall.) Theob. (Meliaceae) and its substitute *Andrographis paniculata* (Burm.f.) Wall. Ex Nees (Acanthaceae).
  Supervisor: Prof. R. M. Dharmadasa, Director, Herbal Technology Section

- Standardization of *Gyrinnops Walla* Gaertn. (Thymalaeaceae): Newly discovered, fragrant industrial potential, endemic plant from Sri Lanka
  Supervisor: Prof. R. M. Dharmadasa, Director, Herbal Technology Section

Professional placement (December 2012); Industrial Technology Institute, Bio-Technology Section, Bauddhaloka Mawatha, Colombo 07, Sri Lanka

- Studied rice varieties to grow in dry zones of Sri Lanka
  Supervisor: Dr. (Mrs.) Siddhika G. Senaratne, Director, Bio-Technology Section

- Sequenced a newly identified cinnamon species
  Supervisor: Dr. (Mrs.) Siddhika G. Senaratne, Director, Bio-Technology Section

RESEARCH PUBLICATIONS

Adhihetty, P. K.; Halder, S.; Fu, X.-A.; Nantz, M. H. (2022). Introducing a New Approach for Sensing Trichloroethylene (TCE) in Air. (Manuscript preparing)

Adhihetty, P. K.; Halder, S.; Jasinski, J. B.; Fu, X.-A.; Nantz, M. H. (2022). Harnessing the Cation-π Interactions of Metalated Gold Monolayer-Protected Clusters to Detect Aromatic Volatile Organic Compounds. In Review, *Talanta.*

Xie, Z.; Raju, M. V. R.; **Adhihetty, P. K**.; Fu, X.; Nantz, M. H. (2020). Effect of Thiol Molecular Structure on the Sensitivity of Gold Nanoparticle-Based Chemiresistors toward Carbonyl Compounds. *Sensors 20* (24), 7024.

Sibakoti, T. R.; Stinger, C. R.; **Adhihetty, P. K.**; Zamborini, F. P.; Nantz, M. H. (2019). Tunable Aminooxy-Functionalized Monolayer-Protected Gold Clusters for Nonpolar and Aqueous Oximation Reactions. *Particle & Particle Systems Characterization 36* (7), 1900093.

Dharmadasa, R. M.; Samarasinghe, K.; **Adhihetty, P**. Hettiarachchi, P. L. (2013). Comparative Pharmacognostic Evaluation of Munronia Pinnata (Wall.) Theob. (Meliaceae) and Its Substitute Andrographis paniculata (Burm.f.) Wall. Ex Nees (Acanthaceae). *World J. Agric. Res. 1* (5), 77-81.

Dharmadasa, R. M.; Siriwardana, A.; Samarasinghe, K.; **Adhihetty, P.** (2013). Standardization of Gyrinops Walla Gaertn. (Thymalaeaceae): Newly Discovered, Fragrant Industrial Potential, Endemic Plant from Sri Lanka. *World J. Agric. Res. 1* (6), 101-103.

RESEARCH PRESENTATIONS

Adhihetty, P. K.; Halder, S.; Fu, X.; Nantz, M. H. (2022, March 20-23) Microfabricated gold-based cesium gas sensor to detect trace levels of trichloroethylene (TCE) [Poster presentation]. *ACS Spring 2022 National Meeting & Exposition*, San Diego, USA.

Adhihetty, P. K.; Halder, S.; Smith, D.; Fu, X.; Nantz, M. H. (2021, Oct. 20-22). BTEX detection: Merging MEMS technology with metal ion-functionalized Au MPCs to exploit cation-π interactions [Oral presentation]. *Sensors 2021 International conference and exhibition*, Milan, Italy.

Adhihetty, P. K.; Halder, S.; Fu, X.; Nantz, M. H. (2021, March 11-12). *Employing cation-π interaction for aromatic VOCs sensing* [Poster presentation]. *14th Annual Graduate Student Regional Research Conference*, University of Louisville, Kentucky, USA.

Adhihetty, P. K.; Halder, S.; Fu, X.; Nantz, M. H. (2020, Dec. 14-16). An alkali metal-based Au MPCs chemiresistor sensor array for sensing aromatic VOCs [Poster presentation]. *Superfund Research Program 2020 Annual Meeting*, Texas, USA.

Halder, S.; **Adhihetty, P. K.**; Xie, Z.; Fu, X.; Nantz, M. H. (2020, Dec. 14-16). Fabrication and characterization of a sensor array to detect volatile organic compounds in environmental air [Poster presentation]. *Superfund Research Program 2020 Annual Meeting*, Texas, USA.

Adhihetty, P. K.; Halder, S.; Fu, X.; Nantz, M. H. (2019, Nov. 18-20). Development of a gold nanoparticles chemiresistor microarray for benzene sensing [Oral presentation]. *Superfund Research Program 2019 Annual Meeting*, Seattle, Washington, USA.

Halder, S.; **Adhihetty, P. K**.; Xie, Z.; Fu, X.; Nantz, M. H. (2019, Nov. 18-20). A sensor array for detection of multiple volatile organic compounds in air [Poster presentation]. *Superfund Research Program 2020 Annual Meeting*, Seattle, Washington, USA.

Sibakoti, T.R.; **Adhihetty, P.K.**; Xie, Z.; Zamborini, F. P.; Fu, X.; Nantz, M. H. (2018, Nov. 28-30). Aminooxy-functionalized aminothiols as ligands for gold nanoparticle chemiresistors [Poster presentation]. *Superfund Research Program 2020 Annual Meeting*, Sacramento, California, USA.

Adhihetty, P.; Rathnayaka, M.; Pandithavidana, D. R. (2014, August 2-4). Computational investigation of design and synthesis of cyclic enediynes [Oral Presentation]. *70th Annual Sessions of the Sri Lankan Association for Advancement of Science (SLAAS)*, Colombo, Sri Lanka.

Adhihetty, P.; Dharmadasa R. M.; Samarasinghe, K.; Hettiarachchi, P. L. (2013, Aug. 7-9). Phytochemical, physicochemical and antioxidant activity of *Munronia pinnata* (Wall.) Theob. (Meliaceae) and *Andrographis paniculata* (Burm.f.) Wall. Ex Nees. (Acanthaceae) [Poster presentation]. *69th Annual Sessions of the Sri Lankan Assosiation for Advancement of Science (SLAAS)*, Colombo, Sri Lanka.

AWARDS

Doctoral Dissertation Completion Award - Spring 2022
Graduate School Travel Award – Spring 2022

RESEARCH SKILLS

Familiar with multiple instrumental techniques:

- Nuclear magnetic resonance spectrometer (NMR)
- Fourier-transform infrared spectroscopy (FTIR)
- Gas chromatograph–mass spectrometer (GC-MS)
- Ultra-high performance liquid chromatography-mass spectrometer (UHPLC-MS)
- Scanning electron microscopy (SEM) with energy-dispersiveX-ray spectroscopy (EDS)
- UV-Vis Spectroscopy
- Thermogravimetric Analysis (TGA)
- X-Ray photoemission spectroscopy (XPS)
- Transmission electron microscope (TEM) imaging

POSITIONS HELD

- President, Sri Lankan Student Association, University of Louisville, Louisville, Kentucky, USA (2020-2022)
- Senator Proxy, Graduate Student Council, University of Louisville, Louisville, Kentucky, USA (2020)
- Organizing Committee President (Recruitment), AIESEC in University of Kelaniya, Kelaniya, Sri Lanka (2012)
- Secretary, Aquatic Society, University of Kelaniya, Kelaniya, Sri Lanka (2011-2012)
- Vice Secretary, Society of Molecular Biology and Plant Biotechnology, University of Kelaniya, Kelaniya, Sri Lanka (2011-2012)

AFFILIATIONS

Member of Sri Lanka Association for the Advancement of Science [SLAAS] (2013-2015)

TRAINING PROGRAMS & WORKSHOPS PARTICIPATED

Summer 2021 Mentoring Academy (June 2021 – July 2021), University of Louisville, Louisville, Kentucky, USA

INTERESTS

Volunteering and Community Involvement, Photography, Cooking, and Travelling

REFERENCES

Dr. Michael H. Nantz, Professor of Chemistry, **Address:** Department of Chemistry, University of Louisville, 2320 S Brook St., Chem 138, Louisville, Kentucky, 40292, USA. **Phone:** (+1) 502-852-8069, **Email:** michael.nantz@louisville.edu

Prof. (Mrs) P. A. Paranagama, Senior Professor & Chair of Chemistry, University of Kelaniya; Director, Institute of Indigenous Medicine, University of Colombo **Address:** University of Kelaniya, Kandy Road, Dalugama, Kelaniya 11600, Sri Lanka. **Phone**: +94 (0)112 914 486, **Email**: priyani@kln.ac.lk

Prof. D. R. Pandithavidana, Professor of Chemistry, **Address**: University of Kelaniya, Kandy Road, Dalugama, Kelaniya 11600, Sri Lanka. **Phone**: +94 (0)777 745 720, **Email**: dinesh@kln.ac.lk